Distortional Lateral Torsional Buckling Analysis for Beams of Wide Flange Cross-Sections

Rusul Hassan

Under supervision of
Dr. M. Mohareb

A thesis submitted to the
Faculty of Graduate and Postdoctoral Studies
in partial fulfilment of the requirements for the
MASc degree in Civil Engineering

Department of Civil Engineering
Faculty of Engineering
University of Ottawa

Acknowledgments

I would like to express my deepest gratitude to my supervisor, Dr. Magdi Mohareb, whose expertise, patience, and love of academics has added considerably to my graduate experience. Furthermore, I am especially grateful for all the support and advice Dr. Magdi Mohareb has provided in my young professional career.

A special thanks goes out to my brothers for their moral support and encouragement during my studies. Finally, I would like to thank my parents, whose sacrifice, financial support, and lifelong encouragement allowed me to accomplish many of my academic and personal goals.

Abstract

Structural steel design standards recognize lateral torsional buckling as a failure mode governing the capacity of long span unsupported beams with wide flange cross-sections. Standard solutions start with the closed form solution of the Vlasov thin-walled beam theory for the case of a simply supported beam under uniform moments, and modify the solution to accommodate various moment distributions through moment gradient expressions. The Vlasov theory solution is based on the assumption that cross-sectional distortional effects have a negligible effect on the predicted elastic critical moment. The present study systematically examines the validity of the Vlasov assumption related to cross-section distortion through a parametric study.

A series of elastic shell finite element eigen-value buckling analyses is conducted on simply supported beams subject to uniform moments, linear moments and mid span point loads as well as cantilevers subject to top flange loading acting at the tip. Cross-sectional dimensions are selected to represent structural steel cross-section geometries used in practice. Particular attention is paid to model end connection details commonly used in practice involving moment connections with two pairs of stiffeners, simply supported ends with a pair of transverse stiffeners, simply supported ends with cleat angle details, and built in fixation at cantilever roots.

The critical moments obtained from the FEA are compared to those based on conventional critical moment equations in various Standards and published solutions. The effects of web slenderness, flange slenderness, web height to flange width ratio, and span to height ratios on the critical moment ratio are systematically quantified. For some combinations of section geometries and connection details, it is shown that present solutions derived from the Vlasov theory can overestimate the lateral torsional buckling resistance for beams.

Contents

List of Figures

List of Tables

Chapter 1
Introduction

1.1. Lateral Torsional Buckling

The flexural resistance of long span laterally unsupported beams is typically governed by lateral torsional buckling. The AISC defines lateral torsional buckling as a "buckling mode of a flexural member involving deflection out of the plane of bending occurring simultaneously with twist about the shear center of the cross section." Fig. 1.1 depicts the beam's cross section position prior to loading, after loading at the onset of buckling, and in the final buckled configuration after lateral torsional buckling has occurred. As the Figure suggests, the applied load causes the cross section to deflect vertically by w from its initial position, and if the load is of sufficient magnitude (referred to as the critical load), the beam translates laterally by displacement u and twists about the shear center by an angle ϕ. At this point, the beam is considered to have failed and is unable to resists additional forces. Lateral torsional buckling is widely recognized as a failure mode in various structural steel design standards. However, closed form solutions for the problem are available only for very limited cases (e.g., Timoshenko and Gere 1961).

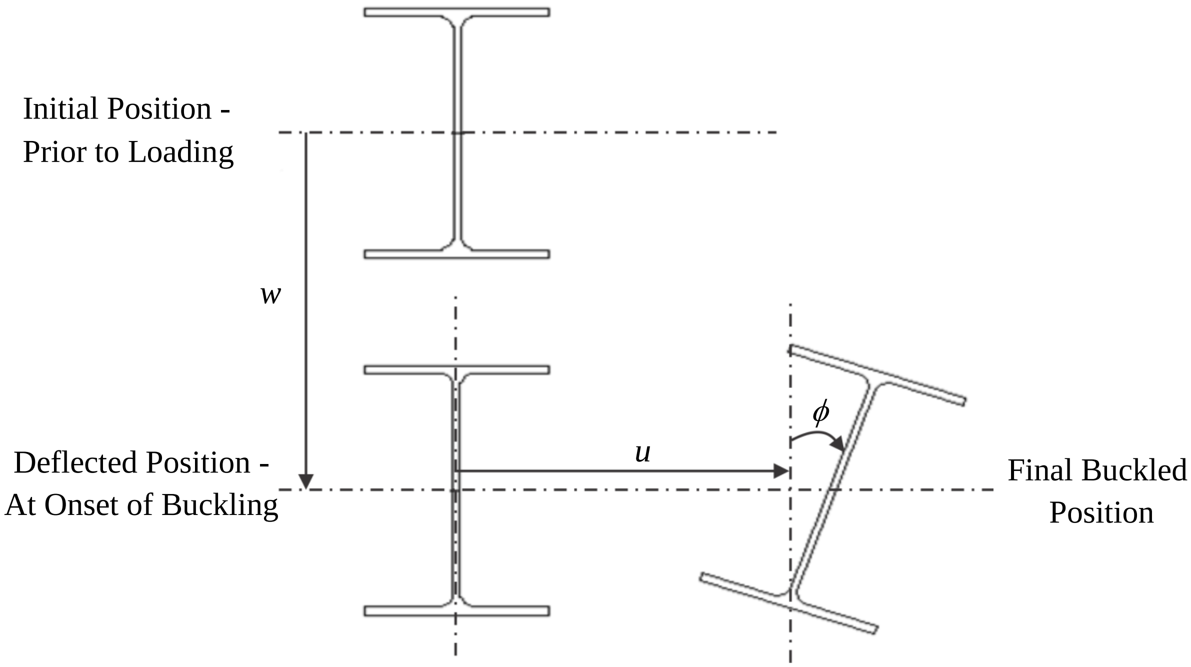

Fig. 1.1- Cross-section during lateral torsional buckling at the initial configuration, at onset of buckling, and in the final position

1.2. Distortion

The classical lateral solution developed by Timoshenko and Gere (1961) is derived under the assumption that when a beam undergoes buckling, the cross section does not exhibit any local deformations and acts as a rigid disk (Fig. 1.2(a)). However, in reality, the cross section does not act as a rigid disk and is thus susceptible to distortional changes (Fig. 1.2(b)). As depicted in Fig. 1.2, distortion is characterized by deformation of the web which causes the angle of twist of the top flange to be different from the angle of twist of the bottom flange.

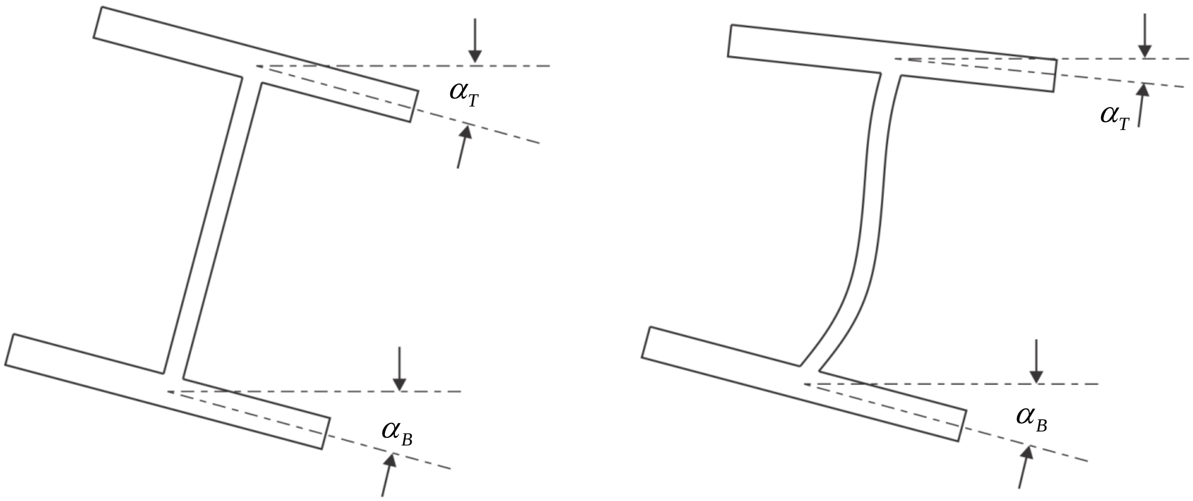

(a) $\alpha_T = \alpha_B$ (a) $\alpha_T \neq \alpha_B$

Fig. 1.2- Assumed buckled configuration of a cross-section: (a) Classical lateral torsional buckling, and (b) Distortional lateral torsional buckling

1.3. Outline of Thesis

The general focus of the thesis is to assess the effects of distortion on the elastic lateral torsional buckling capacity of beams. Towards this aim, the body of the thesis consists of six chapters (Chapter 2 through 7). The content of these chapters are as follows:

- Chapter 2 provides 1) reviews of the Standards' design procedures for doubly symmetric wide flange sections susceptible to failure in a lateral torsional buckling mode, and 2) a review of available literature on distortional lateral torsional buckling of doubly symmetric wide flange cross sections.

- In Chapter 3, a dimensional analysis is conducted in order to determine the dimensionless parameters influencing the distortional buckling moment ratio. The Canadian Institute of Steel Construction (CISC) Structural Selection Tables (SST) database is statistically analyzed and representative sections of the database are selected for parametric investigation. A series of Finite Element Analysis (FEA) is carried out and the effects of each dimensionless parameter are analyzed and discussed. Finally, a sample of 54 beams based on real cross-sections from the CISC SST is analyzed through FEA and a simplified solution which predicts the distortional moment ratio for simply supported beams subject to uniform moments is developed.

- Chapter 4 focuses on investigating the effects of distortion on the critical moment when beams are subject to linear moment gradients. Comparisons are made with the moment gradient factors presented by CAN/CSA S16-09, ANSI/AISC 360-10, EN 1993-1-1, and AS 4100-1998 for various end conditions based on practical details.

- Chapter 5 investigates distortional lateral torsional moment results through FEA of real sections and most common simple connection details, (i.e., bolted web cleat). Attention is given to the partial twisting restraints at the ends as provided by the cleat angles. A database of FEA runs is generated for the problem and the results are used to develop a design procedure which accounts for partial twist restraints and distortional effects.

- Chapter 6 focuses on the behaviour of laterally unsupported cantilever beams subject to tip point loads acting at the top flange. Methods proposed by the various standards are critically evaluated and compared to FEA results, and a new design equation is developed for the problem.

- Chapter 7 provides conclusions reached through the FEA studies in each chapter and provides recommendations for future research.

Chapter 2

Literature Review

2.1. *General*

The literature review in this chapter is divided into four parts. A general background on the classical lateral torsional buckling solution is provided in Section 2.2. Section 2.3 provides a review of the lateral torsional buckling design provisions in various standards. A concise survey of various studies on moment gradient effects is then presented in Section 2.4. The chapter is concluded with Section 2.5 which provides a detailed review of studies on distortional lateral torsional buckling.

2.2. *Classical Lateral Torsional Buckling Solution*

When quantifying the lateral torsional buckling capacity of a beam with a doubly symmetric wide flange section, various structural steel design standards utilize, as a starting point, the classical closed form expression of the critical moment M_u for a simply supported beam under uniform moments

[2.1] $$M_u = \frac{\pi}{L_u}\sqrt{EI_yGJ + \left(\frac{\pi E}{L_u}\right)^2 I_y C_w}$$

in which L_u is the length of unbraced segment of a beam, E is the modulus of elasticity of steel, I_y is the out of plane moment of inertia, G is the shear modulus of elasticity of steel, J is the torsional constant, and C_w is the warping constant. The critical moment solution M_u is derived under the assumption that both ends are simply supported relative to the lateral displacement u and angle of twist θ, i.e. $u = u'' = \theta = \theta'' = 0$ at both ends.

The standards then apply various modification factors to the expression to adapt it to other forms of loading and boundary conditions. However, the classical solution as provided by Eq. [2.1] is based on the Vlasov theory assumptions (Vlasov 1961), i.e., throughout deformation 1) any cross-section acts as a rigid disk within its own plane, and 2) shear strains within the middle surface of the beam are considered negligible. The first Vlasov assumption neglects possible distortional effects within the beam cross-section. As a result, it provides a stiffer representation of the actual beam and is thus expected to overestimate the elastic critical moments. Therefore, the adoption of the Vlasov theory based equation in design standards implies the neglect of such distortional effects. This issue has been recognized in the analysis and design of cold formed cross sections, but has generally been thought of as negligible in the analysis of rolled wide flange sections. One of the objectives of the present thesis is to assess the implications of such a simplifying assumption on the predicted critical moments. Towards this goal, Chapter 3 provides a study on the effect of various geometric parameters of a beam on it is ability to attain the critical moment as predicted by Eq. [2.1] for the case of uniform moments.

In addition to neglecting distortional effects, the formulation of the classical lateral torsional buckling solution is based on specific boundary conditions at both ends. These are full lateral restrain and full twist restrain, but free rotation about the weak axis and zero warping restrain at both ends of the beam. In real life conditions, such idealized support conditions are seldom encountered. Thus, another objective of the present study is to assess the effect of realistic boundary conditions on the lateral torsional buckling resistance of beams. This includes beams with end stiffeners (Chapters 3 and 4), cleat angles (Chapter 5), and cantilevers (Chapter 6).

2.3. Standard Design Provisions

The flexural resistance of a laterally unsupported beam bent about the strong axis is governed by one of three possible modes of failure. These are: 1) elastic lateral torsional buckling, 2) inelastic lateral torsional buckling, and 3) yielding of the cross-section. The standards examined in this study (CAN/CSA S16-09, ANSI/AISC 360-10, AS4100-1998, and EN 1993-1-1:2005) introduce various methods for quantifying a beams resistance under each failure mode.

For the elastic lateral torsional buckling mode, all standards use the classical lateral torsional buckling solution Eq. [2.1] as a starting point to quantify the critical moment for a hypothetical simply supported beam subject to uniform moments and account for non-uniform moment distributions by the introduction of standard dependent moment gradient factors. The moment gradient factors in the various standards fall into one of two categories, based on either 1) the ratio of end moments for linear moment distributions, or 2) moments at quarter span points of the beam for more general moment distributions.

The first category of methods is used for beams subject to linear moment distributions. The moment gradient factor C takes a quadratic form $C = a_1 + a_2\kappa + a_3\kappa^2$, where the end moment ratio κ is the absolute value of the smaller factored moment to that of the larger factored moment at ends of the unbraced length. The ratio κ is taken as positive for double curvature and negative for single curvature.

The second category of methods, known as quarter point methods, is used for general moment distributions and is a function of the absolute values of the moment M_a at quarter span, moment M_b at mid-span, and moment M_c at three quarter span in addition to the maximum moment $M_{\max}$ within the unsupported span of the beam.

Regarding the yielding strength of beams, all standards classify beam cross-sections into three categories: 1) those that are thick enough (compact) to attain their plastic resistance prior undergoing buckling, 2) those of moderate thickness (or non-compact) and thus exhibit local buckling after attaining their yield moment strength but before developing their plastic moment resistance, and 3) those that are too thin (slender) to develop their yield moment capacity prior exhibiting local buckling. For common rolled sections and steel grades, most sections are either compact or non-compact. The yield strength of compact sections is taken as the plastic moment while that of non-compact sections is taken as the yield moment.

Each standard uses their own set of terminologies for the classes or categories. For example while the ANSI/AISC 360-10 and AS 4100-1998 use the terms Compact/ Non-Compact/ Slender, the equivalent terms in CAN/CSA S16-09 and EN 1993-1-1:2005 are Class 1 or 2/ Class 3/ Class 4. In all design standards, the inelastic lateral torsional buckling resistance of a member is determined based on standard specific empirical equations which depend upon the flexural yield strength and the elastic lateral torsional buckling resistance of the member.

CAN/CSA S16-09

For laterally unsupported beams of doubly symmetric cross-sections bent about their strong axis, CAN/CSA S16-09 provides the following procedure for determining the flexural resistance.

Depending on the section class, the yield resistance is determined either based on the plastic moment $M_p = Z_x F_y$ or the elastic resistance $M_y = S_x F_y$, in which Z_x is the plastic section modulus taken about the *x*-axis, S_x is the elastic section modulus taken about the *x*-axis, and F_y is the specified minimum yield stress. Also, the elastic critical lateral torsional buckling moment is determined by multiplying the classical lateral torsional buckling moment for the case of uniform moment as determined from Eq. [2.1] by a moment gradient factor C_{CAN} given by

[2.2] $$M_{cr} = C_{CAN} M_u = C_{CAN} \frac{\pi}{L_u} \sqrt{EI_y GJ + \left(\frac{\pi E}{L_u}\right)^2 I_y C_w}$$

The Canadian CAN/CSA S16-09 Standard provides designers with two solutions for determining the moment gradient factor C_{CAN}. The general equation provided for use with any moment distribution is a quarter point method which was introduced by Wong and Driver (2010). The solution is given as

[2.3] $$C_{CAN-Gen} = \frac{4M_{max}}{\sqrt{M_{max}{}^2 + 4M_A{}^2 + 7M_B{}^2 + 4M_C{}^2}} \le 2.5$$

The standard also supports the use of an end moment ratio equation when the moment distribution is linear based on a slight variation of the solution introduced by Salvadori (1955)

[2.4] $$C_{SALV} = 1.75 + 1.05\kappa + 0.3\kappa^2 \le 2.3$$

In CAN/CSA S16-09, a slightly higher value of 2.5 is specified as an upper limit, i.e.,

[2.5] $$C_{CAN-Lin} = 1.75 + 1.05\kappa + 0.3\kappa^2 \le 2.5$$

If $M_{cr} < 0.67M_P$ for Class 1 or 2 sections or $M_{cr} < 0.67M_y$ for Class 3 sections, the resistance of the member will be governed by elastic lateral torsional buckling and the resisting moment is

[2.6] $$M_r = \phi M_{cr}$$

in which $\phi = 0.90$ is a resistance factor. If $M_{cr} \geq 0.67 M_p$ for Class 1 and 2 sections, or $M_{cr} \geq 0.67 M_y$ for Class 3 sections, the member resistance will be governed by either inelastic lateral torsional buckling as determined by

[2.7] $$M_r = \phi 1.15 M_p \left[1 - \frac{0.28 M_p}{M_{cr}}\right] \quad \text{when } \phi 1.15 M_p \left(1 - 0.28 M_p / M_{cr}\right) < \phi M_p$$

or by yielding as determined by

[2.8] $$M_r = \phi M_p \quad \text{when } \phi 1.15 M_p \left(1 - 0.28 M_p / M_{cr}\right) > \phi M_p$$

For non-compact (Class 3) sections, similar equations are obtained after replacing the plastic moment resistance M_p by the yield moment resistance M_y.

ANSI/AISC 360-10

ANSI/AISC 360-10 utilizes two limiting spans L_p and L_r to determine the failure mode. Span L_r, which corresponds to the condition $M_u = 0.7 M_y$ is known as the limiting laterally unbraced length for the limit state of inelastic lateral torsional buckling. For a doubly symmetric section, it is given by

[2.9] $$L_r = 1.95 r_{ts} \frac{E}{0.7 F_y} \sqrt{\frac{J}{S_x h_o} + \sqrt{\left(\frac{J}{S_x h_o}\right)^2 + 6.76 \left(\frac{0.7 F_y}{E}\right)^2}}$$

where h_o is the distance between flange centroids and r_{ts} is the effective radius of gyration given by

[2.10] $$r_{ts}^2 = \frac{\sqrt{I_y C_w}}{S_x}$$

The limiting laterally unbraced length for the limit state of yielding, L_p is given by

[2.11] $$L_p = 1.76 r_y \sqrt{\frac{E}{F_y}}$$

in which r_y is the radius of gyration about the *y*-axis.

When $L_u > L_r$, the resistance is governed by elastic lateral torsional buckling and the nominal moment resistance for a wide flange doubly symmetric section is given by

[2.12] $M_n = F_{cre} S_x \le M_p$

in which

[2.13] $F_{cre} = \dfrac{C_{AISC}\pi^2 E}{\left(\dfrac{L_u}{r_{ts}}\right)^2}\sqrt{1 + 0.078\dfrac{J}{S_x h_0}\left(\dfrac{L_u}{r_{ts}}\right)^2}$

Equations [2.12] and [2.13] are an equivalent form of the equation

[2.14] $M_n = C_{AISC}\dfrac{\pi}{L_u}\sqrt{EI_y GJ + \left(\dfrac{\pi E}{L_u}\right)^2 I_y C_w}$

where C_{AISC} is the ANSI/AISC 360-10 moment gradient factor given by

[2.15] $C_{AISC} = \dfrac{12.5M_{max}}{2.5M_{max} + 3M_A + 4M_B + 3M_C} \le 3.0$

This is a slightly altered version of a the moment gradient factor expression proposed by Kirby and Nethercot (1979) which took the form

[2.16] $C_{K\&N} = \dfrac{12M_{max}}{2.5M_{max} + 3M_A + 4M_B + 3M_C}$

When $L_p < L_u \le L_r$, the resistance is governed by inelastic lateral torsional buckling and the nominal moment resistance is given by

[2.17] $M_n = C_{AISC}\left[M_p - \left(M_p - 0.7F_y S_x\right)\left(\dfrac{L_u - L_p}{L_r - L_p}\right)\right] \le M_p$

When $L_u \le L_p$, the resistance is governed by yielding and the nominal moment resistance is calculated by $M_n = Z_x F_y$ for compact sections or $M_n = S_x F_y$ for subcompact sections.

AS 4100-1998

The Australian standard provides a single equation which takes into account both elastic and inelastic lateral torsional buckling. For compact sections, the nominal moment resistance is given by

[2.18] $M_n = C_{AUS}\alpha_s M_p \le M_p$

In Eq. [2.18], C_{AUS} is the AS 4100-1998 moment gradient factor given as a

[2.19] $C_{AUS} = \dfrac{1.7M_{max}}{\sqrt{M_A{}^2 + M_B{}^2 + M_C{}^2}} \le 2.5$

and α_s is referred to as the slenderness reduction factor and accounts for reduction in strength due to member global slenderness. It is given as

[2.20] $\alpha_s = 0.6\left[\sqrt{\left[\left(\dfrac{M_p}{M_o}\right)^2 + 3\right]} - \left(\dfrac{M_p}{M_o}\right)\right]$

in which M_o is a modified version of the classical lateral torsional buckling solution M_u given by

[2.21] $M_o = \dfrac{\pi}{L_e}\sqrt{EI_y GJ + \left(\dfrac{\pi E}{L_e}\right)^2 I_y C_w}$

where $L_e = k_t k_l k_r L_u$ is an effective span which accounts for end twist restraint through a constant k_t, for load height with respect to the shear center through a coefficient k_l, for weak axis restraint k_r, and for the member span L_u. AS 4100-1998 provides recommendations for constants k_t, k_l, and k_r for common end restrains. For small effective spans, M_o takes a large value, the corresponding M_p/M_o ratio is small, and Eq. [2.20] yields a value in proximity of unity. For instance, when $M_p/M_o = 0.1$, the corresponding slenderness parameter α_s takes the value 0.981. In such a case, for a typical moment gradient greater than unity, the member capacity will be dictated by the plastic moment. Conversely, when the effective span is large, M_o is small, the corresponding M_p/M_o ratio is large and Eq. [2.20] yields a small value. For instance when $M_p/M_o = 10$, the corresponding slenderness parameter takes the value 0.089, signifying that the critical moment is a small fraction of the plastic moment.

EN 1993-1-1:2005

Under EN 1993-1-1:2005, the elastic lateral torsional buckling moment M_u for the case of uniform moments is first determined. The standard does not provide a method for determining

M_u. However, the Designers Guide (2005) suggests calculating M_u by the classical LTB solution (Eq. [2.1]) and accounting for non-uniform moment distributions through M_{cr} which is calculated by

[2.22] $M_{cr} = C_{EURO} M_u$

in which C_{EURO} is a moment gradient factor. No equations are provided for C_{EURO}. Rather, the commentary provides tables which give various loading patterns and support conditions and their respective moment gradient factors. Table 2.1 provides the moment gradient factors for the various loading conditions of interest in the present study.

Table 2.1 EN 1993-1-1 Guide moment gradient factors

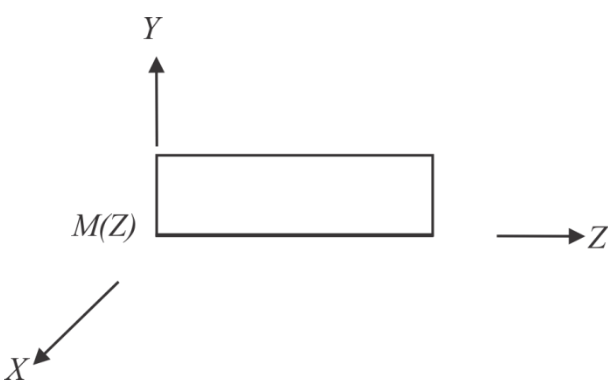	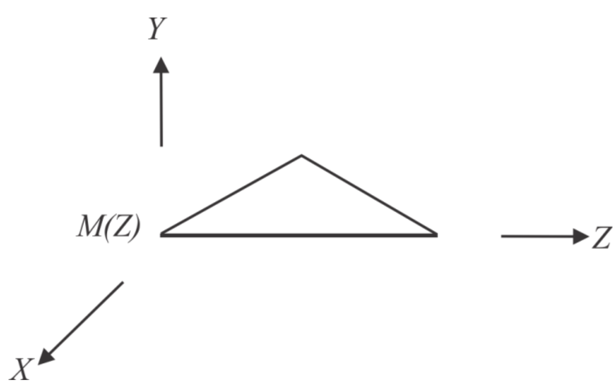
$C_{EURO} = 1.0$	$C_{EURO} = 1.365$
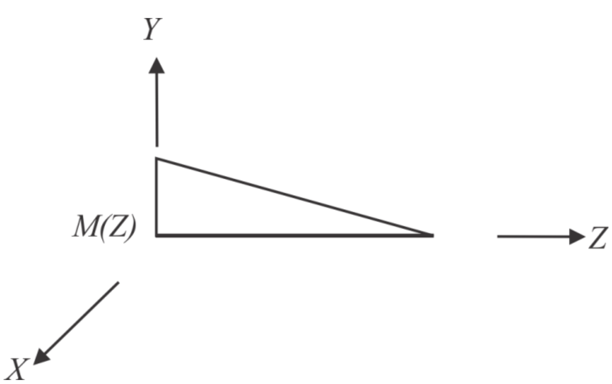	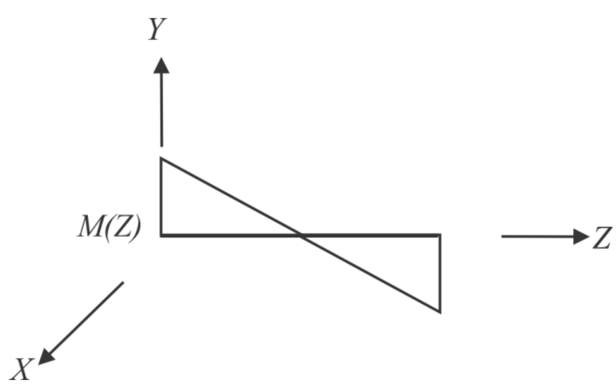
$C_{EURO} = 1.879$	$C_{EURO} = 2.752$

For Class 2 sections, the non-dimensional slenderness parameter $\bar{\lambda}_{LT}$ for lateral torsional buckling is given as the square root of the ratio of plastic moment to the elastic critical moment ratio, i.e.,

[2.23] $\bar{\lambda}_{LT} = \sqrt{\dfrac{Z_x F_y}{M_{cr}}}$

For a Class 3 section, the plastic section modulus Z_x needs to be replaced by the elastic section modulus S_x. Given the slenderness parameter, the dimensionless imperfection parameter Φ_{LT} is determined from

[2.24] $\Phi_{LT} = 0.5\left[1 + \alpha_{LT}\left(\bar{\lambda}_{LT} - 0.2\right) + \bar{\lambda}_{LT}^2\right]$

in which α_{LT} is an imperfection factor which is taken as 0.21 for rolled sections when the beam depth to width ratio $d/b \le 2$ and 0.34 when $d/b > 2$. Based on the slenderness parameter $\bar{\lambda}_{LT}$ and the dimensionless imperfection parameter, one can then determine the reduction factor χ_{LT} for lateral torsional buckling through

[2.25] $\chi_{LT} = \dfrac{1}{\Phi_{LT} + \sqrt{\Phi_{LT}^2 - \bar{\lambda}_{LT}^2}} \le 1.0$

where the upper bound corresponds to the case of short span members. In such a case the design is governed by yielding. The corresponding nominal flexural resistance for a Class 2 section is then given by

[2.26] $M_n = \chi_{LT} Z_x F_y$

Again, for a Class 3 section, the plastic section modulus Z_x needs to be replaced by the elastic modulus S_x. The factored resistance M_r is given by dividing the nominal flexural resistance by the partial safety factor for resistance to instability γ_{M1} taken as unity, i.e.,

[2.27] $M_r = M_n = \chi_{LT} Z_x F_y / \gamma_{M1}$

2.4. Overview of Studies on Critical Moments in Beams with Non-Uniform Moments

2.4.1. Simply Supported Beams

There is a wealth of studies on the moment gradient factor starting with the early work of Salvadori (1955) which resulted in a moment gradient equation applicable for linear moment distributions that is still being used (in CAN/CSA S16-09) with a slight modification. Nethercot and Rockey (1972) investigated the elastic lateral torsional buckling resistance of simply supported beams with restrained warping at the end, restrained lateral rotations, and completely fixed end supports. They also considered three different loading positions with respect to the shear center. With this, they provided 41 different moment gradient factors. Kirby and Nethercot (1979) proposed a general quarter-point method moment gradient factor equation applicable for simply supported beams subjected to any bending moment distribution. Their equation is being used by ANSI/AISC 360-10 with a minor modification. Instead of providing a table of values for specific moment distributions, Trahair (1993) conducted a study where he was able to provide several equations for moment distributions by curve fitting of numerical data. Through the use of finite element analyses, Greiner et al. (1999) conducted a comprehensive numerical study on lateral torsional bulking and provided moment gradient factors for numerous moment diagrams. In their work, Greiner et al. (1999) also investigated lateral torsional buckling for beams with upper and lower flange restraints and presented their findings. On a study on the moment gradient factor in lateral-torsional buckling of wide flange steel sections, Suryotamono and Ho (2002) used finite difference to solve the governing differential equations of lateral torsional buckling numerically and compiled a table of factors and case specific equations for beams subject to linear moment distributions, point loads, and various non-linear moment distributions. Lim et al. (2003) conducted a finite element based study on the elastic lateral torsional buckling of I-beams under linear moment gradients. In their study, Lim et al. (2003) investigated simply supported, warping prevented, and both lateral bending and warping prevented support restraints and highlighted the inadequacy of the AISC standard equation for these cases. Through a study on equivalent uniform moment factors for lateral-torsional buckling of steel members, Serna et al. (2006) introduced a new quarter-point based solution by curve fitting of numerical data which includes a new coefficient which accounts both for moment distribution and lateral, rotational, and warping restrains at brace points. Using numerical data published by various studies, Wong and Driver (2010) conducted a study on the equivalent moment factor procedures for laterally unsupported beams. Using previously published equations for quantifying moment gradient effects, Wong and Driver (2010) studied 12 distinct bending moment distributions for simply supported beams and compared results against published numerical results. Through the vast database of numerical results, Wong and Driver (2010) introduced a new quarter point based method which was adopted by CAN/CSA S16-09.

2.4.2. Cantilevers

Although pervious work which investigated the buckling of cantilevers was conducted by Poley (1956) and Timoshenko and Gere (1961), their research was limited to loading at the shear center. Additional work on the subject was carried out by Kerenskey et al. (1956). However, they neglected to consider the effects of warping.

On his paper on the buckling of cantilevers, Nethercot (1973) investigated the influence of loading type and lateral support on the lateral buckling of cantilevers. The work of Nethercot (1973) is a continuation of previous studies in which warping and flange loading effects were examined. Through comparisons with previously published literature, the author was able to show the adequacy of using eight beam finite elements to model cantilevers.

Results presented by Nethercot (1973) suggest that top flange loading expedites the onset of lateral buckling. To account for the large reduction in stability due top flange loading on cantilevers, the author suggested altering loading position coefficients for simply supported beams introduced by Nethercot and Rockey (1972). The author has shown that his new coefficients produce results within 5% of finite element results.

2.5. *Detailed Review of Studies on Distortional Lateral Torsional Buckling*

2.5.1. Simply Supported Beams

Roberts and Jhita (1983)

Roberts and Jhita (1983) conducted an analytical/ numerical study on lateral, local and distortional buckling of I-Beams. The study developed energy formulations based on plate theory and compared results against finite element results. A computer program was developed to solve the resulting eigen-value problem in order to determine the buckling moments for beams including distortional effects. Roberts and Jhita (1983) presented results for three loading conditions for simply supported beams with symmetric I cross-sections. Loading cases investigated were: 1) uniform moment, 2) midspan concentrated load acting at the section centroid, and 3) midspan concentrated load acting on the top flange. The reference beam investigated had a web thickness $w = 10mm$ and a height $h = 400mm$, flange thickness $t =$ $15mm$ and a span $L = 3200mm$ with a depth to web thickness ratio of $d/w = 40$ and a flange thickness to web thickness ratio or $t/w = 1.5$. The flange width b was varied to investigate the effect of the flange width to depth ratio b/d on the critical moment.

The authors' results suggested that the buckling resistance of I-beams with stocky cross-sections is governed by lateral buckling or coupled lateral local buckling. However, coupled lateral local buckling was observed to occur only after the point at which plastic yielding would govern. The authors also pointed out that I-beams with slender cross sections, particularly those with high flange thickness to web thickness ratios t/w, experience a reduction in critical moment due to distortion. However, this reduction was observed to be insignificant in beams of practical dimensions.

Bradford (1986)

Bradford (1986) developed a finite element formulation for the prediction of inelastic distortional buckling of determinate hot-rolled I-beams. The finite element formulation uses a lengthwise subdivision of a beam into one-dimensional elements. The study assumes that the beam cross-section consists of two rigid flanges (within the plane of the cross-section) connected by a flexible web which is allowed to bend in the plane of the cross-section as the beam undergoes buckling. The resulting element consists of two nodes with six degrees of freedom at each node. The degrees of freedom correspond to the lateral displacements, flange rotations in the plane of bending, and angles of twist of each flange. Bradford (1986) conducted convergence studies in which he compared his results with numerical results by Bradford and Trahair (1981), and Hancock (1978) and showed that only three elements per half span were needed to produce results within 1% accuracy of published results.

Three loading and restraint conditions were considered; 1) simply supported beam under uniform bending, 2) beam on a seat subjected to uniform moments, and 3) beam with continuous restraint at the tension flange under various linear moment gradients. Two cross-sections with stocky flanges and slender webs, 838x292UB176 and 457x152UB52 were selected to promote distortion during buckling. Dimensions of the 838x292UB176 were: beam depth $d = 816mm$, flange width $b = 292mm$, flange thickness $t = 18.8mm$, and web thickness $w = 14.0mm$, while dimensions of the 457x152UB52 were $d = 439mm$, $b = 152mm$, $t = 10.9mm$, $w = 7.6mm$. By comparing results with simply supported beams in uniform bending, the author observed there is a maximum reduction in the critical moment of 5% for both the elastic and inelastic buckling due to distortion while for beams on a seat the decrease was observed to be 6% and 12% respectively.

Bradford (1992)

In a discussion on lateral-distortional buckling of steel I-section members, Bradford (1992) surveyed the literature and discussed advances made in Australian research pertaining to elastic and inelastic distortional buckling. The author indicated that short beams with slender webs will exhibit distortional buckling at loads much lower than those based on elastic lateral buckling based on classical theories which neglect distortion. This behaviour was observed to be more pronounced for mono-symmetric I-beams with the smaller flange in compression. The author suggested that for the majority of short beams, plastic yielding will occur before severe reductions caused distortion may come into play. However, he highlighted that for certain beam geometries and restraint conditions, the effects of distortion should not be neglected.

Pi and Trahair (2000)

Pi and Trahair (2000) studied the effects of web distortion and warping restraints induced by various end support conditions on the lateral torsional buckling resistance of doubly symmetric I-beams. Several finite element and finite strip models were used towards obtaining simplified approximations for the distortional LTB capacity of beams. The authors conducted elastic buckling analyses based on PRFELB (Papangelis et al. 1995), the finite strip program THIN-WALL (Hancock and Papangelis 1998), a finite element model developed by Pi and Trahair (1997), and a shell finite element analysis within ABAQUS. Two sets of beams were analyzed. The first beam had a web height $h = 640mm$, a flange width $b = 160mm$, a flange thickness $t = 10mm$, a web thickness $w = 5mm$, and spans ranging from $L = 1,600mm$ to $L = 5,400mm$. The dimensions of the second beam were $h = 240mm$, $b = 100mm$, $t = 10mm$, $w = 2.5mm$, and had spans ranging from $L = 1,000mm$ to $L = 6,000mm$. In ABAQUS, a load application scheme consisting of two equal and opposite longitudinal tractions applied at both flanges at both ends was used to simulate a uniform moment distribution. To simulate simply supported boundary conditions, vertical and horizontal nodal translations and twist rotations about the longitudinal axis of the beams were restricted at all nodes of both ends, and the longitudinal displacement at the centroid of one beam was also restrained. Results of the distortional buckling analysis revealed that the classical LTB solution overestimates the capacity of beams that do not have substantial flange torsional rigidities.

To investigate the effect of warping restraints of various end supports, the authors used the finite element developed in Pi and Trahair (1997) and ABAQUS. Through the use of ABAQUS, the authors were able to simulate web cleat, end plate, web plate, web open web stiffener, and web box stiffener details. Through the combination of distortional and warping restraint analysis, the authors proposed a modification of the classical LTB solution where the torsional and warping rigidities GJ and EI are replaced with effective torsional and warping rigidities GJ_e and EI_e.

Poon and Ronagh (2004)

Poon and Ronagh (2004) developed a model which idealizes flanges of I-beams as beam elements assumed to act rigidly within the plane of the cross-section while webs of I-beams were idealized as plate elements whose deformation is modeled through a fifth order polynomial along the web height. Their model is capable of handling elastic restraints and flange level loading. Through the use of a beam with distance between flange centroids $h_o = 440mm$, flange width $b = 100mm$, flange thickness $t = 10mm$, and web thickness $w = 7.8mm$, the authors have shown that their solution diverges from the classical LTB solution as the beam span decreases. For beam spans of 20*m*, the authors' solutions were found to exactly match the classical elastic lateral torsional buckling moment while for spans of 3*m*, the classical solution was observed to overestimate the critical moments by 9.9%. For beams with mid-span point load with varying flange widths and for beams with slender webs, the use of a fifth order polynomial representation was observed to be important in capturing distortional buckling compared to lower order polynomials.

Ng and Ronagh (2004)

Ng and Ronagh (2004) introduced an analytical solution similar to that of Bradford and Trahair (1981) and Bradfrod (1986), where a one dimensional beam element method is used to discretize the beam in the longitudinal direction. However their method differs in the way lateral deflections and twists were discretized. While Bradford and Trahair (1981) and Bradford (1986) modeled the lateral deflections and twists of the members as cubic polynomials, their study adopted Fourier Series, in which the number of Fourier terms is specified by the user. The buckling loads and modes were determined from the model based on minimal computational efforts. The authors conducted convergence studies in which predictions made by their model were compared with results in previous studies. It was demonstrated that for beams under uniform bending, only one Fourier term is needed to achieve accurate results while for a beam with a central point load, four Fourier terms were needed to produce results within 1% accuracy.

A beam with a distance between flange centroids $h_o = 400mm$, a flange width $b = 100mm$, a flange thickness $t = 10mm$, and a web thickness $w = 2mm$ was subjected to uniform bending and the span was varied between 3,000 to 20,000*mm*. The authors' results suggested that distortional effects decrease as the length increases. A decrease in predicted moment capacity of 9.7% was observed in beam a span of $3m$ while a beam span of $20m$ no distortion is observed and the distortional critical moment was found equal to the classical critical moment.

Zirakian and Showkati (2007)

Zirakian and Showkati (2007) experimentally investigated the occurrence of distortion in the buckling of I-beams through full scale experimental testing. The testing consisted of six I-beams fabricated from hot rolled IPE12 and IPE14 cross sections. The webs of the cross-sections were removed just above and below the web to flange junctions and longitudinal plates were welded in place of the removed webs with the aim of providing test specimens with more slender webs. The sections fabricated from a IPE12 section had a depth $d = 180mm$, a flange width $b = 64mm$, a flange thickness $t = 6.3mm$, and a web thickness $w = 4.85mm$. The IPE14 sections had a depth $d = 210mm$, a flange width $b = 73mm$, a flange thickness $t = 6.9mm$, and a web thickness $w = 4.9mm$. Three spans of each beam ($3,600mm$, $4,400mm$, and $5,200mm$) were loaded through a mid-span point load and an effective lateral brace was introduced at the location of the load. Through the use of strain gauges, Zirakian and Showkati (2007) were able to experimentally verify the occurrence of distortion in the buckled configuration of the beams.

Kalkan and Buyukkaragoz (2012)

Kalkan and Buyukkaragoz (2012) investigated distortional buckling of double-symmetric steel I-beams through numerical and analytical studies. The numerical study simulated the loading and bracing conditions of the beams experimentally investigated by Zirakian and Showkati (2007). The analysis was conducted through the use of Solid45 elements in the finite element program ANSYS. Hexagonal elements were used instead of quadratic elements to include the fillets at the web-to-flange junctions. The numerical study was successful in predicting buckling modes identical to those observed in Zirakian and Showkati (2007) and buckling loads with accuracy ranging from 10 to 40%. Through their numerical study, Kalkan and Buyukkaragoz (2012) demonstrated that as the web slenderness increases, significant reductions in buckling moments are observed compared to beams with thicker webs.

2.5.2. Cantilever Beams

Bradford (1992)

Bradford (1992) investigated the effects of distortion on the lateral torsional buckling of doubly symmetric cantilever beams. Bradfrod (1992) altered the finite element formulation developed in Bradfrod and Trahair (1981) to produce results which account for loading above the shear center.

To determine the suitable number of elements, the author conducted a convergence study in which the cantilever was loaded at the shear centre.

The author conducted a series of parametric runs in which the dimensionless parameters (web slenderness ratio h_o/w, span to height ratio L/h_o, width to thickness ratio b/t, and flange to width ratio b/h_o) and loading position with respect to the shear center are varied. The author's results suggest the following factors would lead to a decrease in the critical moment ratio; 1) a decrease in the span to height ratio (L/h_o), 2) a decrease in the web slenderness (h_o/w), 3) an increase in the beam width to height ratio (b/h_o), and 4) changing the load position with respect to the load center. The author highlighted that the effects of span to height ratio and web slenderness are most pronounced but that at short beam spans, yielding would govern. It is also demonstrated that although moving the load position either above or below the shear center causes a decrease in the critical moment ratio, moving above the shear center produces more pronounced reductions. The author also investigated the effect of distortion on the inelastic buckling resistance in which distortional moment obtained through FEA was substituted into a solution which predicts the inelastic buckling moment for a simply supported beam due to a combination of local and lateral buckling. Through this, it was shown that distortional effects could reduce the inelastic buckling moment by up to 15%.

Dowswell (2004)

In a study which investigates lateral torsional buckling of wide flange cantilever beams, Dowswell (2004) conducted a FEA consisting of 216 models which includes variations in spans, loading conditions, and restraint for three commonly used wide flange sections. The FEA program used in the analysis was BASP, a shell based finite element program developed at the University of Texas Austin. The FEA mesh consisted of four elements along the web height, one element for the flange width and 10 elements along the span of the beams. Through curve fitting of FEA results, Dowswell (2004) suggested altering the cantilever critical moment equation proposed by Trahair (1983, 1993) to include coefficients which account for various load heights with respect to the shear center and many types of bracing. Dowswell (2004) suggested the continued use of the moment distribution coefficient already included in the critical moment solution. The reader is referred to Chapter 6 for further discussion regarding the equations introduced by Dowswell (2004).

2.5.3. Summary of Studies Incorporating Distortion

Table 2.2 provides a summary of the studies which focus on distortional lateral torsional buckling for wide flange beams. The table presents the study along with the methodology used for obtaining solutions, the support type investigated, the type of loading, and whether load position with respect to the shear center was studied.

Table 2.2 Summary of studies on distortional lateral torsional buckling

Study	**Methodology**	**Support Type**	**Loading Type**	**Load Position Effect Considered**
Roberts and Jhita (1983)	Energy Formulations and FEA	Simply supported	Uniform moment & mid-span load	Yes
Bradford (1986)	FEA	Simply supported	Uniform moment & linear moment	No
Bradford (1992)	FEA	Cantilever	Tip point load	Yes
Pi and Trahair (2000)	FEA, Finite Strip	Simply supported	Uniform moment	No
Dowswell (2004)	FEA	Cantilever	Tip point load & UDL	Yes
Ng and Ronagh (2004)	Energy Formulation - Fourier Series	Simply supported	Uniform moment & mid-span load	Yes
Poon and Ronagh (2004)	FEA	Simply supported	Uniform moment & mid-span load	Yes
Zirakian and Showkati (2007)	Experimental	Simply supported	Mid-span load	No
Kalkan and Buyukkaragoz (2012)	FEA	Simply supported	Mid-span load	No

2.6. Aim of Thesis

As discussed in Section 2.4, there is a wealth of literature which investigates and quantifies the effects of moment gradient on lateral torsional buckling. However, these studies do not incorporate distortion and thus possibly err on the un-conservative side. The current studies on laterally unsupported beams susceptible to lateral torsional buckling which also consider distortion are summarized in Table 2.2. Although many of these studies are based on detailed finite element based analysis, each is only based on a handful of beam cross sections and is thus possibly non-representative of the complete database of sections commonly used in practice. The aim of the present study is to investigate the effects of distortion on lateral torsional buckling for representative cross-section dimensions and realistic design scenarios.

2.7. Notation for Chapter 2

a_i	constants for the end moment based moment gradient equation
b	flange/ beam width
C	standard dependent moment gradient factor
C_{AISC}	ANSI/AISC 360-10 moment gradient factor
C_{AUS}	AS 4100-1998 moment gradient factor
C_{CAN}	CAN/CSA S16-09 moment gradient factor
$C_{CAN-Gen}$	CAN/CSA S16-09 general moment distribution moment gradient factor
$C_{CAN-Lin}$	CAN/CSA S16-09 linear moment distribution moment gradient factor
C_{EURO}	EN 1993-1-1 moment gradient factor
$C_{K\&N}$	moment gradient factor proposed by Kirby and Nethercot (1979)
C_{SALV}	moment gradient factor proposed by Salvadori (1955)
C_w	warping constant
d	beam depth
E	modulus of elasticity of steel
F_y	specified minimum yield stress
F_{cre}	critical stress
G	shear modulus of elasticity of steel
h	web height
h_0	distance between flange centroids

I_e	effective out of plane moment of intertia
I_y	out of plane moment of inertia
J	torsional constant
J_e	effective torsional constant
k_l	load height factor
k_r	lateral rotation restraint factor
k_t	twist restraint factor
L	length of beam
L_e	effective length
L_p	limiting laterally unbraced length for the limit state of yielding
L_r	limiting laterally unbraced length for the limit state of inelastic LTB
L_u	length of unbraced segment of beam
M_a	factored bending moment at one-quarter point of unbraced segment
M_b	factored bending moment at mid-point of unbraced segment
M_c	factored bending moment at three-quarter point of unbraced segment
M_{cr}	elastic critical lateral torsional buckling moment
$M_{\max}$	maximum factored bending moment magnitude in unbraced segment
M_n	nominal moment resistance
M_o	modified classical lateral torsional buckling solution
M_p	plastic moment resistance
M_r	factored moment resistance
M_u	classical lateral torsional buckling solution
M_y	yield moment resistance
r_{ts}	effective radius of gyration
r_y	radius of gyration about the y-axis
S_x	elastic section modulus taken about the x-axis
t	flange thickness
u	lateral displacement
w	web thickness
Z_x	plastic section modulus taken about the x-axis
α_s	slenderness reduction factor
α_{LT}	imperfection factor

γ_{M1}	partial factor for resistance of members to instability assessed by member checks
θ	angle of twist
κ	ratio of smaller to larger factored moment at ends of unbraced length
$\bar{\lambda}_{LT}$	non-dimensional slenderness parameter
Φ_{LT}	dimensionless imperfection parameter
ϕ	CAN/CSA S16-09 structural steel resistance factor
χ_{LT}	reduction factor for lateral torsional buckling

Chapter 3

Distortional Lateral Torsional Buckling in Simply Supported Beams under Uniform Moments

3.1. Objective and Scope

The adoption of the Vlasov theory based equation in design standards implies the neglect of distortional effects. This issue has been recognized in the analysis of cold formed cross sections, but has generally been thought of as negligible in the analysis of rolled wide flange sections. Within the above context, the present study aims at determining the conditions under which distortional effects can be neglected when assessing the buckling strength for beams of common cross-sectional geometries. Towards this goal, a shell finite element based parametric study is conducted to determine the critical moments M_{cr} including distortional effects.

3.2. Dimensional Analysis

According to the Buckingham Pi theorem, if there are n variables in a problem and these variables contain m independent physical quantities, then the equation relating all variables will have a set of $(n-m)$ independent dimensionless groups constructed from the original variables. Buckingham referred to these groups as π groups. In the present study aimed at investigating the critical moment of a simply supported beam under uniform moment, there are eight variables which are related through

[3.1] $f(M_{cr}, b, t, h, w, l, E, G) = 0$

in which M_{cr} = elastic critical moment capturing the effects of distortional buckling, b = flange width, t = flange thickness, h = distance between flange centroids, w = web thickness, l = length of unbraced portion of beam, E = elastic modulus of steel, and G = shear modulus of steel. In general, any physical quantity can be expressed as a combination of force F, length L, or time T. As a notation convention, the dimension of a variable will be denoted by a bracket surrounding the variable, e.g., $\left[M_{cr}\right]=FL$, which signifies that the dimension of M_{cr} is force F multiplied by length L. In a similar manner $\left[b\right]=L$, $\left[t\right]=L$, $\left[h\right]=L$, $\left[w\right]=L$, $\left[l\right]=L$, $\left[E\right]=FL^{-2}$, and $\left[G\right]=FL^{-2}$. For the problem under investigation, Time T does not appear, thus, the above variables are expressed in terms of only two independent physical quantities; Force F and Length L. The Buckingham Pi theorem allows the reduction of the eight variables appearing in Eq. [3.1] into six independent dimensionless parameters. Therefore, the number of independent parameters is six dimensionless groups denoted as $\pi_i\ (i=1...6)$. A π_i term is the product of the eight variables, each raised to an exponent as follows

[3.2] $\left[\pi_i\right]=\left[M_{cr}\right]^{\alpha_1}\left[b\right]^{\alpha_2}\left[t\right]^{\alpha_3}\left[h\right]^{\alpha_4}\left[w\right]^{\alpha_5}\left[l\right]^{\alpha_6}\left[E\right]^{\alpha_7}\left[G\right]^{\alpha_8}$

where exponents α_1 through α_8 must satisfy the following condition

[3.3] $(FL)^{\alpha_1}(L)^{\alpha_2}(L)^{\alpha_3}(L)^{\alpha_4}(L)^{\alpha_5}(L)^{\alpha_6}\left(FL^{-2}\right)^{\alpha_7}\left(FL^{-2}\right)^{\alpha_8}=F^{0}L^{0}$

For Eq. [3.3] to hold true, the following two identities must be satisfied

[3.4] $\alpha_1+\alpha_7+\alpha_8=0$

[3.5] $\alpha_1+\alpha_2+\alpha_3+\alpha_4+\alpha_5+\alpha_6-2\alpha_7-2\alpha_8=0$

In a matrix form, the above two equations can be expressed as

[3.6] $\left[A\right]_{2\times 8}\left\{\alpha\right\}_{8\times 2}=\left\{0\right\}_{2\times 1}$

in which matrix $\left[A\right]$ is given by

[3.7] $\left[A\right]=\begin{bmatrix}1 & 0 & 0 & 0 & 0 & 0 & 1 & 1\\ 1 & 1 & 1 & 1 & 1 & 1 & -2 & -2\end{bmatrix}$

and $\left\langle\alpha\right\rangle^{T}=\left\langle\alpha_1\quad\alpha_2\quad\alpha_3\quad\alpha_4\quad\alpha_5\quad\alpha_6\quad\alpha_7\quad\alpha_8\right\rangle$. Any solution for vector $\left\{\alpha\right\}_i$ which meets Eq. [3.6], leads to an admissible π_i term. The following is a possible set of six independent vectors $\left\{\alpha\right\}_i$ which satisfy Eq. [3.6]

$$[3.8]\quad \left[\{\alpha\}_1,\{\alpha\}_2,\{\alpha\}_3,\{\alpha\}_4,\{\alpha\}_5,\{\alpha\}_6\right]=\left[\begin{Bmatrix}0\\0\\0\\-1\\1\\0\\0\\0\end{Bmatrix}\begin{Bmatrix}0\\-1\\1\\0\\0\\0\\0\\0\end{Bmatrix}\begin{Bmatrix}0\\1\\0\\-1\\0\\0\\0\\0\end{Bmatrix}\begin{Bmatrix}0\\0\\0\\-1\\0\\1\\0\\0\end{Bmatrix}\begin{Bmatrix}0\\0\\0\\0\\0\\0\\1\\-1\end{Bmatrix}\begin{Bmatrix}1\\0\\0\\0\\0\\-3\\-1\\0\end{Bmatrix}\right]$$

Each vector $\{\alpha\}_i$ corresponds to the terms $\pi_1 = w/h$, $\pi_2 = t/b$, $\pi_3 = b/h$, $\pi_4 = l/h$, $\pi_5 = E/G$ and $\pi_6 = M_{cr}/El^3$. According to the π theorem, a linear combination $\sum_{i=1}^{6}\beta_i\{\alpha\}_i$ in which β_i are arbitrary constants also leads to an additional (albeit dependent) dimensionless parameter. The classical solution for the elastic critical moment M_u for a simply supported beam subject to a uniform moment is given by

$$[3.9]\quad M_u = \frac{\pi}{l}\sqrt{EI_yGJ + \left(\frac{\pi E}{l}\right)^2 I_y C_w}$$

The critical moment M_{cr} as predicted through an FEA buckling analysis, captures the effect of distortional buckling. This contrasts with the elastic critical moment M_u which neglects such effects. It would be of interest to normalize M_{cr} with respect to $M_u(b,t,h,w,l,E,G)$ in order to quantify the effects of distortional buckling. Thus, it would be desirable to substitute the last Pi term $\pi_6 = M_{cr}/El^3$ with the more physically meaningful ratio $\pi_{6i} = M_{cr}/M_u$. Starting with the six independent vectors $\{\alpha\}_i$ introduced in Eq. [3.8], Appendix A provides the proof that M_{cr}/M_u can be used as the sixth π term π_{6i} rather than $\pi_6 = M_{cr}/El^3$. With this substitution we have

$$[3.10]\quad f_2\left(\frac{M_{cr}}{M_u},\frac{w}{h},\frac{t}{b},\frac{b}{h},\frac{l}{h},\frac{E}{G}\right)=0$$

For steel, the dimensionless parameter E/G is essentially constant, or

[3.11] $\frac{M_{cr}}{M_u} = f\left(\frac{w}{h}, \frac{t}{b}, \frac{b}{h}, \frac{l}{h}\right)$

This signifies that the ratio of critical moment including distortional effects to the classical critical moment depends upon only four dimensionless parameters which are w/h, t/b, b/h, and l/h. Thus, in the following sections, a systematic parametric study is conducted to investigate the effect of the above four parameters on M_{cr}/M_u.

3.3. Representativeness of Cross-Sectional Geometry of Real Sections

The objective of the present section is to determine a cross-section geometry that is representative of steel sections commonly used in practice. The selection of the cross-section is based on three of the four parameters identified in Eq. [3.11] namely, (w/h, t/b, b/h). Towards this goal, the complete list of wide flange sections available in Structural Selection Tables (SST) of the Canadian Institute of Steel Construction (CISC 2001) was surveyed. The list consists of 281 sections ranging from W100x19 (the lightest section) to W920x1191 (the heaviest section). Nominal heights varied from 100 to 1,100*mm*. Table 3.1 provides the range of dimensionless parameters of the sections in the database. Values for w/h, t/b, and b/h were selected around mid-range to define a "reference section". Also, care was taken to select a t/w ratio for the reference section near its mid-range value. It is noted that the above defined reference section meets Class 1 requirements for a yield strength of 350*MPa*. The reference section will serve as a base value in the parametric study from which variations for the various dimensionless parameters will be made, and the corresponding M_{cr}/M_u will be determined.

Table 3.1 Dimensionless parameters of the sections in the SST database

	h (mm)	b (mm)	t (mm)	w (mm)	w/h	t/b	b/h	t/w
Minimum	106	100	4.9	4.3	0.0154	0.0434	0.3037	1.1042
Maximum	1118	457	125	78	0.1757	0.2753	1.1345	1.900
Mean	570	286	31	19	0.0384	0.01019	0.6109	1.6315
Reference Section	**500**	**305**	**21.034**	**14.706**	**0.0294**	**0.0690**	**0.6100**	**1.4300**

3.4. *Selection of Upper and Lower Bounds of Span*

3.4.1. Selection of Upper Bound for Span

No explicit upper bounds for maximum spans are given for beams in various standards. Beam maximum spans are typically determined by serviceability criteria such as deflections under live loads or vibration control requirements. It is reasoned that flexural members are at best equally prone to vibrations as tension members and therefore a similar maximum slenderness ratio is adopted in the present study. Larger spans were reasoned to be uncommonly used. Thus, a value of $l_{\max} = 300r_{\min}$ (in which $r_{\min}$ is the minimum radius of gyration of the chosen section) is adopted as a possible upper limit for the span. Although the utilization of $l_{\max} = 300r_{\min}$ could lead to excessive lengths for certain sections, it was chosen so a wide range of lengths could be analyzed in the parametric study.

3.4.2. Selection of Lower Bound for Span

The minimum span of a member is taken as the maximum unsupported beam length under a uniform moment gradient. For Class 3 sections, this length is calculated by equating the nominal yield moment $M_y = S_x F_y$ to the nominal inelastic lateral torsional moment resistance M_{in} as predicted in the Canadian standards (CAN/CSA S16-09), in which S_x is the elastic section modulus, and F_y is the specified minimum yield strength taken as 350*MPa* in the present study. For Class 3 Section, M_{in} is given by

[3.12] $$M_{in} = 1.15 M_y \left[1 - \frac{0.28 M_y}{M_u} \right]$$

For Class 1 and 2 sections, the plastic moment $M_p = Z_x F_y$ (Z_x being the plastic section modulus) is instead equated to the inelastic lateral torsional moment resistance M_{in} in Eq. [3.12] (instead of the yield moment M_y). The condition $M_y = M_{in}$ (or $M_p = M_{in}$ as applicable) is then used to solve for the elastic critical moment M_u and the corresponding unsupported length $l_{\min} = l$ is determined from Eq. [3.9]. The capacity of beams with spans less than $l_{\min}$ will be governed by yield rather lateral torsional buckling capacity and thus the spans less than $l_{\min}$

would be of no practical interest. The parametric study is performed on spans within the range $l_{\min} \le l \le l_{\max}$. Span l is normalized with respect to the geometric dimension h. The bounds of interest $l_{\min}/h$ and $l_{\max}/h$ will be computed and examined for each section in the parametric runs. For the reference section (Table 3.1), $l_{\min} = 4,270mm$ and $l_{\max} = 21,237mm$ which correspond to the dimensionless bounds of $l_{\min}/h = 8.5$ and $l_{\max}/h = 42.5$. A reference span of 13,000*mm* is selected for the reference section.

3.5. End Details

Three types of web stiffening arrangements (Fig. 3.1) were investigated. These are a) Unstiffened web (ST0) to simulate the case of simple shear connection, b) Stiffened web with a pair of bearing stiffeners (ST1) to simulate the case where the beam is bearing on base plates, and c) Stiffened web with two pairs of transverse stiffeners (ST2) to simulate the case of a welded moment connection. For Detail (ST1), the stiffener was 9.5*mm* thick, while that of double stiffeners included two scenarios. In the first scenario (ST2A), the stiffener was 9.5*mm* thick. Which, for the reference section, corresponds to a web thickness to stiffener thickness w/w_{st} of 1.54. While in the second scenario (ST2B), the thickness was taken equal to that of the flange. The second scenario was chosen to simulate the configuration of a beam-column moment connection between a beam and a column with the same cross-sections.

3.6. Load Application Scheme

The loading case considered is uniform moment (Fig. 3.2). The results of beams subject to uniform moment are of particular interest since the classical solution for the elastic critical moment M_u is by definition derived under the application of uniform moment. End moments were applied through one of two different schemes (equal and opposite longitudinal tractions (L) applied at both flanges, and two transverse equal and opposite forces (T)). The load application scheme is illustrated in Fig. 3.1. The last letter of each identifier takes the values L or T to denote the load application scheme.

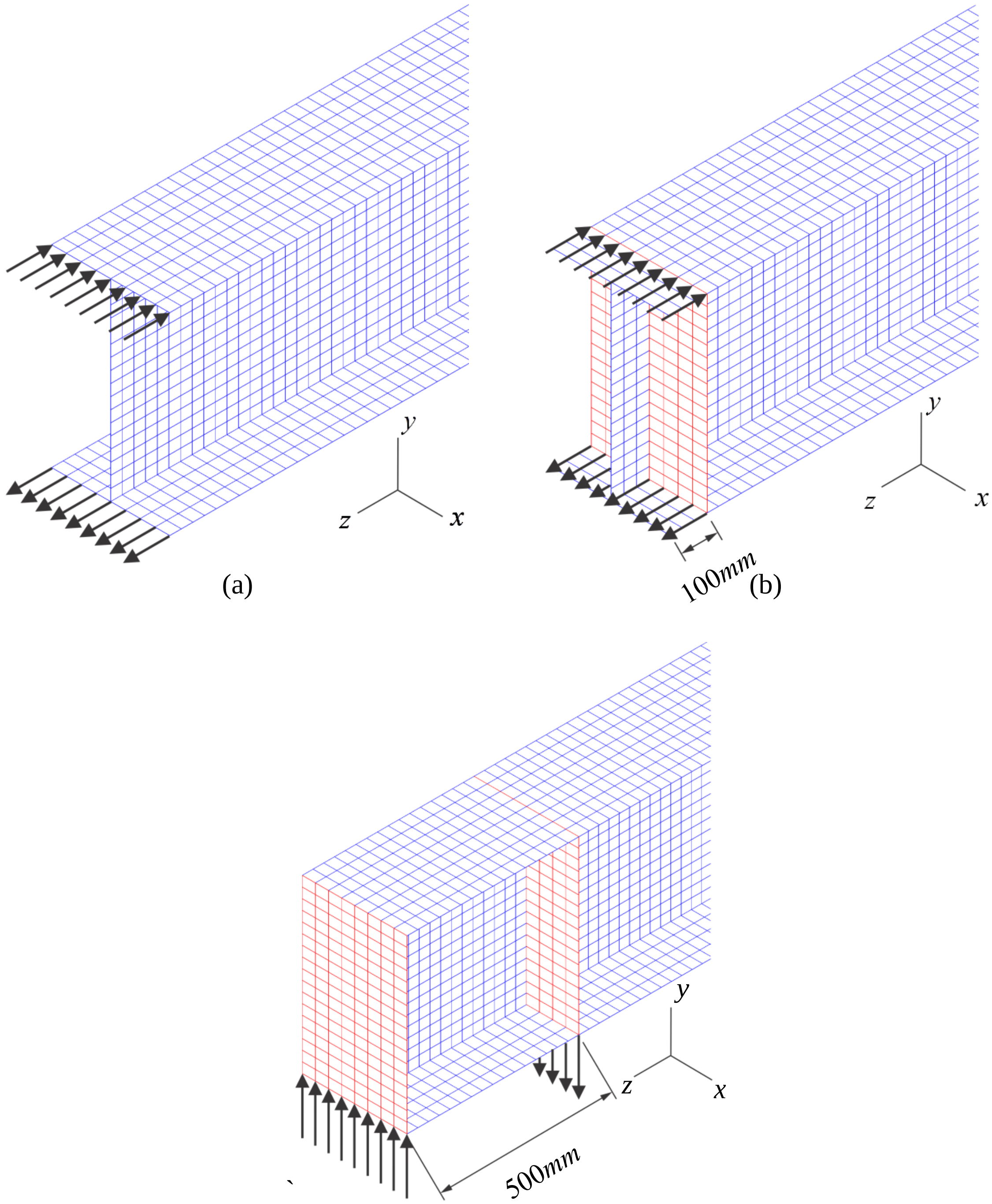

(c)

Fig. 3.1- Details of load application schemes and stiffener arrangements: (a) ST0-L (No stiffener-longitudinal forces applied), (b) ST1-T (Single stiffener- transverse forces applied), and (c) ST2A-T/ ST2B-T (Double stiffeners- transverse forces applied)

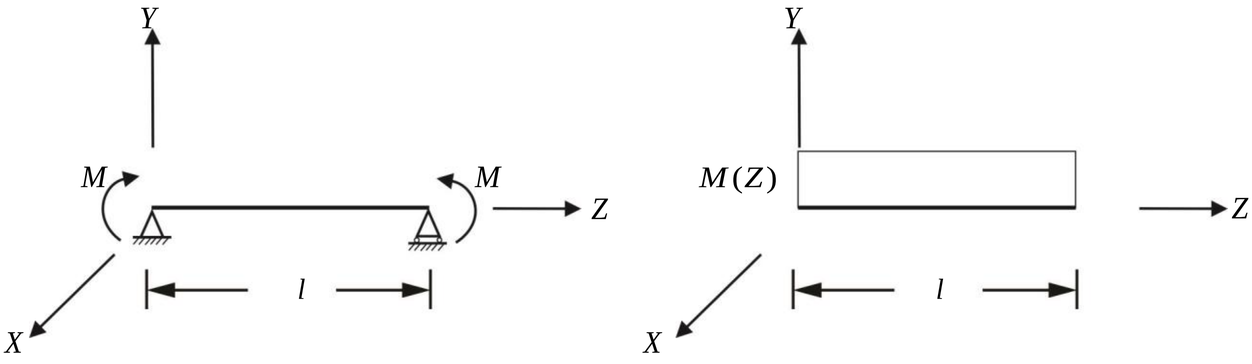

(a) (b)

Fig. 3.2- Uniform moment (a) Schematic, and (b) Moment diagram

3.7. Boundary Conditions

To be consistent with the assumptions made in the derivation of the classical solution for the elastic critical moment M_u (beam is simply supported relative to the lateral displacement and angle of twist), all beams analyzed were restrained in such a manner to simulate simply supported boundary conditions. At one end of the beam (Fig. 3.3(a)), displacement along the *x*, *y*, and *z* axis is restrained at the bottom web-flange junction and displacement along the *x* axis is restrained at the top web-flange junction. At the other end of the beam (Fig. 3.3(b)) displacement along the *x* and *z* axis is restrained at the bottom web-flange junction and displacement along the *x* axis is restrained at the top web flange junction. For the ST0-L detail, the boundary conditions (Fig. 3.3) were imposed at the beam ends while for the ST1-L detail they were imposed at the location of the stiffener (Fig. 3.1b). As for the ST2A-T/ ST2B-T details, boundary conditions were imposed at the mid-point between the end stiffeners (Fig. 3.2c).

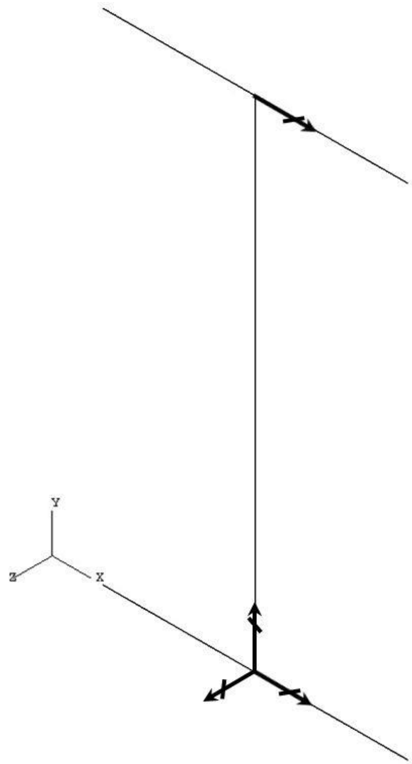

(a)

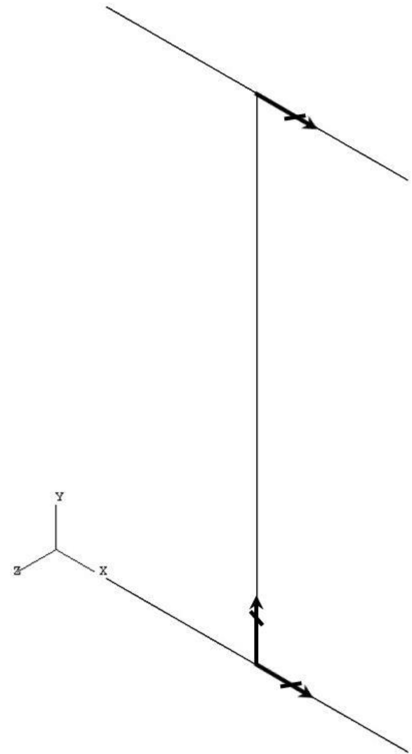

(b)

Fig. 3.3- Boundary conditions (crossed arrows denote restrained displacements)

3.8. Finite Element Model

3.8.1. Software & Model Definition

Abaqus/CAE 6.10-1 is used to create the FEA model. Abaqus/CAE is a software application that is part of the Abaqus Product Suite. The beams are modeled in a 3D modeling space using a deformable part. Abaqus/CAE User's Manual defines a deformable part as "a part that can deform under load; the load can be mechanical, thermal, or electrical". The beams are assigned elastic isotropic material behaviours with Young's Modulus $E = 200,000MPa$ and Poisson's Ratio $\mu = 0.3$.

3.8.2. Model Seeding

Prior to meshing the beam, the model is seeded. Seeding is the process by which the user specifies the mesh density. Because a uniform mesh is desired for the entire beam, global seeds are assigned. An approximate global size of 0.03 is used, which corresponds to an element size of approximately $30mm \times 30mm$. For the reference case (Fig. 3.4) this gives 17 elements along the section height, four elements along half flange width, and 433 elements along the longitudinal direction for a total of 14,289 elements.

3.8.3. Element Used

The S4R element was chosen to mesh the beam. The S4R element is a 4-node, quadrilateral stress/ displacement shell element with reduced integration and a large-strain formulation. The S4R element falls under "General-purpose conventional shell elements." These elements allow transverse shear deformation and they use a hybrid shell– thick shell theory.

3.8.4. Analysis Type

As it is of interest to conduct an eigenvalue buckling analysis, the beams are analyzed using linear perturbation buckling analysis. A buckling analysis is conducted by defining a reference load in the eigenvalue buckling analysis. The magnitude of the reference load is not important since it is scaled by load multipliers found in the eigenvalue problem which is presented as follows

[3.13] $\left(\left[K\right]-\lambda_i\left[K_G\right]\right)\left\{u_i\right\}=\left\{0\right\}$

in which $\left[K\right]=$ the elastic stiffness matrix, $\lambda_i =$ the eigenvalues, $\left[K_G\right]=$ the geometric stiffness matrix due to the reference loads, and $\left\{u_i\right\}=$ the buckling mode shapes, also known as eigenvectors. It is important to note that the buckling mode shapes, $\left\{u_i\right\}$ do not predict the actual deformation magnitudes. They are normalized so that the maximum displacement is equal to 1.0. Abaqus/CAE offers two types of eigenvalue extraction methods, the Lanczos and Subspace iteration methods. The Lanczos method is generally faster when a large number of Eigen modes is desired. Since in this study a small number of Eigen modes are required, the Subspace iteration method is utilized. In the various runs, four eigenvalues were extracted. Extracting four eigenvalues served as a check to ensure the beam was modeled correctly. When the beam was modeled and loaded symmetrically, the first four eignevalues will be two sets of equal eigenvalues with one positive and one negative eigenvalue. A negative eigenvalue indicates that the beam would buckle if the loads were applied in the opposite direction.

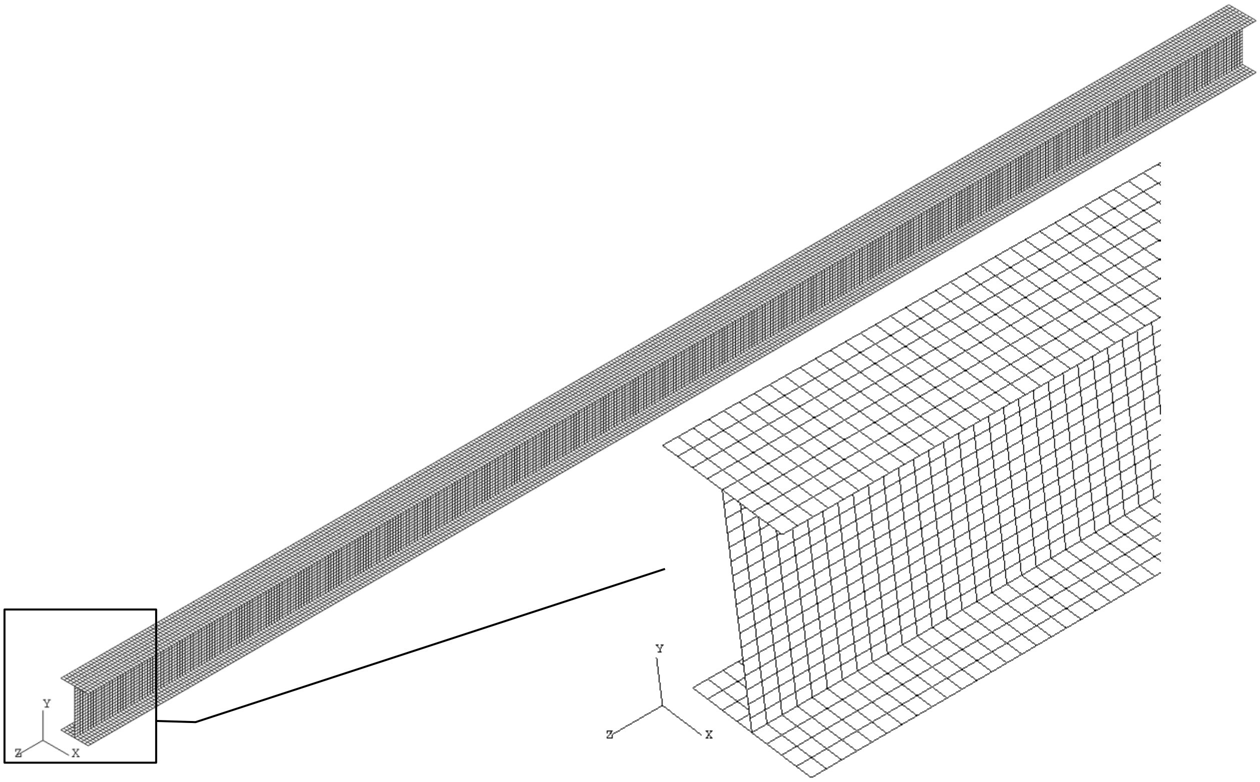

Fig. 3.4- Undeformed reference case

3.9. *Ranges of Dimensionless Parameters Used*

Using the methods outlined in Section 3.3 the following maximum and minimum values for the dimensionless parameters were used

Table 3.2 Minimum & maximum values of dimensionless parameters

	w/h	t/b	b/h	l/h
Min	0.0222	0.0555	0.48	9
Max	0.0370	0.0909	0.81	42

With a practical range of interest established, each dimensionless parameter is varied one at a time and the dimensions of the corresponding sections are determined. The complete set of all parametric runs conducted is tabulated in Appendix B. All sections studied have the same $h = 500mm$. Sections will be assigned identification numbers consisting of two letters and a number. The first two letters represent the parameter being varied and the number corresponds to the last three significant digits of the ratio. For example, the section corresponding to $w/h = 0.0222$ will have an identification number of wh222.

3.10. Results

Subsection 3.10.1 provides a verification of the dimensionless analysis results. Each of the following subsections is dedicated to discussing the effect of each dimensionless parameter, one at a time on the M_{cr}/M_u ratio. Subsections 3.10.2 through 3.10.5 present the results of varying w/h, t/b, b/h, and l/h respectively while subsection 3.10.6 presents FEA results of real sections.

3.10.1. Verification of Dimensionless Analysis Results

An important point to note is that the actual dimensions of a given section have no influence on the resulting M_{cr}/M_u as long as the dimensionless ratios w/h, t/b, b/h, and l/h are specified. Rather, it is the ratios of the dimensionless parameters which dictate the value of M_{cr}/M_u. Two sections with completely different dimensions will yield identical values of M_{cr}/M_u as long as both sections have the same dimensionless ratios. Take for example the reference section ($h = 500mm$, $b = 305mm$, $t = 21.034mm$, $w = 14.706mm$, and $l = 13000mm$) and another section ($h = 600mm$, $b = 366mm$, $t = 25.241mm$, $w = 17.647mm$, and $l = 15600mm$). Although both sections have completely different physical dimensions, they both have identical ratios of w/h, t/b, b/h, and l/h thus yielding an identical value of M_{cr}/M_u equaling 0.987. This finding is a direct result of the Bucklingham Pi theorem and has been numerically verified by the finite element analyses conducted in the present study.

3.10.2. Effect of Web Slenderness

In order to determine the effect of web slenderness, the dimensionless parameter w/h was varied from 0.0222 to 0.0370 while other parameters t/b, b/h and l/h were held constant at the reference values. This is achieved by varying the web thickness w. As shown in Fig. 3.5, when the web slenderness increases (w/h decreases), M_{cr}/M_u decreases for the un-stiffened detail

ST0-L, and to a lesser extent in the single stiffener detail ST1-L, and double stiffeners with 9.5*mm* thick plates ST2A-T ($w/w_{st} = 1.54$). This is the case because slender webs are more prone to distortional effects, which in turn reduces M_{cr}/M_u. The highest buckling capacity is observed for beams with double stiffeners with thicknesses matching that of the flanges (ST2B-T). As a general observation, the presence of stiffeners reduces the distortional tendency of the web end and thus increases the M_{cr}/M_u ratio. The thicker stiffeners also provide partial warping restraint resulting in higher M_{cr}/M_u ratios.

Fig. 3.6(a-b) displays isometric and cross section views of buckled configurations of a ST0-L beam with $w/h = 0.0370$ and Fig. 3.7(a-b) displays isometric and cross section views of buckled configurations of a ST0-L beam with $w/h = 0.0222$. Fig. 3.6(a) illustrates that web distortion is minimal and corresponds to $M_{cr}/M_u = 0.96$. More distortional effects are visible for the thinner web ($w/h = 0.0222$) for which M_{cr}/M_u was observed to drop to 0.93 (Fig. 3.7(a)).

Table 3.3 presents M_{cr}/M_u results of all w/h values. Fig. 3.6(c) and Fig. 3.7(c) show isometric contour plots of the ST0-L detail with $w/h = 0.0370$ and 0.0222 respectively. These Figures demonstrate that the test specimens are buckling in a lateral torsional mode. A closer look at the FEA models shows that no lateral displacement occurs at the ends which prove that the boundary conditions are enforced properly.

Table 3.3 Effect of web slenderness FEA results

ID#	$\frac{w}{h}$	M_u (kNm)	ST0-L M_{cr} (kNm)	ST0-L $\frac{M_{cr}}{M_u}$	ST1-L M_{cr} (kNm)	ST1-L $\frac{M_{cr}}{M_u}$	ST2A-T M_{cr} (kNm)	ST2A-T $\frac{M_{cr}}{M_u}$	ST2B-T M_{cr} (kNm)	ST2B-T $\frac{M_{cr}}{M_u}$
wh222	0.0222	523.5	485.8	0.928	514.5	0.983	525.9	1.005	558.4	1.067
wh244	0.0244	529.8	496.0	0.936	521.5	0.984	533.3	1.007	565.3	1.067
wh270	0.0270	539.0	508.9	0.944	531.4	0.986	543.5	1.008	575.0	1.067
(Ref.)	**0.0294**	**548.8**	**521.3**	**0.950**	**541.8**	**0.987**	**554.1**	**1.010**	**585.0**	**1.066**
wh313	0.0313	557.5	531.5	0.953	550.7	0.988	563.2	1.010	593.7	1.065
wh339	0.0339	571.5	547.5	0.958	565.1	0.989	577.9	1.011	607.6	1.063
wh370	0.0370	590.7	568.3	0.962	584.8	0.990	597.7	1.012	626.5	1.061

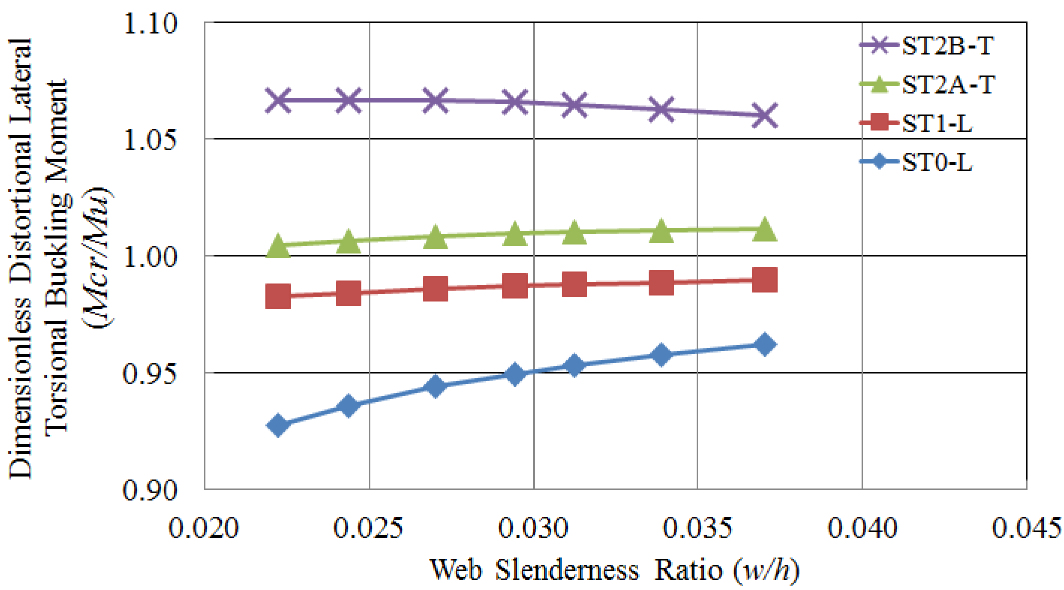

Fig. 3.5- Effect of web slenderness

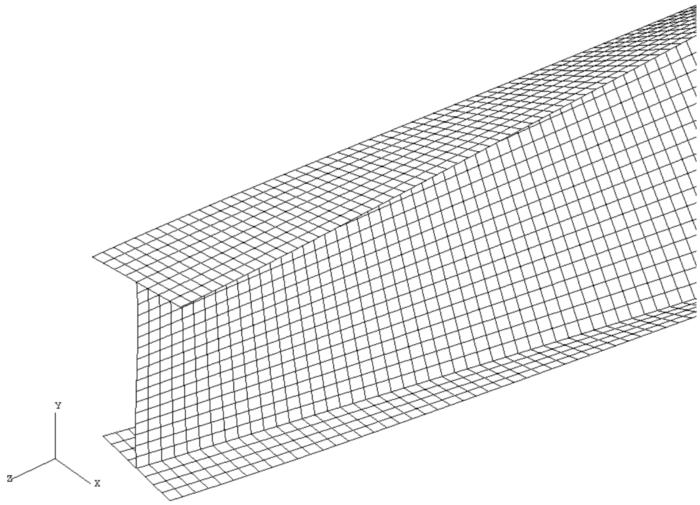

(a)

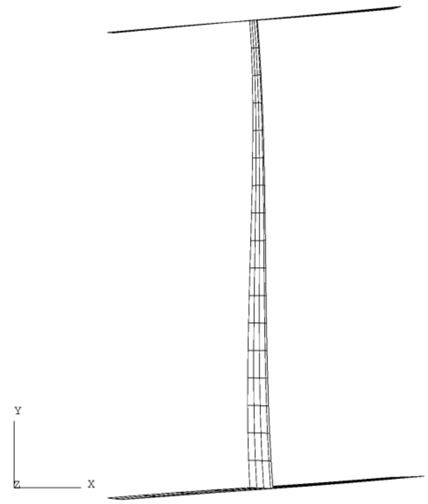

(b)

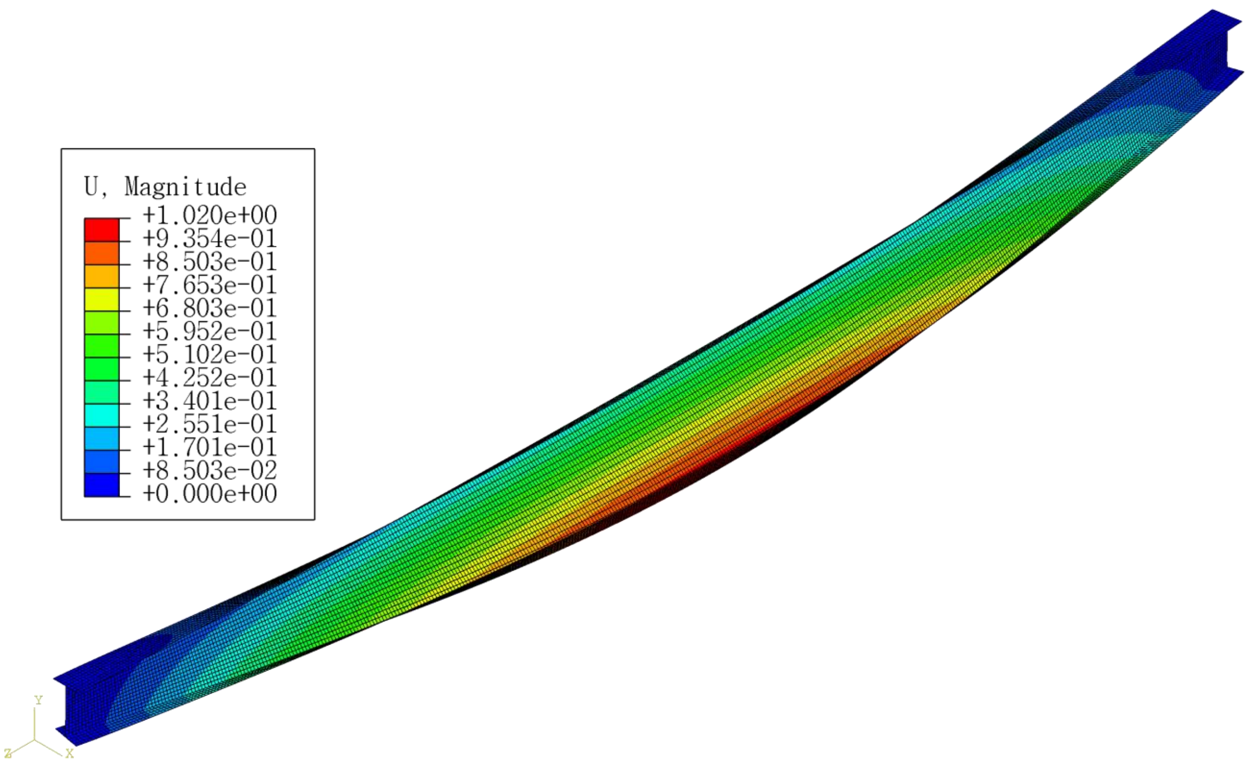

(c)

Fig. 3.6- $w/h = 0.0370$ Buckled configurations of ST0-L detail: (a) Isometric end, (b) Cross section, and (c) Isometric contour plot for the lateral displacement

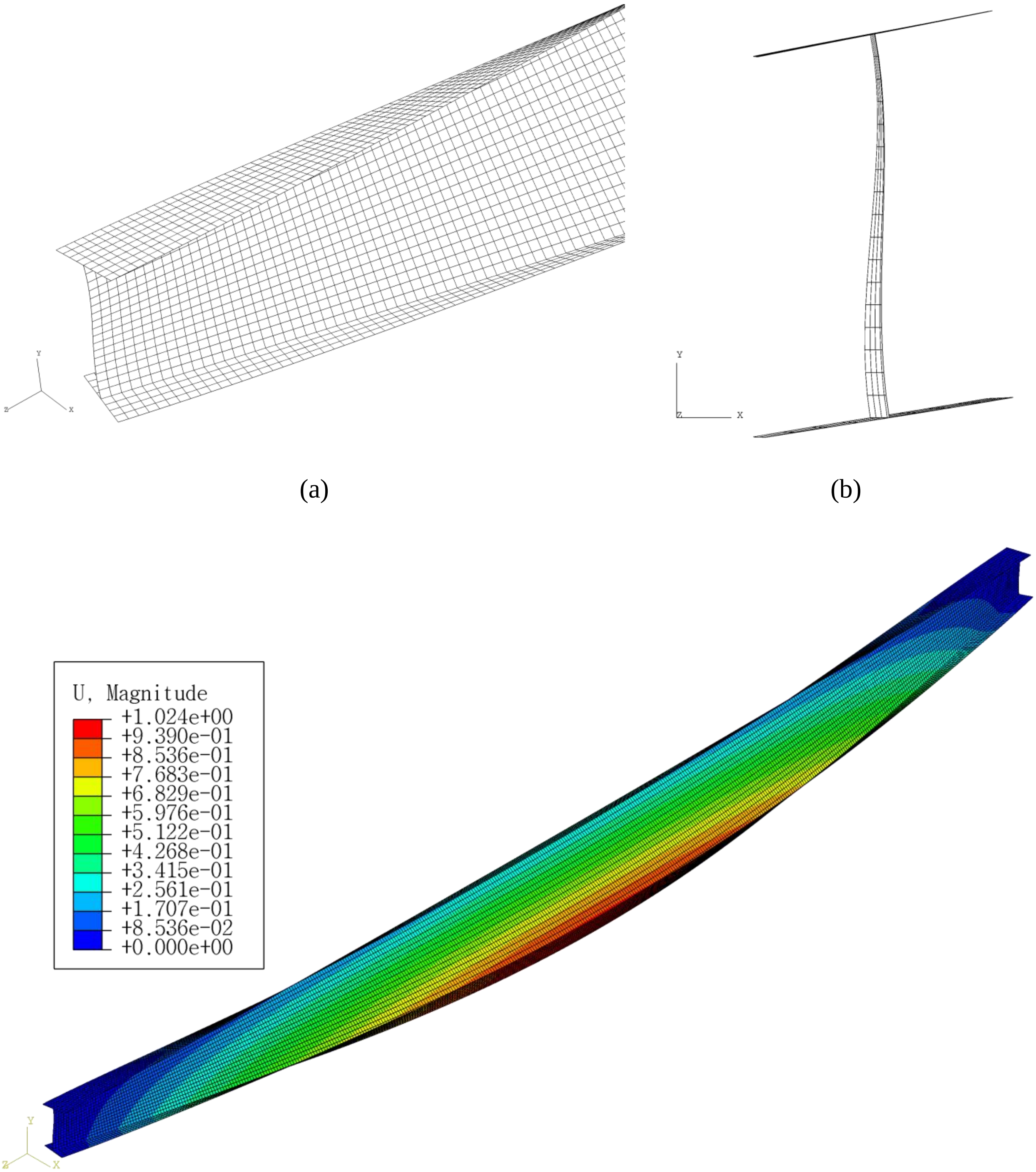

(a) (b)

(c)

Fig. 3.7- $w/h = 0.0222$ Buckled configurations of ST0-L detail: (a) Isometric end, (b) Cross section, and (c) Isometric contour plot for the lateral displacement

3.10.3. Effect of Flange Slenderness

In this section, the flange width to thickness ratio t/b is varied from 0.0555 to 0.0909 while holding parameters w/h, b/h and l/h at their reference values. As displayed in Table 3.4, this is achieved by maintaining h, w, b at the reference values while varying flange thickness *t*. As shown in Fig. 3.8, M_{cr}/M_u decreases as t/b increases for configurations ST0-L, ST1-L, and ST2A-T. When t/b increases (i.e., t increases), the top flange attracts more compressive stresses. This further destabilizes the member, and increases the web proneness to undergo distortion. This is illustrated for the ST0-L Detail in Fig. 3.9(b) for t/b=0.0909 and Fig. 3.10(b) for t/b=0.0555. In the latter case, where the thickness is small, the distortion of the web is observed to be less pronounced than that of the former (with a thicker flange). As expected, the corresponding critical moment ratio M_{cr}/M_u takes a lower value of 0.91 for the thicker flange while has a high value of 0.97 for the case of the thinner flange. Tabulated M_{cr}/M_u results are presented in Table 3.4 and contour plots of the ST0-L detail corresponding to t/b=0.0909 and t/b=0.0555 are displayed in Fig. 3.9(c) and Fig. 3.10(c) respectively.

For the ST2B-T detail, an increase in t/b (i.e., an increase in flange thickness) is associated with two phenomena: 1) an increased destabilizing effect of the web due to the additional compressive stresses attracted by the thicker top flange, making the member more prone to distortional effects, and 2) an increase in the matching thickness of the stiffener, which is associated with an increased distortional restraint to the web (thus counteracting the destabilizing effect in (1)). As a result, for the ST2B-T Detail, there is no clear trend between t/b and M_{cr}/M_u .

Table 3.4 Effect of flange slenderness FEA results

ID#	$\frac{t}{b}$	M_u (kNm)	ST0-L M_{cr} (kNm)	ST0-L $\frac{M_{cr}}{M_u}$	ST1-L M_{cr} (kNm)	ST1-L $\frac{M_{cr}}{M_u}$	ST2A-T M_{cr} (kNm)	ST2A-T $\frac{M_{cr}}{M_u}$	ST2B-T M_{cr} (kNm)	ST2B-T $\frac{M_{cr}}{M_u}$
tb556	0.0556	405.4	391.8	0.966	403.0	0.994	412.4	1.017	428.8	1.058
tb588	0.0588	437.7	421.4	0.963	434.4	0.992	444.4	1.015	464.1	1.060
tb635	0.0635	486.8	465.9	0.957	481.9	0.990	493.0	1.013	517.6	1.063
(Ref.)	**0.0690**	**548.8**	**521.3**	**0.950**	**541.8**	**0.987**	**554.1**	**1.010**	**585.0**	**1.066**
tb741	0.0741	611.3	576.2	0.943	601.7	0.984	615.4	1.007	652.5	1.067
tb816	0.0816	711.9	662.5	0.931	697.6	0.980	713.4	1.002	760.1	1.068
tb909	0.0909	848.7	776.2	0.915	826.9	0.974	845.5	0.996	906.1	1.068

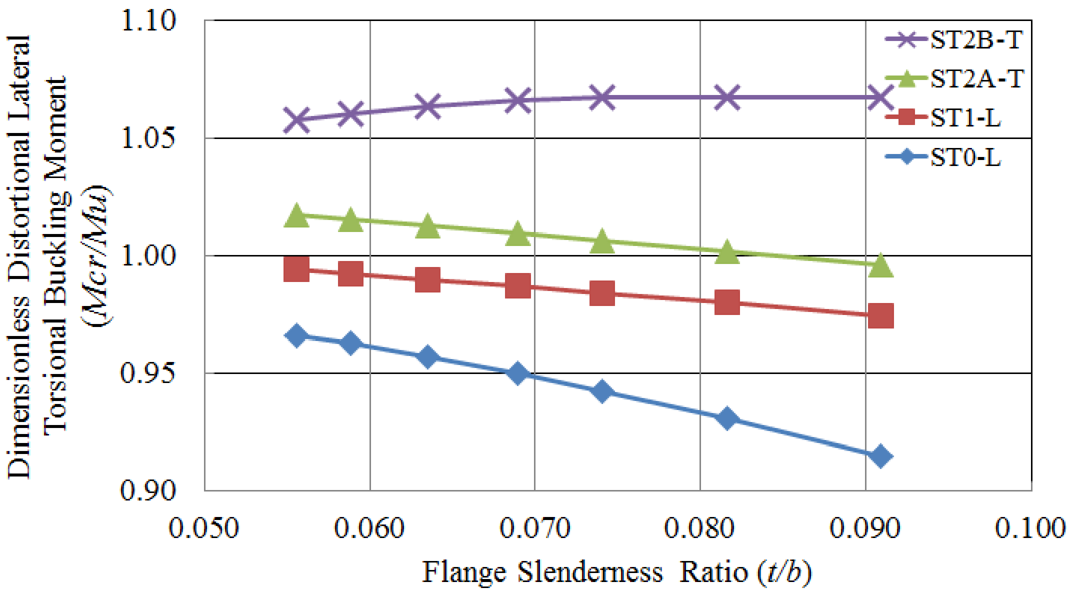

Fig. 3.8- Effect of flange slenderness

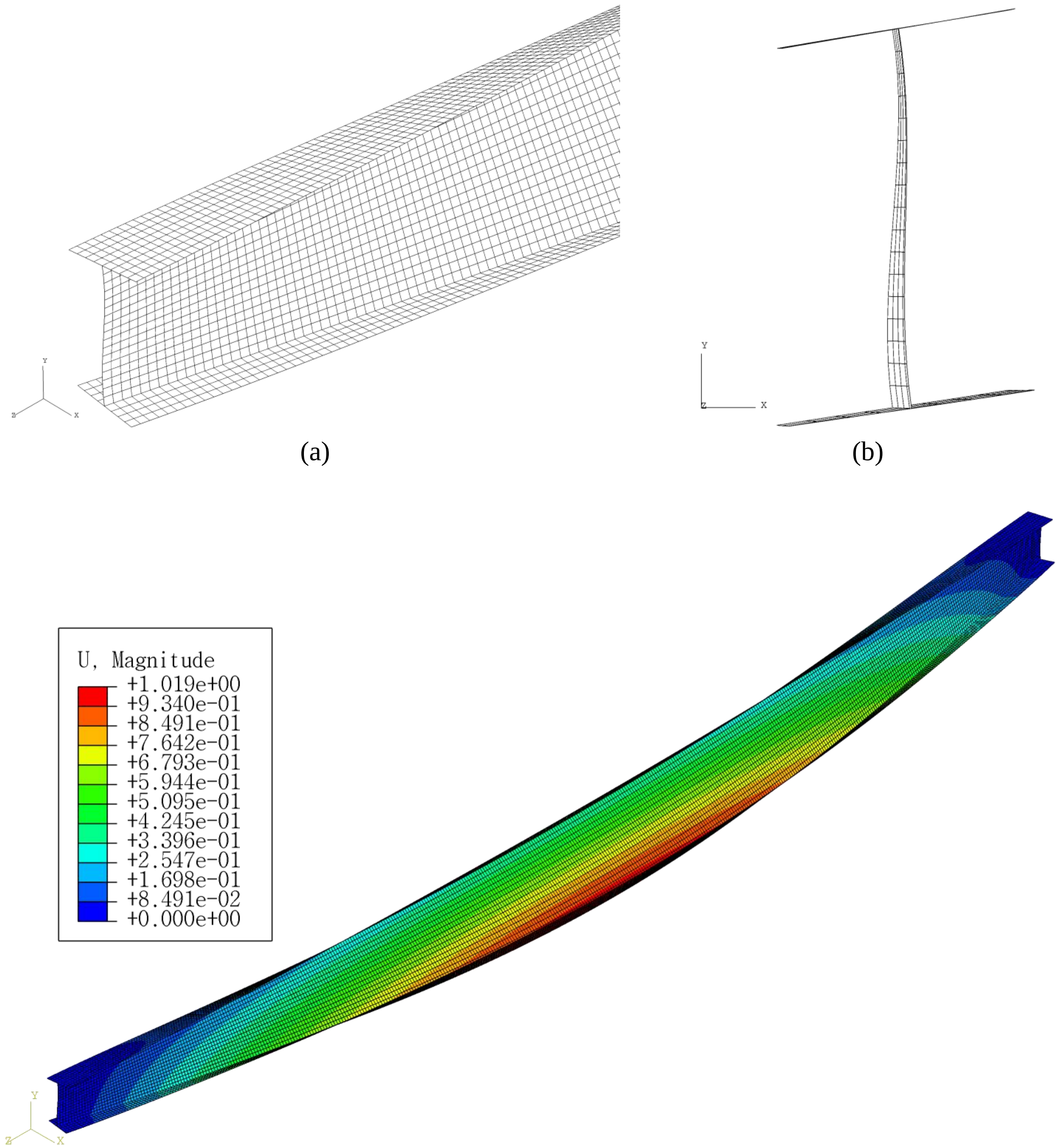

Fig. 3.9- $t/b = 0.0909$ Buckled configurations of ST0-L detail: (a) Isometric end, (b) Cross section, and (c) Isometric contour plot for the lateral displacement

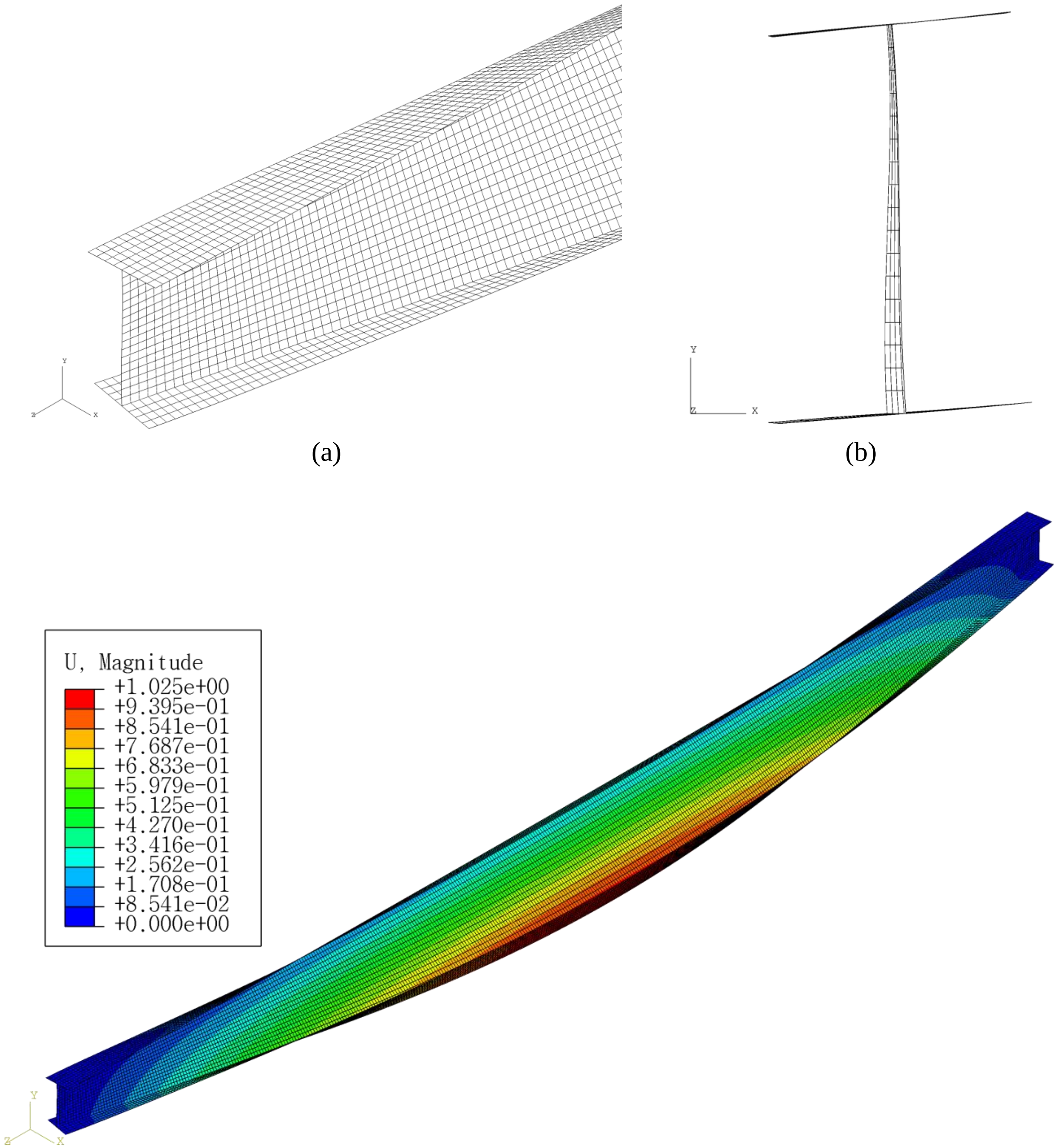

(c)

Fig. 3.10- $t/b = 0.0555$ Buckled configurations of ST0-L detail: (a) Isometric end, (b) Cross section, and (c) Isometric contour plot for the lateral displacement

3.10.4. Effect of Width to Height Ratio

In this series of simulations, the ratio b/h was varied from 0.48 to 0.81 while keeping the ratios w/h, t/b, and l/h constants and equal to the reference values. This is achieved by keeping h, w, and l constant while varying the flange width b and thickness t (so that t/b remains constant at the reference value). The results are depicted in Fig. 3.11. A wider flange relative to the section height is observed to result in a lower M_{cr}/M_u for the ST0-L, ST1-L, and ST2A-T details, all other factors being constant. In contrast, for detail ST2B-T, the ratio M_{cr}/M_u is observed to increase as b/h increases. This is due to the following: a) with an increase in flange width, the stiffeners also become wider and thus provide more resistance to web distortion and b) for a constant height h an increase in b/h is associated with an increase in the flange width b. For a constant t/b ratio, the flange thickness *t* also increases, and since the stiffener thickness for detail ST2B-T matches thickness t, the increase of b/h provides additional distortional restraints to the web. For detail ST2B-T, the beneficial distortional restraining effect of the wider stiffener more than offsets the destabilizing effect induced by the wider flange geometry. Fig. 3.12 and Fig. 3.13 display the buckled configurations of a ST0-L beam with b/h= 0.48 and 0.81. For the higher b/h ratio, the web exhibits more distortion. As a result, the M_{cr}/M_u ratio drops from 0.97 for b/h=0.40 to 0.92 for b/h=0.81.

Table 3.5 Effect of width to height ratio FEA results

			ST0-L		ST1-L		ST2A-T		ST2B-T	
ID#	$\frac{b}{h}$	M_u (kNm)	M_{cr} (kNm)	$\frac{M_{cr}}{M_u}$	M_{cr} (kNm)	$\frac{M_{cr}}{M_u}$	M_{cr} (kNm)	$\frac{M_{cr}}{M_u}$	M_{cr} (kNm)	$\frac{M_{cr}}{M_u}$
bh048	0.48	235.8	228.2	0.968	234.4	0.994	240.3	1.019	248.3	1.053
bh052	0.52	309.7	298.1	0.963	307.2	0.992	314.7	1.016	327.5	1.057
bh057	0.57	428.7	409.7	0.956	424.0	0.989	434.0	1.012	455.4	1.062
(Ref.)	**0.61**	**548.8**	**521.3**	**0.950**	**541.8**	**0.987**	**554.1**	**1.010**	**585.0**	**1.066**
bh068	0.68	823.5	773.2	0.939	810.3	0.984	827.4	1.005	882.1	1.071
bh075	0.75	1197.0	1117.2	0.933	1176.3	0.983	1199.1	1.002	1289.7	1.077
bh081	0.81	1611.9	1486.6	0.922	1579.0	0.980	1606.9	0.997	1741.1	1.080

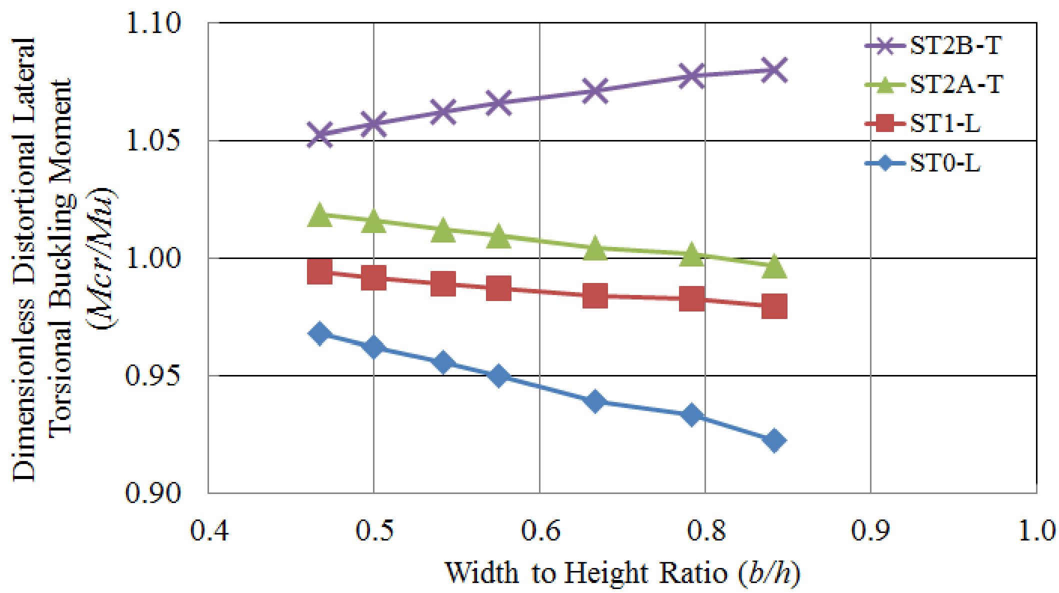

Fig. 3.11- Effect width to height ratio

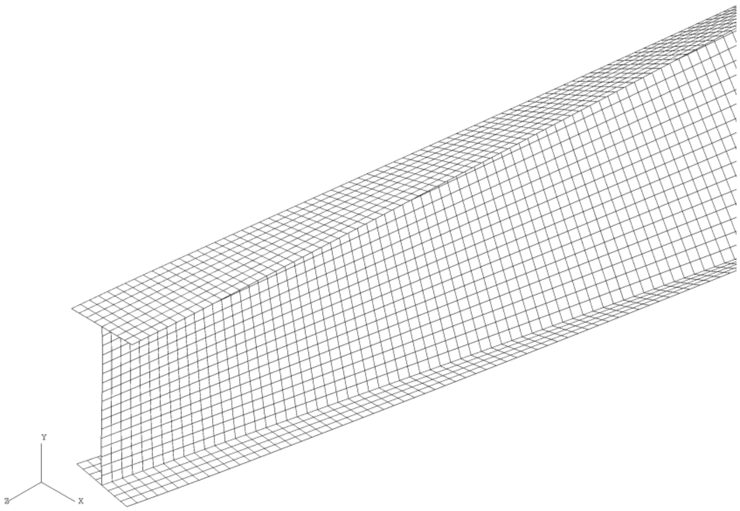

(a)

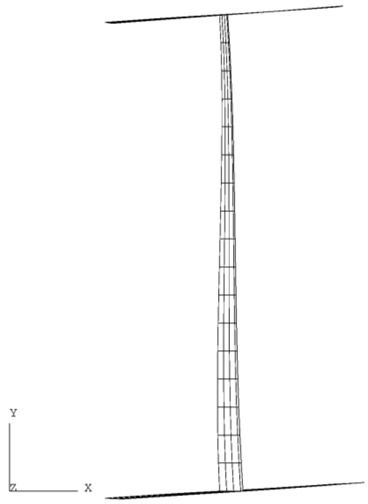

(b)

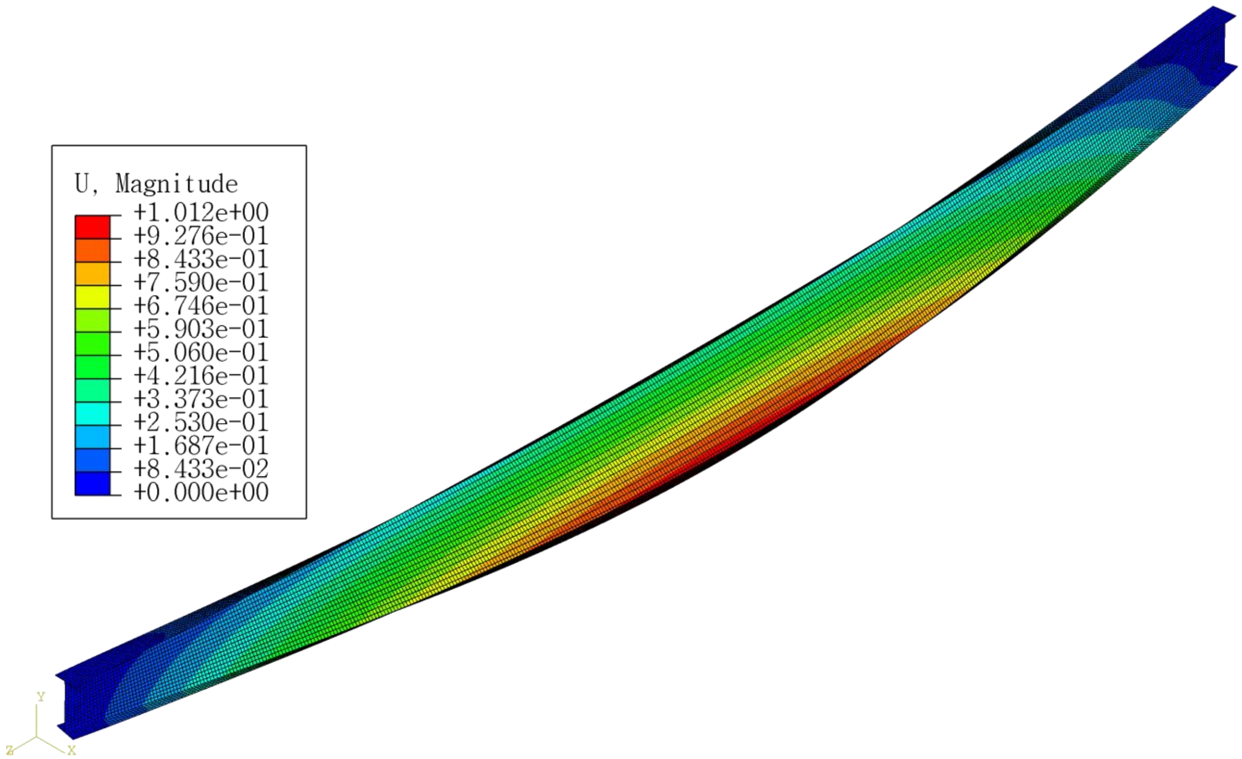

(c)

Fig. 3.12- $b/h = 0.48$ Buckled configurations of ST0-L detail: (a) Isometric end, (b) Cross section, and (c) Isometric contour plot for the lateral displacement

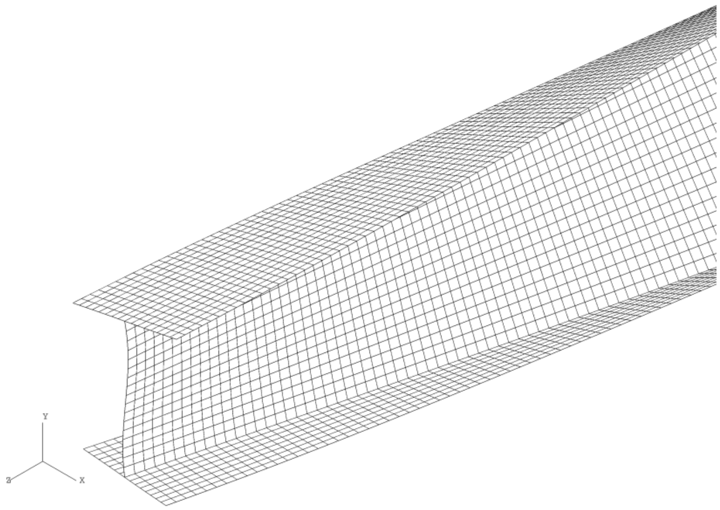

(a)

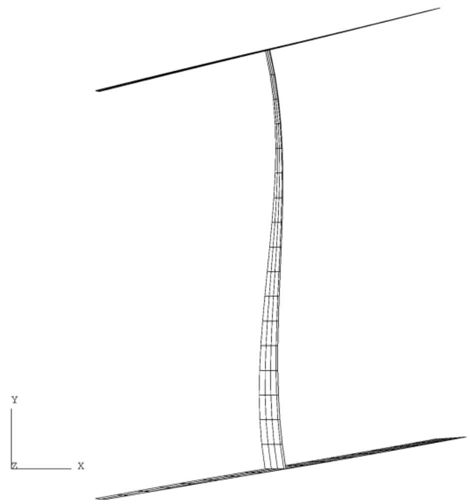

(b)

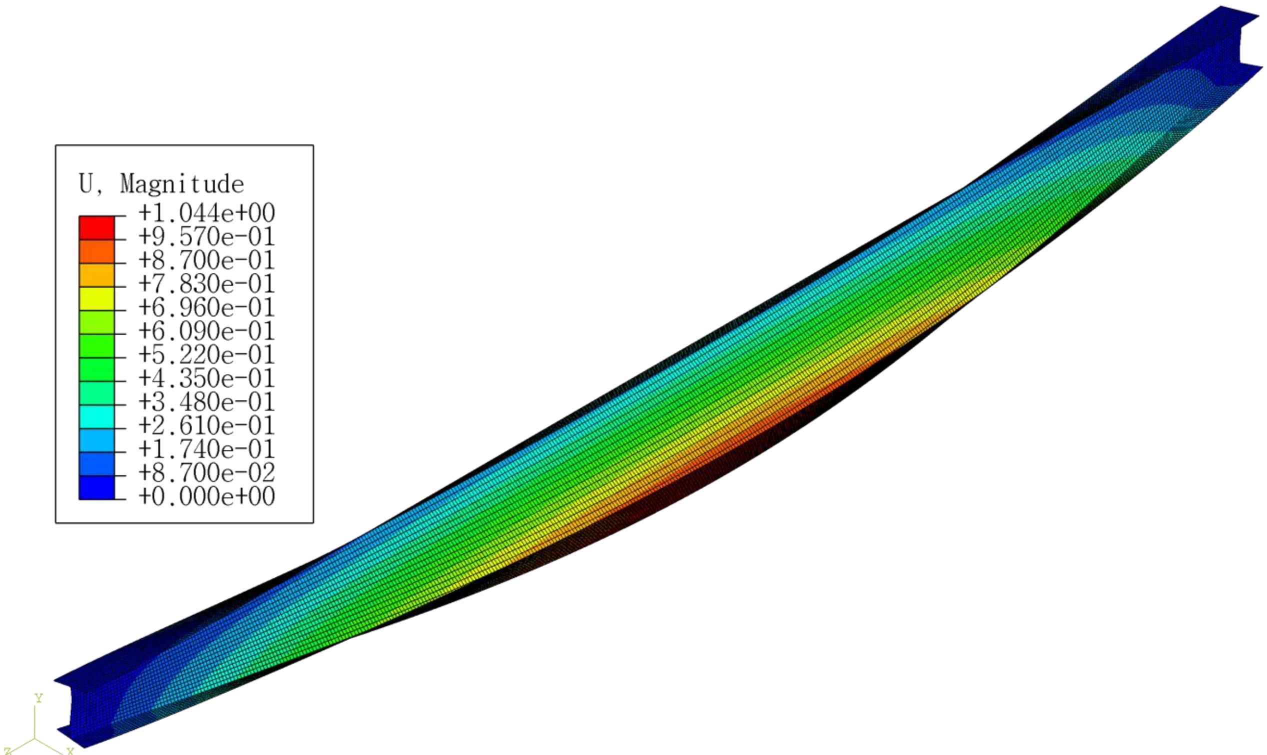

(c)

Fig. 3.13- $b/h = 0.81$ Buckled configurations of ST0-L detail: (a) Isometric end, (b) Cross section, and (c) Isometric contour plot for the lateral displacement

3.10.5. Effect of Span to Height ratio

In order to investigate the effect of span to height ratio l/h, the reference section was chosen and the span to height ratio l/h was varied from 9 to 42. This is achieved by maintaining *h*, *w*, *b*, and *t* at the reference values while varying the span length *l*. The relationship between M_{cr}/M_u and l/h is depicted in Fig. 3.14. For ST0-L and ST1-L, M_{cr}/M_u exhibits a slight decrease with l/h, i.e., shorter spans tend to undergo more distortional effects than longer span. For details ST2A-T and ST2B-T, a similar trend is observed. However, for shorter span beams (l/h=9.0), a sharp decline is observed in M_{cr}/M_u. When the span is small, the critical moment is high and the transverse forces applied to simulate the moment increase accordingly. These forces prematurely buckle the stiffeners prior to buckling the beam in a lateral torsional mode. As suggested by Fig. 3.14, this phenomenon is more pronounced for the ST2A-T detail. The corresponding isometric buckled configuration is illustrated in Fig. 3.15.

Table 3.6 Effect of span to height ratio FEA results

			ST0-L		ST1-L		ST2A-T		ST2B-T	
ID#	$\frac{l}{h}$	M_u (kNm)	M_{cr} (kNm)	$\frac{M_{cr}}{M_u}$	M_{cr} (kNm)	$\frac{M_{cr}}{M_u}$	M_{cr} (kNm)	$\frac{M_{cr}}{M_u}$	M_{cr} (kNm)	$\frac{M_{cr}}{M_u}$
lh9	9.00	2773.5	2621.4	0.945	2712.8	0.978	2506.8	0.904	2823.3	1.018
lh15	15.00	1189.0	1124.7	0.946	1172.8	0.986	1192.0	1.003	1272.3	1.070
lh21	21.00	728.5	690.3	0.948	719.4	0.987	735.8	1.010	781.2	1.072
(Ref.)	**26.00**	**548.8**	**521.3**	**0.950**	**541.8**	**0.987**	**554.1**	**1.010**	**585.0**	**1.066**
lh31	31.00	440.8	419.7	0.952	434.8	0.986	444.2	1.008	466.4	1.058
lh36	36.00	368.8	352.0	0.954	363.6	0.986	370.9	1.005	387.5	1.051
lh42	42.00	309.0	295.6	0.957	304.4	0.985	309.9	1.003	322.1	1.043

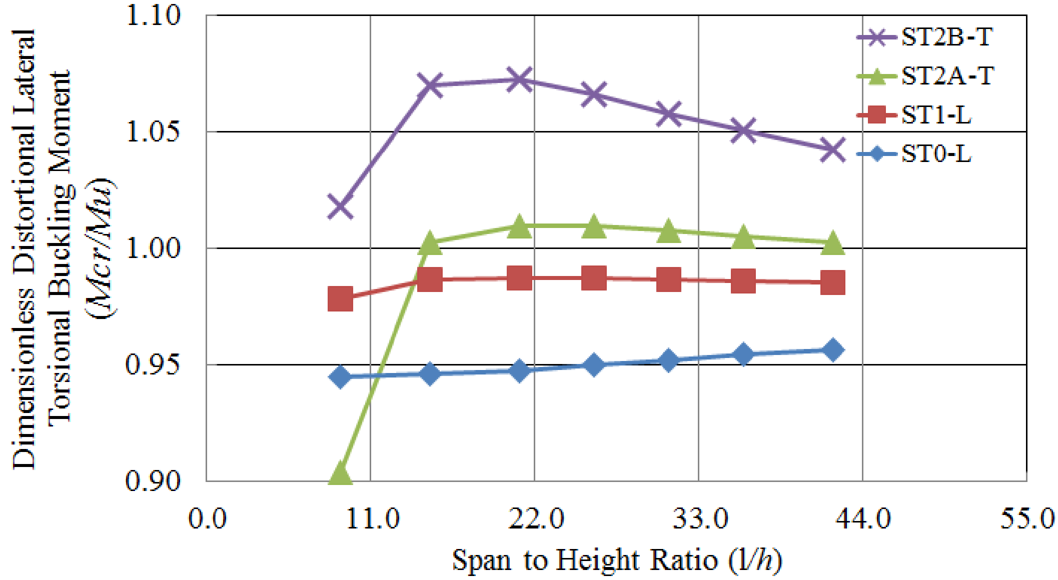

Fig. 3.14- Effect span to height ratio

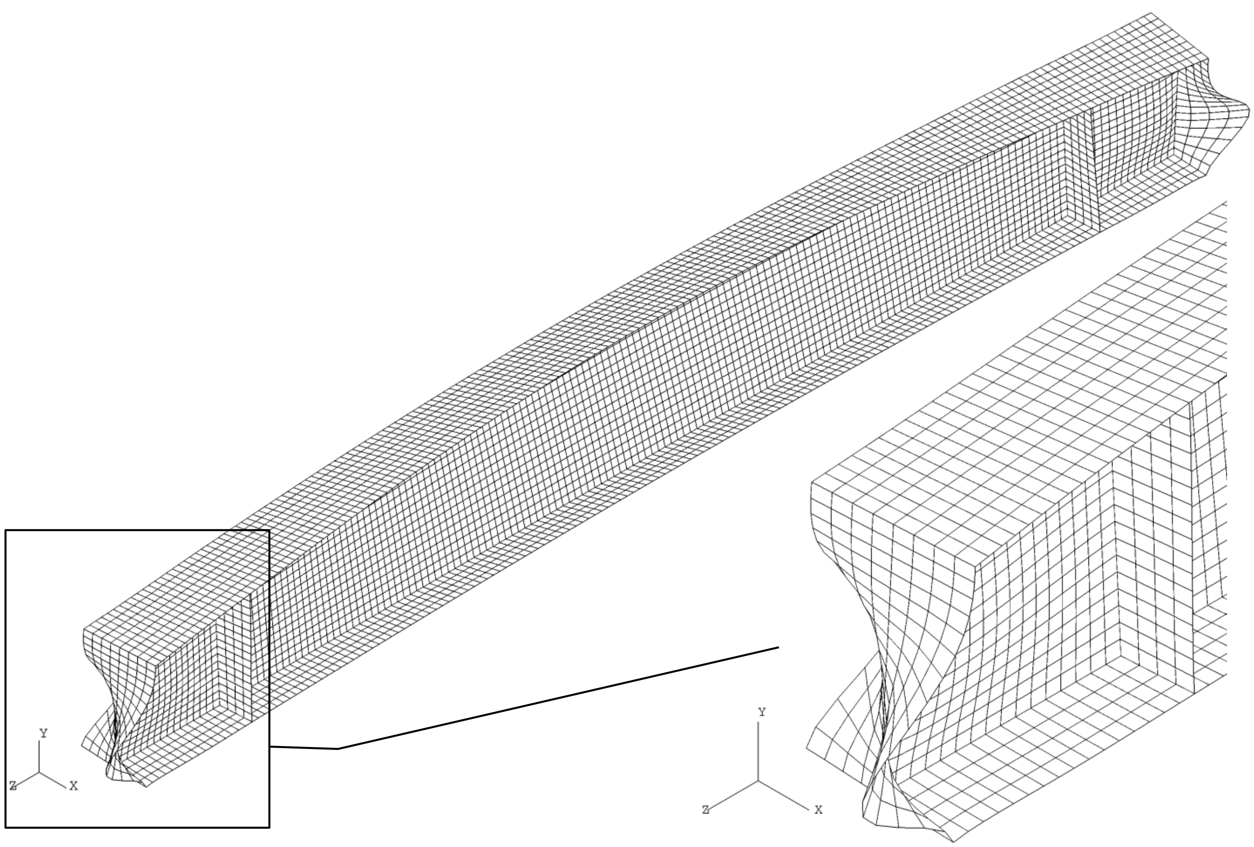

Fig. 3.15- Stiffener buckling, $l/h = 9$

3.10.6. FEA of Real Sections

As presented in sections 3.10.2 through 3.10.5, variations in w/h, t/b, b/h, and l/h influence a beam's M_{cr}/M_u ratio. The influence that a variation of l/h has on the resulting M_{cr}/M_u ratio is negligible compared to the other parameters, thus, it can be reasoned that a beams M_{cr}/M_u is governed by the remaining three dimensionless parameters, w/h, t/b, and b/h. Although the above study provides an understanding of how each dimensionless parameter influences M_{cr}/M_u, it fails to explain what effect a combined variation of all parameters would have on the resulting M_{cr}/M_u ratio. As such, a FEA of 54 real sections from the CISC SST was carried out. The sections were chosen to be representative of the entire database. The studied sections ranged from the W150 to W1000 designation classes. The results of the FEA are presented in Table B.2 of Appendix B. As shown in the table, M_{cr}/M_u values range from 0.830 (W460x64) to 0.977 (W310x21). As for the dimensionless parameters, w/h ranges from 0.0154 to 0.1551, t/b ranges from 0.0488 to 0.2398, while b/h ranges from 0.3037 to 1.1345. A comparison of the above mentioned ranges with Table 3.1 confirms that the sample of chosen sections is representative of the entire SST database. A linear regression analysis of various combinations of three dimensionless parameters was conducted. Table 3.7 presents results of the linear regression analysis. For each parameter combination analyzed, equations of best fit and 95% confidence are displayed. As presented in Table 3.7, the combination of the three dimensionless parameters gives the strongest correlation with an R^2 value of 0.955.

Table 3.7 Regression analysis results

Parameter(s)	R^2	Equation	
t/b	0.547	[3.14] $\frac{M_{cr}}{M_u} = 0.9717 - 0.4904\frac{t}{b}$	Best Fit
		[3.15] $\frac{M_{cr}}{M_u} = 0.9593 - 0.6145\frac{t}{b}$	95% Confidence
$t/b, w/h$	0.592	[3.16] $\frac{M_{cr}}{M_u} = 0.9693 - 0.3197\frac{t}{b} - 0.3350\frac{w}{h}$	Best Fit
		[3.17] $\frac{M_{cr}}{M_u} = 0.9752 - 0.5065\frac{t}{b} - 0.6547\frac{w}{h}$	95% Confidence
$t/b, w/h, b/h$	0.955	[3.18] $\frac{M_{cr}}{M_u} = 1.0536 - 1.0447\frac{t}{b} + 1.2681\frac{w}{h} - 0.1224\frac{b}{h}$	Best Fit
		[3.19] $\frac{M_{cr}}{M_u} = 1.0443 - 1.1406\frac{t}{b} + 1.0772\frac{w}{h} - 0.1347\frac{b}{h}$	95% Confidence

3.11. Notation for Chapter 3

b flange width

C_w warping constant

E elastic modulus of steel (200 000 MPa assumed)

F physical quantity force

F_y specified minimum yield stress

f function relating variables

f_2 function relating dimensionless groups

G shear modulus of steel (77 000 MPa assumed)

h distance between flange centroids

I_y out of plane moment of inertia

J torsional constant

K elastic stiffness matrix

K_G geometric stiffness matrix

L	physical quantity length
l	length of unbraced portion of beam
$l_{\max}$	upper limit of length in FEA study
$l_{\min}$	lower limit of length in FEA study
M_{cr}	elastic critical moment capturing the effects of distortional buckling
M_{in}	nominal inelastic lateral torsional moment resistance
M_p	plastic moment resistance
M_u	classical lateral torsional buckling solution
M_y	nominal yield moment resistance
m	independent physical quantities in the Buckingham π theory
n	variables in a problem in the Buckingham π theory
$r_{\min}$	minimum radius of gyration
S_x	elastic section modulus
T	time
t	flange thickness
u_i	buckling mode shapes
w	web thickness
w_{st}	stiffener thickness
Z_x	plastic section modulus
α_i	Buckingham π theory exponents
λ_i	eigenvalues
μ	Poisson’s Ratio
π_i	Buckingham pi parameters

Chapter 4
Distortional Lateral Torsional Buckling of Beams under Linear Moment Gradients

4.1. Objective and Scope

Structural steel members with linear moment gradients are commonly encountered in steel construction. Various structural steel design standards relate the elastic lateral torsional buckling resistance M_r of the member to that of a beam with identical dimensions subjected to uniform moments M_u through

[4.1] $M_r = C_{st} M_u$

in which C_{st} is a standard dependent coefficient which accounts for the actual moment distribution within the beam. The uniform moment equation M_u is based on ideal simply supported conditions for a beam under uniform moments. It is based on the Vlasov thin-walled beam theory which neglects section distortion. Moment gradient coefficients C_{st} do not account for distortional effects nor do they account for the effect of details including presence/ absence of stiffeners, or the load transfer details at member ends.

Within this context, the study in this chapter aims at quantifying the effect of end details and section distortion on the critical moment of beams with linear moment gradients through a series of shell finite element linear eigenvalue analyses. Beams with various practical end details are modeled to mimic, as closely as possible, real design applications and the critical moments M_{cr} are determined. Subsequent comparisons are performed on the M_{cr}/M_u ratios as determined form the shell finite element model to the moment gradient factors C_{st} in various design standards.

4.2. *Members Subject to Triangular Moment Distributions*

Theoretically, flexural members with triangular moment distribution (Fig. 4.1) arise when a concentrated end moment M is applied at one end of a simply supported beam. Such a loading case is uncommon in design applications. A more common loading case with a triangular moment distribution is depicted in Fig. 4.2, in which a mid-span point load P is applied on a laterally unsupported simply supported beam of span $2l$ with an intermediate lateral restraint at the point of application of the load. This will result in triangular distributions in the two laterally unsupported segments, each of span l .

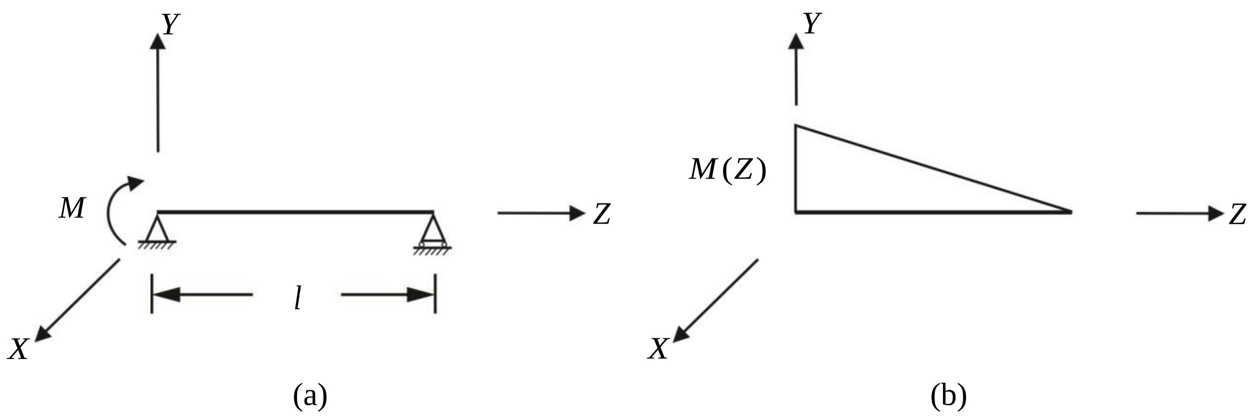

Fig. 4.1- Triangular moment (a) Schematic, and (b) Moment diagram

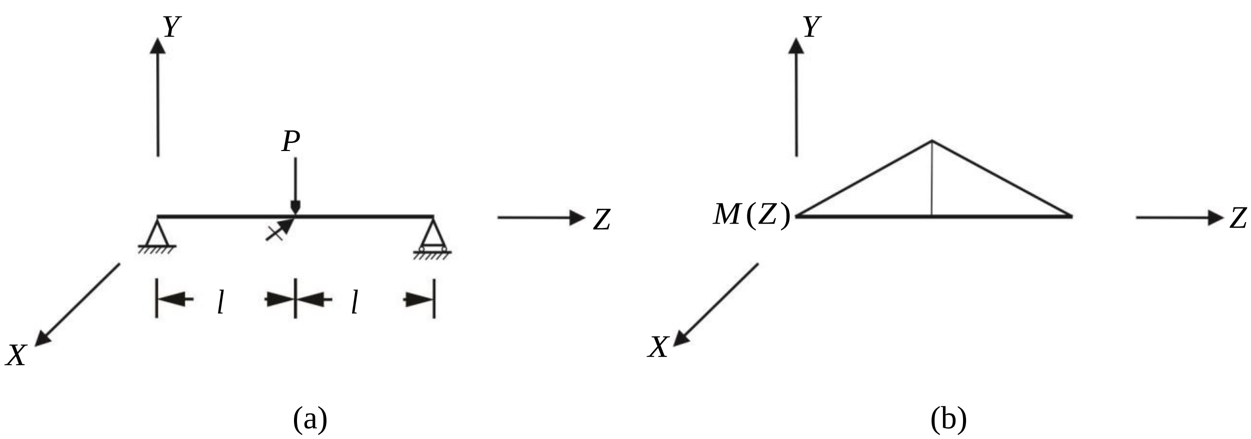

Fig. 4.2- Triangular moment through mid-span point load application (a) Schematic, and (b) Moment diagram

In another type of application, a triangular moment distribution is encountered when a lateral point load is applied at the top of a simply supported portal or gable frame with columns that are pinned at the bases. Portal frames are commonly used in prefabricated steel structures. In these types of structures, the exterior siding is usually made of sheet metal which possibly transmits lateral wind forces to the top of the portal frame. Fig. 4.3 depicts a schematic of such a gable frame subjected to a lateral force at the top of the column.

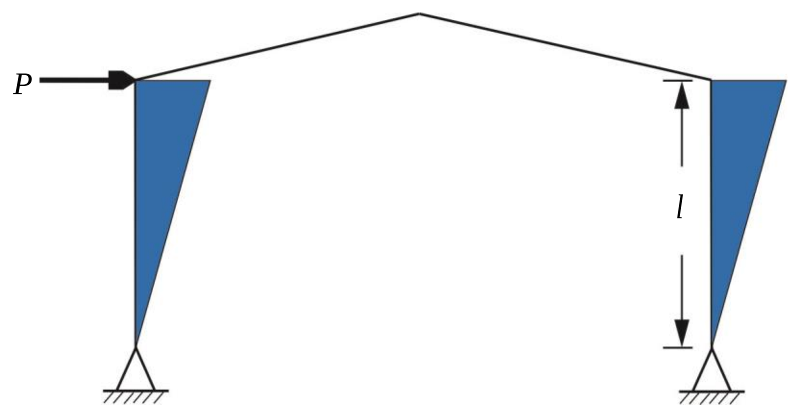

Fig. 4.3- Bending moment in a gable frame

Using the code dependent moment gradeint equations introduced in Chapter 2, the moment gradient factors for beams under triangular moment distributions are tabulated. Based on the quarter-point methods stipulated in ANSI/AISC 360-10, CAN/CSA S16-09, and AS 4100-1998, and using the quarter point moment values $M_a = 0.75M_{\max}$, $M_b = 0.50M_{\max}$, and $M_c = 0.25M_{\max}$, one obtains the moment gradient factors in Table 4.1. For the CAN/CSA S16-09 linear moment equation, the end moment ratio was set to zero, i.e., $\kappa = 0$.

Table 4.1 Standard based moment gradient factors for beams subject to triangular moment

Standard	Moment Gradient Factor
ANSI/AISC 360-10	1.667
CAN/CSA S16-09 General	1.746
CAN/CSA S16-09 Linear	1.750
AS 4100-1998	1.817
EN 1993-1-1 Guide	1.879

4.3. *Members Subject to Reverse Moment Distributions*

As depicted in Fig. 4.4, reverse moments are theoretically achieved when applying equal and opposite end moments at ends of a beam. In a manner similar to the triangular moment case, reverse moments can are practically encountered when a lateral point load is applied to a portal or gable frame at the top of a column level. A reverse moment is obtained when the column bases are fixed. This can be achieved by shop welding the column to a thick base plate, which would then be fastened to a pier or footing via cast in place anchor rods placed outside the footprint of the column or a similar anchoring scheme.

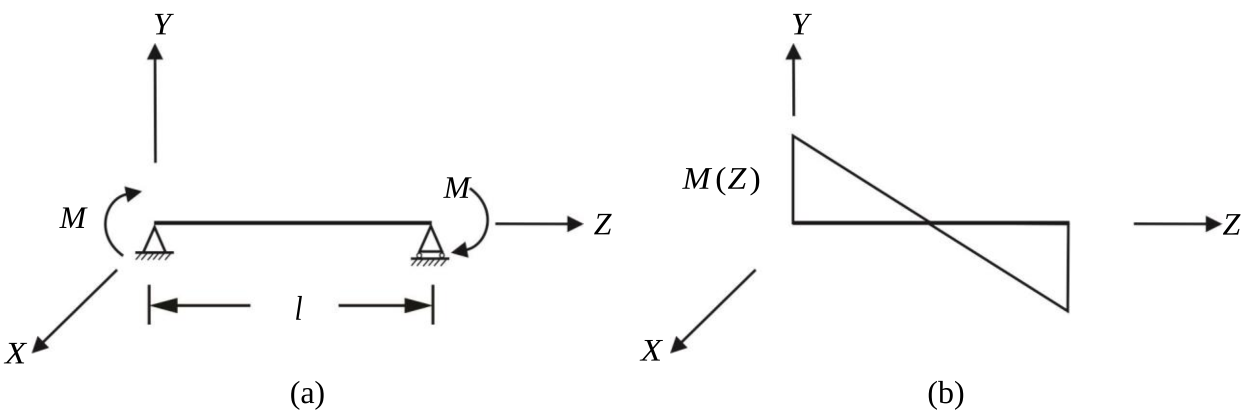

Fig. 4.4- Reverse moment (a) Schematic, and (b) Moment diagram

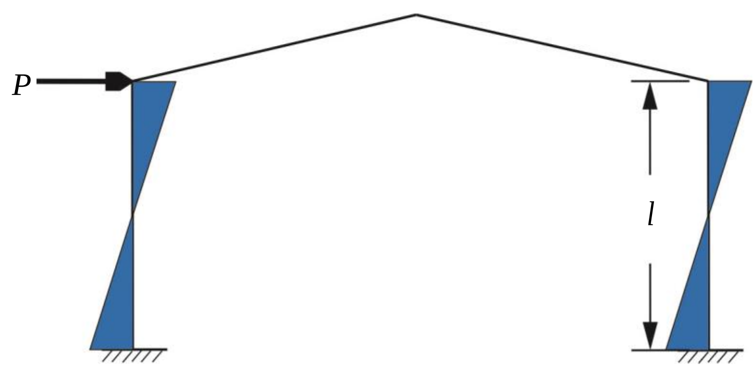

Fig. 4.5- Fixed supported portal frame

For the case of full reversed moments (i.e., equal and opposite moments at both ends), quarter point moment values of $M_a = 0.50M_{\max}$, $M_b = 0.00M_{\max}$, and $M_c = 0.50M_{\max}$ are used to determine moment gradient factors for quarter-point based methods available in ANSI/AISC

360-10, CAN/CSA S16-09, and AS 4100-1998. In the linear moment based equation available in CAN/CSA S16-09, an end moment ratio $\kappa = -1$ was taken. The resulting moment gradient values are summarized in Table 4.2

Table 4.2 Standard based moment gradient factors for beams subject to reverse moment

Standard	Moment Gradient Factor
ANSI/AISC 360-10	2.273
CAN/CSA S16-09 General	2.309
AS 4100-1998	2.404
CAN/CSA S16-09 Linear	2.500
EN 1993-1-1 Guide	2.752

4.4. Applicability of End Details

It is noted that moment gradient equations in various codes depend solely on the moment distribution, with no distinction between the various possible end details at the member end. To expand on this discussion, the beam introduced in Fig. 4.2 has been enlarged and reproduced in Fig. 4.6. For this beam, A and B denote the ends of the unbraced segment which would be used to determine LTB resistance for segment AB. Code equations treat End A as a support in a manner similar to End B even though Ends A and B can be detailed very differently. End A may consist of welded web cleats that are used to support the secondary beam framing perpendicularly to the beam (Fig. 4.7(a)). In this case, the shop welded web cleats would behave as stiffeners similar to the ST1-L detail in Chapter 3. Alternatively, the perpendicular secondary beam could be supported via a bolted single angle or WT section (Fig. 4.7(b-c)), which would result in behavior somewhere between a ST0-L and ST1-L detail. End B could be detailed in a variety of methods which include, but are not limited to, bolted web cleats (Fig. 4.8(a)), welded web cleats (Fig. 4.8(b)), and a stiffened beam sitting on a embedded steel plate on concrete corbel (Fig. 4.8(c)). The above connection details would behave in a similar manner to ST0-L and ST1-L details.

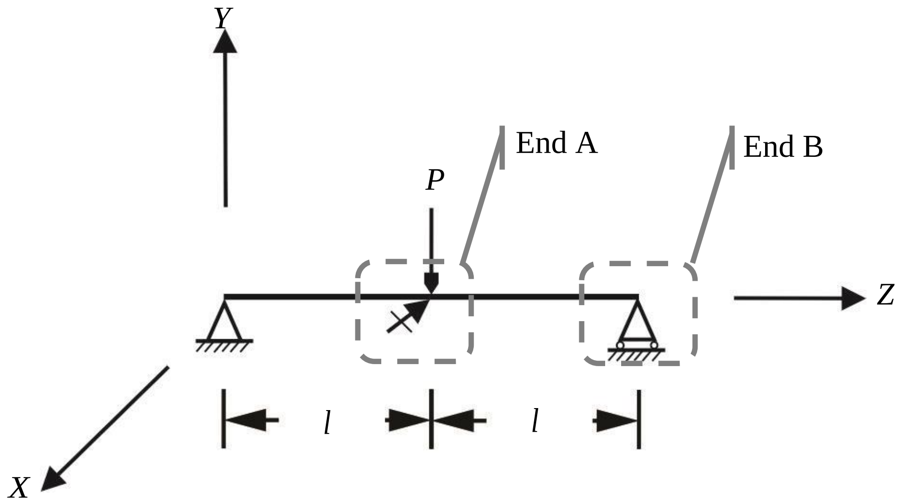

Fig. 4.6- Support identification

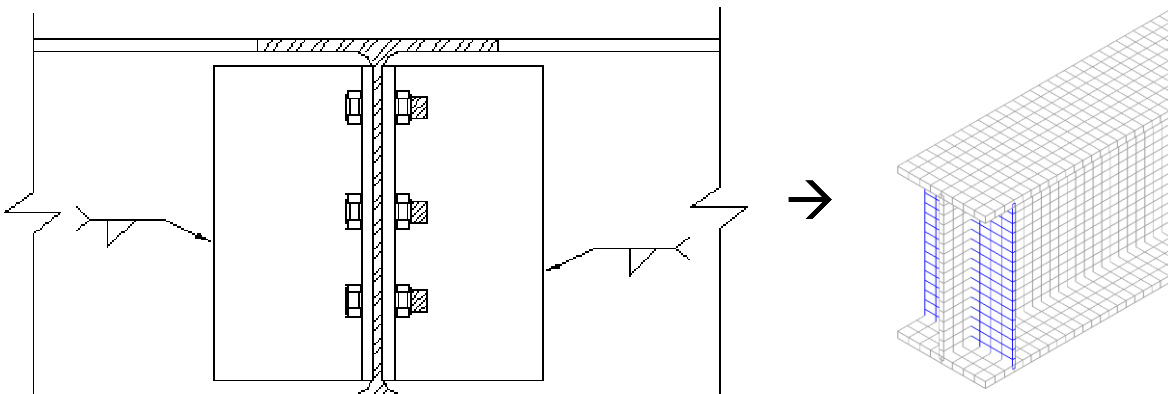

(a)

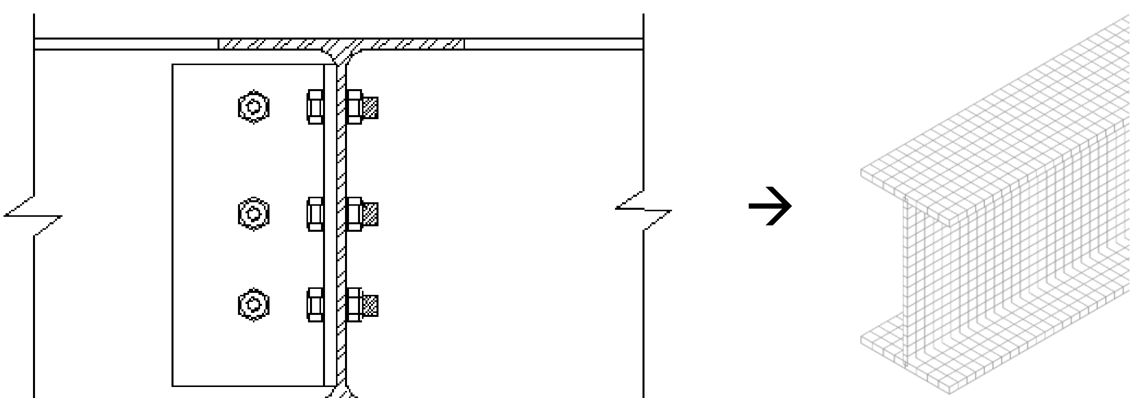

(b)

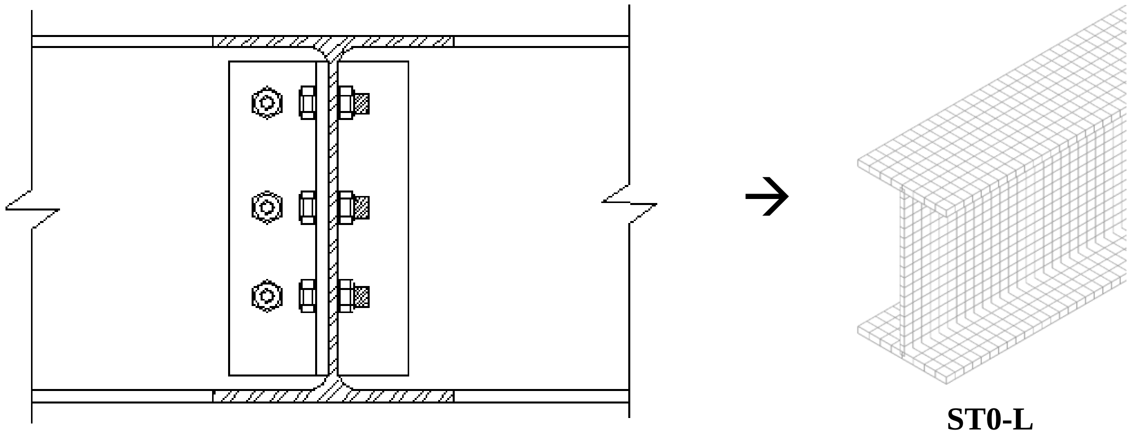

(c)

Fig. 4.7- End A deisgn scenarios and thier corresponding idealizations: (a) Welded web cleats, (b) Bolted angle, and (c) Bolted WT section

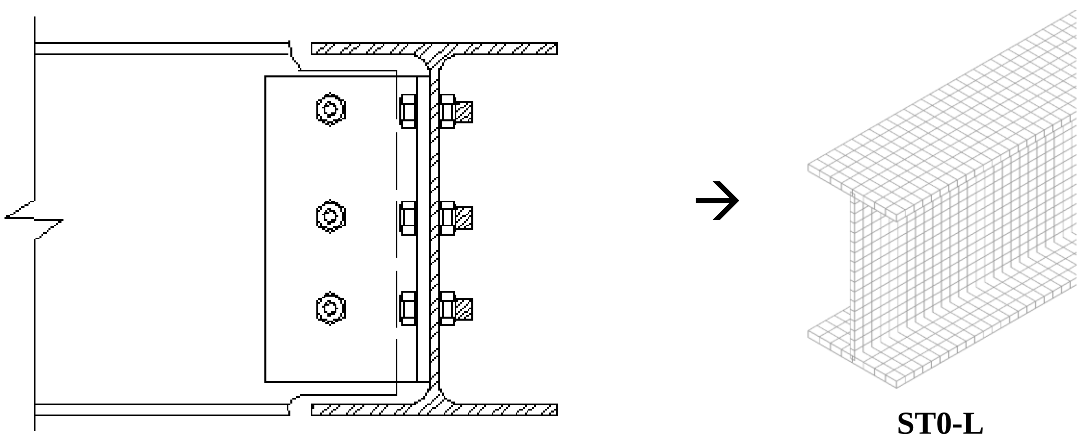

(a)

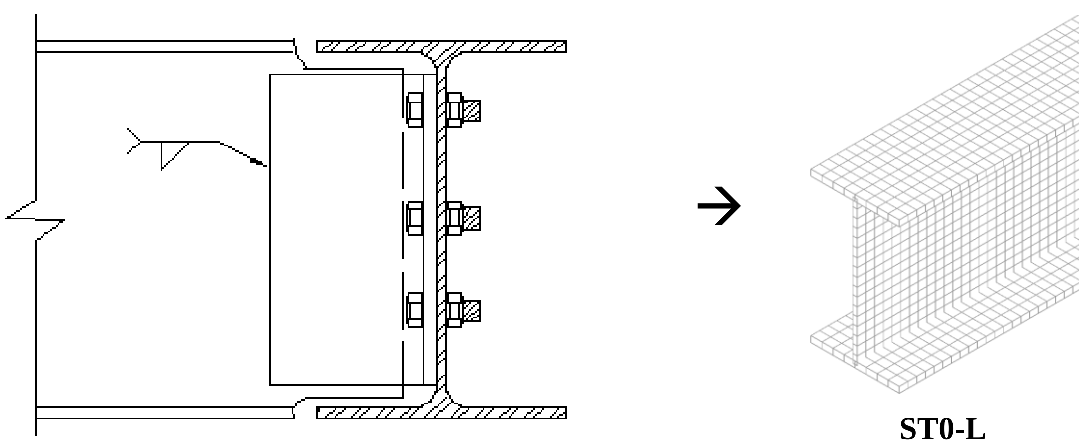

(b)

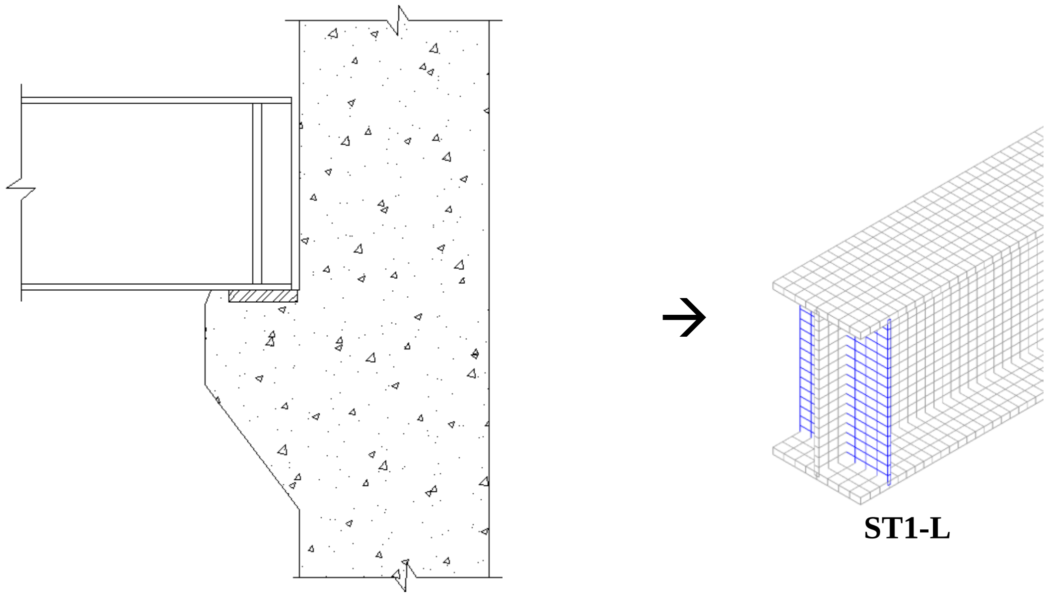

(c)

Fig. 4.8- End B details and their corresponding idealizations: (a) Bolted web cleat, (b) Welded angle, and (c) Stiffened beam on corbel

4.5. Evaluation of Code Moment Gradient Factors

Using the procedures outlined in Sections 3.3 through 3.9, a parametric study is conducted to assess the effect of variations in the various dimensionless parameters on the resulting M_{cr}/M_u ratios. The reference section in Chapter 3 is used again as a basis from which variations in dimensionless parameters are made. One recalls the dimensions of the reference section are $h = 500mm$, $b = 305mm$, $t = 21.034mm$, and $w = 14.706mm$, which correspond to the dimensionless parameters of $w/h = 0.0294$, $t/b = 0.6993$, $b/h = 0.6100$, and $t/w = 1.430$.

4.6. Results

The results presented in Subections 4.6.1 through 4.6.4 investigate the effect of w/h, t/b, b/h, and l/h for different moment gradients (uniform (extracted from chapter 3), triangular, and fully reversed). One of the dimensionless parameters was varied at a time while maintaining the other three dimensionless parameters at their reference values.

4.6.1. Effect of Web Slenderness

Fig. 4.9(a-c) provide the moment gradient factors as determined by FEA (i.e., M_{cr}/M_u) versus the web slenderness w/h for all details considered for the cases of uniform, triangular, and fully reversed moment distributions.

Table 4.3 to Table 4.5 provide an assessment of the ability of each Standard in predicting moment gradient factors for various end details. The tables provide comparisons of the standard predicted moment gradient factor to FEA predicted moment gradient factor. Lowest, average, and highest moment gradient ratios for various standards are provided for w/h when subject to triangular and fully reversed moment.

Fig. 4.9(a-c) reveals that regardless of the moment distribution, the effect of varying w/h produces trends similar to those based on a uniform moment case. That is, for the ST0-L, ST1-L and ST2A-T details, an increase in w/h results in an increase of the moment gradient ratio M_{cr}/M_u due to a reduction in the level of distortion in relatively thicker webs. For the ST2B-T detail there is no clear trend between M_{cr}/M_u versus w/h.

The following observations can be made about the studied Standards; ANSI/ASIC 360-10, CAN/CSA S16-09, AS 4100-1998, and EN 1993-1-1 Guide:

1) While the FEA results show that the moment gradient factors vary depending upon end details and web slenderness, various standard moment gradient factors do not recognize the differences between such details.

2) ANSI/ASIC 360-10 and CAN/CSA S16-09 provide conservative moment gradient predictions for most web slenderness and end detail combinations considered in the study

3) The EN 1993-1-1 Guide moment gradient predictions tend to err on the un-conservative side for most combinations.

4) The Australian standards AS 4100-1998 seem to mostly err on the conservative side for fully reversed moments and on the un-conservative side for the triangular moment distributions.

Results supporting the second point are presented in Table 4.4 and Table 4.5. One example of this occurs for CAN/CSA S16-09 when the beam is subject to a triangular moment distribution. It can be seen that the standard prediction changes from an underestimation of 11.4% for the ST2B-T detail to a slight overestimation of 3.5% for the ST0-L detail. ANSI/AISC 360-10 provides the most conservative predictions by underestimating the critical moment by up to 21.5% for a beam with a stocky web subject to reverse moment. For the web slenderness and end details considered in this section, it is the only standard to never overestimate the critical moments of a beam.

The third point is clearly depicted in Fig. 4.9(b-c) where EN 1993-1-1 overestimates all variations of web slenderness for the ST0-L, ST1-L, and ST2A-T when subject to triangular and full reversed moment gradient distributions. The degree of overestimation ranges from 1.2% for the ST2A-T detail to 12.7% for the ST0-L detail when subject to a fully reversed moment distribution.

Supporting observations for the fourth point can be made by a comparison of the results for the AS 4100-1998 when a beams web is slender, i.e., w/h is low, in Table 4.4 and Table 4.5. The results suggest that when a beam is subject to triangular moment, AS 4100-1998 overestimates the moment gradient factor by 7.5%. On the contrary, when the beam is subject to fully reversed moments, AS 4100-1998 provide a conservative estimate of 1.6%.

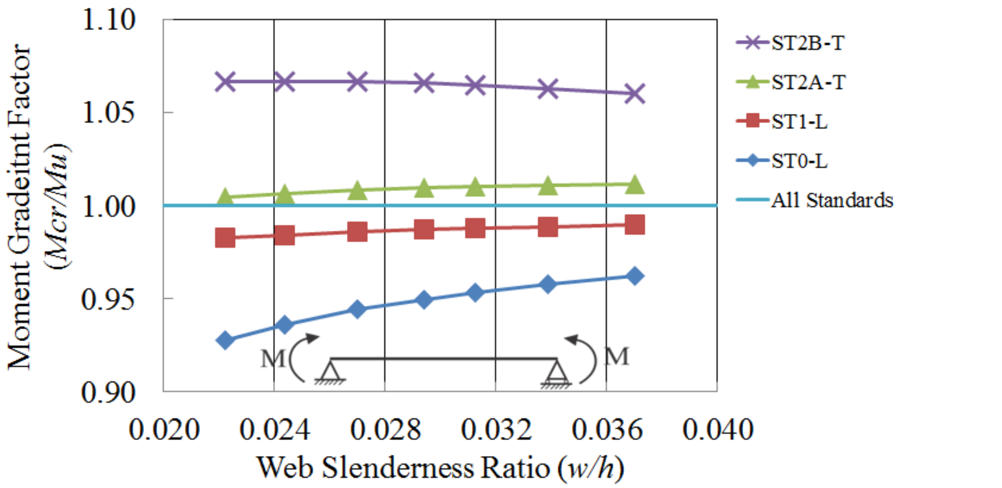

(a)

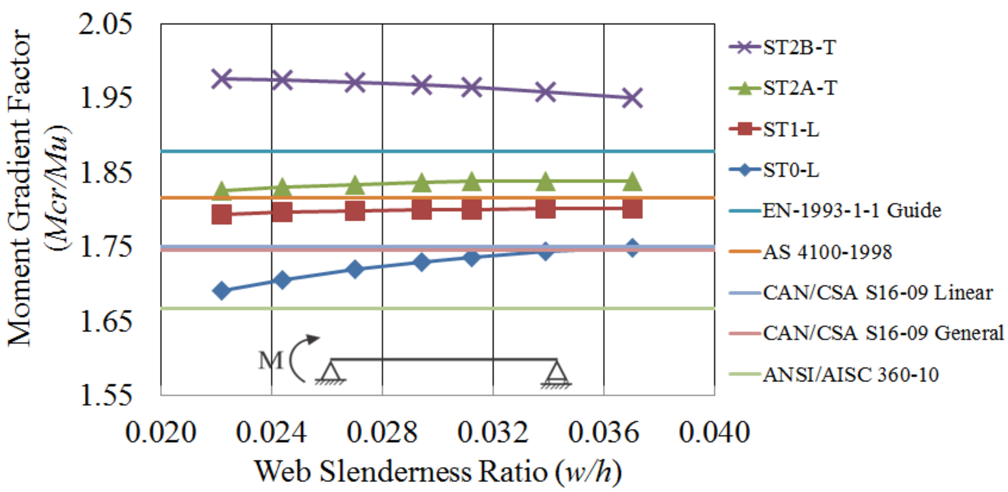

(b)

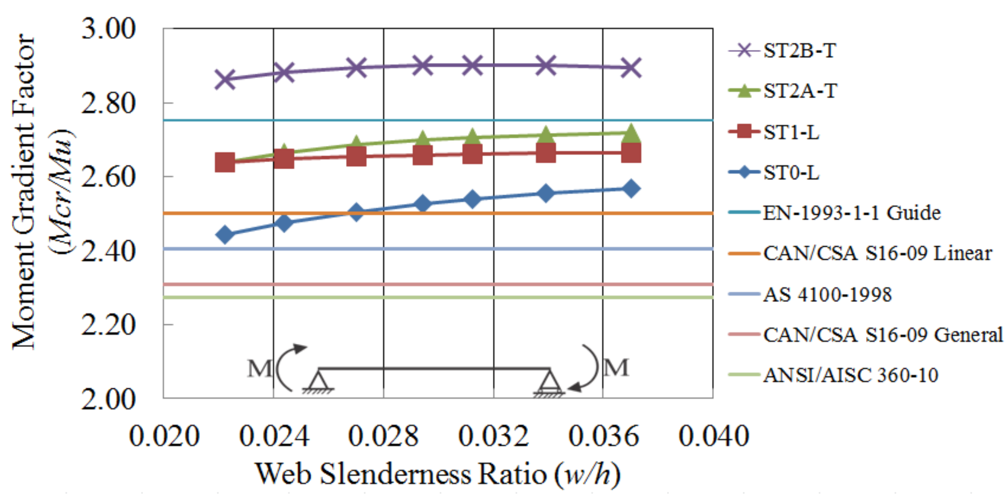

(c)

Fig. 4.9- Effect of web slenderness on FEA predicted moment gradient factors for beams subject to (a) Uniform, (b) Triangular, and (c) Reverse moments

Table 4.3 Effect of web slenderness ratio w/h on percentage difference between standard moment gradients and FEA moment gradients for the case of uniform Moment distribution

		ST0-L	ST1-L	ST2A-T	ST2B-T
All Standards	Low	7.2%	1.7%	-0.5%	-6.7%
	Average	5.3%	1.3%	-0.9%	-6.5%
	High	3.8%	1.0%	-1.2%	-6.1%
All percentages are calculated by $(C_{st} - C_{FEA})/C_{FEA}$. Positive values indicate that applicable standards overestimate member capacity (un-conservative)					

Table 4.4 Effect of web slenderness ratio w/h on percentage difference between standard moment gradients and FEA moment gradients for the case of triangular Moment distribution

		ST0-L	ST1-L	ST2A-T	ST2B-T
ANSI/AISC 360-10	Low	-1.4%	-7.1%	-8.7%	-15.6%
	Average	-3.4%	-7.4%	-9.1%	-15.2%
	High	-4.7%	-7.5%	-9.4%	-14.6%
CAN/CSA S16-09	Low	3.5%	-2.5%	-4.1%	-11.4%
	Average	1.4%	-2.7%	-4.6%	-11.0%
	High	0.0%	-2.9%	-4.8%	-10.3%
AS 4100-1998	Low	7.5%	1.3%	-0.4%	-8.0%
	Average	5.3%	1.0%	-1.0%	-7.6%
	High	3.8%	0.8%	-1.2%	-6.9%
EN 1993-1-1 GUIDE	Low	11.1%	4.7%	3.0%	-4.9%
	Average	8.9%	4.4%	2.4%	-4.5%
	High	7.4%	4.3%	2.2%	-3.7%
All percentages are calculated by $(C_{st} - C_{FEA})/C_{FEA}$. Positive values indicate that applicable standards overestimate member capacity (un-conservative)					

Table 4.5 Effect of web slenderness ratio w/h on percentage difference between standard moment gradients and FEA moment gradients for the case of full reversed moment distribution

		ST0-L	ST1-L	ST2A-T	ST2B-T
ANSI/AISC 360-10	Low	-6.9%	-13.9%	-13.9%	-20.6%
	Average	-9.6%	-14.4%	-15.5%	-21.4%
	High	-11.5%	-14.7%	-16.4%	-21.5%
CAN/CSA S16-09 GENERAL	Low	-5.4%	-12.5%	-12.5%	-19.4%
	Average	-8.2%	-13.0%	-14.1%	-20.1%
	High	-10.1%	-13.4%	-15.1%	-20.2%
AS 4100-1998	Low	-1.6%	-8.9%	-8.9%	-16.1%
	Average	-4.4%	-9.5%	-10.6%	-16.9%
	High	-6.3%	-9.8%	-11.6%	-17.0%
CAN/CSA S16-09 LINEAR	Low	2.4%	-5.3%	-5.3%	-12.7%
	Average	-0.6%	-5.8%	-7.0%	-13.5%
	High	-2.6%	-6.2%	-8.1%	-13.6%
EN 1993-1-1 GUIDE	Low	12.7%	4.3%	4.2%	-3.9%
	Average	9.4%	3.6%	2.3%	-4.8%
	High	7.2%	3.3%	1.2%	-4.9%
All percentages are calculated by $\left(C_{st}-C_{FEA}\right)/C_{FEA}$. Positive values indicate that applicable standards overestimates member capacity					

4.6.2. Effect of Flange Slenderness

Fig. 4.10(a-c) provides the moment gradient factors as determined by FEA versus the flange slenderness t/b for all details considered for uniform, triangular, and fully reversed moment distributions. Table 4.6 - Table 4.8 provide assessments of Standards in determining moment gradient factors for various end details for low, average and high values of t/b when subject to triangular and fully reversed moment.

For ST0-L, ST1-L, and ST2A-T, the moment gradient factor is observed to decrease as the flange thickness-to-width ratio increases. A thicker flange can be thought of as attracting more compressive stresses and thus destabilizing the member and making it more prone to undergo distortional buckling (in comparison to the classical solution which neglects the effect of distortion). This deduction is confirmed by examining Fig. 4.11, in which a section with the smallest flange to thickness-to-flange ratio is observed to exhibit less distortion than the section with the largest thickness-to-flange ratio. For the ST2B-T detail, the trend is found to reverse. An increase in flange thickness-to-width ratio is found to be associated with an increase in the moment gradient factor. Detailed explanations of these trends and supporting data obtained through FEA were provided in Subsection 3.10.3 for the case of uniform moments and remain valid for other linear moment gradients in this chapter.

For triangular moment distributions, depending on the end detail considered and the flange slenderness, the M_{cr}/M_u ratio is observed to range from 1.657 for the ST0-L detail to 1.987 for the ST2B-T, both for the thickest slenderness considered of $t/b = 0.0909$. The corresponding code predictions range from 1.667 for ANSI/AISC 360-10 to 1.879 for EN 1993-1-1. For fully reversed moment distributions, the M_{cr}/M_u ratio ranges from 2.398 for the ST0-L detail to 2.905 for the STB-T detail for the same slenderness of $t/b = 0.0909$.

Fig. 4.10(b-c) suggests that all Standards underestimate the M_{cr}/M_u ratio for the ST2B-T detail regardless of the linear moment distribution or the flange slenderness and ANSI/ASIC 360-10 conservatively estimates M_{cr}/M_u ratio for all details and flange slenderness ratios except for the ST0-L detail when the flange is stocky.

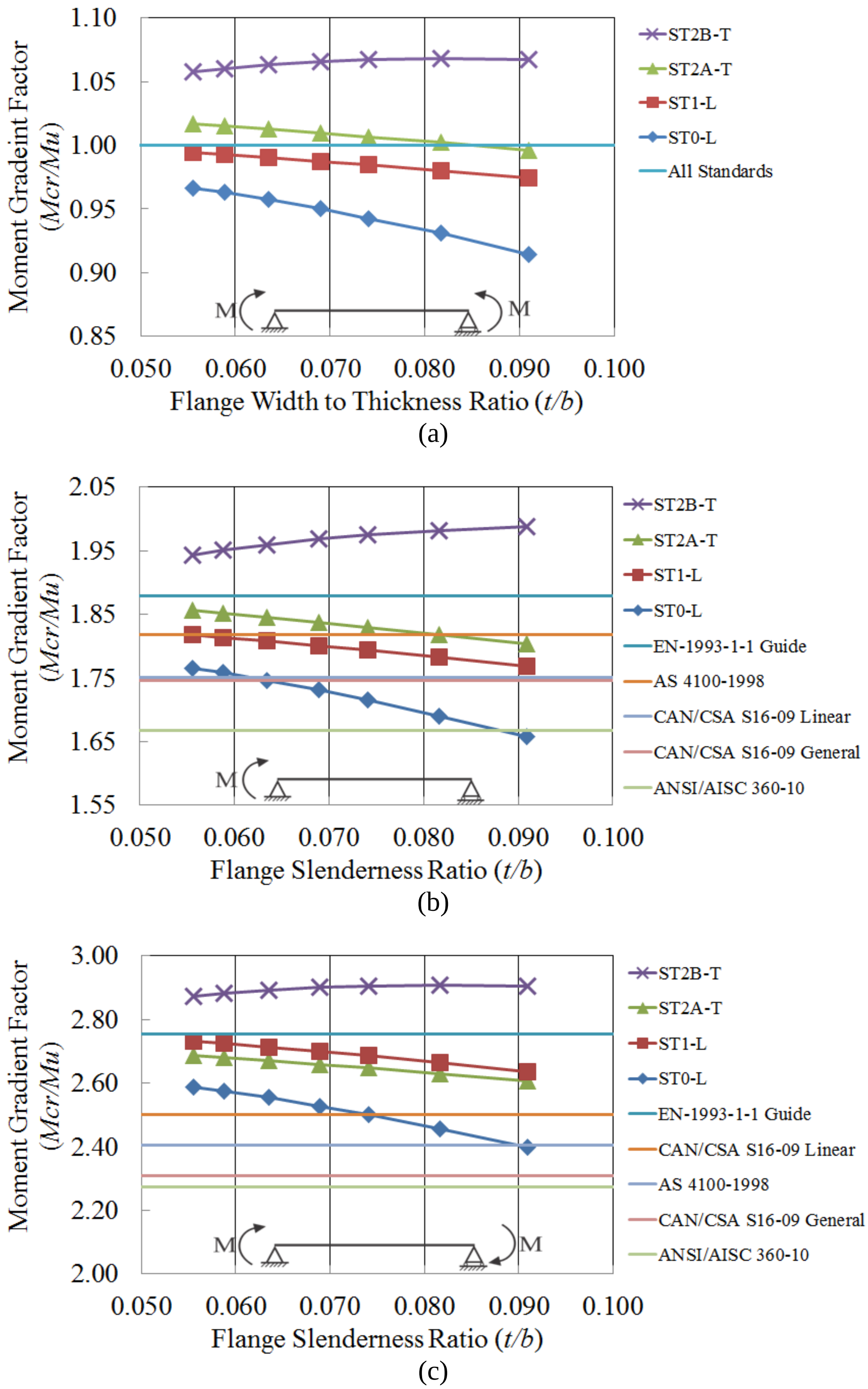

Fig. 4.10- Effect of flange slenderness on FEA predicted moment gradient factors for beams subject to (a) Uniform, (b) Triangular, and (c) Reverse moments

Table 4.6 Effect of flange slenderness ratio t/b on percentage difference between standard moment gradients and FEA moment gradients for the case of uniform moment distribution

		ST0-L	ST1-L	ST2A-T	ST2B-T
All Standards	Low	3.4%	0.6%	-1.7%	-5.8%
	Average	5.4%	1.4%	-0.9%	-6.4%
	High	8.5%	2.6%	0.4%	-6.8%
All percentages are calculated by $(C_{st} - C_{FEA})/C_{FEA}$. Positive values indicate that applicable standards overestimate member capacity (un-conservative)					

Table 4.7 Effect of flange slenderness ratio t/b on percentage difference between standard moment gradients and FEA moment gradients for the case of triangular moment distribution

		ST0-L	ST1-L	ST2A-T	ST2B-T
ANSI/AISC 360-10	Low	-5.6%	-8.3%	-10.2%	-14.2%
	Average	-3.3%	-7.3%	-9.1%	-15.2%
	High	0.6%	-5.7%	-7.5%	-16.1%
CAN/CSA S16-09	Low	-0.8%	-3.7%	-5.7%	-10.0%
	Average	1.6%	-2.6%	-4.6%	-11.0%
	High	5.6%	-1.0%	-2.9%	-11.9%
AS 4100-1998	Low	2.9%	-0.1%	-2.1%	-6.5%
	Average	5.5%	1.1%	-1.0%	-7.6%
	High	9.7%	2.8%	0.8%	-8.6%
EN 1993-1-1 GUIDE	Low	6.5%	3.4%	1.2%	-3.3%
	Average	9.1%	4.5%	2.4%	-4.5%
	High	13.4%	6.3%	4.2%	-5.4%
All percentages are calculated by $(C_{st} - C_{FEA})/C_{FEA}$. Positive values indicate applicable standards overestimate member capacity (un-conservative)					

Table 4.8 Effect of flange slenderness ratio t/b on percentage difference between standard moment gradients and FEA moment gradients for the case of full reversed moment distribution

		ST0-L	**ST1-L**	**ST2A-T**	**ST2B-T**
ANSI/AISC 360-10	Low	-12.2%	-15.4%	-16.8%	-20.9%
	Average	-9.6%	-14.3%	-15.6%	-21.5%
	High	-5.2%	-12.8%	-13.8%	-21.8%
CAN/CSA S16-09 GENERAL	Low	-10.8%	-14.0%	-15.5%	-19.6%
	Average	-8.1%	-13.0%	-14.3%	-20.2%
	High	-3.7%	-11.4%	-12.4%	-20.5%
AS 4100-1998	Low	-7.1%	-10.5%	-12.0%	-16.3%
	Average	-4.4%	-9.4%	-10.7%	-17.0%
	High	0.3%	-7.8%	-8.8%	-17.2%
CAN/CSA S16-09 LINEAR	Low	-3.4%	-6.9%	-8.5%	-13.0%
	Average	-0.5%	-5.8%	-7.2%	-13.6%
	High	4.3%	-4.1%	-5.2%	-13.9%
EN 1993-1-1 GUIDE	Low	6.3%	2.5%	0.7%	-4.2%
	Average	9.5%	3.7%	2.2%	-4.9%
	High	14.8%	5.6%	4.4%	-5.3%
All percentages are calculated by $\left(C_{st} - C_{FEA}\right)/C_{FEA}$. Positive values indicate that applicable standards overestimates member capacity					

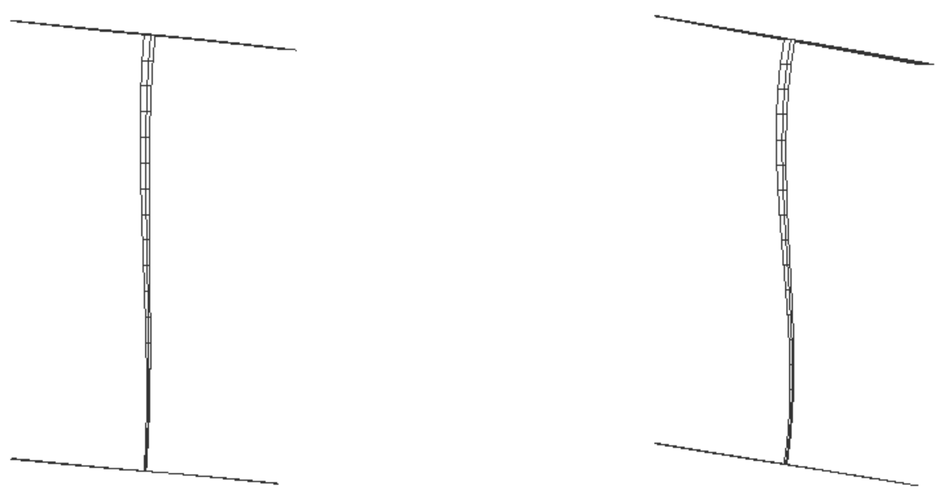

(a) (b)

Fig. 4.11- Buckled configurations of ST0-L detail: (a) $t/b = 0.0556$, and (b) $t/b = 0.0909$

4.6.3. Comparative Evaluation of Effect of End Details

As suggested by Fig. 4.10(a-c), depending on the values of the section dimensionless parameters, the choice of end detail has a significant contribution on the resulting M_{cr}/M_u ratio. The most pronounced example was observed to take place in beams subject to fully reversed moment gradient distributions with thick flanges (t/b is high). As depicted in Fig. 4.12 (a-d), M_{cr}/M_u varies from 2.398 (ST0-L detail) to 2.905 (ST2B-T detail). From the FEA, it is concluded that the ST0-L detail always corresponds to the lowest M_{cr}/M_u values. Thus, a moment gradient factor equation M_{cr}/M_u for the ST0-L detail, would be conservative for all four end details.

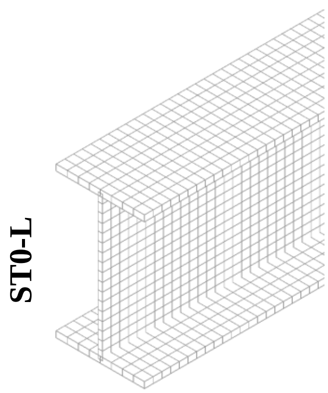

$$\frac{M_{cr}}{M_u} = 2.398$$

(a)

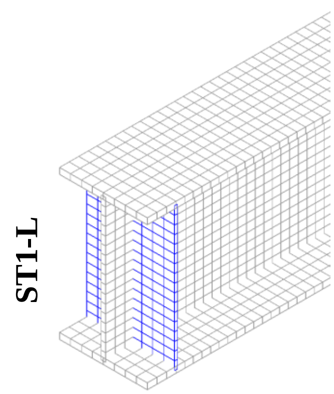

$$\frac{M_{cr}}{M_u} = 2.606$$

(b)

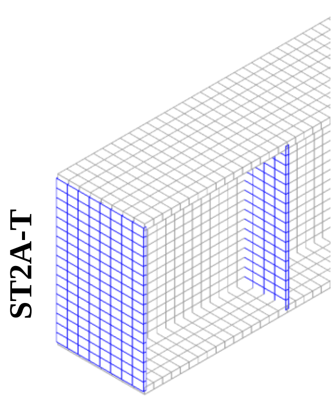

$$\frac{M_{cr}}{M_u} = 2.636$$

(c)

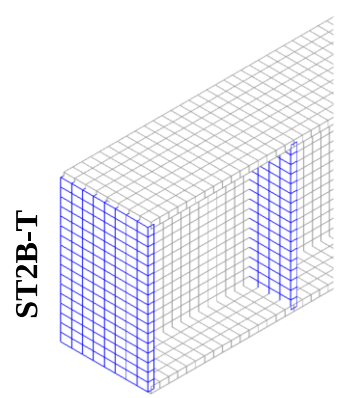

$$\frac{M_{cr}}{M_u} = 2.905$$

(d)

Fig. 4.12- Comparison of end details (a) ST0-L, (b) ST1-T, (c) ST2A-T, and (d) ST2B-T

4.6.4. Effect of Width to Height Ratio

Fig. 4.12(a-c) provides the moment gradient factors as determined by FEA versus the web to height ratio b/h for all details considered when subject to uniform, triangular, and fully reversed moment distributions. A comparison of moment gradient factors as determined from the FEA in the present study to those predicted by the various standards is presented in Table 4.9 - Table 4.11. Finally, Fig. 4.14 presents buckled configurations of the ST2A-T detail when the beam is subject to a triangular moment distribution for $b/h = 0.81$.

A comparison of Fig. 4.12(a-c) suggests that with the exception of sudden drops in the moment gradient factors, the general trends of the change in M_{cr}/M_u when a beam is subject to a linear moment distribution is the same as those of a beam subject to a uniform moment. The reader is referred to Subsection 3.10.4 for supporting explanations.

As for the sudden declines in the M_{cr}/M_u ratio, Table 4.10 and Table 4.11 suggest that all standards grossly overestimate the M_{cr}/M_u ratio when $b/h = 0.81$. The overestimation is most significant for EN 1993-1-1 where it is observed to be 27.5%. To explain this observation, Fig. 4.14(a-c) depicts various buckled configuration snapshots of the ST2A-T detail while subject to a triangular moment distribution for $b/h = 0.81$. It is evident from the Figures that the beam is not failing in a LTB mode, but rather a localized failure of the web stiffeners is taking place. This is due to the combination of the large magnitude of forces and the load application scheme. The reader is referred to Section 3.7 for information pertaining to the load application scheme. The observed localized mode of failure is not a lateral torsional buckling failure mode and, potentially, should not be considered when formulating standards lateral torsional buckling provisions. Nevertheless, it remains an important design criterion governing that should be recognized and accounted for when designing the end connections.

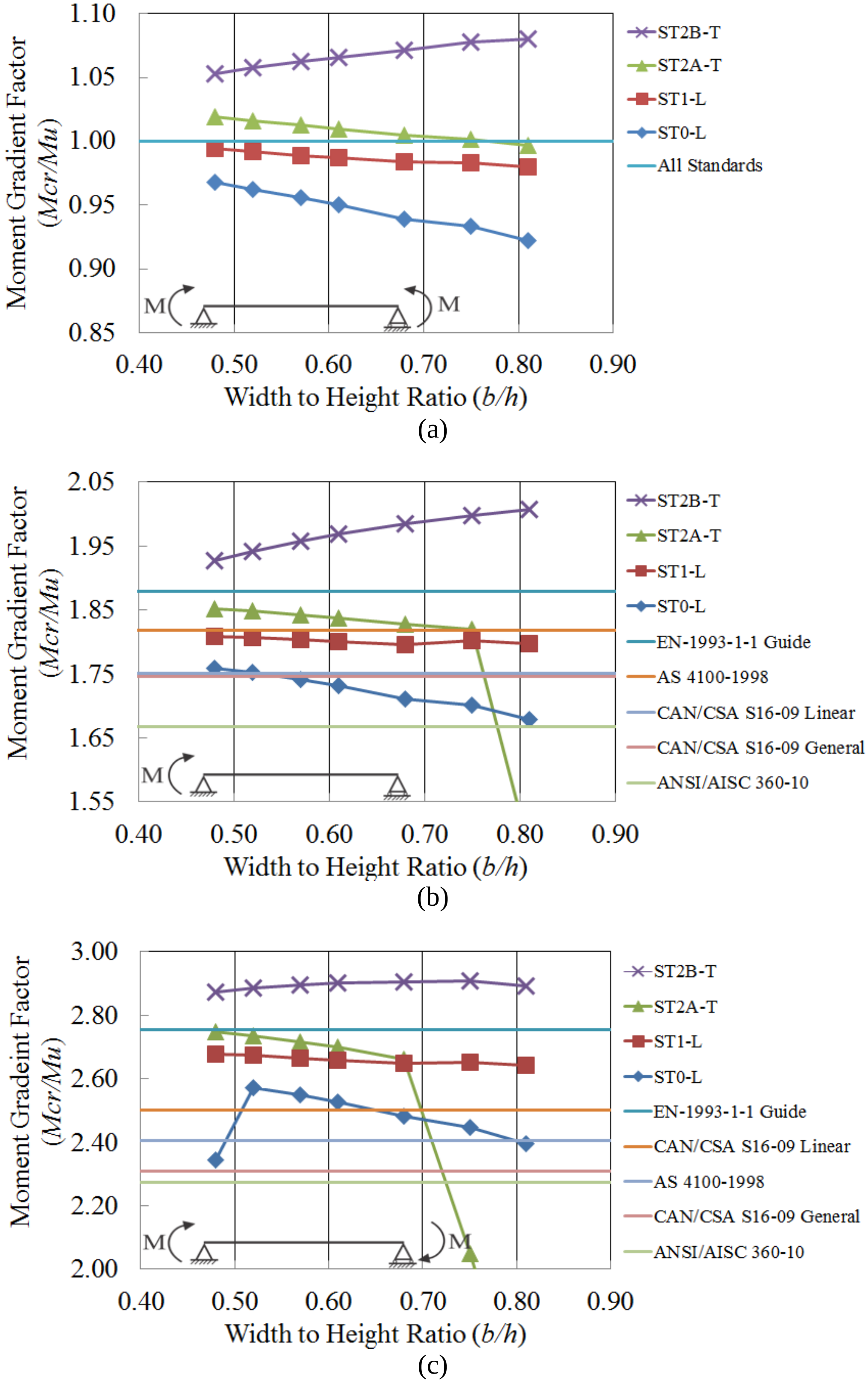

Fig. 4.13- Effect of aspect Ratio on FEA predicted moment gradient factors for beams subject to (a) Uniform, (b) Triangular, and (c) Reverse moments

Table 4.9 Effect of aspect ratio b/h on percentage difference between standard moment gradients and FEA moment gradients for the case of uniform moment distribution

		ST0-L	ST1-L	ST2A-T	ST2B-T
All Standards	Low	3.2%	0.6%	-1.9%	-5.3%
	Average	5.3%	1.3%	-0.9%	-6.7%
	High	7.8%	2.0%	0.3%	-8.0%
All percentages are calculated by $\left(C_{st}-C_{FEA}\right)/C_{FEA}$. Positive values indicate that applicable standards overestimate member capacity (un-conservative)					

Table 4.10 Effect of aspect ratio b/h on percentage difference between standard moment gradients and FEA moment gradients for the case of triangular moment distribution

		ST0-L	ST1-L	ST2A-T	ST2B-T
ANSI/AISC 360-10	Low	-5.2%	-7.8%	-9.9%	-13.5%
	Average	-3.3%	-7.5%	-6.6%	-15.3%
	High	-0.7%	-7.2%	13.1%	-16.9%
CAN/CSA S16-09	Low	-0.5%	-3.2%	-5.5%	-9.2%
	Average	1.5%	-2.9%	-2.0%	-11.1%
	High	4.3%	-2.6%	18.7%	-12.8%
AS 4100-1998	Low	3.3%	0.5%	-1.8%	-5.7%
	Average	5.4%	0.8%	1.8%	-7.7%
	High	8.3%	1.1%	23.3%	-9.4%
EN 1993-1-1 GUIDE	Low	6.8%	3.9%	1.5%	-2.5%
	Average	9.0%	4.3%	5.2%	-4.6%
	High	12.0%	4.6%	27.5%	-6.3%
All percentages are calculated by $\left(C_{st}-C_{FEA}\right)/C_{FEA}$. Positive values indicate that applicable standards overestimates member capacity					

Table 4.11 Effect of aspect ratio b/h on percentage difference between standard moment gradients and FEA moment gradients for the case of full reversed moment distribution

		ST0-L	**ST1-L**	**ST2A-T**	**ST2B-T**
ANSI/AISC 360-10	Low	-3.0%	-15.1%	-17.3%	-20.8%
	Average	-8.1%	-14.5%	-6.8%	-21.4%
	High	-5.0%	-13.9%	54.1%	-21.4%
CAN/CSA S16-09 GENERAL	Low	-1.5%	-13.7%	-16.0%	-19.6%
	Average	-6.6%	-13.2%	-5.4%	-20.2%
	High	-3.5%	-12.6%	56.5%	-20.2%
AS 4100-1998	Low	2.6%	-10.2%	-12.5%	-16.3%
	Average	-2.8%	-9.6%	-1.5%	-16.9%
	High	0.5%	-9.0%	63.0%	-16.9%
CAN/CSA S16-09 LINEAR	Low	6.7%	-6.6%	-9.0%	-12.9%
	Average	1.1%	-6.0%	2.5%	-13.6%
	High	4.5%	-5.3%	69.5%	-13.6%
EN 1993-1-1 GUIDE	Low	17.5%	2.8%	0.1%	-4.1%
	Average	11.3%	3.5%	12.8%	-4.9%
	High	15.0%	4.2%	86.6%	-4.9%
All percentages are calculated by $\left(C_{st} - C_{FEA}\right)/C_{FEA}$. Positive values indicate that applicable standards overestimates member capacity					

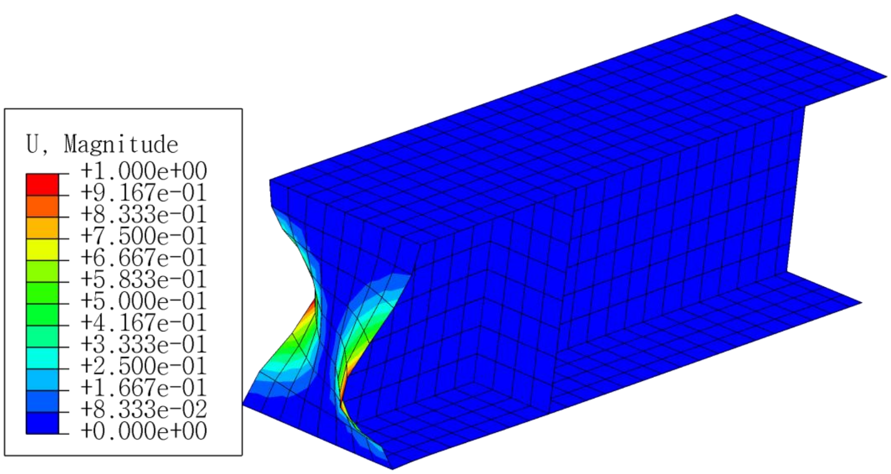

(a)

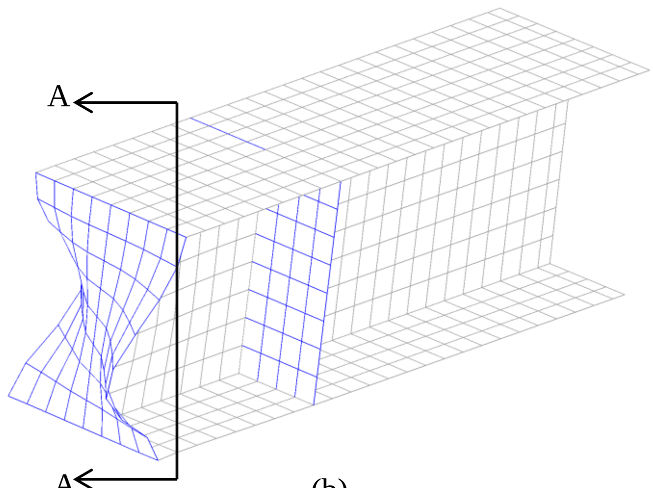

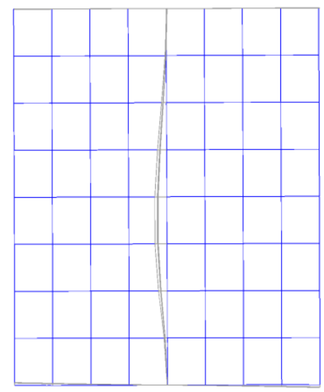

Fig. 4.14- Triangular moment distribution - $b/h = 0.81$ buckled configurations of ST0-L detail: (a) Isometric end contour plot for the lateral displacement, (b) Isometric end, and (c) Cross section

4.6.5. Effect of Beam Span to Section Height Ratio

Fig. 4.15(a-c) provides the moment gradient factor as determined by FEA versus the beam span to section height ratio l/h and a comparison of moment gradient factors as determined from the FEA in the present study to those predicted by the various standards is presented in Table 4.12 - Table 4.14.

FEA studies reveal sharp drops in M_{cr}/M_u from small l/h ratios. This is primarily due to the fact that beams tend to fail in a localized mode at lower load magnitudes than those corresponding to lateral torsional buckling failures. As such, Section 4.6.6 is dedicated to a buckling mode study which investigates this phenomenon in details.

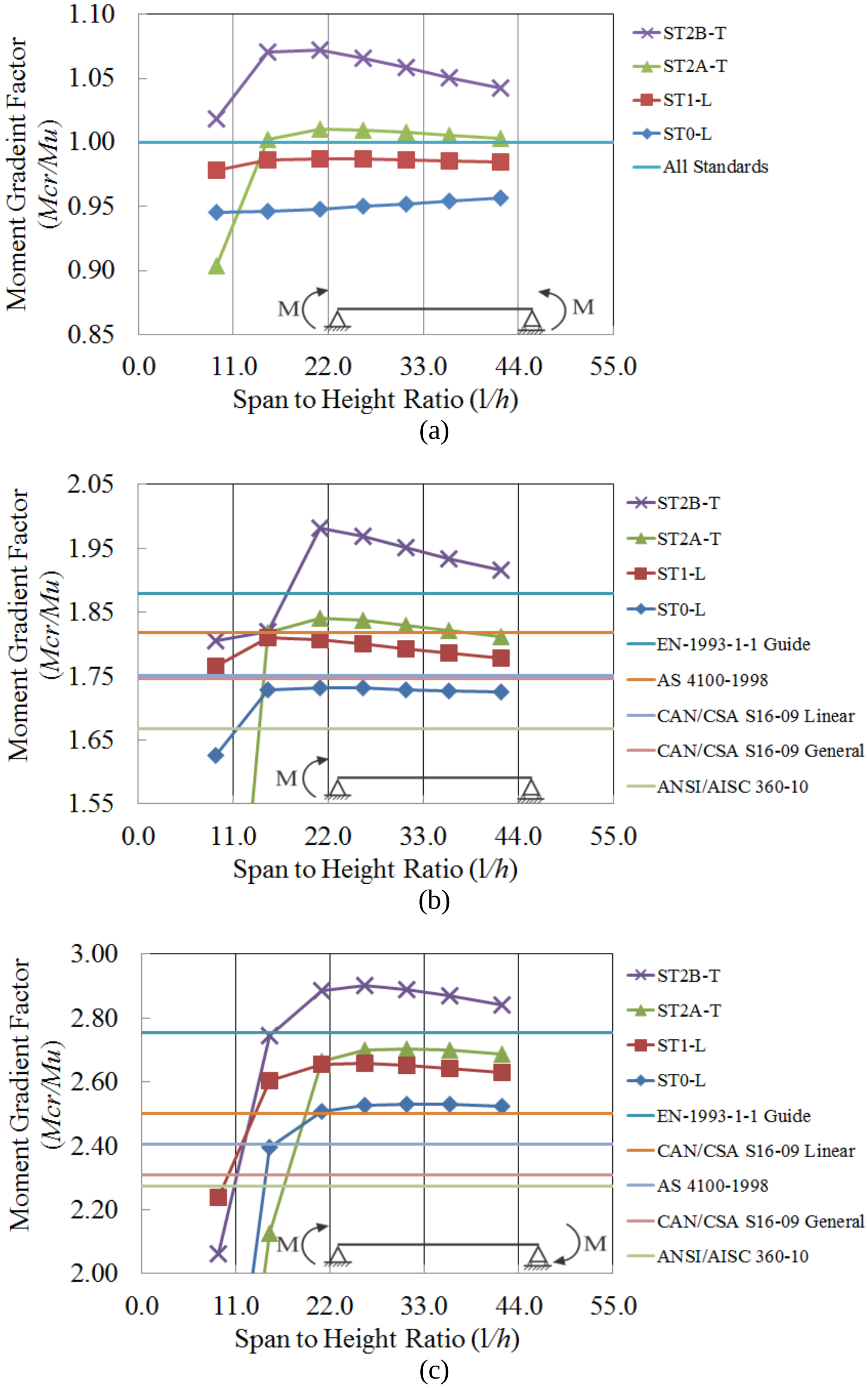

Fig. 4.15- Effect of span to height ratio on FEA predicted moment gradient factors for beams subject to (a) Uniform, (b) Triangular, and (c) Reverse moments

Table 4.12 Effect of span to height ratio l/h on percentage difference between standard moment gradients and FEA moment gradients for the case of uniform moment distribution

		ST0-L	ST1-L	ST2A-T	ST2B-T
All Standards	Low	5.5%	2.2%	9.6%	-1.8%
	Average	5.0%	1.5%	0.8%	-5.4%
	High	4.3%	1.5%	-0.3%	-4.3%
All percentages are calculated by $\left(C_{st} - C_{FEA}\right)/C_{FEA}$. Positive values indicate that applicable standards overestimate member capacity (un-conservative)					

Table 4.13 Effect of span to height ratio l/h on percentage difference between standard moment gradients and FEA moment gradients for the case of triangular moment distribution

		ST0-L	ST1-L	ST2A-T	ST2B-T
ANSI/AISC 360-10	Low	-5.2%	-7.8%	-9.9%	-13.5%
	Average	-3.3%	-7.5%	-6.6%	-15.3%
	High	-0.7%	-7.2%	13.1%	-16.9%
CAN/CSA S16-09	Low	-0.5%	-3.2%	-5.5%	-9.2%
	Average	1.5%	-2.9%	-2.0%	-11.1%
	High	4.3%	-2.6%	18.7%	-12.8%
AS 4100-1998	Low	3.3%	0.5%	-1.8%	-5.7%
	Average	5.4%	0.8%	1.8%	-7.7%
	High	8.3%	1.1%	23.3%	-9.4%
EN 1993-1-1 GUIDE	Low	6.8%	3.9%	1.5%	-2.5%
	Average	9.0%	4.3%	5.2%	-4.6%
	High	12.0%	4.6%	27.5%	-6.3%
All percentages are calculated by $\left(C_{st} - C_{FEA}\right)/C_{FEA}$. Positive values indicate that applicable standards overestimates member capacity					

Table 4.14 Effect of span to height ratio l/h on percentage difference between standard moment gradients and FEA moment gradients for the case of full reversed moment distribution

		ST0-L	ST1-L	ST2A-T	ST2B-T
ANSI/AISC 360-10	Low	89.7%	1.6%	149.0%	10.4%
	Average	-1.8%	-12.0%	-3.5%	-17.1%
	High	-9.9%	-13.5%	-15.3%	-20.0%
CAN/CSA S16-09 GENERAL	Low	92.7%	3.2%	152.9%	12.1%
	Average	-0.3%	-10.6%	-2.0%	-15.7%
	High	-8.5%	-12.1%	-14.0%	-18.7%
AS 4100-1998	Low	100.7%	7.5%	163.3%	16.8%
	Average	3.8%	-6.9%	2.1%	-12.3%
	High	-4.8%	-8.5%	-10.5%	-15.4%
CAN/CSA S16-09 LINEAR	Low	108.7%	11.8%	173.8%	21.4%
	Average	8.0%	-3.2%	6.1%	-8.8%
	High	-1.0%	-4.8%	-6.9%	-12.0%
EN 1993-1-1 GUIDE	Low	129.7%	23.0%	201.4%	33.7%
	Average	18.9%	6.6%	16.8%	0.4%
	High	9.0%	4.8%	2.5%	-3.1%
All percentages are calculated by $\left(C_{st}-C_{FEA}\right)/C_{FEA}$. Positive values indicate that applicable standards overestimates member capacity					

4.6.6. Buckling Mode Study

Analysis of the results produced through the parametric study discussed in Subsections 4.6.4 and 4.6.5 revealed that for short spans, there is a significant drop in M_{cr}/M_u. This observation held true both for triangular and fully reversed moment distributions. Since beams subject to reverse moment distributions were more susceptible to the decrease in M_{cr}/M_u, the present discussion will focus on reverse moment distributions for beams with the ST2B-T detail. Fig. 4.16 displays the deformed contour plot for the lateral displacement with $l/h=9.0$ (shortest span to depth investigated). Fig. 4.17 presents various buckled configuration snapshots of the same beam. A look at the buckled configurations suggests that the decrease in M_{cr}/M_u is attributed to localized buckling of the web in the connection region. To further assess the implications of this phenomenon on the design of beams, a FEA study on the buckling modes of a real section is conducted. A W310x52 section was chosen for the study. As presented in Table 4.15, the dimensionless parameters for the chosen section are close to the average values of the dimensionless parameters in the CISC SST section database, and are thus believed to be reasonably representative of practical section geometries.

Table 4.15 W310x52 and CISC SST mean dimensionless parameters

	w/h	t/b	b/h
W310X52	0.0249	0.0790	0.5479
CISC SST Mean	0.0384	0.1019	0.6109

The study on the W310x52 section included numerous FEA simulations which ranged from a span of 4000*mm* to 13000*mm*. Spans greater than 13000*mm* were discarded for two reasons: 1) it is unlikely that a span of 13000*mm* for a beam of such a low weight would be encountered in practice and 2) the purpose of the present study is to determine if non-LTB modes could govern design of <u>short</u> beams. The rationale behind a minimum span of 4000*mm* is based on the fact that LTB would be a contributing design factor only when the critical moment M_{cr} is less than the plastic moment resistance M_p. Given the conservative possibility of using a high grade steel with a specified minimum yield strength as high as $F_y = 700MPa$, the FEA study predicted a lateral torsional buckling moment $M_{cr} = 672.7kNm$ at a span of 4,000*mm*. This compares to a plastic moment of 583.4*kNm* at $F_y = 700MPa$. As such, spans less than 4,000*mm* can be omitted from the study since their design would be governed by yielding. Table 4.16 and Fig. 4.18 present the results of the FEA study.

Fig. 4.18 displays the first five buckling loads as a function of span. The first two loads were based on global LTB (Fig. 4.19(a)) corresponding to critical loads that are significantly lower than those based on local buckling of the web in the connection region. The black plot line in Fig. 4.18 highlights modes of failures due local buckling of the web (Fig. 4.19(b)). A complete set buckling modes is provided in Appendix C. The corresponding buckling loads are observed to be independent of spans. As such, the drop in M_{cr}/M_u values observed in Subsections 4.6.4 and 4.6.5 would only be of theoretical interest for the section considered. This study suggests that, at least for common section geometries, web local buckling in the connection region will not govern the design. A more comprehensive study on other cross-sections would be needed to confirm or disprove this hypothesis.

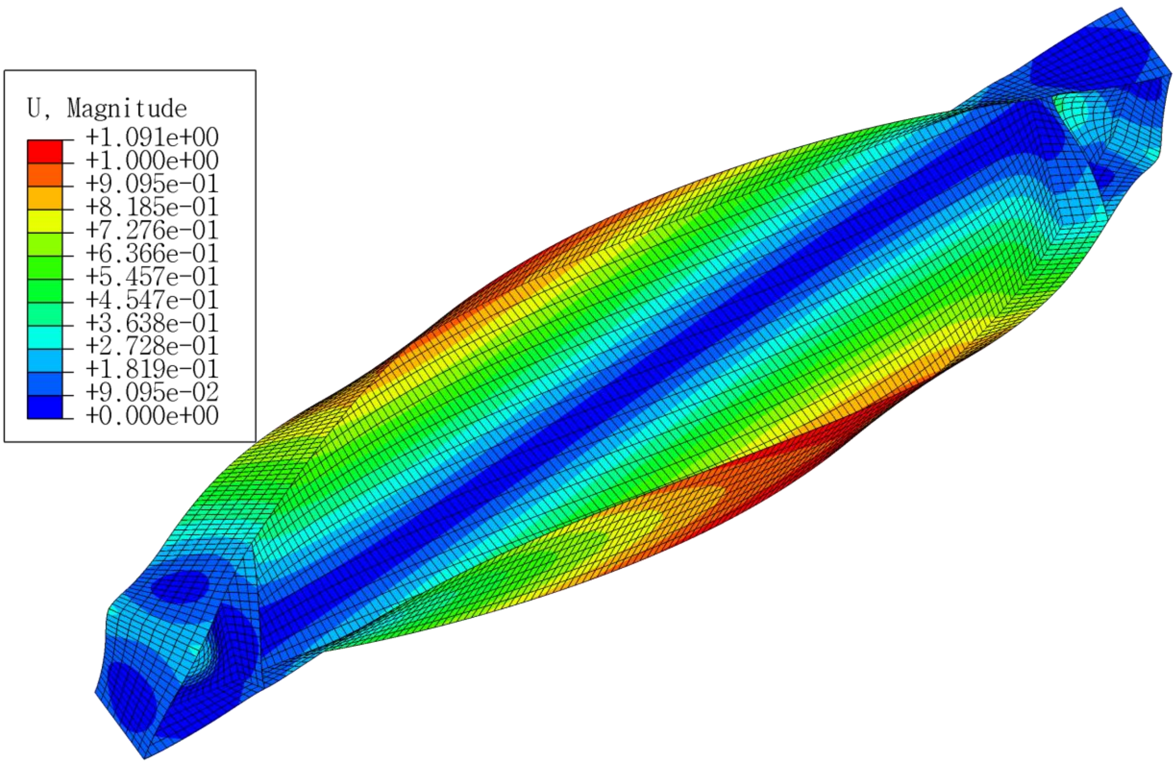

Fig. 4.16- ST2B-T Detail subject to reverse moment $l/h = 9$ isometric contour plot for the lateral displacement

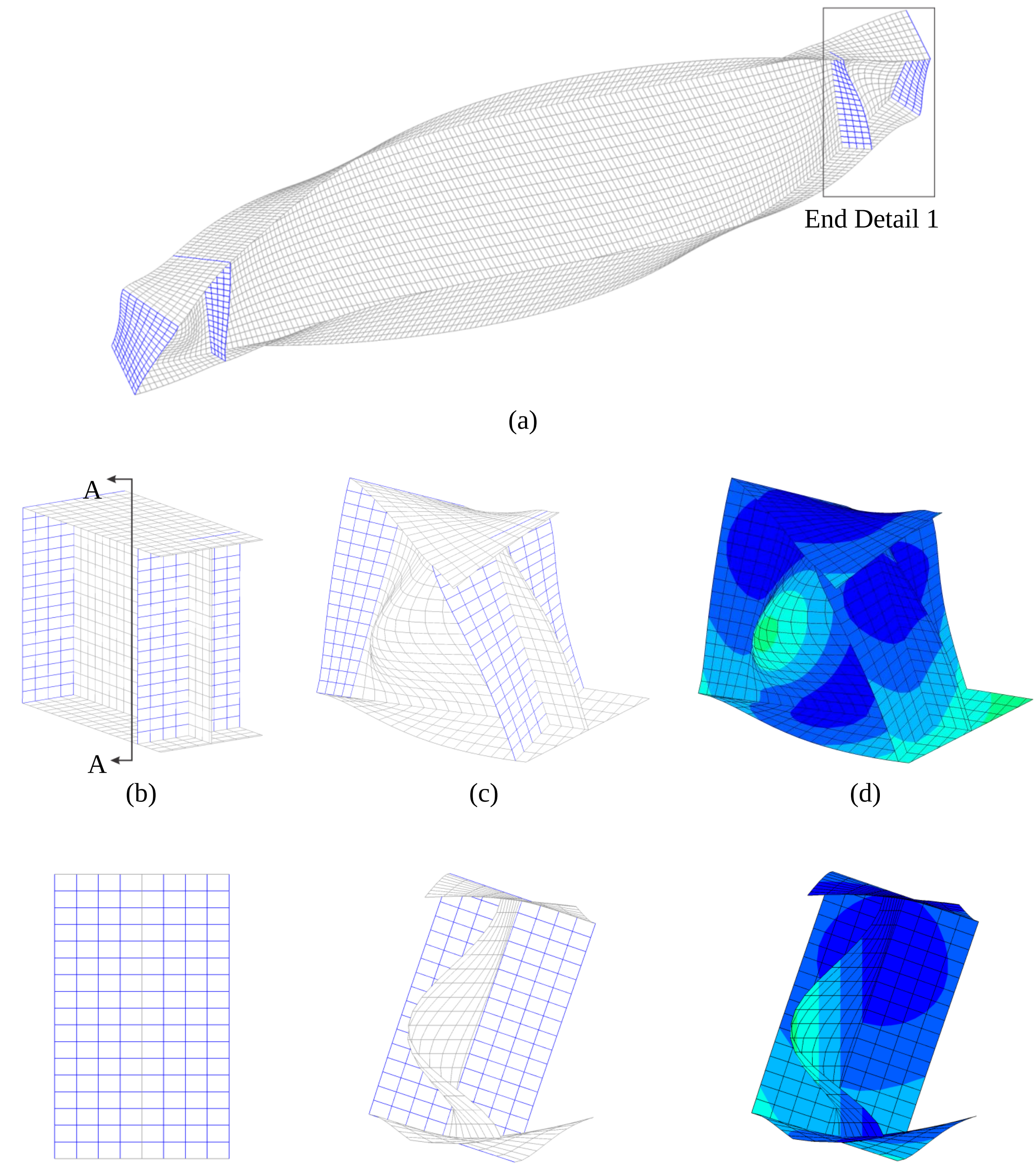

Fig. 4.17- ST2B-T Detail subject to reverse moment $l/h = 9$: (a) Overall buckled configuration, (b) End detail 1 - undeformed, (c) End detail 1- buckled, (d) End detail 1- displacement contour, (e) Section A-A - undeformed, (f) Section A-A - buckled, and (g) Section A-A – contour

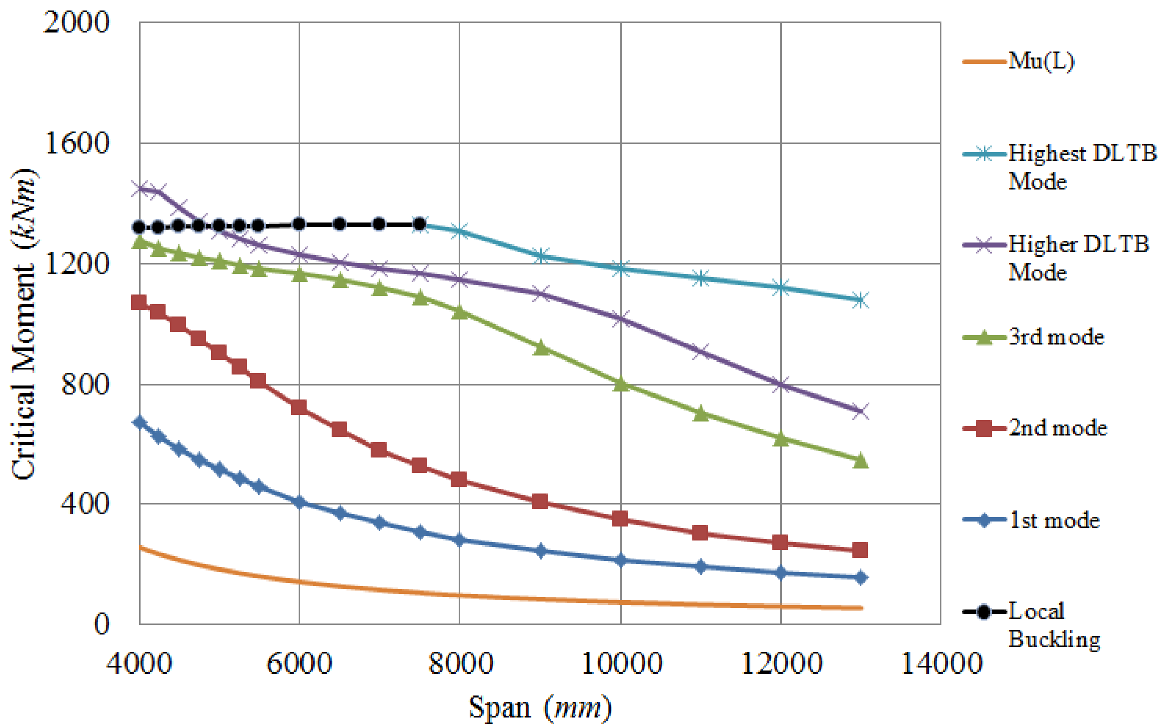

Fig. 4.18- W310x52 FEA critical moment results plot

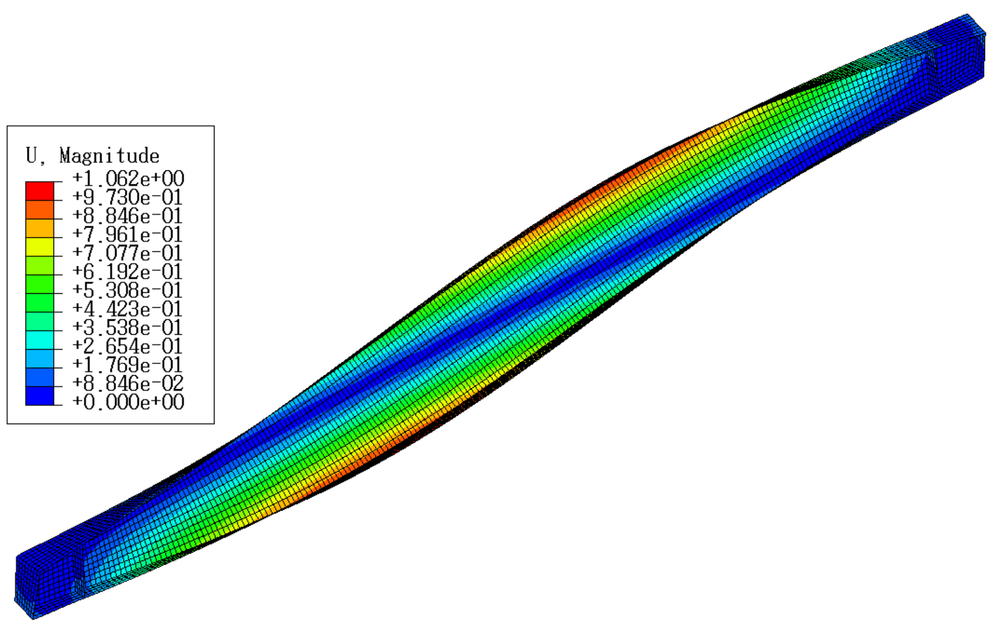

(a)

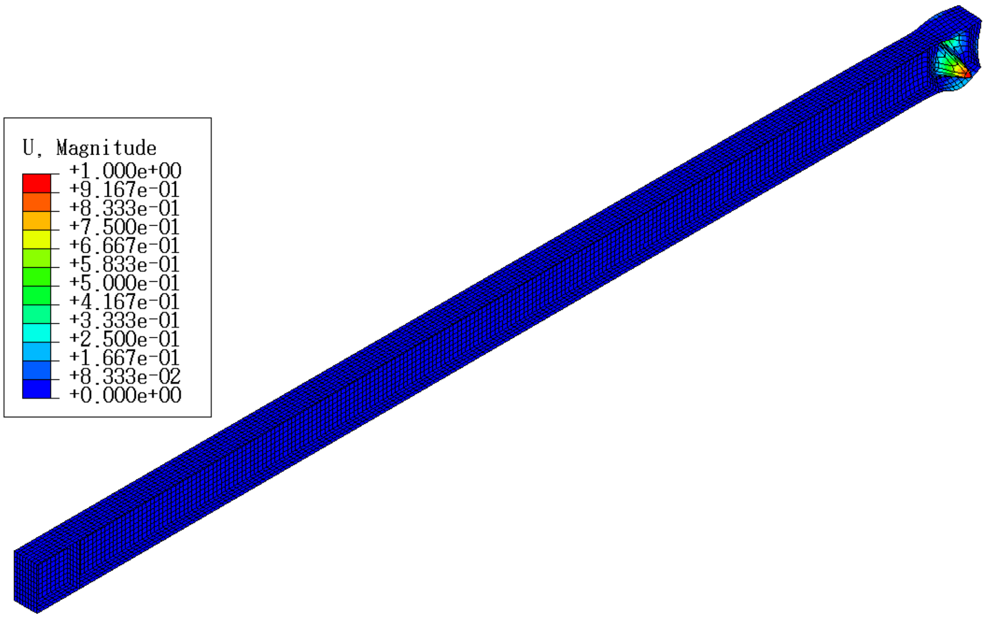

(b)

Fig. 4.19- Deformed contour plots of (a) 1st Mode LTB, and (b) Local buckling

Table 4.16 W310x52 FEA critical moments for first five buckling modes

	Critical Moment (kNm) based on various buckling modes							
l (mm)	1st	2nd	3rd	Higher DLTB Mode	Highest DLTB Mode	Local Buckling	M_u (kNm)	$\frac{M_{cr}}{M_u}$
4000	672.7	1070	1274	1446	-	1319	257.7	2.610
4250	627.3	1036	1253	1435	-	1320	234.7	2.673
4500	586.2	995.1	1235	1385	-	1322	215.2	2.724
4750	548.9	949.9	1220	1341	-	1322	198.6	2.764
5000	515.2	902.2	1207	1307	-	1324	184.3	2.795
5250	484.8	854.0	1195	1281	-	1325	171.8	2.822
5500	457.3	807.1	1185	1260	-	1326	160.9	2.842
6000	409.6	720.5	1166	1227	-	1327	142.6	2.872
6500	370.0	645.3	1146	1203	-	1328	128.1	2.888
7000	336.9	581.0	1122	1183	-	1329	116.3	2.897
7500	308.7	526.2	1089	1165	-	1330	106.4	2.901
8000	284.7	479.5	1043	1147	1310	-	98.18	2.900
9000	245.9	404.9	923.9	1099	1225	-	85.03	2.892
10000	216.0	348.7	803.9	1016	1184	-	75.06	2.878
11000	192.4	305.3	701.9	905.1	1154	-	67.23	2.862
12000	173.4	270.9	618.3	799.4	1122	-	60.91	2.847

4.7. Summary and Conclusions

The following observations can be made about the moment gradient factor for triangular moment distributions. Only applicable admissible FEA runs which were observed to fail in pure LTB mode were considered in providing the following conclusions.

- EN 1993-1-1 provides the least conservative predictions of M_{cr}/M_u by consistently overestimating moment gradient factors for all details except the ST2B-T detail.

- Depending on the values of the dimensionless ratios (w/h, t/b, b/h, l/h), the ratio M_{cr}/M_u may agree or vary from standard dependent moment gradient factors, making some of the standard predictions conservative in some cases or un-conservative in other cases. An example of this can be found in Subsection 4.6.2 where depending on the value of t/b, both ANSI/AISC 360-10 and CAN/CSA S16-09 can yield acceptably conservative results or unacceptable overestimations.

- When assessing the moment gradient factor predictions in various standards, ANSI/AISC 360-10 provides the most conservative predictions of the moment gradient. Only one out of the 96 admissible FEA runs was overestimated by ANSI/AISC 360-10.

For fully reversed moment gradients ANSI/AISC 360-10 and CAN/CSA S16-09 provide conservative moment gradient factor predictions for all admissible FEA results. With the exception of three out of the 90 admissible FEA results, AS 4100-1998 normally provides conservative predictions for the moment gradient factor.

4.8. Notation for Chapter 4

b	flange width
C_{st}	standard dependent moment gradient factor
C_{FEA}	moment gradient factor as determined by FEA
F_y	specified minimum yield stress
h	distance between flange centroids
l	length of unbraced portion of beam
M	applied moment
M_a	factored bending moment at one-quarter point of unbraced segment
M_b	factored bending moment at mid-point of unbraced segment
M_c	factored bending moment at three-quarter point of unbraced segment
M_{cr}	elastic critical moment capturing the effects of distortional buckling
$M_{\max}$	maximum factored bending moment magnitude in unbraced segment
M_p	plastic moment resistance
M_r	elastic lateral torsional buckling resistance

M_u classical lateral torsional buckling solution

P applied point load

t flange thickness

w web thickness

κ ratio of smaller factored moment to the larger factored moment at ends of unbraced length

Chapter 5

Distortional Lateral Torsional Buckling of Simply Supported Beams with Mid-span Loads

5.1. Objective and Scope

In this chapter, the distortional lateral torsional buckling moments are determined for simply supported beams with realistic cross-sections, end details, and loading conditions subjected to mid-span loads. This is achieved by conducting a series of FEA runs on commonly used cross-sections in the CISC database. Attention is focused on beams with web cleat end details subject to mid-span load.

5.2. Description of Web Cleats

One of the most common steel connections in steel framed structures is a web cleat. Web cleats are used as simple shear connections and consist of double angles of equal size. Fig. 5.2 illustrates a web cleat connection. Commonly, the supported beam is connected to the web cleats through bolts and the web cleats are attached to the supporting member either thorough bolts or fillet weld. Standard A325 bolts with 20*mm* diameters are commonly used in steel buildings. Therefore, all bolts in the present study are assumed to be 20*mm* in diameter.

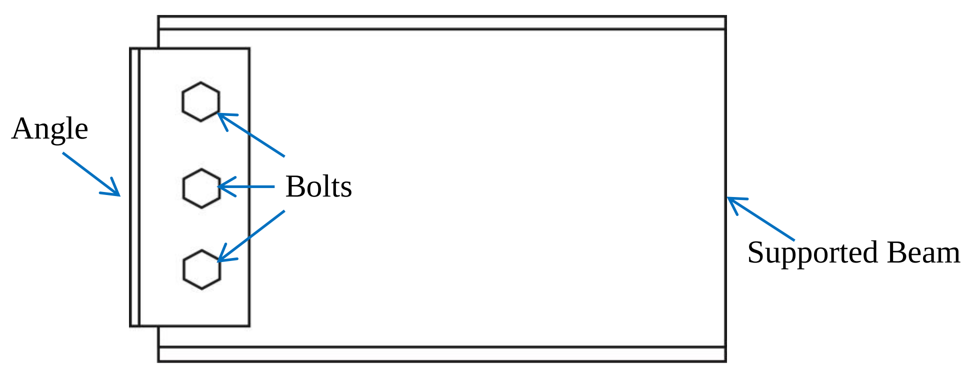

Fig. 5.1- Web cleat connection schematic

5.3. *Description of Finite Element Model*

Simulation of Web Cleat Connection

In order to fully capture the contact between the various elements of the web cleat connections during beam failure in a LTB mode, the web cleat/ bolt connection would have to be modeled as 3-dimensional solids. However, since the purpose of the present study is to capture the global effect of end connections details on web distortion throughout buckling, as opposed to local influence of bolts on the web, a full 3-dimensional solids model was judged unnecessary. As an efficient alternative, the FEA models are built using shell elements. The beam and all four angles are modeled as separate parts and are then combined into a single assembly where the beam is connected to the angles through modelling features which approximately simulate the effects of bolts. Simulation of bolt connections is discussed in the latter part of this section. Fig. 5.2(a-b) displays Abaqus snapshots of the web cleats alone and within the entire assembly.

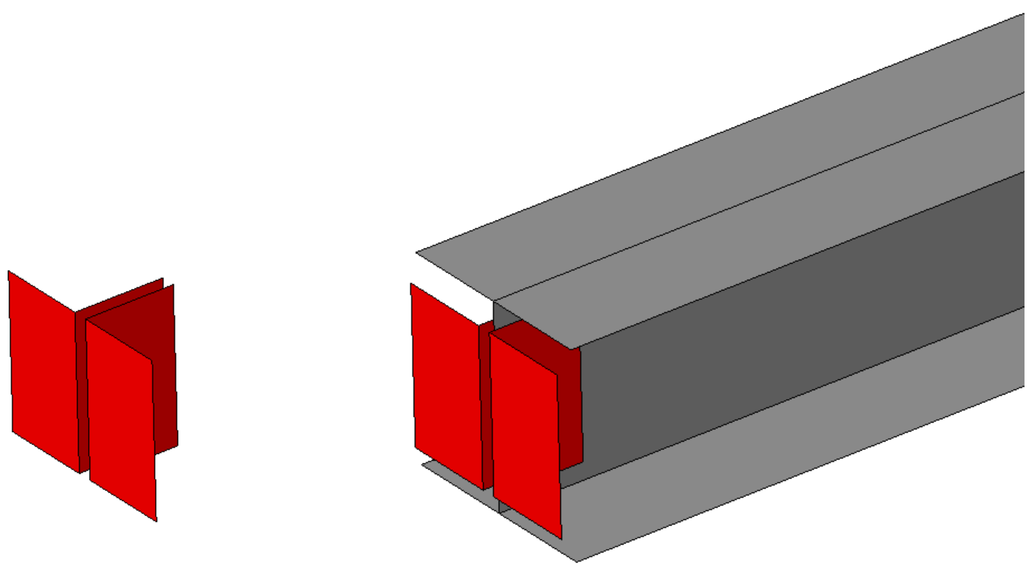

(a) (b)

Fig. 5.2- Abaqus modeling snapshots of (a) Web cleats, and (b) Web cleat & beam assembly

Simulation of Boundary Conditions

The boundary conditions were chosen to simulate a welded connection between the angle toes and the supporting member (typically a column). This is representative of typical field assembly practice where the supporting member would be shipped with welded angles and the beam would be simply dropped into place and the two components fastened on site. To simulate the boundary conditions of a weld, nodal translations in the x, y, and z axes were restrained along the entire length of the angle toe. A schematic of the boundary conditions is depicted in Fig. 5.3.

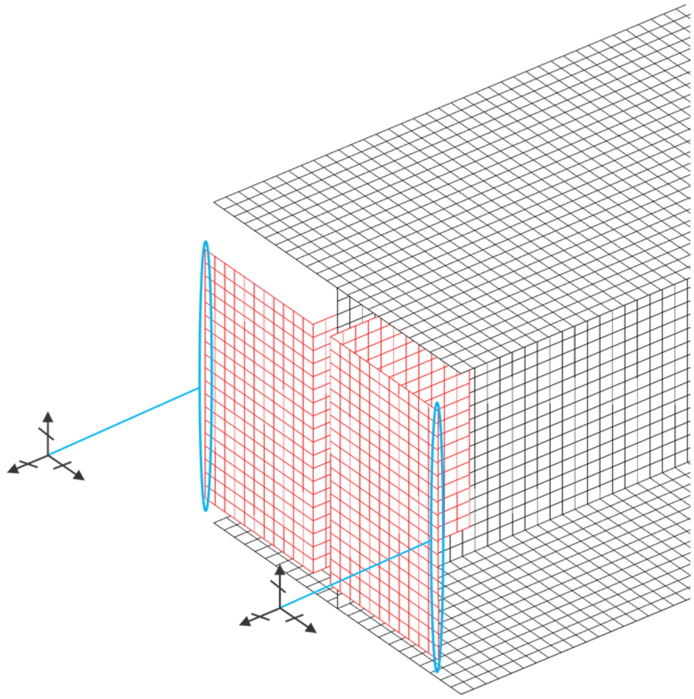

Fig. 5.3- Boundary conditions simulating a web cleat connection

Simulation of Loading

The loading scheme chosen for the FEA runs in this chapter is a point load at mid span. A schematic of a mid-span point load and its corresponding moment diagram can be seen in Fig. 5.4(a-b).

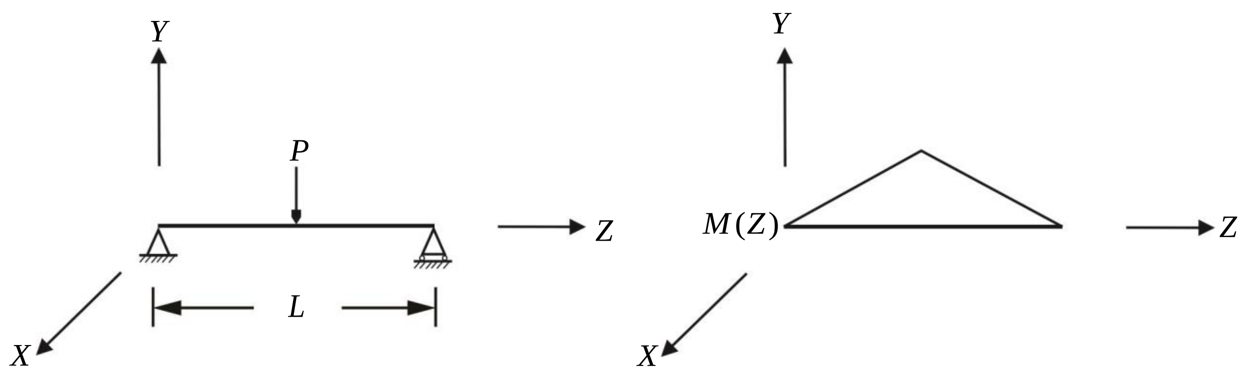

(a) (b)

Fig. 5.4- Point load at mid-span (a) Schematic, and (b) Bending moment diagram

In the FEA model, the applied load P at mid-span was simulated by applying two equal point loads $P/2$ acting both at the top and bottom web to flange junctions at the beam mid-span. The decision to simulate the single point load with the use of two loads serves two purposes: a) by splitting the force and applying it at both web to flange junctions, local distortion around the point load is eliminated, and b) the resultant of the forces is equivalent to that of a single point load acting at web mid-span which is consistent with code based solutions which do not account for load position effect relative to the section shear centre. The load application scheme is illustrated in Fig. 5.5.

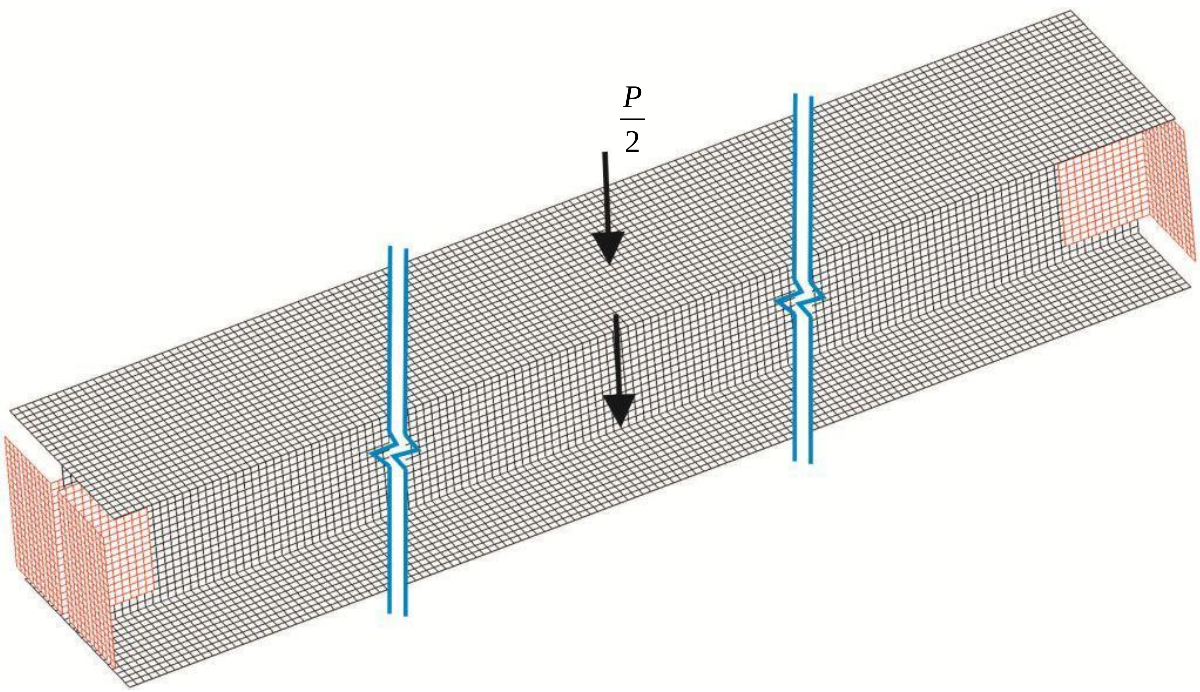

Fig. 5.5- Abaqus model point load application

Using the equations introduced in Chapter 2, the moment gradient factor for simply supported beams under the action of a mid-span point load are provided in Table 5.1. For quarter-point methods in ANSI/AISC 360-10, CAN/CSA S16-09, and AS 4100-1998, the moment values at quarter points are $M_a = 0.50M_{\max}$, $M_b = M_{\max}$, and $M_c = 0.50M_{\max}$ as a proportion of the maximum moment $M_{\max}$ at mid-span.

Table 5.1 Code moment gradient factors for beams subject to mid-span point load

Standard	Moment Gradient Factor
ANSI/AISC 360-10	1.316
CAN/CSA S16-09 General	1.265
AS 4100-1998	1.388
EN 1993-1-1 Guide	1.365

Simulation of Bolt Connections

Bolts were simulated through the use of the “Discrete Fasteners” feature in Abaqus. The modeling process involves choosing the surfaces that are to be fastened. In the present problem, this would be the beam and both angles. This is then followed by specifying the quantity, location and radius of influence of the points on each surface that are needed for fastening (for the present application, this would be the number of bolts, the location of the bolts, and the radius of each bolt). Finally, a choice of the coupling type must be specified. For the purpose of this study “Structural Coupling” was chosen.

Abaqus/CAE User’s Manual describes structural coupling as “a method which couples the translation and rotation of each fastening point to the translation and the rotation motion of the group of coupling nodes on each of the fastened surfaces.” In the present study, the rotation and motion of the nodes within the radius of influence on the web cleats is coupled to the rotation and motion of the nodes within the radius of influence on the beam web. It is important to note that the above mentioned procedure is different from node to node coupling. Rather, it is a weighted average of the rotations and translations of the nodes within the radius of influence on the beam that is taken, and all the nodes within the radius of influence on the web cleats are coupled to that weighted average. Fig. 5.6(a-b) displays Abaqus model snapshots of the radius of influence and the fasteners.

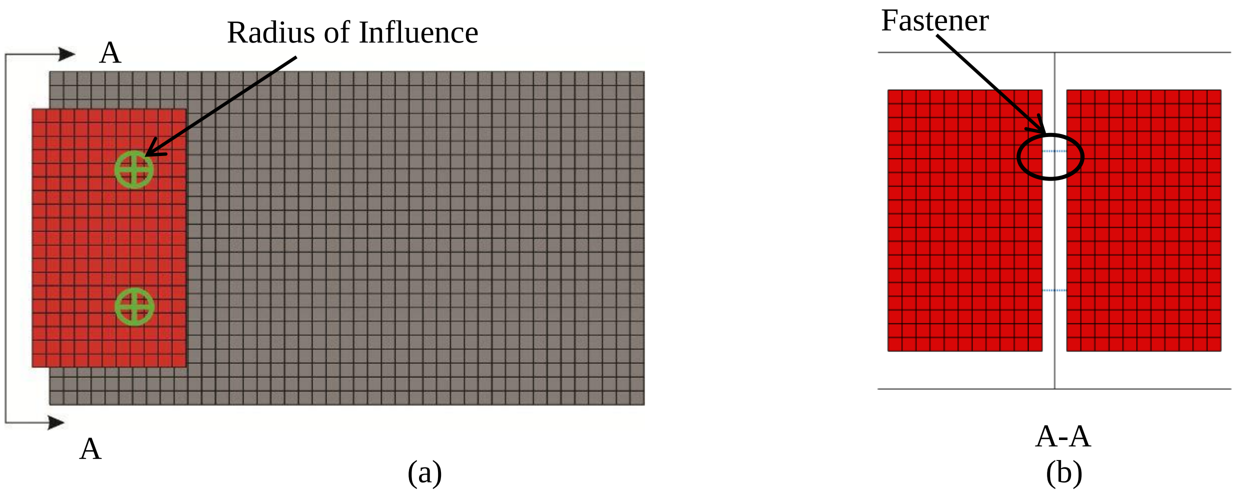

Fig. 5.6- Abaqus model's representation of (a) Radius of influence, and (b) Fasteners

Finite Element Mesh

The use of fasteners in Abaqus introduces additional constraints on the selection of the mesh fineness. To simulate a 20*mm* bolt, a radius of influence of 10*mm* must be defined. In order for the surfaces to be coupled, the specified radius of influence must contain at least three nodes. There are two ways to satisfy this condition, either by increasing the number of nodes per unit area or by increasing the radius of influence. Since the radius of influence is dictated by the 20*mm* bolt size, the condition must be satisfied by increasing the mesh fineness, thus increasing the number of nodes per unit area. A mesh sensitivity analysis for several W310 sections was conducted and it was determined that an approximate global size of 0.008 is most suitable when seeding the mesh. Within the Abaqus environment, the approximate global size is a factor of the basic unit of measurement chosen for modeling and analysis. The basic unit of measurement used is one meter. Since $0.008 \times 1m = 8mm$, this results in an element size of approximately $8mm \times 8mm$.

5.4. Parametric Runs

5.4.1. Selection of Cross-Sections

The FEA study of real sections was conducted for W310, W200, and W150 series sections from the CISC SST tables. All sections in the W200 and W150 sections were analyzed while for the W310s only sections W310x21 through W310x107 were studied. It was reasoned that W310 sections heavier than W310x107 would be predominantly used as columns rather than beams and thus would not be of interest in the present study aiming at investigating lateral torsional buckling for pure flexural members.

5.4.2. Selection of Spans

The purpose of this study is to investigate distortional effects on the LTB capacity of beams while mimicking, as close as possible, realistic design conditions. To remain consistent with this objective, beam spans were chosen to ensure that an elastic LTB mode to take place based on standards predictions. As such, for Class 1 and 2 sections, limiting span values $l_{\lim}$ were calculated by equating the inelastic lateral torsional buckling moment M_{in} to $0.67M_p$ and solving for the span $l_{\lim}$ yielding

$$l_{\lim} = \frac{\pi}{\sqrt{\dfrac{-\left(GJEI_y\right)C_{st}{}^2 + \sqrt{\left(GJEI_y\right)^2 C_{st}{}^4 + 4\left(0.44\right)\left(M_p\right)^2 E^2 I_y C_w}}{2C_{st}{}^2 E^2 I_y C_w}}} \qquad [5.1]$$

For Class 3 sections a similar equation is used while replacing of the plastic moment M_p with the yield moment M_y. The presence of the moment gradeint factor constant C_{st} is noted in Eq. [5.1]. If the moment gradient factor C_{st} is conservatively taken equal to unity in the calculation, the corresponding limiting span $l_{\lim}$ would correspond to the smallest value possible for the span. Beams with spans less than $l_{\lim}$ would not fail in an elastic LTB mode (according to Standard provisions), but rather in an inelastic buckling mode. For the purpose of determining $l_{\lim}$, the quarter point method based CAN/CSA S16-09 value of $C_{CAN-Gen} = 1.265$ was used. Various span values $L > l_{\lim}$ were investigated with spans L rounded up to the nearest $100mm$. Lastly, an upper limit of $l_{\max} = 12000mm$ was enforced to ensure realistic spans were chosen in the database of simulations.

5.4.3. Selection of Cleat Angles

With the exception of two simulations, angles with L89x89x6.4 cross-sections were adopted in all FEA simulations. The two extra runs used angles with L89x89x9.5, and L89x89x13 cross-sections to investigate the effect of twisting end restraint provided by the cleat angle on the LTB resistance of the beam. For all runs, the depth h_c of the angles varied depending upon the beam depth. Design aids provided in CAN/CSA S16 (2009) were used as a guideline for the selection of angle length and bolt spacing.

Summary of Parametric Runs

Table 5.2 provides a summary of all FEA runs conducted. The distance of angle heel to bolt centerline for all runs is taken as $L_c = 52.6mm$ while the depth h_c of cleat angles depends on the beam depth and is provided in the table. In total, there are 38 runs. Runs 1-15 are for W310 sections, 16-29 are for W200 sections and 30-38 for W150 sections. It is noted that runs 16-18 have the same cross-section (W200x100) and span (12,000*mm*), but different cleats in order to investigate the effect of partial twisting restraint provided by the web cleat on the LTB resistance of the supported beam.

Table 5.2 Summary of FEA runs

Run #	Beam		Angle Cleat		Run #	Beam		Angle Cleat	
	Section	span (*mm*)	Section L89x89x	h_c (*mm*)		Section	span (*mm*)	Section L89x89x	h_c (*mm*)
1	W310x107	12000	6.4	230	20	W200x71	12000	6.4	150
2	W310x97	12000	6.4	230	21	W200x59	10300	6.4	150
3	W310x86	11200	6.4	230	22	W200x52	10400	6.4	150
4	W310x79	10500	6.4	230	23	W200x46	9300	6.4	150
5	W310x74	8200	6.4	230	24	W200x42	7200	6.4	150
6	W310x67	7700	6.4	230	25	W200x36	7100	6.4	150
7	W310x60	7200	6.4	230	26	W200x31	5100	6.4	150
8	W310x52	5700	6.4	230	27	W200x27	5000	6.4	150
9	W310x45	5300	6.4	230	28	W200x21	4500	6.4	150
10	W310x39	5400	6.4	230	29	W200x22	3400	6.4	150
11	W310x31	5000	6.4	230	30	W200x19	3400	6.4	150
12	W310x33	3100	6.4	230	31	W200x15	3100	6.4	150
13	W310x28	2900	6.4	230	32	W150x37	8200	6.4	100
14	W310x24	2600	6.4	230	33	W150x30	7600	6.4	100
15	W310x21	2800	6.4	230	34	W150x22	6100	6.4	100
16	W200x100	12000	13	150	35	W150x24	4800	6.4	100
17	W200x100	12000	9.5	150	36	W150x18	3800	6.4	100
18	W200x100	12000	6.4	150	37	W150x14	3600	6.4	100
19	W200x86	12000	6.4	150	38	W150x13	3500	6.4	100

5.5. *Results*

5.5.1. Critical Moment Results and Mode Shapes

The results of each designation are presented separately for each of the W310, W200, and W150 series. The results for each set consist of a table which lists the section designations investigated along with their respective span L, critical moment M_u as predicted by the classical equation for the case of uniform moment, the critical moment M_{FEA}, as determined by the FEA model, and the ratio M_{FEA}/M_u.

5.5.1.1. Results for W310 Series

Table 5.3 and Fig. 5.7 summarize the results for the W310 series of sections. M_{FEA}/M_u values range from 1.227 (for W310x52) to 1.337 (for W310x21). The M_{FEA}/M_u ratio can be regarded as a factor accounting for moment gradient, distortion effects, and any other effects accounted for in the finite element model but not in the classical beam solution for the critical moment. This factor will be subsequently denoted C_{FEA}. Buckled configurations of the beams excluding web cleats, and isometric contour plots for the W310x21 and W310x52 sections can be seen in Fig. 5.8(a-c) as sample results. The Figures show that the W310x52 beam exhibits more distortion compared to the W310x21. This is consistent with a smaller moment gradient factor C_{FEA} for W310x52 than for the W310x21 section.

Table 5.3 FEA results for W310 series

Run #	Section Designation	Span $L\ (mm)$	Critical uniform moment based on code equation $M_u\ (kNm)$	Critical Moment Based on FEA $M_{FEA}\ (kNm)$	Moment Ratio $C_{FEA} = \frac{M_{FEA}}{M_u}$
1	W310x107	12000	351.4	439.0	1.249
2	W310x97	12000	292.7	369.5	1.262
3	W310x86	11200	232.6	288.7	1.241
4	W310x79	10500	208.4	262.8	1.261
5	W310x74	8200	214.0	263.4	1.231
6	W310x67	7700	188.7	234.3	1.241
7	W310x60	7200	169.2	210.4	1.243
8	W310x52	5700	153.0	187.8	1.227
9	W310x45	5300	129.3	160.2	1.239
10	W310x39	5400	100.0	125.6	1.256
11	W310x31	5000	77.4	98.9	1.278
12	W310x33	3100	83.7	104.4	1.248
13	W310x28	2900	71.2	90.5	1.272
14	W310x24	2600	59.1	77.1	1.304
15	W310x21	2800	42.8	57.2	1.337

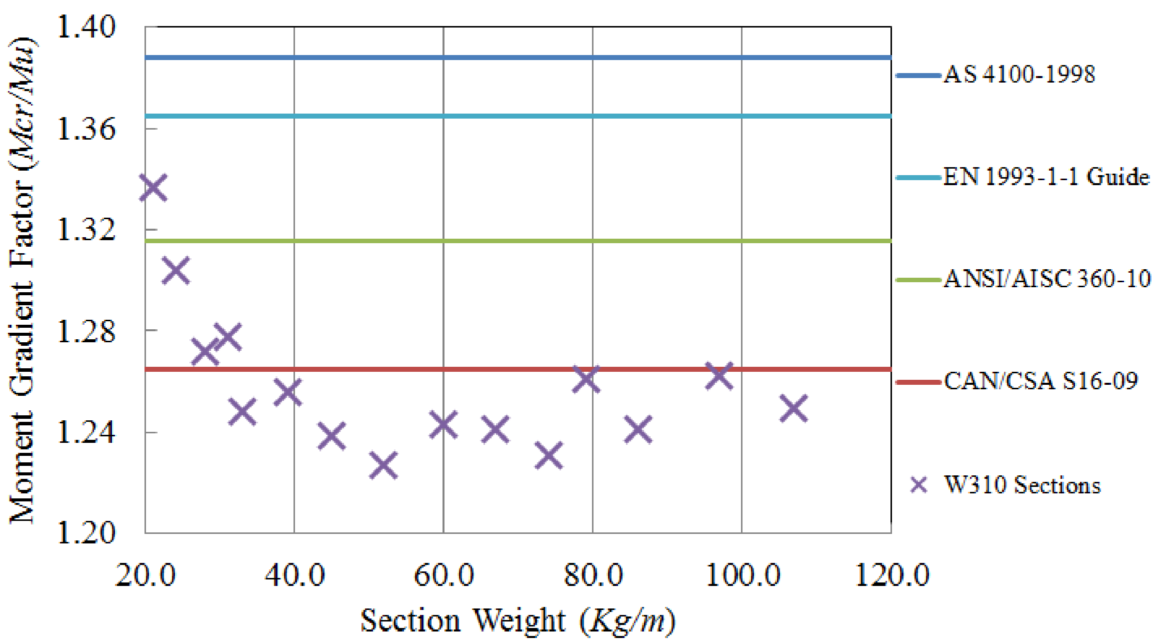

Fig. 5.7- Moment gradient ratio M_{FEA}/M_u for W310 series

Fig. 5.7 shows that all four design standards generally overestimate the moment gradient factor as determined by FEA C_{FEA}, with AS 4100-1998 and EN 1993-1-1:2005 overestimating the capacity of every W310 section investigated in the present study. Table 5.4 provides a comparison of the moment gradient factor based on all four design standards compared to the moment gradient factor as determined by the finite element analysis. On average, the Canadian code is observed to overestimate the lateral torsional buckling resistance only by 0.5%. In comparison, the American, European, and Australian standards overestimate the resistance, on average, by 4.5%, 8.4% and 10.4% respectively.

Table 5.4 W310 series comparison of code moment gradient factors C_{st} against moment gradient factors C_{FEA} as determined from FEA

Run #	Section Designation	Span (mm)	$C_{FEA} = \left(\frac{M_{FEA}}{M_u}\right)$	$\frac{C_{CAN}}{C_{FEA}}$	$\frac{C_{AISC}}{C_{FEA}}$	$\frac{C_{EUR}}{C_{FEA}}$	$\frac{C_{AUS}}{C_{FEA}}$
1	W310x107	12000	1.249	1.013	1.053	1.093	1.111
2	W310x97	12000	1.262	1.002	1.042	1.081	1.100
3	W310x86	11200	1.241	1.019	1.060	1.100	1.118
4	W310x79	10500	1.261	1.003	1.043	1.082	1.101
5	W310x74	8200	1.231	1.028	1.069	1.109	1.128
6	W310x67	7700	1.241	1.019	1.060	1.100	1.118
7	W310x60	7200	1.243	1.017	1.058	1.098	1.116
8	W310x52	5700	1.227	1.031	1.072	1.112	1.131
9	W310x45	5300	1.239	1.021	1.062	1.102	1.120
10	W310x39	5400	1.256	1.007	1.047	1.087	1.105
11	W310x31	5000	1.278	0.990	1.030	1.068	1.086
12	W310x33	3100	1.248	1.014	1.054	1.094	1.112
13	W310x28	2900	1.272	0.995	1.035	1.073	1.091
14	W310x24	2600	1.304	0.970	1.009	1.047	1.064
15	W310x21	2800	1.337	0.946	0.984	1.021	1.039
			Mean	1.005	1.045	1.084	1.103

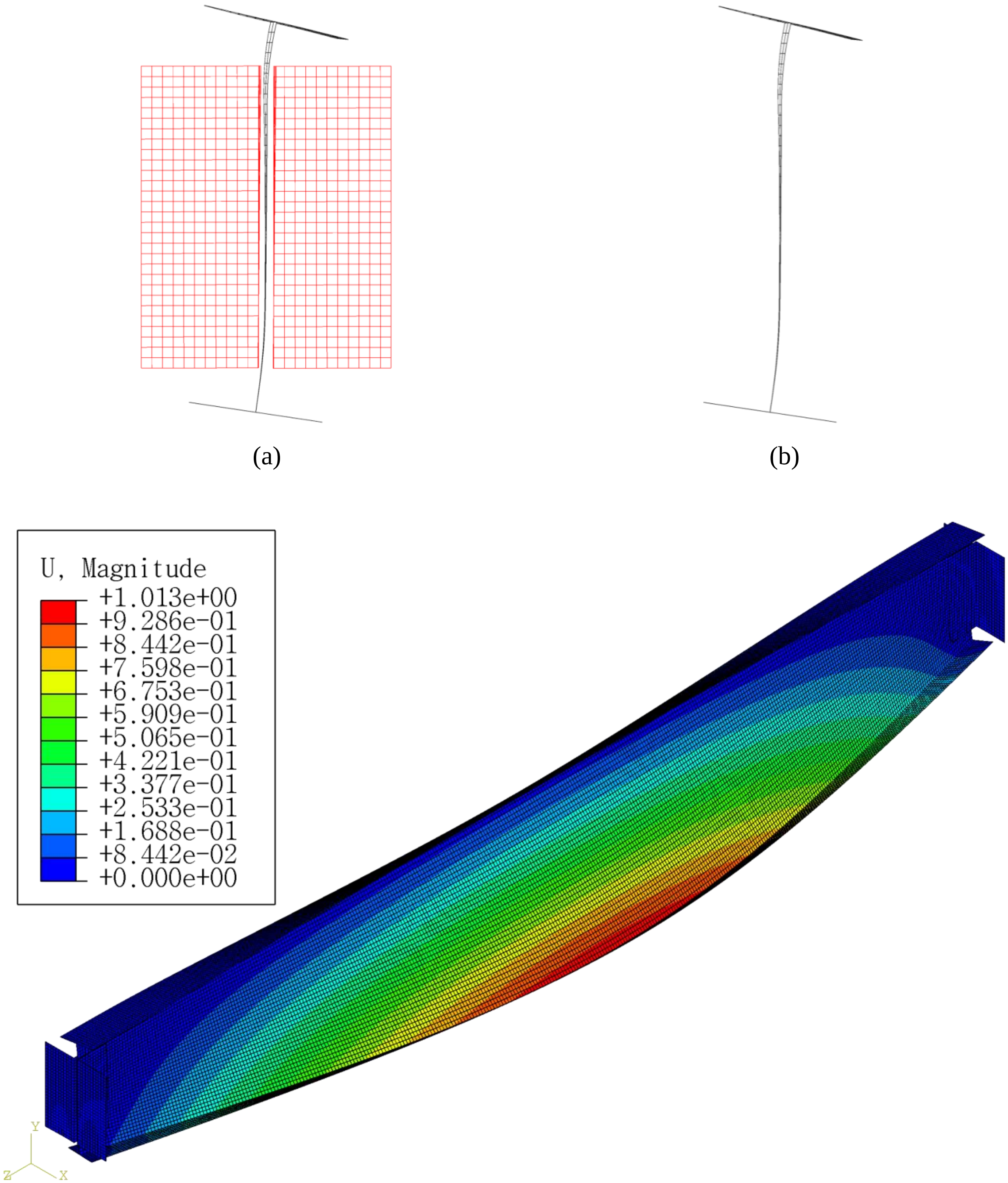

(c)

Fig. 5.8- W310x21 buckled configuration: (a) Cross section, (b) Cross section excluding web cleats, and (c) Isometric contour plot

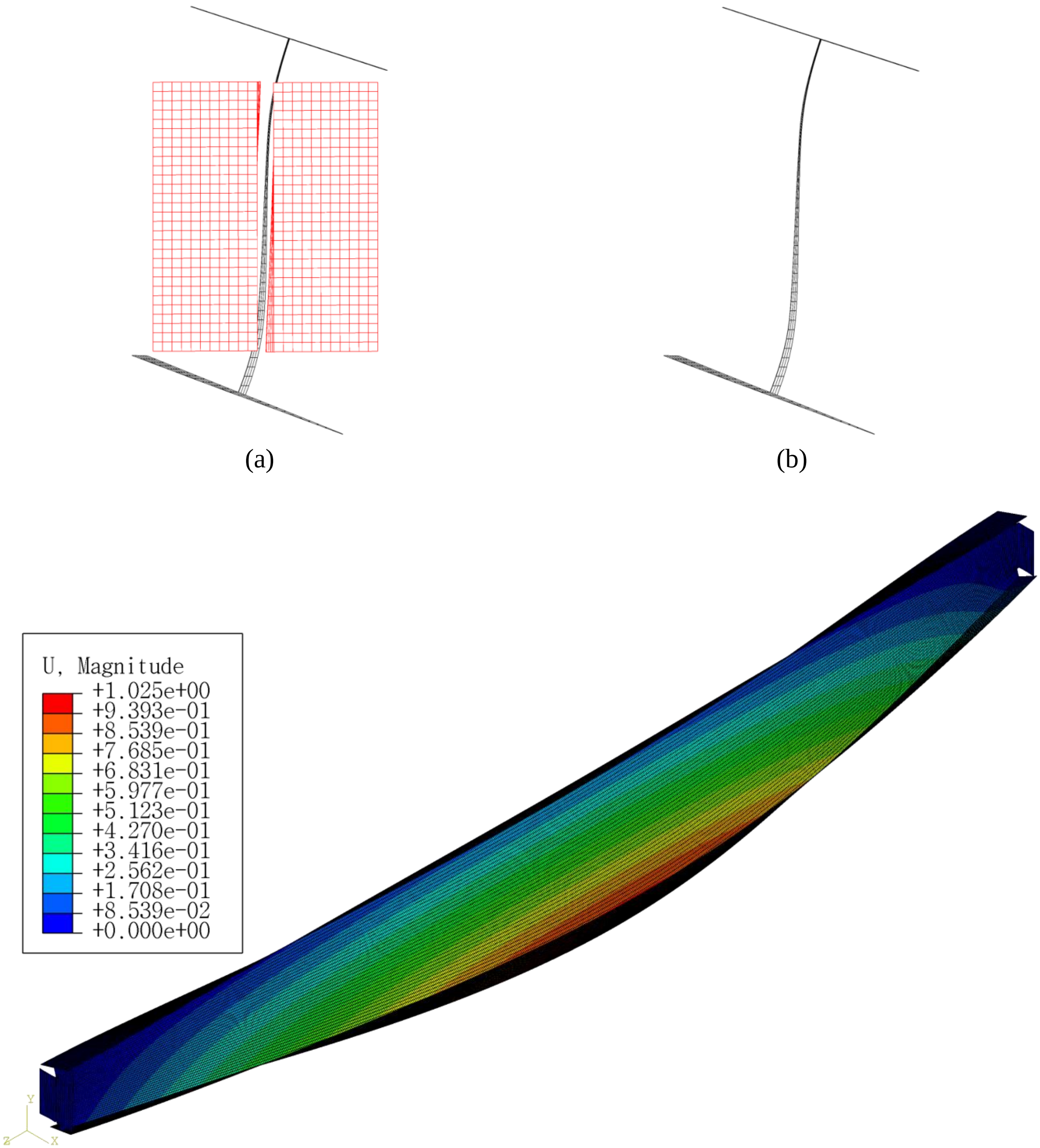

Fig. 5.9- W310x52 buckled configuration: (a) Cross section, (b) Cross section excluding web cleats, and (c) Displacement contour plot

5.5.1.2. Results for W200 Series

Table 5.5 presents FEA results for Runs 16-31 for the W200 sections investigated. Results are also plotted in Fig. 5.11. Values for M_{FEA}/M_u are found to range from 1.159 to 1.360. This variation of 20.1% is quite larger than that of the M_{FEA}/M_u results for the W310 sections. However, as depicted in Fig. 5.11, the W200x100 (run 18) M_{FEA}/M_u value of 1.159 significantly deviates from the mean. An examination of the W200x100 buckled configuration (Fig. 5.10(a-b)) suggests that the significant reduction in M_{FEA}/M_u is not based on distortion. Instead, it is observed that, given that web cleats are unable to provide a large enough torsional restraint to the beam ends, the beam is unable to attain its the full LTB resistance based on an infinite twist rigidity at the end. The fact that the web cleats have been adequately designed for shear (with an h_c/w_c ratio of 23.4) does not necessarily mean they were able to provide full torsional restraint the relatively stocky W200x100 beam cross-section with a web slenderness h/w of 12.5. Depending on the degree of torsional restraint provided by the web cleats to the ends of the beam, beam ends in all runs were observed to undergo twisting deformation to various degrees. This phenomenon is illustrated by comparing the results of runs 16-18, all of which having W200x100 cross-sections and 12,000*mm* spans but different cleat angles.

It is observed that W200x86, W200x71, and W200x59 also undergo significant twisting deformation. Therefore, even though moment gradient C_{FEA} for these sections as determined by FEA is lower than the rest of the sections, they are observed to exhibit little distortion. In contrast, the W200x42 section is observed to exhibit the most distortion. Cross sectional cuts and contour plots of the buckled configurations of the W200x15 and W200x42 can be seen in Fig. 5.12 and Fig. 5.13.

Significant distortion can be seen in the cross section of the W200x42 beam compared to W200x15. As presented in Fig. 5.11, the AS 4100-1998 moment gradient factor overestimates the critical moments for all W200 sections, while the EN 1993-1-1:2005 and ANSI/AISC 360-10 overestimate all but one section in the case of EN 1993-1-1:2005 and four sections in the case of ANSI/AISC 360-10. Values of normalization of the various code moment gradient factors with respect to C_{FEA} along with their means are tabulated in Table 5.6. For W200 sections, it appears that the Canadian Standards yield the best results by slightly underestimating beam LTB resistance capacity by 0.8% while the Australian Standards on average overestimate the resistance by 8.8%.

Table 5.5 FEA results for W200 series (All cleat angles are L89x89x6.4 unless noted otherwise)

Run #	Section Designation	Span $L\ (mm)$	Critical uniform moment based on code equation $M_u\ (kNm)$	Critical Moment Based on FEA $M_{FEA}\ (kNm)$	Moment Ratio $C_{FEA} = \frac{M_{FEA}}{M_u}$
16	W200x100(1)	12000	287.6	374.2	1.301
17	W200x100(2)	12000	287.6	356.7	1.240
18	W200x100	12000	287.6	333.3	1.159
19	W200x86	12000	216.9	260.4	1.200
20	W200x71	12000	149.7	183.7	1.227
21	W200x59	10300	119.3	150.0	1.257
22	W200x52	10400	92.7	118.1	1.273
23	W200x46	9300	81.4	104.6	1.286
24	W200x42	7200	80.8	101.8	1.260
25	W200x36	7100	62.0	79.2	1.277
26	W200x31	5100	60.4	76.2	1.263
27	W200x27	5000	44.5	57.9	1.302
28	W200x21	4500	34.2	45.7	1.334
29	W200x22	3400	38.9	51.9	1.332
30	W200x19	3400	29.1	40.1	1.376
31	W200x15	3100	22.4	30.4	1.360

(1) Cleat angle is L89x89x13
(2) Cleat angle is L89x89x9.5

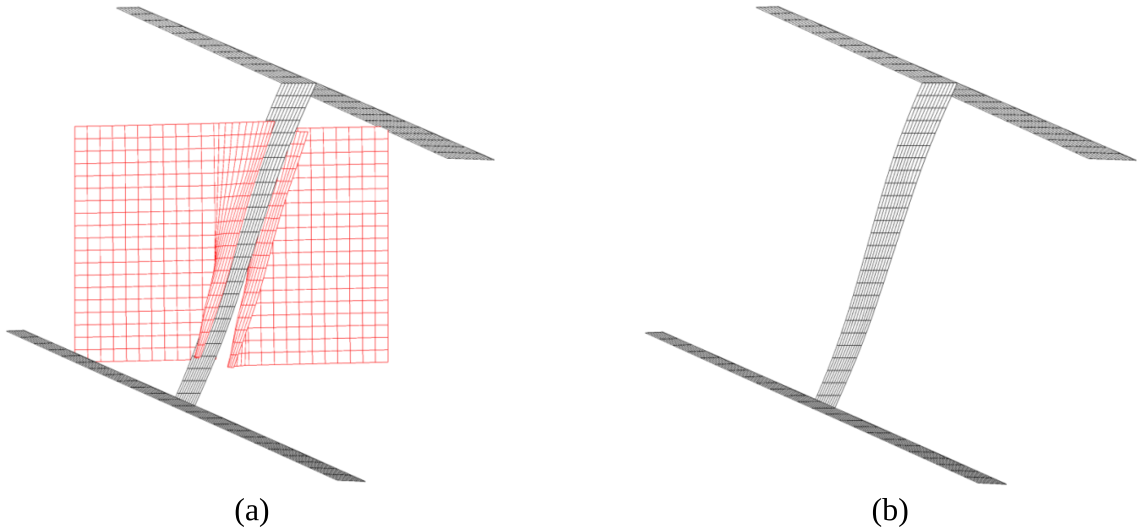

Fig. 5.10- W200x100 buckled configuration: (a) Cross section, and (b) Cross section excluding web cleats

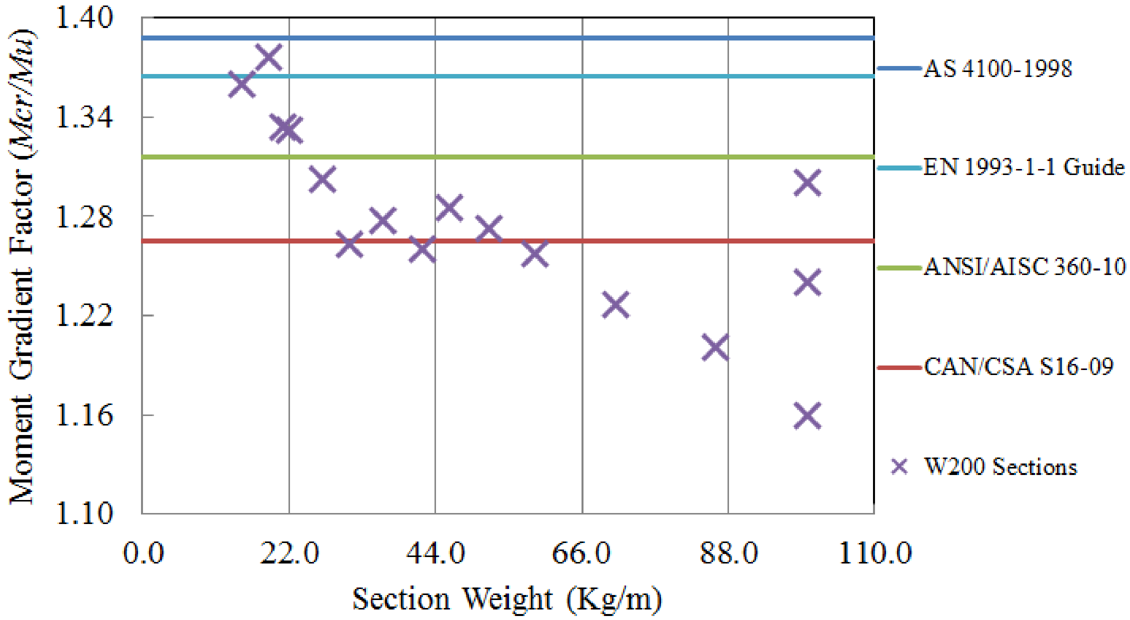

Fig. 5.11- Moment gradient ratio M_{FEA}/M_u for W200 series

Table 5.6 W200 series comparison of code moment gradient factors C_{st} against moment gradient factors C_{FEA} as determined from FEA (All cleat angles are L89x89x6.4 unless noted otherwise)

Run #	Section Designation	$C_{FEA} = \left(\frac{M_{FEA}}{M_u}\right)$	$\frac{C_{CAN}}{C_{FEA}}$	$\frac{C_{AISC}}{C_{FEA}}$	$\frac{C_{EUR}}{C_{FEA}}$	$\frac{C_{AUS}}{C_{FEA}}$
16	W200x100(1)	1.301	0.972	1.011	1.049	1.067
17	W200x100(2)	1.240	1.020	1.061	1.101	1.119
18	W200x100	1.159	1.091	1.135	1.178	1.197
19	W200x86	1.200	1.054	1.096	1.137	1.156
20	W200x71	1.227	1.031	1.073	1.113	1.131
21	W200x59	1.257	1.006	1.047	1.086	1.104
22	W200x52	1.273	0.994	1.034	1.072	1.090
23	W200x46	1.286	0.984	1.023	1.062	1.080
24	W200x42	1.260	1.004	1.044	1.083	1.102
25	W200x36	1.277	0.990	1.030	1.069	1.087
26	W200x31	1.263	1.002	1.042	1.081	1.099
27	W200x27	1.302	0.971	1.010	1.048	1.066
28	W200x21	1.334	0.948	0.986	1.023	1.040
29	W200x22	1.332	0.949	0.988	1.025	1.042
30	W200x19	1.376	0.919	0.956	0.992	1.009
31	W200x15	1.360	0.930	0.968	1.004	1.021
		Mean	0.992	1.032	1.070	1.088

(1) Cleat angle is L89x89x13
(2) Cleat angle is L89x89x9.5

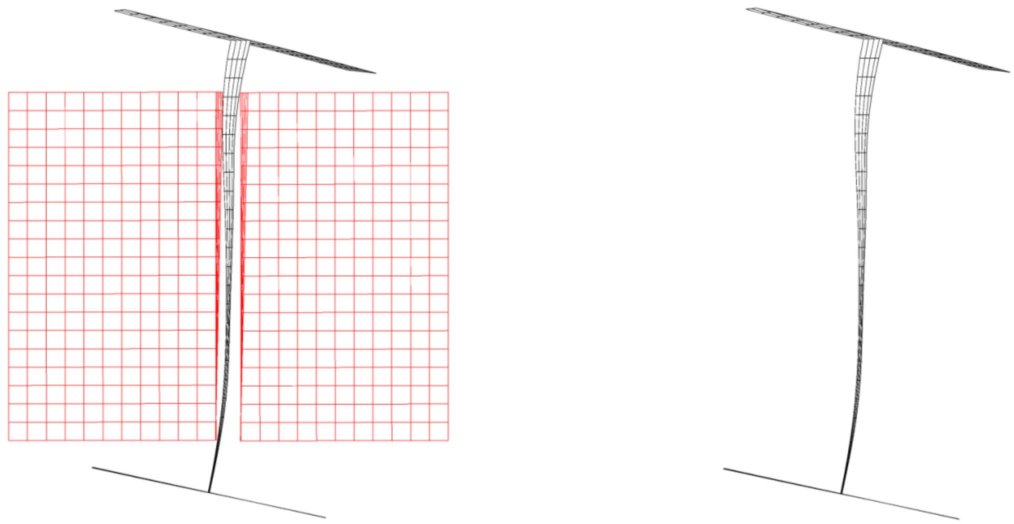

(a) (b)

Fig. 5.12- W200x15 buckled configuration: (a) Cross section, and (b) Cross section excluding web cleats

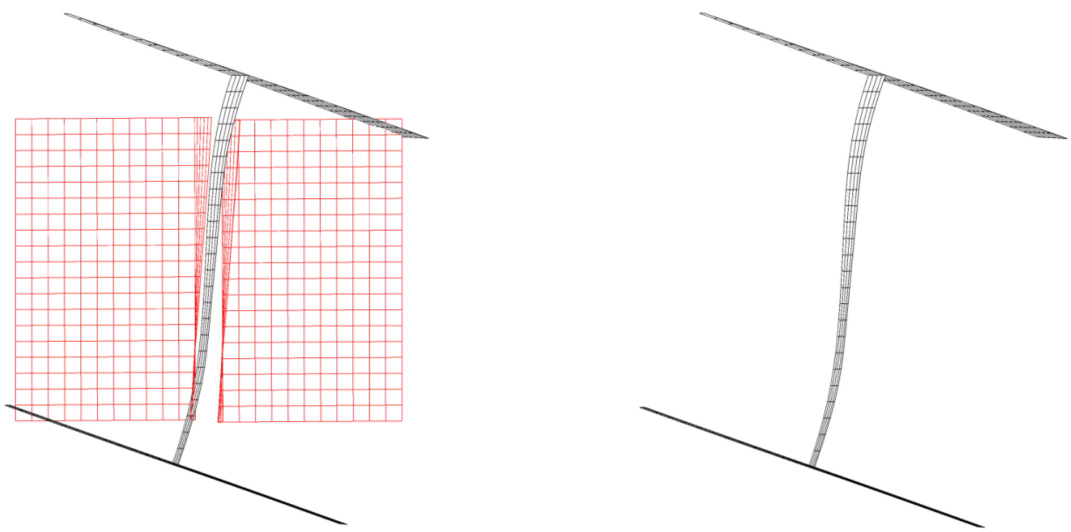

(a) (b)

Fig. 5.13- W200x42 buckled configuration: (a) Cross section, and (b) Cross section excluding web cleats

5.5.1.3. Results for W150 Series

The results of all seven W150 sections modeled are presented in Table 5.7 and plotted in Fig. 5.14. The M_{FEA}/M_u values are observed to range from 1.278 for W150x37 to 1.401 for W150x13. Cross sectional cuts of buckled configurations of both beams are displayed in Fig. 5.15 and Fig. 5.16. It is evident that the W150x37 beam exhibits more distortion than the

W150x13. As shown in the bottom entries in Table 5.8, depending on the standards, a beam's LTB resistance ranges from an underestimation of 5.2% on average by the Canadian standards to an overestimation of 4.0% on average by the Australian Standards. The American Standards best predicts the moment gradient for or W150 sections by conservatively underestimating the LTB resistance by 1.4% on average.

Table 5.7 FEA results for W150 Series

Run #	Section Designation	Span L (mm)	Critical uniform moment based on code equation M_u (kNm)	Critical Moment Based on FEA M_{FEA} (kNm)	Moment Ratio $C_{FEA}=\frac{M_{FEA}}{M_u}$
32	W150x37	8200	56.8	72.6	1.278
33	W150x30	7600	40.0	52.3	1.307
34	W150x22	6100	28.8	39.0	1.352
35	W150x24	4800	34.7	44.5	1.283
36	W150x18	3800	24.6	33.3	1.356
37	W150x14	3600	16.2	22.3	1.375
38	W150x13	3500	14.4	20.1	1.401

Table 5.8 W150 series comparison of code moment gradient factors C_{st} against moment gradient factors C_{FEA} as determined from FEA

Run #	Section Designation	$C_{FEA}=\left(\frac{M_{FEA}}{M_u}\right)$	$\frac{C_{CAN}}{C_{FEA}}$	$\frac{C_{AISC}}{C_{FEA}}$	$\frac{C_{EUR}}{C_{FEA}}$	$\frac{C_{AUS}}{C_{FEA}}$
32	W150x37	1.278	0.990	1.030	1.068	1.087
33	W150x30	1.307	0.968	1.007	1.044	1.062
34	W150x22	1.352	0.935	0.973	1.009	1.026
35	W150x24	1.283	0.986	1.026	1.064	1.082
36	W150x18	1.356	0.933	0.971	1.007	1.024
37	W150x14	1.375	0.920	0.957	0.993	1.010
38	W150x13	1.401	0.903	0.939	0.975	0.991
		Mean	0.948	0.986	1.023	1.040

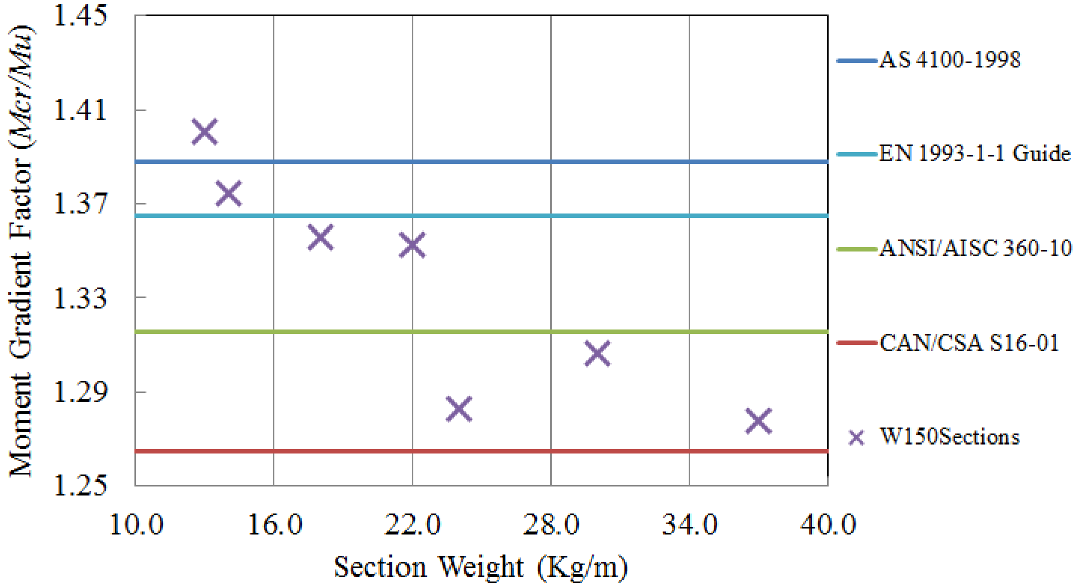

Fig. 5.14- Moment gradient ratio M_{FEA}/M_u for W150 series

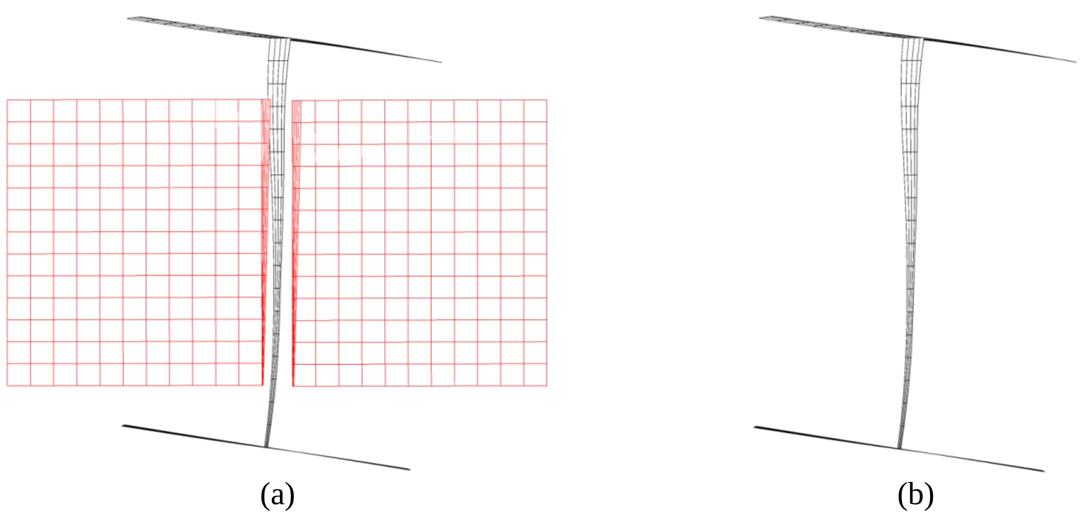

Fig. 5.15- W150x13 buckled configuration: (a) Cross section, and (b) Cross section excluding web cleats

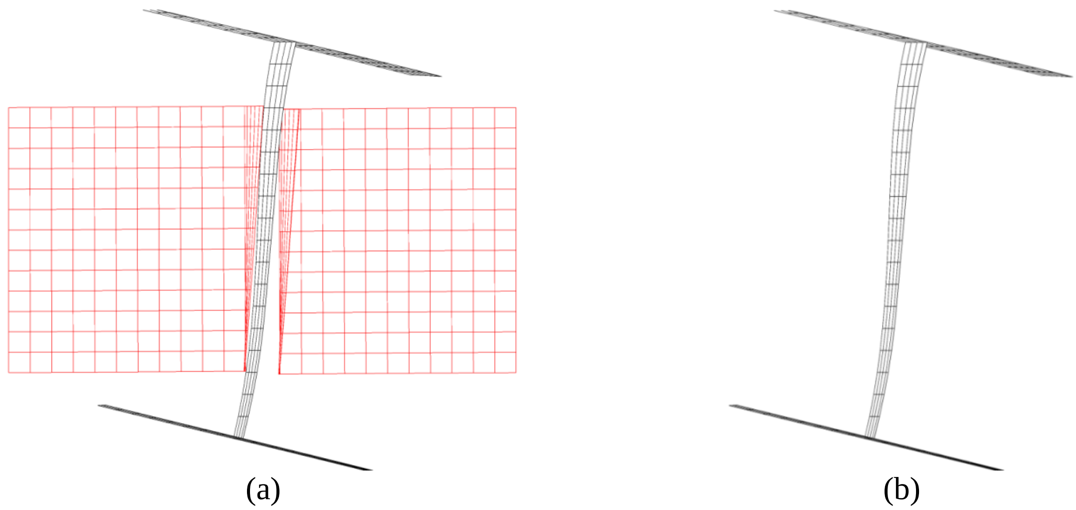

Fig. 5.16- W150x37 buckled configuration: (a) Cross section, and (b) Cross section excluding web cleats

5.5.1.4. Summary of Critical Moment Results

In the previous three sections, the suggested equivalent uniform moment factor C_{st} of the various codes was compared with M_{FEA}/M_u results for each beam group separately. In this section, a global comparison of C_{FEA}, which looks at all W310, W200, and W150 results simultaneously. Fig. 5.17 displays results of all sections studied along with code predicted moment gradient factors.

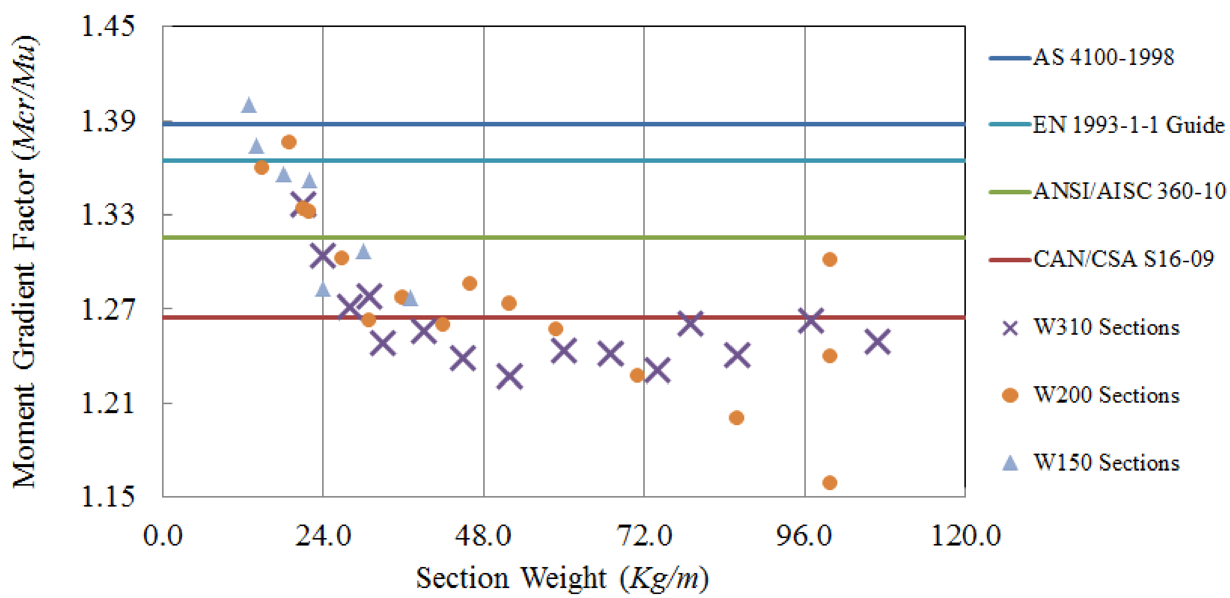

Fig. 5.17- M_{FEA}/M_u results for all sections studied

Table 5.9 Global average of normalization of M_{FEA}/M_u with C_{FEA}

Series	# of Sections Analyzed	$\frac{C_{CAN}}{C_{FEA}}$	$\frac{C_{AISC}}{C_{FEA}}$	$\frac{C_{EUR}}{C_{FEA}}$	$\frac{C_{AUS}}{C_{FEA}}$
W310	15	1.005	1.045	1.084	1.103
W200	16	0.992	1.032	1.070	1.088
W150	7	0.948	0.986	1.023	1.040
	Weighted Mean	0.989	1.029	1.067	1.085

The weighted mean values presented in Table 5.9 suggest that on average, the Canadian Standards would underestimate the LTB resistance of W150, W200, and W310 beams by 1.1%. In comparison, the American, European, and Australian standards would overestimate their resistance by 2.9%, 6.7%, and 8.5% respectively.

5.6. Observations about Buckling Mode Shapes

5.6.1. Presence of End Twist

The classical lateral torsional buckling solution given by Eq. [2.1] is derived under the assumption that beams are fully restrained from twist at both ends. The assumption implied is that beam ends are subject to infinite twist restraints at the ends. The finite element results in the present study show that for cleat angle details, this is not the case as the beam ends were shown to undergo some twist. The implications of this simplifying assumption in the classical solution thus need to be examined.

To assess the torsional stiffness of web cleats, twist angles at both ends and mid-span of the beams are calculated from finite element results. Since all beams studied have symmetrical cross-sections and are symmetrically loaded, twist angles at both beam ends are expected to yield identical results. In all finite element analyses conducted, the angles of twist at both ends were ensured to be equal in the mode shape corresponding to the lower critical value. To determine the angle of twist at a section z along the beam span, nodal translations along the lateral direction at the top and bottom web to flange junctions are extracted from the finite element results. As a matter of notation, displacements and rotations are denoted A for the left end and B for the right end. Also, the beam mid-span is assigned subscript M. Nodal translations along the lateral direction at the top web to flange junction is denoted u_t while that at the bottom web to flange junction is denoted u_b. Using this identification scheme, nodal translation at the top web to flange junction at End A of the beam would be $u_{t,A}$. The twist angle ϕ_A for End A is then calculated by

[5.2] $$\phi_A = \frac{u_{t,A} - u_{b,A}}{h}$$

and h is the beam height, from the mid-surface of the bottom flange to that of the top flange. Angles of twists at End B and Mid-span section M are calculated using similar equations by substituting their respective nodal translations.

Table 5.10 - Table 5.12 present results of twist deformation and the web cleat connection's twist stiffness which is determined by

[5.3] $$R = \frac{GJ_c}{L_c} = \frac{2G\left(\frac{1}{3}h_c t_c{}^3\right)}{L_c}$$

where J_c is St.Venant torsional constant of a single angle and L_c is the cleat span and is equal to the distance from the angle heal at face of the supporting column to the bolt line, in which h_c is the height of the cleat angle and t_c is the thickness of the angle and the coefficient 2 is to account for the double cleat angles.

As presented in Table 5.10 - Table 5.12, the beam ends exhibit twist when buckling. This signifies that the assumption made in the classical lateral torsional buckling solution that when a beam undergoes buckling, its ends experience no twist, is not valid.

Table 5.10 W310 Series twist deformation results

Run #	Section Designation	ϕ_A $(rads)$	ϕ_M $(rads)$	$\frac{\phi_A}{\phi_M}$	R (kNm/rad)
1	W310x107	0.1689	2.319	0.0728	58.5
2	W310x97	0.1524	2.425	0.0629	58.5
3	W310x86	0.1512	2.262	0.0669	58.5
4	W310x79	0.1415	2.445	0.0579	58.5
5	W310x74	0.1729	2.374	0.0728	58.5
6	W310x67	0.1730	2.568	0.0674	58.5
7	W310x60	0.1857	2.764	0.0672	58.5
8	W310x52	0.2174	2.715	0.0801	58.5
9	W310x45	0.2284	2.921	0.0782	58.5
10	W310x39	0.2102	3.006	0.0699	58.5
11	W310x31	0.2114	3.185	0.0664	58.5
12	W310x33	0.2233	2.969	0.0752	58.5
13	W310x28	0.2159	3.113	0.0694	58.5
14	W310x24	0.1923	3.238	0.0594	58.5
15	W310x21	0.1363	3.249	0.0419	58.5

Table 5.11 W200 Series twist deformation results (All cleat angles are L89x89x6.4 unless noted otherwise)

Run #	Section Designation	ϕ_A $(rads)$	ϕ_M $(rads)$	$\frac{\phi_A}{\phi_M}$	R (kNm/rad)
16	W200x100(1)	0.0961	1.701	0.0565	359
17	W200x100(2)	0.1453	1.692	0.0859	125
18	W200x100	0.2834	1.725	0.1643	38.3
19	W200x86	0.2344	1.879	0.1248	38.3
20	W200x71	0.1994	2.111	0.0945	38.3
21	W200x59	0.1902	2.647	0.0719	38.3
22	W200x52	0.1655	2.837	0.0583	38.3
23	W200x46	0.1673	3.258	0.0514	38.3
24	W200x42	0.2116	3.268	0.0647	38.3
25	W200x36	0.1901	3.553	0.0535	38.3
26	W200x31	0.2468	3.672	0.0672	38.3
27	W200x27	0.1917	3.931	0.0488	38.3
28	W200x21	0.1703	4.389	0.0388	38.3
29	W200x22	0.1781	4.079	0.0437	38.3
30	W200x19	0.1079	4.247	0.0254	38.3
31	W200x15	0.1608	4.687	0.0343	38.3

(1) Cleat angle is L89x89x13
(2) Cleat angle is L89x89x9.5

Table 5.12 W150 Series twist deformation results

Run #	Section Designation	ϕ_A $(rads)$	ϕ_M $(rads)$	$\frac{\phi_A}{\phi_M}$	R (kNm/rad)
32	W150x37	0.2026	3.129	0.0648	25.6
33	W150x30	0.1632	3.766	0.0433	25.6
34	W150x22	0.1108	4.888	0.0227	25.6
35	W150x24	0.2134	3.713	0.0575	25.6
36	W150x18	0.1148	4.890	0.0235	25.6
37	W150x14	0.0944	5.565	0.0170	25.6
38	W150x13	0.0449	5.749	0.0078	25.6

To assess the effect of the web cleat twist stiffness on end twist deformation, Run 18 for the W200x100 with (L89x89x6.4 cleat angles with $R = 38.3 kNm/rad$) is chosen and the end rotational restraint is varied by selecting thicker cleat angles L89x89x9.5 ($R = 359\,kNm/rad$) and L89x89x13 ($125\,kNm/rad$), resulting in Runs 16 and 17. This particular section was selected due to the fact that the W200x100 section in Run 16 experiences the highest end to mid-span rotation $\phi_A/\phi_M = 0.1643$. As depicted in Fig. 5.18, an increase in twisting restraint provided by the web cleat connection leads to a significant decrease in the ratio of end to mid span twist deformation. With this observation, it is evident that the LTB mode shape is affected by the twisting stiffness of cleat angles. As such, critical moment equations in standards need to be adjusted to account for partial twist restraint provided by end connection details.

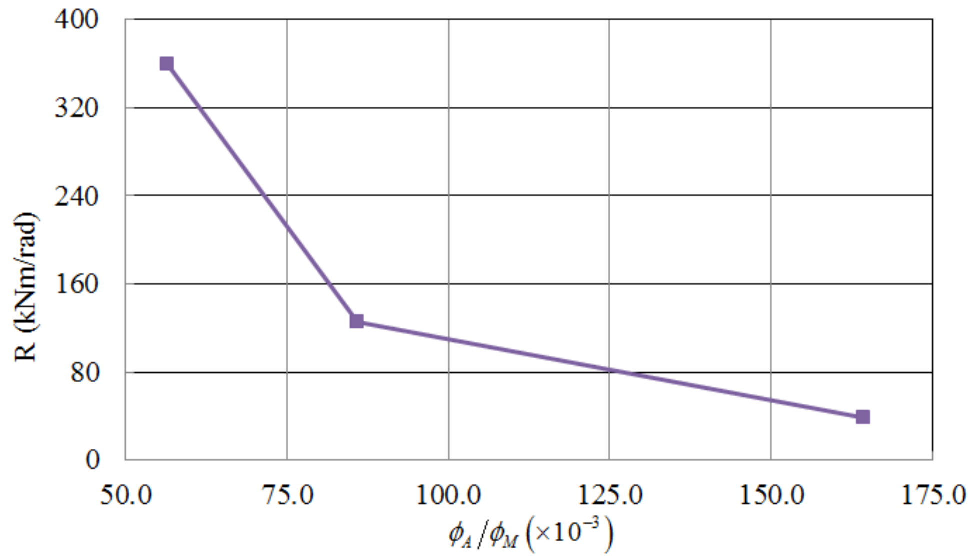

Fig. 5.18- Effect of twist stiffness on the ratio of end to mid-span twist deformation (W200x100 with 12,000mm span)

5.6.2. Absence of End Lateral Displacements

In the derivation of the classical LTB solution, it is assumed that beam ends do not experience lateral displacements. To verify this assumption, normalized end lateral displacement profiles for runs 16-18 for the W200x100 cross section are extracted from Abaqus and plotted in Fig. 5.19. In Abaqus, all displacements are normalized with respect to the largest displacement, which means that the largest displacement would be normalized to equal unity. It is observed that the node corresponding to the mid-height of the web experiences negligible displacement irrespective of the twisting stiffness provided by the cleat angles. As such, the assumption of no lateral displacement at the beams ends appears to be valid.

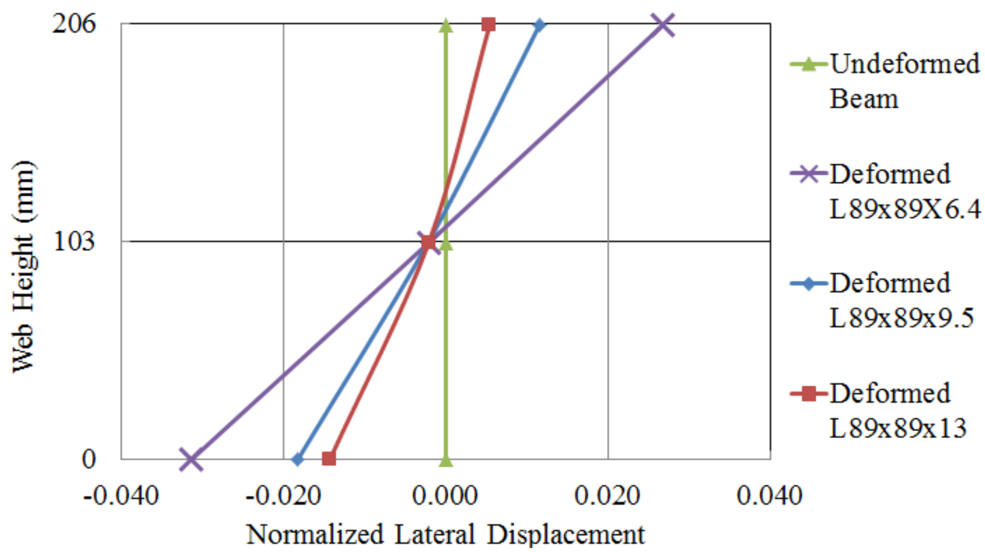

Fig. 5.19- Beam end lateral displacement profile

5.6.3. Presence of Distortion

As discussed in Subsection 5.5.1, the presence of distortion decreases a beam ability to achieve theoretical LTB resistance as predicted by the classical LTB solution. Cross sectional cuts of the buckled configurations in Fig. 5.12 - 5.16 provide a visual representation of distortion.

5.7. Proposed Modifications of Standards Procedures

As outlined in Section 2.2 of Chapter 2, the critical moment of a beam based on the classical LTB solution is given by

[5.4] $$M_u = \frac{\pi}{L}\sqrt{GJEI_y + \left(\frac{\pi E}{L}\right)^2 I_y C_w}$$

This solution is based on three assumptions which are 1) the beam is subject to a uniform moment distribution, 2) ideal simply supported conditions, both in the lateral and torsional directions (i.e., the beam is fully restrained against lateral displacement and twist at both ends) and, 3) the beam cross-section exhibits no distortion.

The first assumption is corrected in various standards through the introduction of moment gradient factors C_{st}. The second assumption has been assessed in Subsections 5.6.1 and 5.6.2, and it is revealed that while the lateral restraint assumption can be valid, torsional restraints are only partial for the case of cleat angle end details. Finally, the third assumption has been shown to be invalid based on the finite element simulation in the present study.

Within this context, modifications to standard procedures are needed which account for partial end twist restraint and cross-sectional distortion. Since the nominal elastic lateral torsional buckling resistance as determined in various standards take the form $M_n = C_{st} M_u$, which neglects distortional effects and partial twist restraint effects, but incorporates the effect of moment gradient through the standard specific coefficient C_{st}, it is proposed in the present research, to apply three modification factors to the above equation, i.e.,

[5.5] $$M_{cr} = D C_R S_{st} \left(C_{st} M_u \right)$$

in which C_R is a coefficient which accounts for the partial twist restraint provided by the cleat angle and depends on the twisting stiffness of the cleat angles relative to the twisting stiffness of the beam. Coefficient D accounts for distortional effects as determined by the results of the FEA and since various design standards have slightly different values regarding the moment gradient factor C_{st}, another standard specific constant S_{st} is introduced to ensure consistency in the safety level between the various standards.

In the following, Section 5.7.1 develops an energy solution which formulates an expression for a coefficient which accounts for partial end twist restraint. Also, Section 5.7.2 uses the finite element results provided in the present study to develop another coefficient which accounts for distortional effects. Both coefficients when applied to the classical critical moment and moment gradient factors in various standards should provide realistic prediction of the critical moment.

5.7.1. Energy Formulation for Critical Moments Accounting for Partial Twist Restraint

It is required to formulate an expression for the critical moment for a simply supported flexural member of a doubly symmetric cross-section subject to a triangular moment distribution $M(z) = (2z/L) M_0$ for $0 \le z \le L/2$ and $M(z) = \left(2(L-z)/L\right) M_0$ for $L/2 \le z \le L$. The beam is assumed to be partially restrained against twist at each end by a rotational spring with a rotational constant R. Distortional effects are to be neglected in the formulation since they will be dealt with subsequently under Section 5.7.2.

The total potential energy π_p is given by

[5.6] $\pi_p = U + V$

where U is the internal strain energy and V is the load potential energy gain by the moments as the beam undergoes lateral torsional buckling. U and V are given by (Trahair 1993) as

[5.7] $U = \frac{1}{2}\int_0^L EI_y u''^2\,dz + \frac{1}{2}\int_0^L GJ\phi'^2\,dz + \frac{1}{2}\int_0^L EC_w\phi''^2\,dz + \frac{1}{2}\times R\left[\phi(0)\right]^2 + \frac{1}{2}\times R\left[\phi(l)\right]^2$

[5.8] $V = \int_0^L M(z)u''\phi dz$

The mode shapes of the shell finite element runs conducted in this study provide a rational basis to assume displacement functions that are more realistic than those based on the classical solution. Approximate displacement (u) and angle of twist (ϕ) functions which meet all essential and natural boundary conditions are

[5.9] $u(z) = A\sin\left(\frac{\pi z}{L}\right)$

[5.10] $\phi(z) = B + C\sin\left(\frac{\pi z}{L}\right)$

It is noted that the introduction of constant B in Eq. [5.10] is consistent with the fact that in the FEA simulations, end rotations were observed not to vanish, in contrast to the classical solution. By substituting Eqs. [5.9] and [5.10] along with their required derivatives into the potential energy expression ($\pi_p = U + V$) and evaluating the integrals, the following equation is found

[5.11] $\pi_p = \frac{1}{4}A^2\left(\frac{\pi^4 EI_y}{L^3}\right) + RB^2 + \frac{1}{4}C^2\left(\frac{\pi^2 GJ}{L} + \frac{\pi^4 EC_w}{L^3}\right) - M_0\left(\frac{4}{L}\right)AB - \frac{M_0}{L}\left(\frac{\pi^2}{4}+1\right)AC$

Evoking the stationary conditions

[5.12] $\frac{\partial A}{\partial \pi_p} = \frac{\partial B}{\partial \pi_p} = \frac{\partial C}{\partial \pi_p} = 0$

yields three expressions which, given in matrix format, are presented as

$$[5.13]\quad \begin{bmatrix} \dfrac{\pi^4 EI_y}{2L^3} & \dfrac{-4M_0}{L} & -\dfrac{M_0}{L}\left(\dfrac{\pi^2}{4}+1\right) \\ \dfrac{-4M_0}{L} & 2R & 0 \\ -\dfrac{M_0}{L}\left(\dfrac{\pi^2}{4}+1\right) & 0 & \dfrac{1}{2}\left(\dfrac{\pi^2 GJ}{L}+\dfrac{\pi^4 EC_w}{L^3}\right) \end{bmatrix} \begin{Bmatrix} A \\ B \\ C \end{Bmatrix} = \begin{Bmatrix} 0 \\ 0 \\ 0 \end{Bmatrix}$$

By setting the determinant of Eq. [5.13] to zero, one recovers the following critical moment expression

$$[5.14]\quad M_0 = \sqrt{\frac{\left(\dfrac{\pi^4 EI_y}{2L}\right)\left(\dfrac{\pi^2 GJ}{L}+\dfrac{\pi^4 EC_w}{L^3}\right)}{2\left(\dfrac{\pi^2}{4}+1\right)^2+\dfrac{8}{R}\left(\dfrac{\pi^2 GJ}{L}+\dfrac{\pi^4 EC_w}{L^3}\right)}}$$

To determine the moment resistance in the hypothetical case where ends are infinitely restrained, one can take the limit of M_0 as R approaches infinity, yielding

$$[5.15]\quad M_\infty = \lim_{R\to\infty} M_0 = \frac{\pi^2}{2\left(\dfrac{\pi^2}{4}+1\right)}\left(\frac{\pi}{L}\right)^2\sqrt{\left(EI_y GJ+\left(\frac{\pi E}{L}\right)^2 I_y C_w\right)} = \frac{\pi^2}{2\left(\dfrac{\pi^2}{4}+1\right)} M_u \approx 1.423 M_u$$

As expected, when the ends of a beam are infinitely restrained, the result is a moment gradient factor multiplied by the classical LTB solution; where the moment gradient factor derived by energy formulation is $C_E = 1.423$. A comparison with the moment gradient factors in Table 5.1 indicates that C_E is slightly larger than the values provides in various standards. This is expected since the displacement and angle of twist functions postulated in Eqs. [5.9] and [5.10] are approximate. Improved values can be obtained by postulating more refined displacement curves. In the present study, the simpler displacement functions are retained in order to preserve the simplicity of the resulting critical moment equation. Defining the moment gradient factor based on the energy solution as

$$[5.16]\quad C_E = \frac{\pi^2}{2\left(\dfrac{\pi^2}{4}+1\right)} = 1.423$$

Eq. [5.14] can be rearranged as

$$[5.17] \quad M_0 = C_E \sqrt{\frac{\left(\frac{EI_y}{L}\right)\left(\frac{\pi^2 GJ}{L} + \frac{\pi^4 EC_w}{L^3}\right)}{1 + \frac{\frac{2\pi^2}{R}\left(\frac{GJ}{L} + \frac{\pi^2 EC_w}{L^3}\right)}{\left(\frac{\pi^2}{4}+1\right)^2}}} = C_E \sqrt{\frac{1}{1+1.642\alpha}} M_u$$

where the dimensionless ratio α is

$$[5.18] \quad \alpha = \frac{1}{R}\left(\frac{GJ}{L} + \frac{\pi^2 EC_w}{L^3}\right)$$

and represents the torsional stiffness of the beam to that of the end elastic rotational restraint of the cleat angle. Eq. [5.17] can be re-written as

$$[5.19] \quad M_0 = C_R \left(C_E M_u\right)$$

in which the partial twisting restraint coefficient C_R is given by

$$[5.20] \quad C_R = \sqrt{\frac{1}{1+1.642\alpha}}$$

C_R is a universal (code independent) reduction factor which accounts for the fact that cleat angles provide a partial twisting restraint, allowing the beam ends to undergo some twist, and thus achieving only a fraction of the LTB resistance obtained by assuming infinite twisting restraints. It is noted that Appendix H of AS 4100-1998 provides a somewhat similar expression for C_R due to partial twist restraints at the ends. However as shown in Appendix D, the present formulation is shown to yield superior buckling predictions for the given pattern. Appendix D illustrates the limitations of the Australian Standards solution compared to the one based on the present formulation

It is emphasized that the formulation behind Eq. [5.17] does not account for distortional effects. These effects will be subsequently incorporated into the formulation based on the finite element run results.

5.7.2. Determining the Distortional Coefficient

For a given finite element run i, a distortional coefficient D_{FEA} is calculated from

[5.21] $$D_{FEA(i)} = \left(\frac{M_{FEA}}{C_R C_E M_u} \right)_i$$

This procedure is applied for all finite element runs in the study and the results compiled in Table 5.13.

Table 5.13 Calculation of parameters accounting for partial end restraint

Designation	M_u (1) (kNm)	M_∞ (2) (kNm)	R (3) (kNm/rad)	α (4)	C_R (5)	$M_0 = C_R M_\infty$ (kNm)	M_{FEA} (kNm)	D_{FEA}
W310x107	351	500	58.8	1.55	0.892	446	439	0.985
W310x97	293	416	58.8	1.2	0.913	380	369	0.972
W310x86	233	331	58.8	1.16	0.916	303	289	0.952
W310x79	208	296	58.8	0.972	0.928	275	263	0.955
W310x74	214	305	58.8	1.36	0.903	275	263	0.958
W310x67	189	269	58.8	1.13	0.918	247	234	0.951
W310x60	169	241	58.8	0.96	0.929	224	210	0.941
W310x52	153	218	58.8	1.11	0.919	200	188	0.938
W310x45	129	184	58.8	0.882	0.934	172	160	0.932
W310x39	100	142	58.8	0.631	0.951	135	126	0.928
W310x31	77.4	110	58.8	0.468	0.963	106	98.9	0.932
W310x33	83.7	119	58.8	0.963	0.928	110	104	0.945
W310x28	71.2	101	58.8	0.791	0.940	94.9	90.5	0.951
W310x24	59.1	84.2	58.8	0.67	0.949	79.9	77.1	0.966
W310x21	42.8	60.9	58.8	0.445	0.965	58.8	57.2	0.973
W200x100	288	409	360	0.376	0.970	397	374	0.943
W200x100	288	409	125	1.08	0.921	377	357	0.947
W200x100	288	409	38.3	3.53	0.794	325	333	1.026
W200x86	217	309	38.3	2.35	0.848	262	260	0.995
W200x71	150	213	38.3	1.38	0.902	192	184	0.956
W200x59	119	170	38.3	0.938	0.930	158	150	0.950
W200x52	92.7	132	38.3	0.654	0.950	125	118	0.942
W200x46	81.4	116	38.3	0.524	0.959	111	105	0.942
W200x42	80.8	115	38.3	0.681	0.948	109	102	0.934
W200x36	62	88.3	38.3	0.467	0.963	85.1	79.2	0.932
W200x31	60.4	85.9	38.3	0.592	0.954	82.0	76.2	0.930

Table 5.13 Continued

Designation	M_u (1) (kNm)	M_∞ (2) (kNm)	R (3) (kNm/rad)	α (4)	C_R (5)	$M_0 = C_R M_\infty$ (kNm)	M_{FEA} (kNm)	D_{FEA}
W200x27	44.5	63.3	38.3	0.391	0.969	61.3	57.9	0.945
W200x21	34.2	48.7	38.3	0.274	0.978	47.6	45.7	0.959
W200x22	38.9	55.4	38.3	0.474	0.963	53.3	51.9	0.972
W200x19	29.1	41.5	38.3	0.327	0.974	40.4	40.1	0.993
W200x15	22.4	31.8	38.3	0.233	0.981	31.2	30.4	0.974
W150x37	56.8	80.8	25.6	0.732	0.944	76.3	72.6	0.951
W150x30	40	56.9	25.6	0.429	0.966	55.0	52.3	0.951
W150x22	28.8	41	25.6	0.256	0.979	40.2	39	0.971
W150x24	34.7	49.4	25.6	0.619	0.952	47.0	44.5	0.947
W150x18	24.6	35	25.6	0.357	0.972	34.0	33.3	0.981
W150x14	16.2	23	25.6	0.201	0.984	22.6	22.3	0.982
W150x13	14.4	20.5	25.6	0.173	0.986	20.2	20.1	0.998

(1) Eq. [5.4] (2) Eq. [5.15] (3) Eq. [5.3] (4) Eq. [5.18] (5) Eq. [5.20]

Conceptually, the distortional coefficient D must depend on the dimensionless parameters w/h, t/b, b/h, and l/h. A linear regression was conducted and equations based on the best fit are provided in Table 5.14

Table 5.14 Linear correlation of distortional coefficient D with dimensionless parameters w/h, t/b, b/h, and l/h.

Parameter(s)	R^2	Equation
w/h	0.069	[5.22] $D_{lin} = 0.9248 - 0.0962\dfrac{w}{h}$
l/h	0.010	[5.23] $D_{lin} = 0.9367 + 0.0006\dfrac{l}{h}$
b/h	0.009	[5.24] $D_{lin} = 0.9265 - 0.0224\dfrac{b}{h}$
t/b	0.001	[5.25] $D_{lin} = 0.9264 - 0.3479\dfrac{t}{b}$
w/h, l/h, b/h, t/b	0.36	[5.26] $D_{lin} = 0.9117 + 1.6105\dfrac{w}{h} - 0.0041\dfrac{l}{h} - 0.8199\dfrac{b}{h} - 0.0111\dfrac{t}{b}$

Results of the linear correlation reveal that use of all four dimensionless parameters (w/h , l/h , b/h , and t/b) would provide the best results. The distortional coefficient obtained through linear correlation, D_{lin} , as given by Eq. [5.26] is calculated and presented in Table 5.15. The ratio of the distortional coefficient obtained through linear correlation to the distortional coefficient obtained by FEA, D_{lin}/D_{FEA}, is then calculated to determine the accuracy of the predictions. As the statistical summary at the bottom of Table 5.15 suggests, the use of D_{lin} , could yield results which underestimate the FEA distortional coefficient D_{FEA} by 49.5%. At best, D_{lin} still provides unacceptable results which underestimate D_{FEA} by 15.1%.

Table 5.15 Accuracy of the predicted distortional coefficient obtained by linear regression (All cleat angles are L89x89x6.4 unless noted otherwise)

Designation	D_{FEA}	D_{lin}	D_{lin}/D_{FEA}	Designation	D_{FEA}	D_{lin}	D_{lin}/D_{FEA}
W310x107	0.985	0.556	0.565	W200x71	0.956	0.532	0.557
W310x97	0.972	0.559	0.575	W200x59	0.950	0.548	0.577
W310x86	0.952	0.559	0.587	W200x52	0.942	0.550	0.584
W310x79	0.955	0.568	0.594	W200x46	0.942	0.557	0.591
W310x74	0.958	0.561	0.585	W200x42	0.934	0.559	0.598
W310x67	0.951	0.569	0.598	W200x36	0.932	0.565	0.607
W310x60	0.941	0.575	0.611	W200x31	0.930	0.571	0.613
W310x52	0.938	0.573	0.611	W200x27	0.945	0.587	0.622
W310x45	0.932	0.587	0.629	W200x21	0.959	0.605	0.631
W310x39	0.928	0.597	0.643	W200x22	0.972	0.589	0.606
W310x31	0.932	0.615	0.660	W200x19	0.993	0.610	0.614
W310x33	0.945	0.556	0.588	W200x15	0.974	0.618	0.635
W310x28	0.951	0.583	0.613	W150x37	0.951	0.553	0.582
W310x24	0.966	0.616	0.637	W150x30	0.951	0.561	0.590
W310x21	0.973	0.629	0.646	W150x22	0.971	0.580	0.598
W200x100(1)	0.943	0.519	0.550	W150x24	0.947	0.547	0.578
W200x100(2)	0.947	0.519	0.548	W150x18	0.981	0.589	0.601
W200x100	1.026	0.519	0.505	W150x14	0.982	0.598	0.609
W200x86	0.995	0.530	0.533	W150x13	0.998	0.608	0.609
				Minimum			0.505
				Average			0.594
				Maximum			0.660

(1) Cleat angle is L89x89x13
(2) Cleat angle is L89x89x9.5

Since the use of distortional coefficient predictions obtained through linear correlation, D_{lin}, yields subpar results, an alternative method is utilized. Regression through minimizing the sum of the weighted squares of errors is utilized. This is achieved through solving for the constants a_1 a_2, a_3, a_4, and a_5 provided by minimizing

[5.27] $$\sum w_i \left[D_{FEA} - \left(a_1 + a_2 \left(\frac{w}{h} \right)_i + a_3 \left(\frac{l}{h} \right)_i + a_4 \left(\frac{b}{h} \right) + a_5 \left(\frac{t}{b} \right) \right) \right] = \min$$

where $w_i = 1$ when results are conservative, i.e., $D_{FEA} < 1$, and $w_i = 10$ when results are non-conservative, i.e., $D_{FEA} \geq 1$. The use of this procedure yields the following solution

[5.28] $$D = 0.9323 + 0.2760 \frac{w}{h}$$

Table 5.16 provides an indication of the accuracy of the predicted distortional coefficient obtained by Eq. [5.28]. As the statistical summary at the bottom of the table suggests, the proposed solution for the distortional coefficient, D provides predictions of D_{FEA} ranging from conservative underestimations of 7.3% to overestimations of a mere 0.1%. On average, the proposed solution underestimates the distortion coefficient by 1.6%.

Table 5.16 Accuracy of the predicted distortional coefficient obtained by minimizing sum of the weighted squared of error regression (All cleat angles are L89x89x6.4 unless noted otherwise)

Designation	D_{FEA}	D	D/D_{FEA}	Designation	D_{FEA}	D	D/D_{FEA}
W310x107	0.985	0.985	0.957	W200x71	0.956	0.950	0.990
W310x97	0.972	0.972	0.969	W200x59	0.950	0.942	0.995
W310x86	0.952	0.952	0.988	W200x52	0.942	0.942	1.002
W310x79	0.955	0.955	0.985	W200x46	0.942	0.934	1.001
W310x74	0.958	0.958	0.982	W200x42	0.934	0.932	1.009
W310x67	0.951	0.951	0.989	W200x36	0.932	0.930	1.010
W310x60	0.941	0.941	0.998	W200x31	0.930	0.945	1.012
W310x52	0.938	0.938	1.001	W200x27	0.945	0.959	0.996
W310x45	0.932	0.932	1.007	W200x21	0.959	0.972	0.980
W310x39	0.928	0.928	1.010	W200x22	0.972	0.993	0.968
W310x31	0.932	0.932	1.005	W200x19	0.993	0.974	0.947
W310x33	0.945	0.945	0.993	W200x15	0.974	0.951	0.963
W310x28	0.951	0.951	0.986	W150x37	0.951	0.951	0.996
W310x24	0.966	0.966	0.970	W150x30	0.951	0.971	0.994
W310x21	0.973	0.973	0.963	W150x22	0.971	0.947	0.972
W200x100(1)	0.943	0.943	1.010	W150x24	0.947	0.981	0.998
W200x100(2)	0.947	0.947	1.005	W150x18	0.981	0.982	0.962
W200x100	1.026	1.026	0.927	W150x14	0.982	0.998	0.958
W200x86	0.995	0.995	0.955	W150x13	0.998	0.950	0.942
					Minimum		0.927
					Average		0.984
					Maximum		1.012

(1) Cleat angle is L89x89x13
(2) Cleat angle is L89x89x9.5

5.7.3. Determining the Consistency Coefficient

The standard specific consistency coefficient, S_{st} is taken as the ratio of the moment gradient factor derived by energy formulation to the Standard specific moment gradient factors i.e., C_E/C_{st}. The proposed coefficient is Standard specific and depends only upon the degree of conservativeness implied in the present standard moment gradient factor. For instance, CAN/CSA S16-09 (Table 5.17) has the lowest moment gradient factor (most conservative) and AS 4100-1998 has the highest moment gradient factor (least conservative). To achieve the same level of implied safety, the consistency coefficient for the Canadian code is 1.125 while that of AS 4100-1998 is a mere 1.025. This ensures that both standards will yield the same solution, regardless of the starting point of the magnitude of the standard dependent moment gradient factor. It is noted that the consistency coefficient is unrelated to the beam properties, span, or loading method.

Table 5.17 Standard dependant consistency coefficient S_{st}

Standard	Standard Moment Gradient Factor C_{st}	Energy Formulation Moment Gradient Factor C_E	Consistency Coefficient $S_{st} = C_E / C_{st}$
ANSI/AISC 360-10	1.316	1.423	1.081
CAN/CSA S16-09 General	1.265	1.423	1.125
AS 4100-1998	1.388	1.423	1.025
EN 1993-1-1 Guide	1.365	1.423	1.042

5.7.4. Design Example 1

A beam with W410x39 cross-section ($F_y = 350MPa$) has a span of 4500*mm*. The beam is subject to a mid-span load. The beam is connected to rigid columns at both ends using double cleat angles at both ends. The cleat angles are L76x76x4.8 and are fastened to the beam web through 3-20*mm* A325 bolts. The distance between the angle heel to the bolt centerline is $l_c = 41mm$ while the cleat angle height is $h_c = 350mm$. It is required to determine the maximum factored load that the beam can withstand. Design checks are to be performed according to present design standards CAN/CSA S16-09, ANSI/AISC 360-10 as well as the proposed design methodology in the present chapter.

Beam properties are beam depth $d = 399mm$, flange width $b = 140mm$, flange thickness $t = 8.8mm$, web thickness $w = 6.4mm$, Saint-Venant constant $J = 110\times10^3 mm^4$, out-of-plane moment of inertia $I_y = 4.40\times10^6 mm^4$, plastic section modulus about the *x*-axis $Z_x =$

$610\times10^3 mm^3$, and warping constant $C_w = 154\times10^9 mm^6$. The cleat angles have a thickness $t_c = 4.8mm$, and a Saint-Venant constant $J_c = 57.5\times10^3 mm^4$.

CAN/CSA S16-09 Solution

The section flange meets Class 2 requirements since $b_{el}/t = 7.95 \le 170\big/\sqrt{F_y} = 9.092$. Also, the web meets Class 2 requirements since $h/w = 399/6.4 = 62.3 \le 1700\big/\sqrt{F_y} = 90.89$. Hence, the section meets Class 2 requirements and the plastic moment resistance is determined as $M_p = Z_x F_y = 255.5kNm$. The elastic lateral torsional buckling moment is $C_{CAN} M_u$ in which the moment gradient factor C_{CAN} is calculated based on the quarter point moment gradient equation (Eq. [2.3]), yielding the value $C_{CAN} = 1.265$ for a beam under mid-span load. The resulting elastic lateral torsional buckling moment is

$$C_{CAN} M_u = C_{CAN} \frac{\pi}{L} \sqrt{GJEI_y + \left(\frac{\pi E}{L}\right)^2 I_y C_w} = (1.265)(96.3) = 121.8kNm$$

Since $C_{CAN} M_u \le 0.67 M_p$, the beam capacity is governed by elastic LTB and the factored flexural resistance is given by $M_r = \phi C_{CAN} M_u = 109.6kNm$ and the corresponding factored load, $P_{f\max}$ is then given by $P_{f\max} = 4M_r/L = 97.4kN$.

ANSI/AIC 360-10 Solution

Since $b_{el}/t = 7.95 \le 0.38\sqrt{E/F_y} = 9.08$ and $h/w = 399/6.4 = 62.3 \le 3.76\sqrt{E/F_y} = 89.88$, ANSI/ AISC 360-10 also predicts Class 2 classification and the plastic moment resistance is $M_p = Z_x F_y = 255.5kNm$. The elastic lateral torsional buckling moment is $C_{AISC} M_u$ in which the moment gradient factor C_{ASIC} is calculated based on the quarter point moment gradient equation (Eq. [2.15]), yielding the value $C_{AISC} = 1.316$ for a beam under mid-span load. The resulting elastic lateral torsional buckling moment is

$$C_{AISC} M_u = C_{AISC} \frac{\pi}{L} \sqrt{GJEI_y + \left(\frac{\pi E}{L}\right)^2 I_y C_w} = (1.316)(96.3) = 126.7kNm$$

Since $C_{AISC}M_u \leq 0.7M_p$, the beam capacity is governed by elastic LTB and the flexural resistance is given by $M_r = \phi C_{AISC}M_u = 114.1kNm$ and the corresponding factored load, $P_{f\max}$ is then given by $P_{f\max} = 4M_r / L = 101.4kN$.

The above solutions do not account for partial twist restraints provided by the cleat angles, nor do they account for distortional effects. In these respects, the proposed design methodology accounts for these effects as described below.

Proposed Solution

To determine the partial twist restraint coefficient C_R, twisting stiffness R for cleat angles are determined

$$R = \frac{GJ_c}{l_c} = \frac{2G\left(\frac{1}{3}h_c t_c^{\ 3}\right)}{l_c} = 48.4kNm/rad$$

and the corresponding dimensionless ratio α is

$$\alpha = \frac{1}{R}\left(\frac{GJ}{L} + \frac{\pi^2 EC_w}{L^3}\right) = 0.1081$$

yielding a C_R value of

$$C_R = \sqrt{\frac{1}{1+1.642\alpha}} = 0.922$$

This signifies that since the twist restrain of the web cleat connection is only partial, a reduction factor of 92.2% needs to be applied to the critical moment as determined based on an idealized infinitely rigid twist connection. The factor accounting for reduction due to distortion, D is determined from

$$D = 0.9323 + 0.2760\frac{w}{h} = 0.937$$

This result suggests that, in order to account for distortional effects, a factor of 0.937 need to be applied to the solution provided by the standard which does not incorporate distortional effects. The corresponding critical moment is

$$
\begin{aligned}
M_{cr} &= DC_R\left(\phi C_{CSA} M_u\right) \\
&= (0.937)(0.922)(109.6) \\
&= 94.7kNm
\end{aligned}
$$

and the corresponding factored load, $P_{f\,\max}$ is then given by $P_{f\,\max} = 4M_{cr}/L = 84.2kN$.

If consistent results are to be obtained under both standards, the consistency coefficients found to $S_{st} = 1.081$ for ANSI/AISC 360-10 and $S_{st} = 1.125$ for CAN/CSA S16-09 need to be applied to the above solution. The resulting critical moments are then obtained as

<u>ANSI/AISC 360-10</u>

$$
\begin{aligned}
M_{cr} &= DC_R S_{st}\left(\phi C_{st} M_u\right) \\
&= (0.937)(0.922)(1.081)(114) \\
&= 106.5kNm
\end{aligned}
$$

$$P_{f\,\max} = \frac{4M_{cr}}{L} = 94.6kN$$

<u>CAN/CSA S16-09</u>

$$
\begin{aligned}
M_{cr} &= DC_R S_{st}\left(\phi C_{st} M_u\right) \\
&= (0.937)(0.922)(1.125)(109.6) \\
&= 106.5kNm
\end{aligned}
$$

$$P_{f\,\max} = \frac{4M_{cr}}{L} = 94.6kN$$

For comparison, the nominal critical moment based on finite element results is 124.1*kNm* and the corresponding factored critical moment is 111.7*kNm*. This value is used in the last column of the table as benchmark solution against which other solutions are assessed. Table 5.18 provides a summary of the moment predictions by the various methods.

For the given problem, CAN/CSA S16-09 procedure underestimates the critical moments by 2%, ANSI/AISC 360-10 overestimates it by 2%, but both solutions do not provide means to quantify distortional effects nor the degree of twist restraint. By disregarding the consistency coefficient, and retaining the partial twist restraint and distortional coefficients, the modified CAN/CSA S16-09 modified is observed to underestimate the critical moment by 15% and the modified ANSI/AISC 360-10 by 12%. After incorporating the consistency coefficients, both standards are found to underestimate the capacity of the beams by 5%.

Table 5.18 Comparison of critical moment predictions for a 4.5m span W410x39 beam (supported by 2xL76xL76x4.8 at both ends)

	Factored Critical Moment Equation (M_{cr} or M_r)	Moment gradient Factor (C_{st})	Partial twist restraint factor (C_R)	Distortion coefficient (D)	Consistency coefficient (S_{st})	Critical Moments (kNm)	$\frac{M_r}{M_{FEA}}$
CAN-CSA S16(1)	$\phi C_{CSA} M_u$	1.265	-	-	-	109.6	0.981
ANSI/AIC 360-10(1)	$\phi C_{AISC} M_u$	1.316	-	-	-	114.1	1.021
CAN-CSA S16 Modified(2)	$\phi D C_R C_{CSA} M_u$	1.265	0.922	0.937	-	94.7	0.848
ANSI/AISC 360-10 Modified(2)	$\phi D C_R C_{AISC} M_u$	1.316	0.922	0.937	-	98.6	0.883
Consistent Procedure (CSA)(3)	$\phi S_{CSA} D C_R C_{CSA} M_u$	1.265	0.922	0.937	1.125	106.5	0.953
Consistent Procedure (AISC)(3)	$\phi S_{AISC} D C_R C_{AISC} M_u$	1.316	0.922	0.937	1.081	106.5	0.953
FEA	ϕM_{FEA}					111.7	1.00

(1) Does not account for distortion or partial twist restraint provided by cleat angles and equations are based on standard dependent moment gradient factors.

(2) Equations based on standard dependent moment gradient factors and accounts for partial twist restraint and distortion.

(3) Equations are standard independent and account for partial twist restraint and distortion.

5.7.5. Design Example 2

It is required to revise the capacity of the beam if the supporting cleat angles are replaced with thick L76x76x9.5. The twist stiffness of the new cleat angles would increase to $R = 375\, kNm/rad$, and the corresponding results are summarized in Table 5.19.

As expected, a thicker cleat angle results in a critical moment as determined by FEA that is higher by about 6.3% compared to that based on the thinner cleat angle (L76x76x4.8). Again, the resisting moment will serve as a basis to assess the quality of other solutions. The difference in resistance in both cases is not captured by present design rules in CAN/CSA S16-09 and ANSI/AISC 360-10 which predict the same buckling resistance as that determined in Example 1, which now predict a lower moment resistance ratios of 92.3% and 96.1%, respectively.

Under the proposed modification to the standard, an increase in the partial twist restraint coefficient C_R is obtained, where it is observed to increase from 0.922 to 0.989, a 7.3% increase. The proximity of the new value of C_R suggests the chosen angle provides near full twist fixity to the beam ends. This increase results in a proportional increase in the predicted capacity of the beam, thus maintaining the predicted moment ratio nearly identical to that based on example 1, i.e., the moment ratios are 0.859 and 0.891 for CAN/CSA S16-09 and ANSI/AISC 360-10, respectively. To achieve consistency under both standards and closer proximity to FEA values, the consistency coefficients for both standards are applied, resulting in both cases in a moment ratio of 0.963.

The above illustrative examples suggest that the proposed methodology is able to successfully account for partial twist restraints and distortional effects in predicting critical moments and illustrate the advantages of the new method compared to present standard methodologies.

Table 5.19 Comparison of critical moment predictions for a 4.5m span W410x39 beam (supported by 2xL76xL76x9.5 at both ends).

	Factored Critical Moment Equation (M_{cr} or M_r)	Moment gradient Factor (C_{st})	Partial twist restraint factor (C_R)	Distortion coefficient (D)	Consistency coefficient (S_{st})	Critical Moments (kNm)	$\frac{M_r}{M_{FEA}}$
CAN-CSA S16(1)	$\phi C_{CSA} M_u$	1.265	-	-	-	109.6	0.923
ANSI/AIC 360-10(1)	$\phi C_{AISC} M_u$	1.316	-	-	-	114.1	0.961
CAN-CSA S16 Modified(2)	$\phi D C_R C_{CSA} M_u$	1.265	0.989	0.937	-	101.6	0.856
ANSI/AISC 360-10 Modified(2)	$\phi D C_R C_{AISC} M_u$	1.316	0.989	0.937	-	105.7	0.891
Consistent Procedure (CSA)(3)	$\phi S_{CSA} D C_R C_{CSA} M_u$	1.265	0.989	0.937	1.125	114.3	0.963
Consistent Procedure (AISC)(3)	$\phi S_{AISC} D C_R C_{AISC} M_u$	1.316	0.989	0.937	1.081	114.3	0.963
FEA	ϕM_{FEA}					118.7	1.000

(1) Does not account for distortion or partial twist restraint provided by cleat angles and equations are based on standard dependent moment gradient factors.

(2) Equations based on standard dependent moment gradient factors and accounts for partial twist restraint and distortion.

(3) Equations are standard independent and account for partial twist restraint and distortion.

5.8. *Notation for Chapter 5*

A	constant in the displacement function
a_i	minimizing sum of weighted squares regression constants
B	constant in the angle of twist function
b	flange/ beam width
b_{el}	width of unstiffened compression element
C	constant in the angle of twist function
C_{AISC}	ANSI/AISC 360-10 moment gradient factor
C_{AUS}	AS 4100-1998 moment gradient factor
C_{CAN}	CAN/CSA S16-09 moment gradient factor
$C_{CAN-Gen}$	CAN/CSA S16-09 general moment distribution moment gradient factor
C_{EURO}	EN 1993-1-1 moment gradient factor
C_{FEA}	moment gradient factor as determined by FEA
C_R	partial twisting restraint coefficient
C_{st}	standard dependent moment gradient factor
C_w	warping constant
D	distortional coefficient
D_{FEA}	distortional coefficient calculated by FEA results
D_{lin}	distortional coefficient obtained through linear corelation
E	modulus of elasticity of steel
F_y	specified minimum yield stress
G	shear modulus of elasticity of steel
h	distance between flange centroids
h_c	depth of cleat angle
I_y	out of plane moment of inertia
J	St. Venant torsional constant
J_c	St. Venant torsional constant of a single angle
L	length of beam
L_c	distance from angle heel to bolt centerline
$l_{\lim}$	limiting minimum span

$l_{\max}$ maximum span

M applied moment

M_a bending moment at one-quarter point of unbraced segment

M_b bending moment at mid-point of unbraced segment

M_c bending moment at three-quarter point of unbraced segment

M_{cr} elastic critical moment capturing the effects of distortional buckling

M_E moment gradient factor derived by energy formulation

M_{FEA} elastic critical moment capturing the effects of distortional buckling as determined by FEA

M_{in} nominal inelastic lateral torsional moment resistance

$M_{\max}$ maximum bending moment magnitude in unbraced segment

M_n nominal moment resistance

M_p plastic moment resistance

M_r factored moment resistance

M_u classical lateral torsional buckling solution

M_y yield moment resistance

M_0 maximum moment in a triangular moment distribution, critical moment expression obtained by energy methods

M_∞ hypothetical critical moment assuming ends are infinitely restrained

P applied point load

$P_{f\,\max}$ maximum factored point load

R web cleat connection twist stiffness

S_{AISC} consistency constant to be used with ANSI/AISC 360-10

S_{CAN} consistency constant to be used with CAN/CSA S16-09

S_{st} standard specific consistency constant

t flange thickness

t_c angle thickness

U internal strain energy

u_b nodal translation at the bottom web to flange junction

u_t	nodal translation at the top web to flange junction
$u(z)$	displacement function
V	load potential energy gain
w	web thickness
w_c	cleat angle thickness
w_i	minimizing sum of weighted squares regression weight constant
Z_x	plastic section modulus taken about the x-axis
α	dimensionless ratio
$\phi(z)$	angle of twist function
ϕ_A	twist angle at beam end A
ϕ_B	twist angle at beam end B
ϕ_M	twist angle at beam mid-span
π_p	total potential energy

Chapter 6

Distortional Lateral Torsional Buckling for Cantilevers Subject to Tip Point Loads

6.1. Cantilevers in Structural Applications

Cantilevers are structural members which are restrained at one end (the root) and free at the other end (the tip). Cantilevers are generally used when support via a beam or column is undesirable or unfeasible at one end. They are frequently used in pipe rack networks in industrial plants, petrochemical plants, and the oil and gas industry. A common configuration of this application is depicted in Fig. 6.1. In this setup, loading from a pipe is transmitted to the cantilever tip through steel plate seats. The load schematic and corresponding bending moment diagram are presented in Fig. 6.2 (a-b).

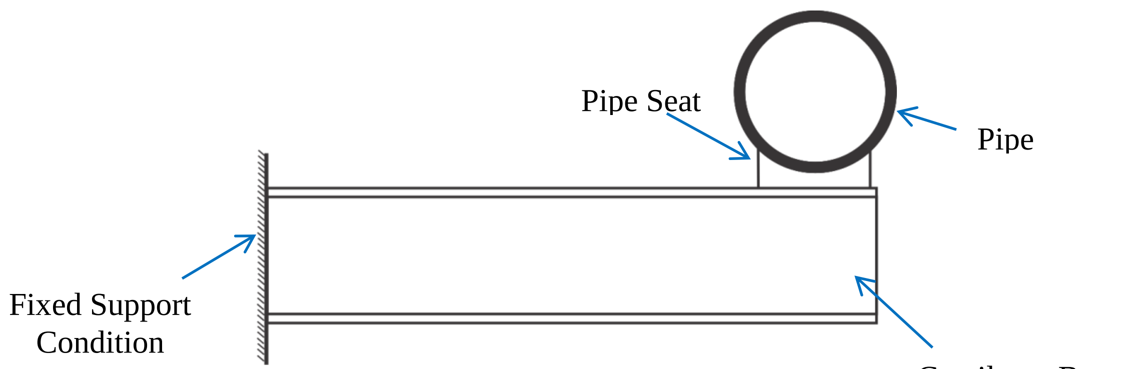

Fig. 6.1- Cantilever beam in a pipe rack

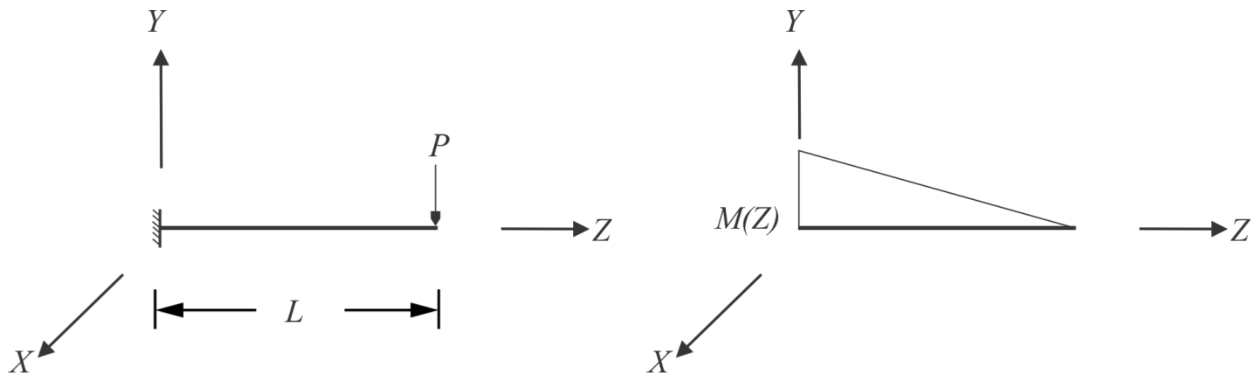

(a) (b)

Fig. 6.2- Tip point load (a) Schematic, and (b) Bending moment diagram

6.2. *Standard Procedures on Lateral Torsional Buckling of Beams*

Various standards (CAN/CSA S16-09, ANSI/AISC 360-10, EN 1993-1-1 and AS 4100-1998) do not provide detailed recommendations for designing cantilevers to resist failure in a LTB mode. While EN 1993-1-1 does not mention cantilevers at all in its section for flexural design, CAN/CSA S16-09 and ANSI/AISC 360-10 codes provide little guidance.

Clause 13.6(a) of CAN/CSA S16-09 on laterally unsupported members in bending, states that; "For unbraced beam segments loaded above the shear centre between brace points, where the method of load delivery to the member provides neither lateral nor rotational restraint to the member, the associated destabilizing effect shall be taken into account using a rational method. For loads applied at the level of the top flange, in lieu of a more accurate analysis, "the critical moment" be determined using "a moment gradient factor $C_{CAN}" = 1.0$ and using an effective length, for pinned-ended beams, equal to $1.2L$ and, for all other cases, $1.4L$." It is not clear whether the intent of the modified span method is applicable to cantilevers. Also, Clause 13.6(d) states that "For cantilever beams, a rational method of analysis taking into account the lateral and torsional restrain conditions at the supports and tip of the cantilever, as well as the loading conditions and the flexibility of the back-span, shall be used." Clause 13.6(a) could be interpreted to suggest that for cantilevers loaded above the shear center, the use of a moment gradient factor of $C_{CAN} = 1.0$ and an effective length of $1.4L$ in the classical LTB solution would produce code conformant results. One of the objectives of the present study is to assess how consistent results based on Clause 13.6(a) are with those based on Clause 13.6(d) for the case of a cantilever subject to a tip concentrated load acting on the top flange.

ANSI/AISC 360-10 does not differentiate between cantilevers and other beam types. However, it stipulates setting the moment gradient factor $C_{AISC} = 1.0$, thus using the classical LTB equation to asses moment resistance of cantilevers. This recommendation has been criticized by Dowswell (2004), who suggested that the classical LTB solution was derived for simply supported beams and its use of for cantilevers may not be correct since the mechanics of buckling for a cantilever beam could differ from those of simply supported beams.

The Australian Standard AS 4100-1998 provides detailed direction in its informative Appendix H about cantilever design for lateral torsional buckling. According to the Appendix solution, a moment modifier factor C_{AUS} should be applied, of the form

[6.1] $$C_{AUS} = \alpha_{mc}\alpha_{lc}$$

where α_{mc} is a moment gradient factor given by

[6.2] $$\alpha_{mc} = \frac{\left(C_3 + C_4 X\right)}{\pi\sqrt{1+X^2}}$$

where for cantilevers subject to tip loads, $C_3 = 4.0$ and $C_4 = 3.7$ should be used. In Eq. [6.1] α_{lc} is a load position factor given by

[6.3] $$\alpha_{lc} = 1 + \frac{\left(\frac{y_L X}{h}\right)}{\sqrt{\left[1+\left(\frac{y_L X}{h}\right)^2\right]}}$$

where y_L is the load height from the section shear centre, taken as positive for loading below the shear center, and h is the distance between flange centroids. Symbol X, initially introduced in Trahair (1983, 1993) represents the ratio of warping stiffness to the Saint-Venant torsional stiffness is given by

[6.4] $$X = \frac{\pi}{l}\sqrt{\frac{EC_w}{GJ}}$$

and will subsequently be referred to as the “dimensionless torsional parameter.” As an observation, there is significant variability between design methods for laterally unsupported cantilevers in terms of the degree of simplicity of the solution and the level of detail involved in the various design procedures. Also, it is not clear whether the proposed solutions account for distortional buckling effects.

6.2.1. Dabbas Study (2002)

Dabbas (2002) investigated the lateral torsional buckling of cantilevers based on a series of shell FEA runs for a W250x58 cantilever with boundary conditions and load application details identical to those outlined and studied in the present study. However, the FEA results presented by Dabbas suppress distortional effects. In his FEA model, Dabbas attempted to simulate the first Vlasov assumption (Vlasov 1961), i.e., throughout deformation, a cross-section is assumed to act as a rigid disk within its own plane. Dabbas enforced this condition through a series of Multi Point Constraints (MPC) offered by Abaqus known as MPC Slider Type.

6.2.2. Dowswell Study (2004)

Dowswell (2004) introduced a procedure where the LTB resistance of a cantilever beam is predicted by replacing the standard dependent moment gradient factor (C_{st}) by a factor C_{DOWS}. The factor C_{DOWS} was determined by curve fitting of buckling moment predictions based on a series of shell based FEA results obtained for several combinations of cross-sections and cantilever spans (summarized in Table 6.1). Dowswell proposed that the critical moment of a cantilever beam is product of a factor (C_L) which depends on the moment diagram, a bracing coefficient (C_B), and a load position factor (C_H) with respect to the shear centre. Since the aim of the present study is to investigate unbraced cantilevers subject to tip point loads acting on the top flange, discussions pertaining to Dowswell’s solution will be limited to his equations for this particular case. As such, Dowswell’s proposed factor, C_{DOWS} which relates the critical moment to the classical LTB M_u (Eq. [2.1]) through $M_{DOWS} = C_{DOWS} M_u$, is given by

[6.5] $$C_{DOWS} = \frac{C_L C_H C_B}{\pi} \sqrt{\frac{GJ}{GJ + \left(\frac{\pi}{l}\right)^2 EC_w}}$$

where coefficient C_L is based on a triangular moment distribution corresponding to a point load at the free end given by

[6.6] $C_L = 3.95 + 3.52X$

Since loading is taken to be applied at the top flange, the corresponding load position factor C_H is given by

[6.7] $C_H = 0.97 - 0.59X + 0.14X^2$

In the absence of lateral and torsional bracing, the bracing coefficient based on Dowswell's study is taken as

[6.8] $C_B = 1.0$

By substituting C_L, C_H, and C_B into Eq. [5.2], the following expression is obtained

[6.9] $$C_{DOWS} = \frac{0.49X^3 - 1.52X^2 + 1.08X + 3.83}{\pi\sqrt{1+X^2}}$$

Therefore, for the conditions investigated in this chapter (cantilever subject to a top flange point load at its free end with no bracing), C_{DOWS} is strictly a function of the dimensionless torsional parameter X .

The Sixth Edition of Structural Stability Research Council (SSRC) Guide to Stability Design Criteria for Metal Structures (Ziemian 2010) essentially adopted a modified form of Dowswell solution, in which the solution was limited to the range $0.5 \le X \le 2.5$ and the load position factor was taken as

[6.10] $C_{H-SSRC} = 0.76 - 0.51X + 0.13X^2$

By replacing C_H in Dowswell solution by C_{H-SSRC} and substituting in Eq. [6.5], the following expression is obtained

[6.11] $$C_{D-SSRC} = \frac{0.46X^3 - 1.28X^2 + 0.66X + 3.00}{\pi\sqrt{1+X^2}}$$

Since the SSRC provides the latest form of the Dowswell solution, comparisons made in the rest of this study will be limited to the SSRC Dowswell solution as expressed in the moment gradient factor C_{D-SSRC}.

6.3. *Root Restrains in Cantilevers*

The restraint conditions adopted by Dabbas (2002) and Dowswell (2004) assume that cantilever roots are infinitely restrained against displacement, twist, and weak axis rotation and warping. In design applications, whether or not this limiting idealized support condition is attained depends on the stiffening details at the root.

Fig. 6.3 (a-c) shows three possible details. Fig. 6.3(a) shows an unstiffened cantilever root which provides little or no warping restraint. Fig. 6.3(b) shows a cantilever root with two pairs of horizontal stiffener which provides partial warping restraint while Fig. 6.3(c) shows a cantilever root with three pairs of stiffeners providing full warping restrains. The studies in Dabbas (2002) and Dowswell (2004) as well as the present study are applicable to the case of full restraint at the cantilever root (i.e., restricted to details such as those in Fig. 6.3(c)).

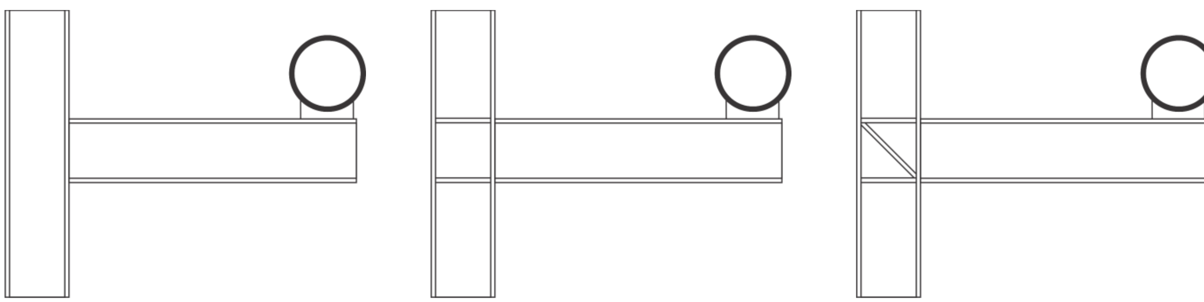

(a) (b) (c)

Fig. 6.3- Cantilever connection arrangements: (a) Unstiffened, (b) Two pairs of horizontal stiffeners, and (c) Three pairs of stiffeners including diagonal stiffening

6.4. *Objective and Scope*

In an effort to provide better guidance for cantilever design than that available in present design standards for cantilevers, this chapter documents a study on a series of buckling FEA runs for cantilevers subject to tip point loads. Focus will be on cantilevers with no lateral or torsional bracing and with loads applied to the top flange. Cross-sections will be selected from those commercially available in the CISC database.

Towards this goal, section and span combinations studied by Dowswell (2004), and Dabbas (2002) will be modeled and analyzed. The database is also augmented by analyzing additional section and span combinations with the goal of providing a more comprehensive representation of practical sections and realistic design scenarios.

6.5. *Selection of Cross-Sections and Spans*

A total of 11 sections and 81 FEA runs are conducted. Four sections and a total of 24 runs are based on cross-sections studied by Dowswell (2004) and Dabbas (2002). These are summarized in Table 6.1. An additional seven cross-sections with a total of 57 runs were selected and modeled. These are presented in Table 6.2.

Table 6.1 Sections studied by Dowswell (2004) and Dabbas (2002)

	Dowswell (2004) Sections			Dabbas (2002) Sections
	W200x22	W310x79	W410x39	W250x58
t/b	0.078	0.057	0.063	0.067
w/h	0.031	0.030	0.016	0.034
b/h	0.515	0.872	0.359	0.851
l (mm)	l/h			
1000	-	-	-	4.19
2000	-	-	-	8.39
2286	11.5	7.84	5.86	-
3000	-	-	-	12.6
3048	15.4	10.5	7.81	-
3810	19.2	13.1	9.76	-
4000	-	-	-	16.8
4572	23.1	15.7	11.7	-
5000	-	-	-	21.0
5334	26.9	18.3	13.7	-
6000	-	-	-	25.2
6096	30.8	20.9	15.6	-

Table 6.2 Additional FEA runs (Section Designations, spans, and dimensionless parameters)

	Designation						
	W360x39	W360x33	W310x21	W310x24	W410x46	W150x30	W1000x584
t/b	0.084	0.067	0.056	0.066	0.080	0.061	0.204
w/h	0.019	0.017	0.017	0.019	0.018	0.045	0.036
b/h	0.374	0.373	0.340	0.339	0.357	0.025	0.317
l (mm)	l/h						
1000	2.92	2.94	3.36	3.35	2.55	6.77	-
1200	3.51	3.52	4.04	4.02	3.06	-	-
1400	4.09	4.11	4.71	4.69	3.57	-	-
1700	4.97	4.99	5.72	5.70	4.34	-	-
2000	5.84	5.87	6.73	6.70	5.1	13.5	-
3000	8.76	8.81	10.1	10.1	7.66	20.3	-
4000	11.7	11.7	13.5	13.4	10.2	27.1	4.03
4600	-	-	-	-	-	-	4.64
5000	14.6	14.7	16.8	16.8	12.8	33.9	5.04
6000	17.5	17.6	20.2	20.1	15.3	40.6	6.05
7000	-	-	-	-	-	-	7.06
8000	-	-	-	-	-	-	8.06

6.5.1. Selection of Representative Sections

A consideration of the dimensionless parameters w/h, t/b, and b/h revealed that the sections chosen by Dowswell (2004) and Dabbas (2002) are not representative of the entire CISC SST database. As presented in Table 6.3, sections studied by Dowswell (2004), and Dabbas (2002) do not include sections at extreme ends of the dimensionless parameters, especially for the t/b ratio. As such, the additional sections listed in Table 6.2 were introduced in the present FEA study.

Table 6.3 Statistical data of dimensionless parameters

	Statistic	t/b	b/h	w/h
Dowswell & Dabbas Sections	Maximum	0.078	0.872	0.034
	Minimum	0.057	0.359	0.016
CISC SST Database Sections	Maximum	0.275	1.134	0.176
	Minimum	0.043	0.304	0.015
All Studied Sections	Maximum	0.204	1.036	0.045
	Minimum	0.056	0.317	0.016

6.5.1.1. Representativeness of Dimensionless torsional parameter X

As depicted in Fig. 6.4, the sections and spans chosen by both Dowswell (2004) and Dabbas (2002) do not adequately represent all possible variations of the dimensionless torsional parameter X of practical interest. The FEA runs conducted by Dowswell are limited to $0.435 \leq X \leq 2.78$. Dabbas' sections and spans include dimensionless torsional parameter values of X up to 4.29; however, his study does not include FEA simulations in the range of $2.14 < X < 4.29$. As such, additional sections and spans are chosen to broaden the range of X while satisfying the needs of sectional representativeness outlined in Subsection 6.5.1. The combination of all sections chosen in the present study broadens the database to correspond to values of the dimensionless torsional parameter in the range $0.435 \leq X \leq 5.40$.

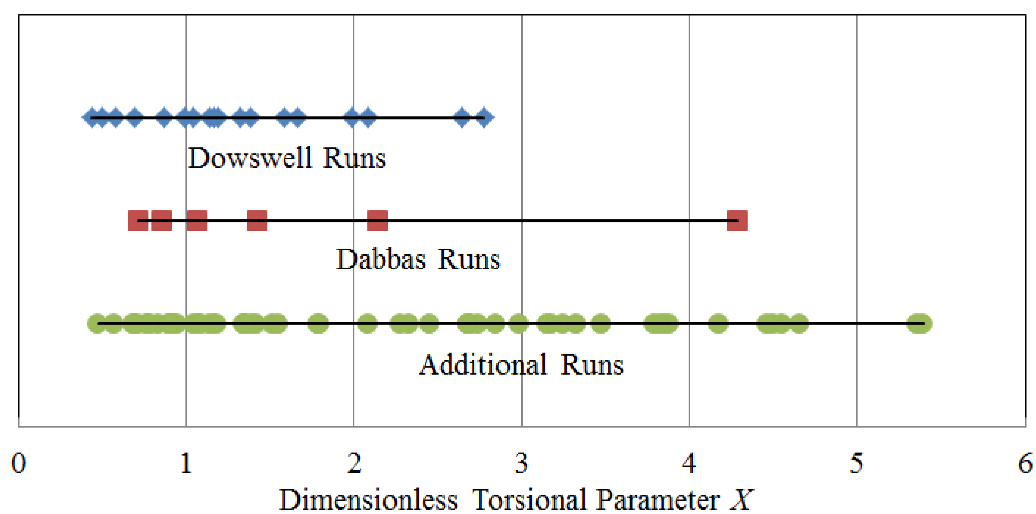

Fig. 6.4- Representativeness of Dimensionless Torsional Parameter X

6.6. FEA Model & Boundary Conditions

The details described in Section 3.8 were used in creating the FEA models of the cantilevers to be simulated in the present study. As in Chapter 3, a global mesh of 0.3 is assigned. As one recalls, this results in an element size of approximately $30mm \times 30mm$. For a W310 beam whose depth is $300mm$ this would results in 10 elements along the height of the web. Several methods are used in the industry to achieve fixed conditions. In general, any connection method which transmits moments to the supporting member is a valid moment connection. The most common types of connections are flange plates and welds. For the purposes of this study, a welded connection is simulated. To achieve this, displacements and rotations of all nodes at the cantilever root of the FEA model are restrained (Fig. 6.5(a)). At the tip, all translational and rotational degrees of freedom are released for all nodes (Fig. 6.5(b)).

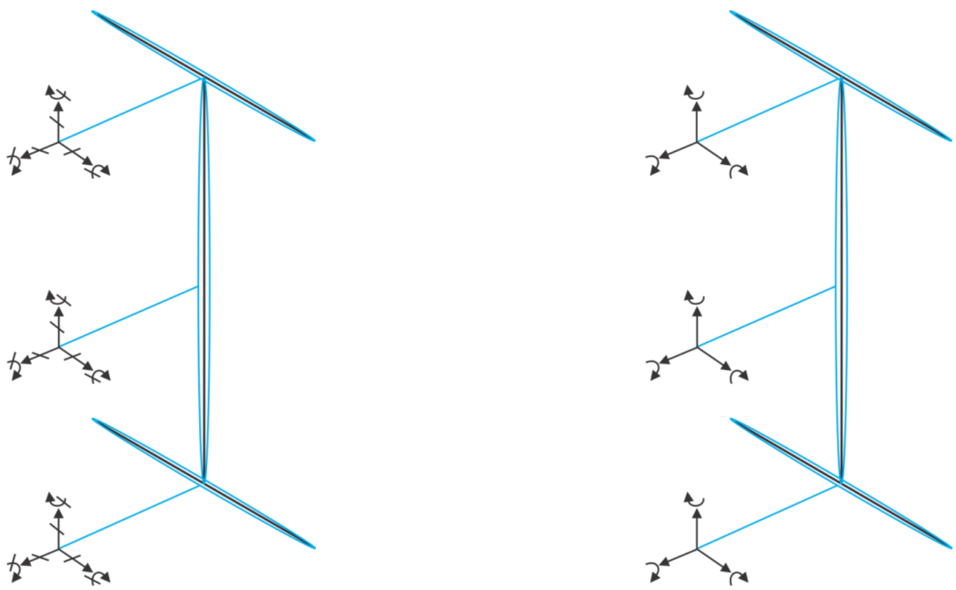

(a) (b)

Fig. 6.5- Nodal translations and rotations at (a) Fixed end, and (b) Free end

6.7. Load Application Scheme

All sections studied exhibited the same load application consisting of a single point load at the top web to flange junction of the free end (Fig. 6.6). This load application was selected because the destabilizing factor introduced by top flange loading amplifies the effect of LTB.

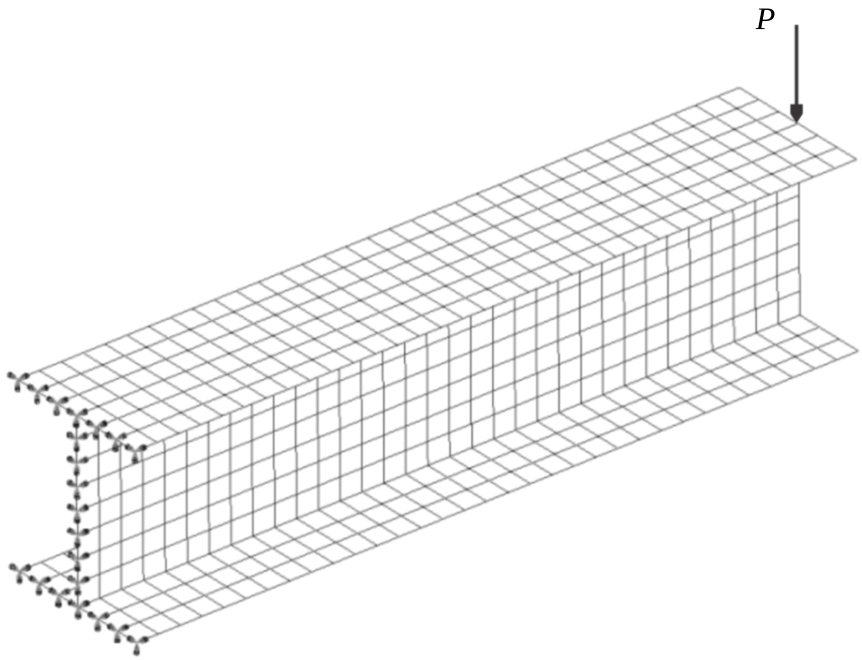

Fig. 6.6- FEA model free end point load

6.8. Results

6.8.1. Dabbas' Sections

FEA results produced by Dabbas (2002) and through the present FEA model are presented in Table 6.4. The results produced slightly lower critical moments than those produced by Dabbas, with the only exception occurring when the span is equal to 1000*mm*. For this span, it was noticed that Dabbas' results over-estimated the moment capacity by 54.5%. The reason for the large discrepancy is attributed to the fact that while Dabbas suppressed distortional effects in his solution, the present solution captures them. For short cantilevers, distortional effects gain significance which explains the larger discrepancy in this case. However, this result based on the 1000*mm* span is of no practical value since the design would be normally be governed by yielding (for common steel grades) for such a short span. As such, this data point will be dismissed in any further analysis or discussion. With this data point removed, Fig. 6.7 suggests that Dabbas' results overestimate moment capacity by 2% for a 6*m* span to 10% for a 2*m* span. This discrepancy is a natural outcome of the fact that Dabbas' results neglect the effects of distortion, thus overestimating the critical moment capacity.

Table 6.4 FEA Results of Dabbas' sections

	l (mm)	$\frac{l}{h}$	M_u (kNm)	M_{DABB} (kNm)	M_{FEA} (kNm)	C_{DABB}	C_{FEA}	$\frac{C_{DABB}}{C_{FEA}}$
W250x58	1000	4.19	4550	1452	661	0.319	0.145	2.196
	2000	8.39	1220	546	496	0.447	0.406	1.100
	3000	12.6	601	366	345	0.609	0.573	1.062
	4000	16.8	379	292	280	0.771	0.740	1.041
	5000	21.0	272	245	241	0.900	0.886	1.016
	6000	25.2	212	216	212	1.020	1.001	1.020
						Minimum		1.020
						Maximum		2.196
						Mean		1.239

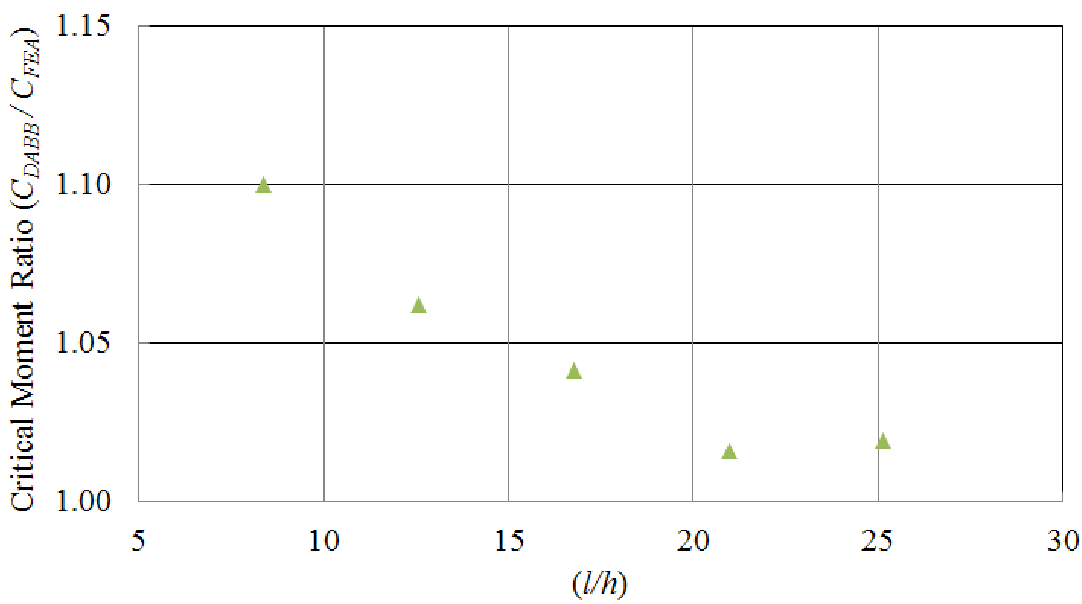

Fig. 6.7- Critical moment ratio of for W250x58

6.8.2. Dowswell's Sections

FEA of the sections and spans chosen by Dowswell are conducted and results are presented in Table 6.5. Results suggest that Dowswell's proposed equation overestimates capacities by up to 42% for short beams. For the 18 combinations of sections and spans considered, there are 15 instances where Dowswell's solution provided conservative results exceeding 10%. However, on average, Dowswell's solutions were observed to underestimate capacities by 14%. As depicted in Fig. 6.8, regardless of the section, Dowswell's solutions diverge from the FEA results as the span of a beam decreases.

Table 6.5 FEA Results of Dowswell's sections

	l (mm)	$\frac{l}{h}$	M_u (kNm)	M_{D-SSRC} (kNm)	M_{FEA} (kNm)	C_{D-SSRC}	$C_{FEA}=\frac{M_{FEA}}{M_u}$	$\frac{C_{D-SSRC}}{C_{FEA}}$
W410x39	2286	5.86	316	162	114	0.512	0.360	1.420
	3048	7.81	185	75.4	82	0.407	0.443	0.919
	3810	9.76	125	54.4	65.9	0.436	0.529	0.825
	4572	11.7	91.5	45.5	56.5	0.498	0.617	0.806
	5334	13.7	71.2	40.1	50.1	0.562	0.703	0.799
	6096	15.6	57.9	36.0	45.4	0.621	0.784	0.792
W310x79	2286	7.84	2350	1120	870	0.479	0.371	1.292
	3048	10.5	1380	563	640	0.407	0.463	0.879
	3810	13.1	934	420	522	0.450	0.559	0.804
	4572	15.7	688	355	453	0.517	0.658	0.785
	5334	18.3	537	313	405	0.583	0.754	0.773
	6096	20.9	438	281	370	0.642	0.845	0.760
W200x22	2286	11.5	69.9	40.1	49.5	0.573	0.707	0.810
	3048	15.4	45.4	31.7	40.3	0.698	0.887	0.787
	3810	19.2	33.4	26.1	34	0.782	1.019	0.767
	4572	23.1	26.4	22.1	29.3	0.838	1.109	0.755
	5334	26.9	21.8	19.1	25.5	0.875	1.168	0.749
	6096	30.8	18.7	16.8	22.5	0.900	1.205	0.747
						Minimum		0.747
						Maximum		1.420
						Mean		0.859

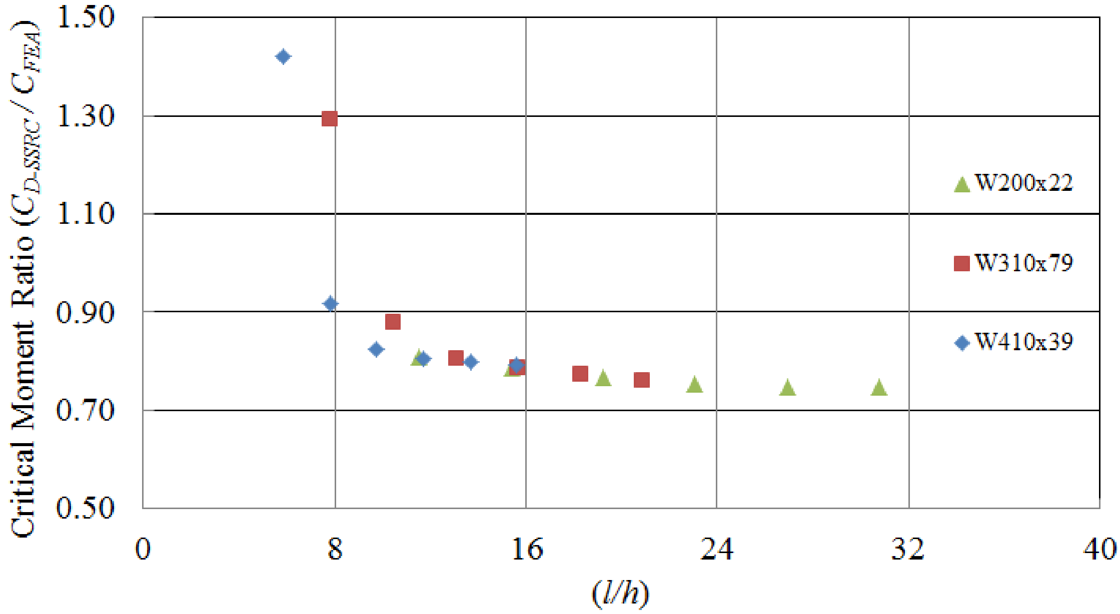

Fig. 6.8- Critical moment ratio of Dowswell's sections

6.8.3. Additional Sections

Results based on additional sections are evaluated against predictions provided by Dowswell using the methodology outlined by the SSRC. Since Dabbas (2002) did not provide a general solution applicable to any section, a comparison with his methodology for the additional sections cannot be made. For clarity, FEA results are presented in Table 6.6 which is split into two pages. Statistics for both tables are compiled in Table 6.7. As the results suggest, predictions provided by Dowswell's solution lead to results which range from conservative predictions of about 26% to gross overestimations which exceed 2100%. On average Dowswell's solution overestimates the critical moments by 152%.

Table 6.6 FEA Results of additional sections

	l (mm)	$\frac{l}{h}$	M_u (kNm)	M_{D-SSRC} (kNm)	M_{FEA} (kNm)	C_{D-SSRC}	$C_{FEA}=\frac{M_{FEA}}{M_u}$	$\frac{C_{D-SSRC}}{C_{FEA}}$
W150x30	1000	6.77	858	456	298	0.532	0.348	1.53
	2000	13.5	247	121	146	0.488	0.591	0.826
	3000	20.3	131	86.6	109	0.662	0.833	0.795
	4000	27.1	87.4	67.7	88.6	0.775	1.014	0.765
	5000	33.9	65.5	55.3	74	0.843	1.129	0.747
	6000	40.6	52.5	46.5	62.9	0.885	1.198	0.739
W360x39	1000	2.92	1290	2000	194	1.542	0.150	10.3
	1200	3.51	908	886	207	0.975	0.228	4.28
	1400	4.09	675	462	193	0.685	0.285	2.40
	1700	4.97	467	227	160	0.486	0.342	1.42
	2000	5.84	345	144	135	0.417	0.390	1.07
	3000	8.76	168	78.2	92.5	0.465	0.550	0.846
	4000	11.7	105	61.3	74.6	0.582	0.709	0.821
	5000	14.6	75.2	51.1	63.9	0.680	0.849	0.800
	6000	17.5	58.2	43.7	56	0.752	0.963	0.781
W360x33	1000	2.94	993	2370	130	2.386	0.131	18.2
	1200	3.52	694	1040	144	1.497	0.207	7.22
	1400	4.11	515	523	138	1.016	0.268	3.79
	1700	4.99	354	231	114	0.652	0.321	2.03
	2000	5.87	260	128	94.1	0.491	0.361	1.36
	3000	8.81	124	52	61	0.419	0.491	0.852
	4000	11.7	75.9	38.6	47.6	0.509	0.627	0.812
	5000	14.7	53.2	32.2	40.3	0.605	0.757	0.800
	6000	17.6	40.6	27.8	35.3	0.685	0.871	0.786
W310x21	1000	3.36	294	481	70.6	1.635	0.240	6.81
	1200	4.04	206	213	60.8	1.032	0.295	3.50
	1400	4.71	153	110	50.5	0.720	0.330	2.18
	1700	5.72	106	53.2	36.6	0.502	0.346	1.45
	2000	6.73	78.3	33.1	32.7	0.423	0.417	1.01
	3000	10.1	38	17.4	21.7	0.457	0.571	0.801
	4000	13.5	23.7	13.6	17.2	0.572	0.725	0.788
	5000	16.8	16.9	11.3	14.6	0.670	0.863	0.777
	6000	20.2	13	9.69	12.7	0.744	0.973	0.764

Table 6.6 continued

	l (mm)	$\frac{l}{h}$	M_u (kNm)	M_{D-SSRC} (kNm)	M_{FEA} (kNm)	C_{D-SSRC}	$C_{FEA}=\frac{M_{FEA}}{M_u}$	$\frac{C_{D-SSRC}}{C_{FEA}}$
W1000X584	4000	4.03	25200	12700	13300	0.505	0.528	0.958
	4600	4.64	20100	11400	12200	0.565	0.606	0.932
	5000	5.04	17700	10600	11600	0.602	0.656	0.916
	6000	6.05	13400	9160	10400	0.681	0.775	0.879
	7000	7.06	10800	8030	9490	0.743	0.878	0.847
	8000	8.06	9030	7140	8690	0.790	0.962	0.821
W310x24	1000	3.35	349	432	89.6	1.238	0.257	4.83
	1200	4.02	245	195	75.8	0.796	0.309	2.57
	1400	4.69	183	105	63.2	0.577	0.346	1.67
	1700	5.7	127	55.9	50.2	0.441	0.396	1.11
	2000	6.7	94.1	38.3	42	0.407	0.446	0.912
	3000	10.1	46.4	23.1	28.8	0.497	0.620	0.801
	4000	13.4	29.4	18.2	23.1	0.620	0.787	0.788
	5000	16.8	21.2	15.2	19.6	0.715	0.926	0.773
	6000	20.1	16.5	12.9	17	0.783	1.031	0.759
W410x46	1000	2.55	2020	4720	211	2.340	0.104	22.4
	1200	3.06	1410	2070	240	1.468	0.170	8.65
	1400	3.57	1050	1040	248	0.997	0.237	4.21
	1700	4.34	720	462	218	0.642	0.303	2.12
	2000	5.1	529	257	184	0.486	0.348	1.40
	3000	7.66	253	106	122	0.420	0.482	0.871
	4000	10.2	155	79.2	95.8	0.512	0.619	0.827
	5000	12.8	109	66	81.4	0.609	0.750	0.811
	6000	15.3	82.7	56.9	71.6	0.688	0.866	0.794

Table 6.7 Statistics for the additional FEA runs

	C_{D-SSRC}	C_{FEA}	$\frac{C_{FEA}}{C_{D-SSRC}}$
Minimum	0.540	0.104	0.739
Maximum	2.478	1.198	22.4
Mean	0.935	0.557	2.52

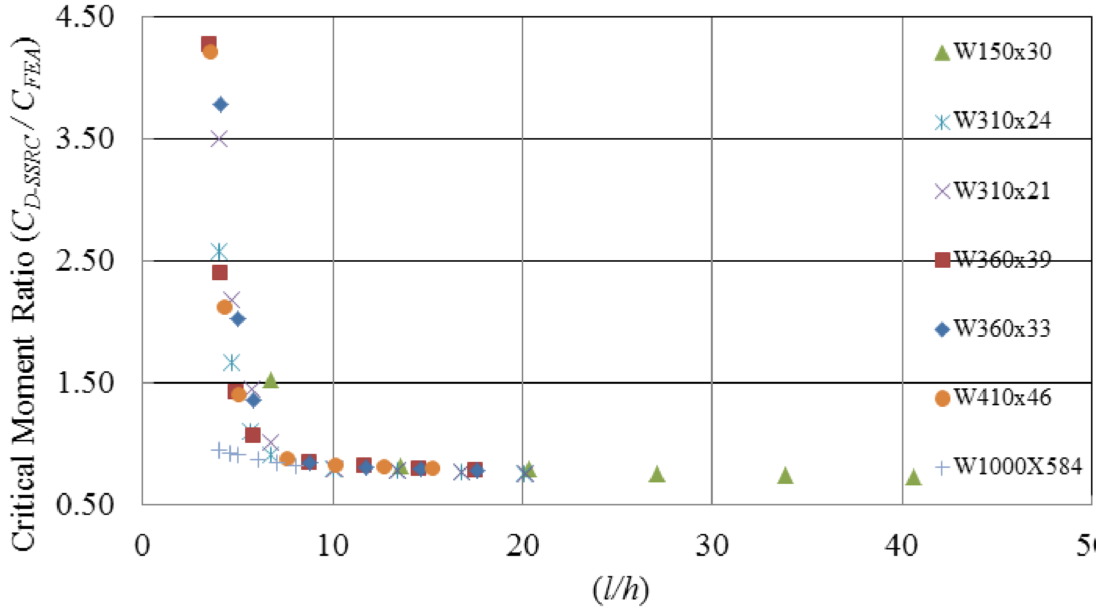

Fig. 6.9- Normalized capacity of additional sections' variation with span

6.8.4. Limitations of Dowswell's Solution

In his paper, Dowswell (2004) does not recommend the use of his procedure (based on the factors C_{DOWS} discussed in Eq. [5.2]) when a beam's failure is governed by inelastic lateral torsional buckling. In addition, as discussed in Subsection 6.2.2, the 6th edition of the Guide to Stability Design Criteria for Metal Structures places a limitation on the dimensionless torsional parameter of $0.5 \leq X \leq 2.5$. Therefore, to assess the procedure proposed by Dowswell within its domain of applicability, cases corresponding to inelastic buckling and cases where the dimensionless torsional parameter values lie outside the range $0.5 \leq X \leq 2.5$ must be discarded. Towards this goal, Fig. 6.10 presents the FEA results for combinations of sections and spans whose failure is governed strictly by elastic LTB and Fig. 6.11 presents the FEA results for combinations of sections and spans whose failure is governed strictly by elastic LTB and whose dimensionless torsional parameter lies within the domain $0.5 \leq X \leq 2.5$.

When assessing the results based on elastic LTB limitation alone, the range of critical moment ratios $M_{D-SSRC}/M_{FEA} = C_{D-SSRC}/C_{FEA}$ are observed to range from 75.9% to 218% signifying that the Dowswell solution ranges from conservative predictions of 24.1% to overestimations of 118% when compared to the critical moments obtained through FEA. While limiting the comparisons to sections governed by a pure elastic LTB mode in fact discards many sections with grossly un-conservative results, Dowswell's solution is still observed to provide inaccurate results for beams with a low span to height ratios. This suggests that the capacity of short span beams which fail in a pure elastic LTB are generally overestimated by Dowswell's solution.

When both limitations are applied (failure in elastic LTB mode and $0.5 \leq X \leq 2.5$), better agreement is obtained between the Dowswell solution and the finite element solution. The variation in results is observed to range from conservative predictions of 24.1% to overestimations of 11.2%. Although the limitations introduced in the SSRC on Dowswell's study provide better results, they happen to discard beams which fail in an elastic LTB mode, leaving designers with no guidance in such cases. As such, a more general solution is needed for a wider range of the dimensionless torsional parameter X.

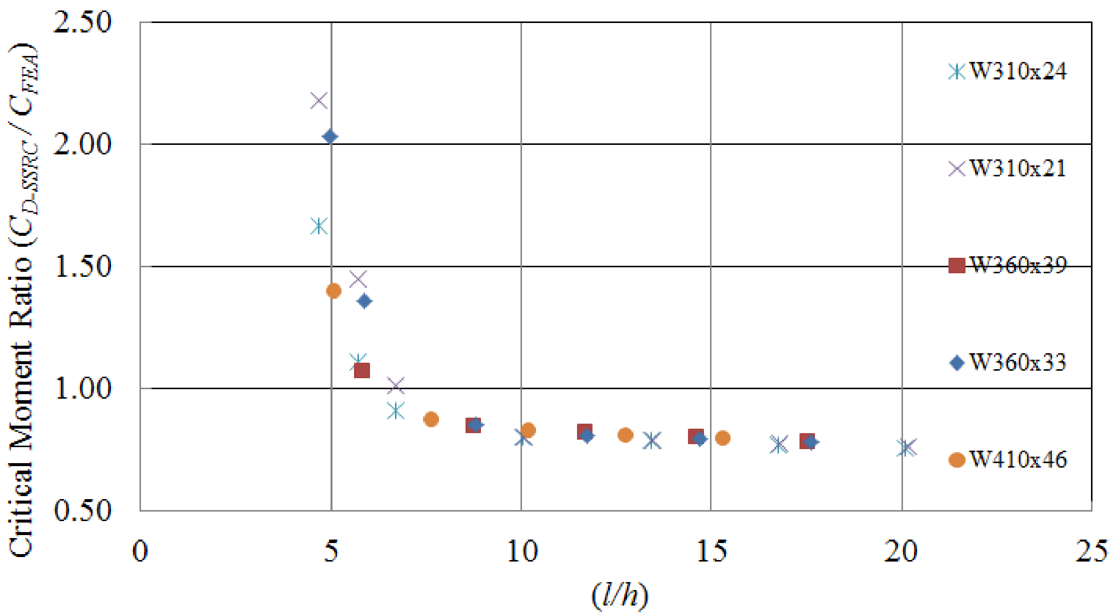

Fig. 6.10- FEA results for additional sections governed by elastic LTB

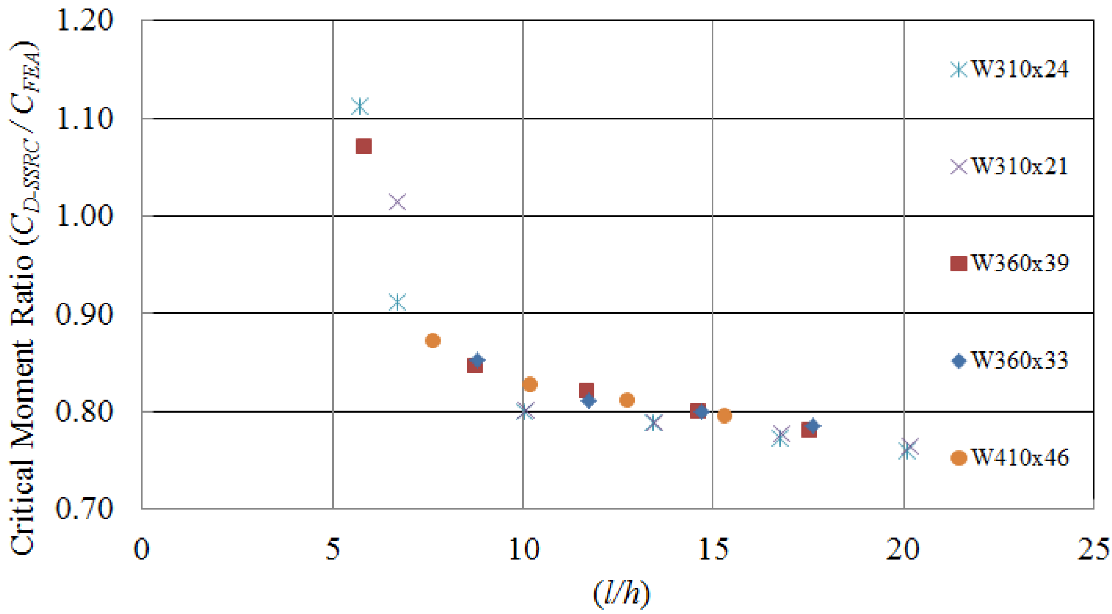

Fig. 6.11- FEA results for additional sections governed by elastic LTB and meeting the constrain $0.5 \leq X \leq 2.5$

6.8.5. Evaluating Dowswell's Predictions

In order to illustrate the trend of Dowswell's equations with the dimensionless torsional parameter X and compare them with the trend obtained by the FEA model, the ratio of critical moment to classical moment value (i.e., predicted moment factor) for all sections and span combinations are plotted in Fig. 6.12. As the reader recalls, the sections are comprised of three sections with various spans analyzed in Dowswell (2004), one section with various spans analyzed in Dabbas (2002), and an additional seven sections with various spans As highlighted in Subsection 6.2.2 and depicted in Fig. 6.12, both of Dowswell's moment factors C_{DOWS} and C_{D-SSRC} show a parabolic trend with minimum value near a value of X close to 2.0. The trend of the finite element agrees reasonably well below X=2.0. For higher values of X, finite element results exhibit a slightly decreasing trend while the Dowswell equations exhibit a sharply increasing trend. The use of Dowswell equations beyond X=2.0 would lead to grossly conservative results.

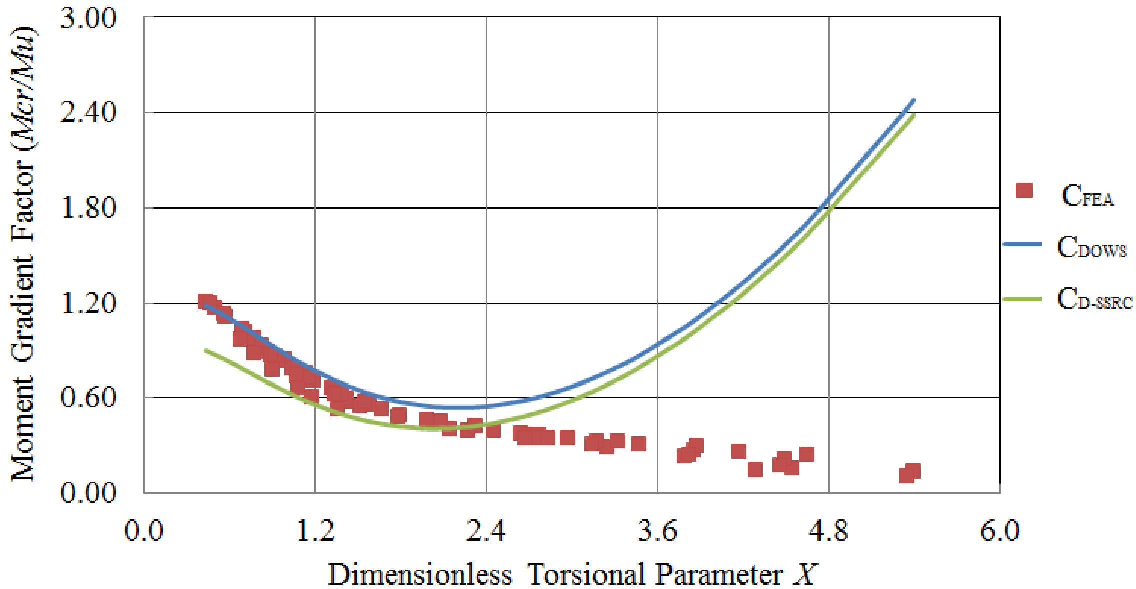

Fig. 6.12- Relation of Dimensionless Torsional Parameter X with moment gradient factor

In order to stay consistent with the goal of providing solutions for design, only those section and span combinations likely to be used in design are retained in the database. Throughout the selection of additional sections, care was taken to avoid sections which are governed by yielding. In addition, to provide a more realistic solution, a deflection limit was enforced such that sections and span combinations whose deflection exceeds $L/100$ were omitted from the regression. With this restriction, all spans of W310x79, W200x22, W250x58, and W150x30 were omitted. Fig. 6.13 presents the resulting reduced (and refined) database. A regression analysis based on an assumed cubic function is conducted. It is found that Eq. [6.12] presented below provides predictions a very good fit with $R^2 = 0.979$.

[6.12] $$C_{cubic} = \frac{M_{cr}}{M_u} = -0.022X^3 + 0.242X^2 - 0.920X + 1.492$$

6.8.6. Comparison of Proposed Solutions

Fig. 6.13 provides a comparison of both methods provided by Dowswell (Dowswell (2004) and Dowswell-SSRC), the ANSI/AISC 360-10 suggestion of using a moment gradient factor of unity, the procedure outlined in Clause 13.6(a) of CAN/CSA S16-09 to use an effective length of $1.4L$, the procedure outlined in the Informative Appendix H of AS 4100-1998, and the new equation developed in the present study through Eq. [6.12]. As observed, the Dowswell-SSRC solution provides conservative results within its limitations of $0.5 \leq X \leq 2.5$. However for beams where $X \geq 2.5$, the solution provides grossly un-conservative results. Using the ANSI/AISC 360-10 solution provides conservative predictions only when $X \leq 0.6$. In most practical ranges, it provides un-conservative predictions. The CAN/CSA S16-09 procedure based on $1.4L$ provides conservative results when $X \leq 1.5$. Appendix H of AS 4100-1998 solution provides the best predictions of all standards studied. The AS 4100-1998 procedure provides conservative results for $X \geq 2.25$ and slightly overestimates capacities for $X \leq 2.25$. In contrast, the solution introduced in this study, provides the best predictions and can be used in the wider range $0.5 \leq X \leq 5.0$. The reader is referred to Appendix D for the data used to generate Fig. 6.13.

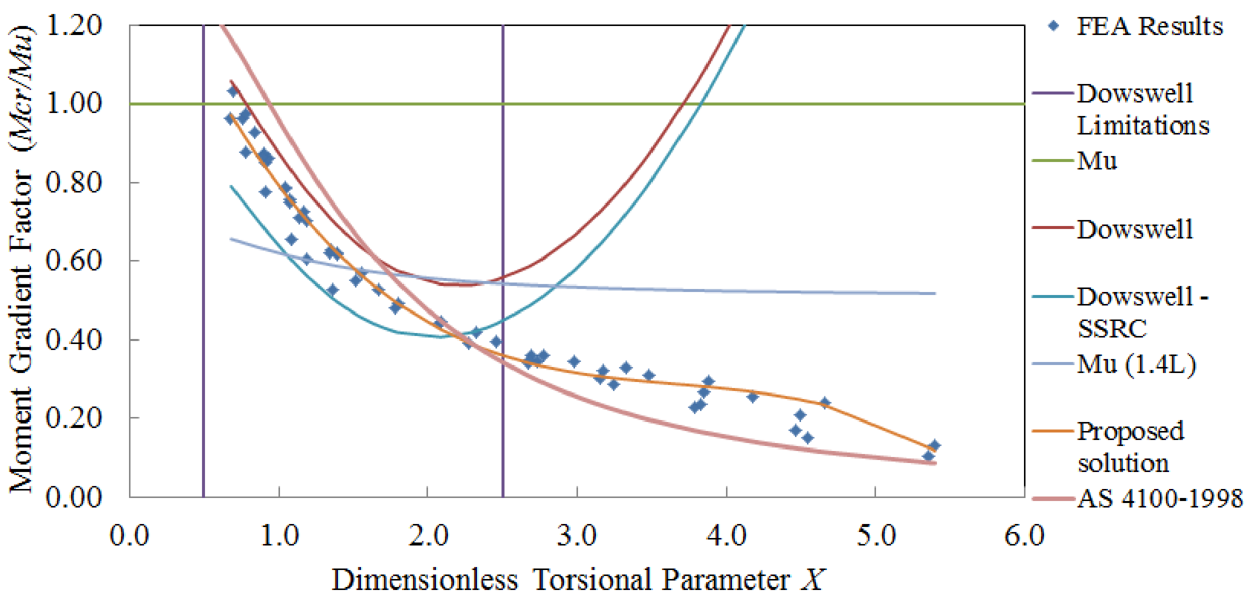

Fig. 6.13- Comparison of proposed methods and their limitations

6.9. *Notation for Chapter 6*

b	flange/ beam width
C_{AISC}	ANSI/AISC 360-10 moment gradient factor
C_{AUS}	AS 4100-1998 moment gradient factor
C_B	bracing coefficient
C_{CAN}	CAN/CSA S16-09 moment gradient factor
C_{cubic}	proposed moment gradient factor which captures effects of distortional buckling
C_{DABB}	moment gradient factor proposed calculated by M_{DABB}/M_u

C_{DOWS}	moment gradient factor proposed by Dowswell (2004)
C_{D-SSRC}	moment gradient factor proposed by SSRC (2010)
C_H	load position factor
C_L	UDL moment distribution coefficient
C_{st}	standard dependent moment gradient factor
C_w	warping constant
$C_{3,4}$	AS 4100-1998 cantilever moment gradient factor equation constants
E	modulus of elasticity of steel
G	shear modulus of elasticity of steel
h	distance between flange centroids
J	St. Venant torsional constant
L	length of beam
M_{cr}	elastic critical moment capturing the effects of distortional buckling
M_{DABB}	elastic critical moment results presented in Dabbas (2002)
M_{DOWS}	elastic critical moment by Dowswell (2004)
M_{D-SSRC}	elastic critical moment by SSRC (2010)
M_u	classical lateral torsional buckling solution
P	applied point load
t	flange thickness
w	web thickness
X	dimensionless torsional parameter
y_L	load height wrt shear center
α_{lc}	AS 4100-1998 cantilever load position factor
α_{mc}	AS 4100-1998 cantilever moment gradient factor

Chapter 7
Conclusions and Recommendations

7.1. Summary and Conclusions

1) Through dimensional analysis, it was shown that the distortional moment ratio M_{cr}/M_u depends upon only four dimensionless geometric parameters. These are the web slenderness ratio w/h, flange slenderness ratio t/b, width to height ratio b/h, and span to height ratio l/h.

2) For simply supported beams under uniform moments, results reveal that the effects of distortion are more pronounced for wide flange section beams with slender webs (low w/h ratios), stocky flanges (high t/b ratios), and compact beam aspect ratios (high b/h ratios). The findings which suggest that beams with slender webs are more susceptible to distortional buckling are in agreement with previous findings by Roberts and Jhita (1983) and Bradford (1986).

3) Through Buckling FEA on 53 beams with sections from the CISC SST database, and subsequent regression analysis of the results, the distortional moment ratio M_{cr}/M_u was expressed as a function of w/h, t/b, and b/h, with a correlation coefficient $R^2 = 0.955$.

4) It was shown that the distortional moment ratio M_{cr}/M_u in simply supported beams subject to linear moment distributions exhibit trends similar to those of beams subject to uniform moment when the web slenderness ratio w/h, flange slenderness ratio t/b, width to height ratio b/h, and span to height ratio l/h are varied.

5) Results for beams with end moments (i.e., with linear moment distributions) suggest that the warping stiffness introduced by commonly used connections in steel construction involving transverse stiffeners lead to higher M_{cr}/M_u than details not involving end stiffeners. In general, the presence of transverse stiffeners lead to moment gradients higher than those based in various design standards.

6) Through simulation of realistic design loading and web cleat connections, three observations regarding assumptions made in the classical LTB solution are made. These are: 1) the assumption made in the classical lateral torsional buckling solution that beams are fully restrained against twist at both ends did not hold true, 2) the assumption made in the classical lateral torsional buckling solution regarding the absence of end lateral displacements of buckled beams held true, and 3) the Vlasov theory assumption postulating cross sections to behave as a rigid disk within the plane of the cross-section did not hold true for all runs, i.e., some beams of real cross-sections and practical spans exhibited distortion.

7) For simply supported beams with end cleat connections subject to mid-span loads, the current study proposed a new procedure to quantify the elastic lateral torsional buckling resistance as a product of the classical lateral torsional buckling term and by three factors, 1) a distortional coefficient D which accounts for distortional effects as determined by FEA results, 2) a partial twist restraint coefficient C_R accounting for the partial twist restraint provided by the cleat angles which depends on the twisting stiffness of the cleat angles relative to the twisting stiffness of the beam, and 3) a standard specific constant S_{st} which ensures consistency in the safety level between the various standards.

8) A series of shell finite element buckling analyses for cantilevers subject to tip point-loads acting at the top flange was conducted. The study has shown that distortional effects are evident and particularly pronounced for short span cantilever, with significant implications on the predicted critical to classical moment ratio.

9) A regression analysis was carried out to relate the distortional moment ratio M_{cr}/M_u to the dimensionless torsional parameter $X = \pi\sqrt{EC_w/GJ}/L$ used by Dowswell (2004). The resulting equation was based on a large number of runs based on cross-section and span combinations solely of practical interest and is applicable to a wide range of X and predicts the critical moments reliably (with a regression coefficient $R^2 = 0.979$) while capturing distortional effects.

10) The cantilever parametric study provided a basis to assess the quality of various solutions in structural steel design standards. The CAN/CSA S16-09 procedure based on an effective span of $1.4L$ was found to lead to un-conservative results for $X \geq 1.5$. Also, the ANSI/AISC 360-10 procedure was found to lead to un-conservative results for $X \geq 0.6$ while the Dowswell-SSRC solution was shown to lead to un-conservative results for $X \geq 2.5$. The AS 4100-1998 Appendix procedure provided the best results.

7.2. Recommendations for Future Research

1) Further investigation pertaining to beams supported by web cleats should be carried out for various loading conditions (multiple loads, udl, load position factor), and development of appropriate distortional coefficients, partial twist coefficients, and standard specific consistency constants. Findings from this research should then be consolidated with the findings from the current study into a unified universal design procedure which accounts for realistic partial twist restraint and distortional effects.

2) Realistic modeling for other practical support conditions should be conducted to quantify effects (similar to partial twist restrain) which alter the LTB capacity of beams. Previous research, while extensive, pays little attention to modeling of practical connection details within lateral torsional buckling restraints. Rather, the majority of studies assume simple nodal translation and twist restraints.

3) The present study has provided a basis for quantifying the limits of applicability of the simplified design procedures in CAN/CSA S16-09, ANSI/AISC 360-10, and AS 4100-1998 for the special case of cantilevers with tip loading applied at the top flange with no lateral or twist restraint. Similar studies need to be conducted for other loading patterns, load position relative the shear centre, and presence of lateral or torsional restraints. The resulting limits of applicability for these simplified procedures need to be recognized in design standards. The user should then be directed to other more comprehensive solutions (such as the one proposed in Chapter 6), for cases beyond the limitations of standard provisions.

4) The study provided in Chapter 4 needs to be expanded for different end moment ratios. Based on these results, it would be of practical interest to develop moment gradient equations for various connection details, possibly as functions of geometric dimensionless parameters.

Appendix A
Derivation of M_{cr}/M_u from the π Terms Introduced in Chapter 3

Contents

In Section 3.2 of Chapter 3, π_{6i} is substituted for π_6 in the dimensional analysis. The following illustrates how π_{6i} is obtained from the dimensionless parameters $\pi_1 = w/h$, $\pi_2 = t/b$, $\pi_3 = b/h$, $\pi_4 = l/h$, $\pi_5 = E/G$ and $\pi_6 = M_{cr}/El^3$ introduced in Chapter 3. For a W section, the sectional properties I_y, C_w, and J are given as

[A.1] $$I_y = \frac{tb^3}{6} + \frac{hw^3}{12} - \frac{tw^3}{12}$$

[A.2] $$C_w = \frac{h^2b^3t}{24}$$

[A.3] $$J = \frac{2bt^3}{3} + \frac{hw^3}{3}$$

Using the already established π terms in chapter 3, it can be shown that the three sectional properties listed normalized relative to the span raised to the appropriate power arise as linear combinations of π_1 through π_4 leading to

[A.4] $$\begin{aligned}&\lambda_1(\pi_1,\pi_2,\pi_3,\pi_4)\\ &= \frac{1}{6}\left(\frac{1}{\pi_4}\right)^4(\pi_3)^4\left(\frac{1}{\pi_1}\right) + \frac{1}{12}\left(\frac{1}{\pi_4}\right)^4\left(\frac{1}{\pi_2}\right)^3 - \frac{1}{12}\left(\frac{1}{\pi_4}\right)^4\left(\frac{1}{\pi_2}\right)^3\left(\frac{1}{\pi_1}\right)(\pi_3)\\ &= \frac{tb^3}{6l^4} + \frac{hw^3}{12l^4} - \frac{tw^3}{12l^4} = \frac{I_y}{l^4}\end{aligned}$$

[A.5] $$\lambda_2(\pi_1,\pi_4) = \left(\frac{1}{\pi_4}\right)^6\left(\frac{1}{\pi_1}\right)(\pi_3)^4 = \frac{h^2b^3t}{24l^6} = \frac{C_w}{l^6}$$

[A.6] $$\lambda_3(\pi_1,\pi_2,\pi_4) = \frac{2}{3}\left(\frac{1}{\pi_4}\right)^4(\pi_3)^4\left(\frac{1}{\pi_1}\right)^3 + \frac{1}{3}\left(\frac{1}{\pi_4}\right)^4\left(\frac{1}{\pi_2}\right)^3 = \frac{2bt^3}{3l^4} + \frac{hw^3}{3l^4} = \frac{J}{l^4}$$

The classical critical moment for a simply supported beam under uniform moments is given by

[A.7] $$M_u = \frac{3.14}{l}\sqrt{EI_y JG + \left(\frac{3.14E}{l}\right)^2 C_w I_y}$$

Moment M_u is normalized with respect to the critical moment including distortional effects M_{cr}, i.e.,

[A.8] $$\frac{M_u}{M_{cr}} = \frac{3.14}{M_{cr} l}\sqrt{EI_y JG + \left(\frac{3.14E}{l}\right)^2 C_w I_y} = 3.14\frac{EL^3}{M_{cr}}\sqrt{\left(\frac{J}{l^4}\right)\left(\frac{I_y}{l^4}\right)\left(\frac{G}{E}\right) + 3.14^2\left(\frac{C_w}{l^6}\right)\left(\frac{I_y}{l^4}\right)}$$
$$= 3.14\left(\frac{1}{\pi_6}\right)\sqrt{\lambda_2\lambda_1\left(\frac{1}{\pi_5}\right) + 3.14^2\lambda_3\lambda_1}$$

By inverting the above relation, one recovers the dimensionless parameter $\pi_{6i} = M_{cr}/M_u$ as a function of π_i $(i = 1..6)$ and $\lambda_j(\pi_i)(j = 1,2,3)$ as

[A.9] $$\pi_{6i} = \frac{M_{cr}}{M_u} = \frac{\pi_6}{3.14\sqrt{\lambda_2\lambda_1\left(\frac{1}{\pi_5}\right) + 3.14^2\lambda_3\lambda_1}}$$

Equation [A.9] signifies that the dimensionless parameter π_6 can be replaced by π_{6i}.

Appendix B
List of Input Parameters and FEA Results for the Parametric Runs in Chapter 3

Contents

Table B.1 presents the input parameter values for the parametric runs conducted in Chapter 3 while Table B.2 provides the results of the FEA discussed in Subsection 3.10.6.

Table B.1 Input parameters for parametric runs in chapter 2

ID#	w/h	t/b	b/h	l/h	$b\,(mm)$	$t\,(mm)$	$w\,(mm)$	$l\,(mm)$
wh222	0.0222	0.0690	0.61	26.00	305	21.034	18.519	13000
wh244	0.0244	0.0690	0.61	26.00	305	21.034	16.949	13000
wh270	0.0270	0.0690	0.61	26.00	305	21.034	15.625	13000
(Ref.)	**0.0294**	**0.0690**	**0.61**	**26.00**	**305**	**21.034**	**14.706**	**13000**
wh313	0.0313	0.0690	0.61	26.00	305	21.034	13.514	13000
wh339	0.0339	0.0690	0.61	26.00	305	21.034	12.195	13000
wh370	0.0370	0.0690	0.61	26.00	305	21.034	11.111	13000
tb556	0.0294	0.0556	0.61	26.00	305	27.727	14.706	13000
tb588	0.0294	0.0588	0.61	26.00	305	24.898	14.706	13000
tb635	0.0294	0.0635	0.61	26.00	305	22.593	14.706	13000
(Ref.)	**0.0294**	**0.0690**	**0.61**	**26.00**	**305**	**21.034**	**14.706**	**13000**
tb741	0.0294	0.0741	0.61	26.00	305	19.365	14.706	13000
tb816	0.0294	0.0816	0.61	26.00	305	17.941	14.706	13000
bh048	0.0294	0.0690	0.48	26.00	240	16.552	14.706	13000
bh052	0.0294	0.0690	0.52	26.00	260	17.931	14.706	13000
bh057	0.0294	0.0690	0.57	26.00	285	19.655	14.706	13000
(Ref.)	**0.0294**	**0.0690**	**0.61**	**26.00**	**305**	**21.034**	**14.706**	**13000**
bh068	0.0294	0.0690	0.68	26.00	340	23.448	14.706	13000
bh075	0.0294	0.0690	0.75	26.00	375	25.862	14.706	13000
bh081	0.0294	0.0690	0.81	26.00	405	27.931	14.706	13000
lh9	0.0294	0.0690	0.61	9.00	305	21.034	14.706	4500
lh15	0.0294	0.0690	0.61	15.00	305	21.034	14.706	7500
lh21	0.0294	0.0690	0.61	21.00	305	21.034	14.706	10500
(Ref.)	**0.0294**	**0.0690**	**0.61**	**26.00**	**305**	**21.034**	**14.706**	**13000**
lh31	0.0294	0.0690	0.61	31.00	305	21.034	14.706	13000
lh36	0.0294	0.0690	0.61	36.00	305	21.034	14.706	15500
lh42	0.0294	0.0690	0.61	42.00	305	21.034	14.706	18000

Table B.2 Complete set of chapter 3 parametric runs

Section Designation	w/h	t/b	b/h	h/l	M_u (kNm)	M_{cr} (kNm)	$\frac{M_{cr}}{M_u}$
W150x13	0.0300	0.049	0.6988	0.0220	6.5	6.3	0.975
W150x30	0.0447	0.0608	1.0359	0.0568	162.8	147.6	0.906
W200x19	0.0295	0.0637	0.5191	0.1310	110.9	106.9	0.965
W200x31	0.032	0.0761	0.6707	0.0999	241.1	224.7	0.932
W200x42	0.0373	0.0711	0.8592	0.0743	325.7	299.1	0.918
W200x52	0.0408	0.0618	1.0548	0.0537	364	333.8	0.917
W200x71	0.0514	0.0845	1.0373	0.0537	595.9	533	0.894
W250x18	0.0195	0.0525	0.4111	0.0410	10.5	10.3	0.977
W250x28	0.0256	0.098	0.408	0.1786	249.1	235.1	0.944
W250x45	0.030	0.0878	0.585	0.1150	433	400.3	0.925
W250x67	0.0369	0.077	0.8454	0.0731	645.6	585.4	0.907
W250x80	0.0391	0.0612	1.0607	0.0546	721.2	654.1	0.907
W310x21	0.0172	0.0564	0.3397	0.0541	14.7	14.4	0.977
W310x28	0.020	0.0873	0.3399	0.2308	293.7	279.7	0.952
W310x45	0.0219	0.0675	0.55	0.1312	525.9	496.2	0.943
W310x67	0.0292	0.0716	0.7001	0.0940	735	680.6	0.926
W310x86	0.0310	0.0642	0.8648	0.0699	919.1	841.2	0.915
W310x97	0.0338	0.0505	1.0424	0.0585	1038	956.2	0.921
W310x118	0.0403	0.0609	1.0396	0.0850	1269	1165	0.918
W310x143	0.0467	0.0741	1.0297	0.0557	1756	1590	0.905
W360x39	0.0190	0.0836	0.3739	0.0566	467.2	443	0.948
W360x57	0.0229	0.0762	0.4987	0.2014	723.7	682.5	0.943
W360x79	0.0279	0.082	0.6079	0.1124	1048	967.3	0.923
W360x110	0.0335	0.0777	0.7527	0.1437	1471	1343	0.913
W360x134	0.0331	0.0488	1.0917	0.0563	1722	1584	0.92
W360x147	0.0362	0.0535	1.0876	0.0549	1881	1735	0.923
W360x216	0.0498	0.0703	1.1345	0.0503	3115	2840	0.912
W360x287	0.0634	0.0917	1.1195	0.0495	4826	4328	0.897
W360x634	0.1199	0.1818	1.0683	0.0284	10640	9401	0.883
W360x818	0.1451	0.222	1.048	0.0241	14400	12650	0.879
W360x900	0.1551	0.2398	1.04	0.0224	15990	14000	0.876
W410x39	0.0164	0.0629	0.3588	0.2054	448.6	430.1	0.959
W410x54	0.0191	0.0616	0.4514	0.1568	663.7	635.6	0.958
W410x67	0.0222	0.0804	0.4525	0.1582	943.4	891	0.944

Section Designation	w/h	t/b	b/h	h/l	M_u (kNm)	M_{cr} (kNm)	$\frac{M_{cr}}{M_u}$
W410x85	0.0273	0.1006	0.4539	0.1534	1210	1126	0.93
W460x60	0.0181	0.0869	0.3464	0.2209	919.6	870	0.946
W460x82	0.0223	0.0838	0.4302	0.1708	1316	1243	0.945
W460x464	0.0776	0.2282	0.6132	0.1661	9248	7679	0.83
W530x66	0.0173	0.0691	0.3213	0.0691	1125	1072	0.952
W530x92	0.0197	0.0746	0.4039	0.2568	1650	1571	0.952
W530x109	0.0223	0.0891	0.4056	0.1848	1969	1858	0.943
W530x138	0.028	0.1103	0.4073	0.1794	2557	2383	0.932
W610x82	0.0171	0.0719	0.3037	0.1751	114.1	110.4	0.968
W610x84	0.0154	0.0518	0.3868	0.0586	1493	1432	0.959
W610x101	0.0179	0.0654	0.3877	0.0584	2127	2031	0.955
W610x125	0.0201	0.0856	0.3866	0.2028	2575	2433	0.945
W610x155	0.0215	0.0586	0.5473	0.1911	3086	2939	0.953
W610x195	0.0258	0.0746	0.5472	0.1260	4439	4178	0.941
W920x1191	0.0622	0.2385	0.4702	0.1299	44820	37280	0.832
W1000x272	0.0172	0.1033	0.3128	0.1092	1021	943.7	0.924
W1000x314	0.0198	0.1197	0.3112	0.0639	1314	1203	0.916
W1000x321	0.0172	0.0775	0.4171	0.0643	1546	1451	0.938
W1000x371	0.0197	0.0903	0.415	0.0533	1986	1844	0.928
						Min	0.830
						Max	0.977
						Mean	0.928

Appendix C
Buckling Mode Study for a Beam under Reverse Moments

Contents

This appendix provides the first five buckling mode shapes and corresponding critical moments (Fig. C.1) for the beam investigated in Subsection 4.65. Cross-section is W310x52, end connection details are ST2B-L, and spans range from 4m to 12m.

Observations

The provided plots show that localized buckling in the connection region corresponds to higher modes, and is thus of no practical importance for the chosen section. For all spans considered, lateral torsional buckling corresponds to the lowest critical moments.

Mode	$l = 4{,}000\,mm$	$l = 6{,}000\,mm$
1st	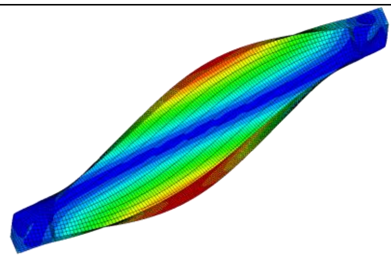	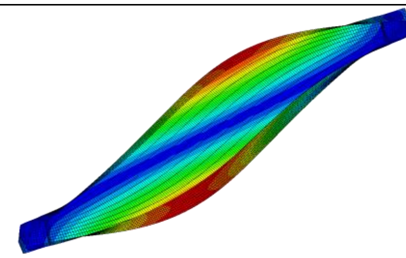
	$M_{cr} = 672.7\,kNm$	$M_{cr} = 409.6\,kNm$
2nd	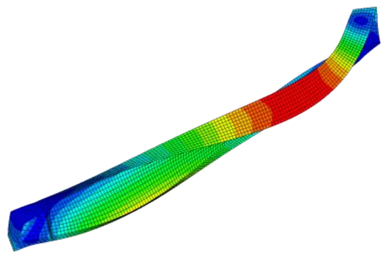	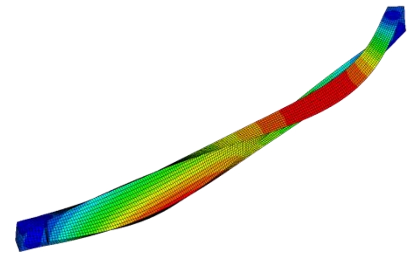
	$M_{cr} = 1070\,kNm$	$M_{cr} = 720.5\,kNm$
3rd	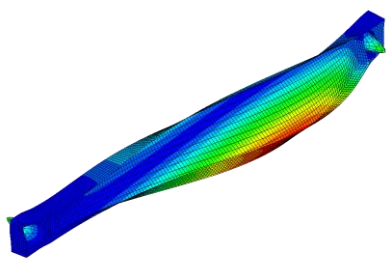	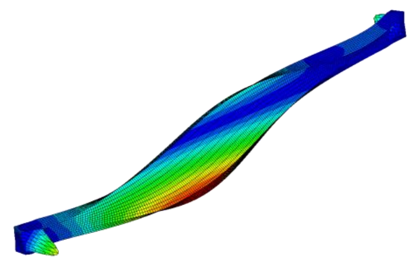
	$M_{cr} = 1274\,kNm$	$M_{cr} = 1166\,kNm$
4th	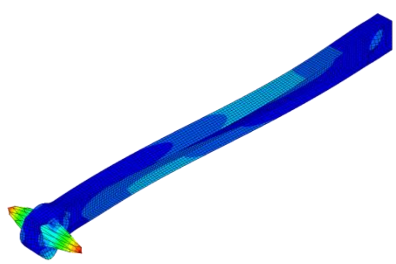	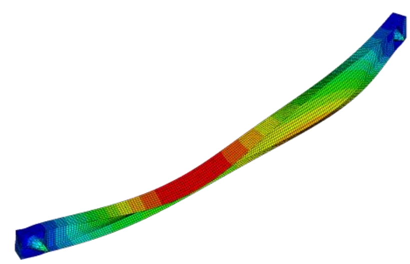
	$M_{cr} = 1319\,kNm$	$M_{cr} = 1227\,kNm$
5th	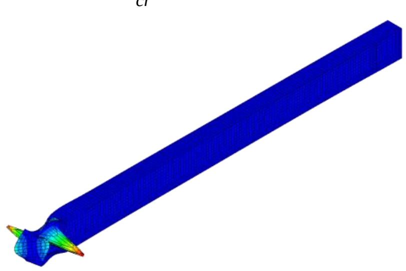	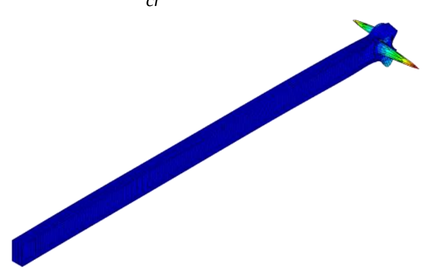
	$M_{cr} = 1447\,kNm$	$M_{cr} = 1327\,kNm$

Mode	$l = 8{,}000\ mm$	$l = 10{,}000\ mm$
1^{st}	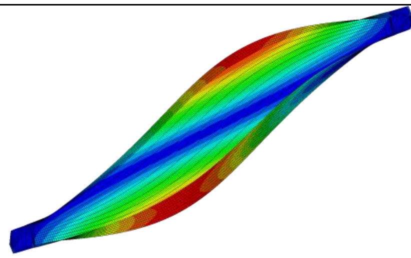 $M_{cr} = 284.7\ kNm$	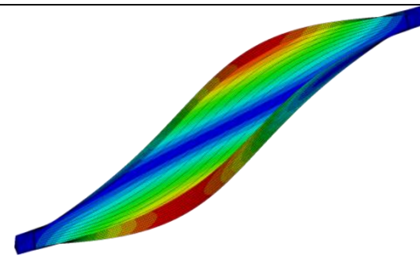 $M_{cr} = 216.0\ kNm$
2^{nd}	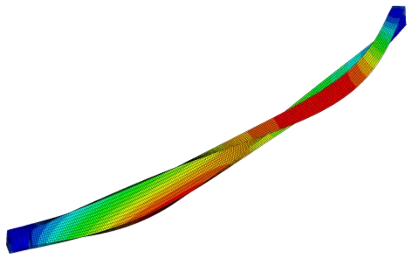 $M_{cr} = 479.5\ kNm$	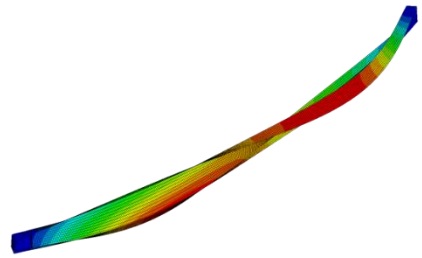 $M_{cr} = 384.7\ kNm$
3^{rd}	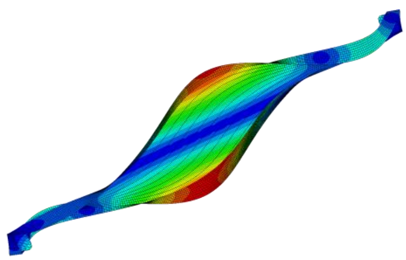 $M_{cr} = 1043\ kNm$	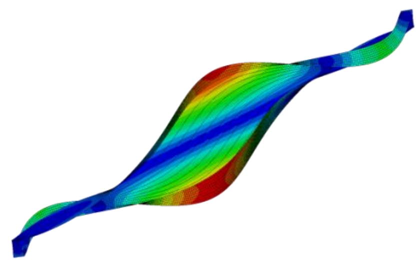 $M_{cr} = 803.9\ kNm$
4^{th}	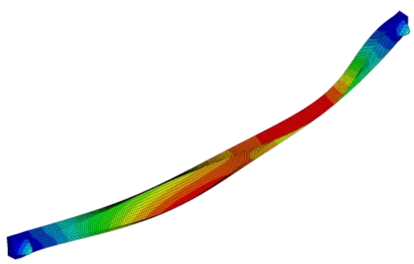 $M_{cr} = 1147\ kNm$	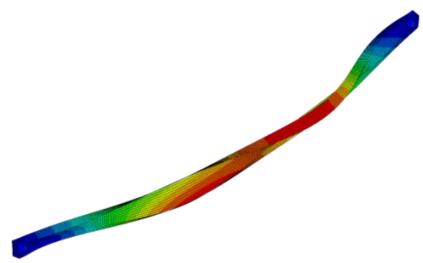 $M_{cr} = 1016\ kNm$
5^{th}	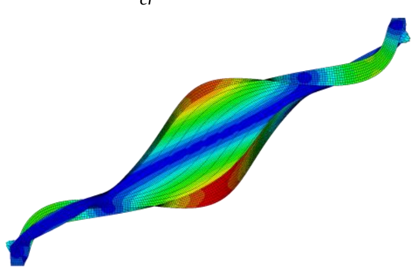 $M_{cr} = 1310\ kNm$	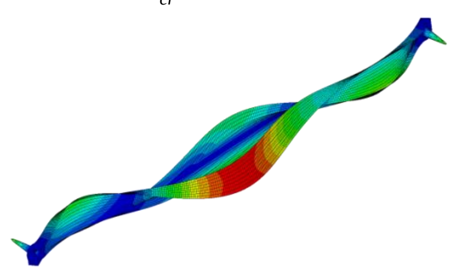 $M_{cr} = 1184\ kNm$

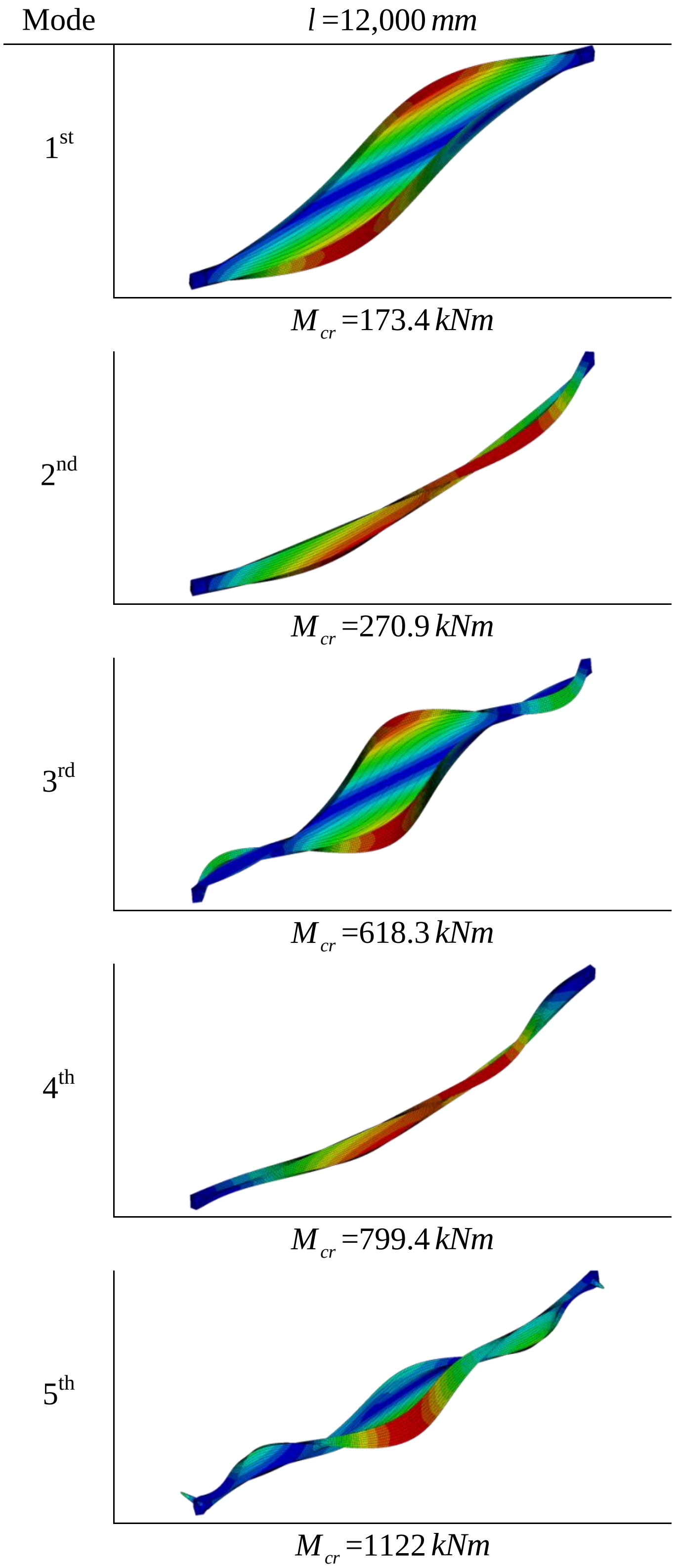

Fig. C.1- Buckling modes for a simply supported W310x52 beam

Appendix D

AS 4100-1998 Informative Appendix H Procedure for Torsional End Restraints in LTB

Contents

This Appendix provides a comparison of the procedures outlined in Appendix H of As 4100-1998 with those presented in Chapter 5. As one recalls, in Chapter 5, a procedure is introduced which accounts for reductions in lateral torsional buckling capacity due to partial twist restraint at supports. This solution is given by

[D.1] $$M_0 = C_R M_u = \sqrt{\frac{1}{1+1.642\alpha}} M_u$$

Where the dimensionless ratio α is given by

[D.2] $$\alpha = \frac{1}{R}\left(\frac{GJ}{L} + \frac{\pi^2 EC_w}{L^3}\right)$$

In Appendix H of AS 4100-1998, the following solution is given which accounts for reductions in critical moment due to partial twist restraints

[D.3] $$M_{cr} = \sqrt{\frac{2\beta_T}{1+\beta_T}} M_u \le M_u$$

where β_T is given by

[D.4] $$\beta_T = \frac{\left(\frac{Rl}{GJ}\right)}{5\left(1+K^2\right)}$$

and

[D.5] $$K = \sqrt{\frac{\pi^2 EC_w}{GJl^2}}$$

By substituting Eqs. [D.4] and [D.5] into Eq. [D.3] and rearranging, it can be shown that

[D.6] $$M_{cr} = \sqrt{\frac{2\beta_T}{1+\beta_T}} M_u = \sqrt{\frac{2}{5\alpha+1}} M_u = C_{R-AUS} M_u \le M_u$$

To assess the validity of C_{R-AUS}, a comparison will be made with C_R using the examples provided in Chapter 5.

Table D.1 Numeric comparisons of proposed partial twist reduction factor and AS 4100-1998 factor

Angle	$R\ (kNm/Rad)$	α	C_R	C_{R-AUS}
L76x76x4.8	48.4	0.1081	0.922	$1.14 \geq 1.0$ therefore $C_{R-AUS} = 1.0$
L76x76x9.5	375	0.01395	0.989	$1.37 \geq 1.0$ therefore $C_{R-AUS} = 1.0$

For the given example, the AS 4100-1998 equation does not recognize the fact that the restrain provided by cleat angles is insufficient in developing the full lateral torsional buckling resistance based on full twist restraint at the end. In addition to this, AS 4100-1998 does not differentiate between restrains provided by L76x76x4.8 vs. L76x76x9.8. This is contrary to the finite element predictions which confirm a 7% increase in the capacity when replacing L76x76x4.8 by L76x76x9.5. This difference is successfully captured by the C_R coefficient developed in the present study, but not the AS 4100-1998 Appendix procedure which treats both end details similar to the case of full end twist restraint.

Appendix E

Cantilever Moment Gradient

Factor Results

Contents

Table E.1 presents result values used in generating Fig. 6.13 in Chapter 6.

Table E.1 Cantilever results

	l (mm)	X	M_u (kNm)	$M_u(1.4l)$ (kNm)	M_{FEA} (kNm)	C_{CAN} (1)	C_{AUS}	C_{DOWS}	C_{D-SSRC}	C_{FEA} (2)	C_{cubic} (3)
W410x39	2286	2.77	316	170	114	0.538	0.291	0.608	0.512	0.36	0.332
	3048	2.08	185	103	82	0.554	0.45	0.542	0.407	0.443	0.427
	3810	1.66	125	71.2	65.9	0.571	0.6	0.604	0.436	0.529	0.53
	4572	1.39	91.5	53.8	56.5	0.588	0.731	0.692	0.498	0.617	0.623
	5334	1.19	71.2	43	50.1	0.603	0.841	0.777	0.562	0.703	0.703
	6096	1.04	57.9	35.7	45.4	0.617	0.932	0.852	0.621	0.784	0.772
W310x79	2286	2.65	2350	1270	870	0.54	0.314	0.581	0.479	0.371	0.344
	3048	1.99	1380	771	640	0.558	0.48	0.549	0.407	0.463	0.447
	3810	1.59	934	537	522	0.576	0.633	0.625	0.45	0.559	0.553
	4572	1.32	688	408	453	0.593	0.765	0.718	0.517	0.658	0.647
	5334	1.13	537	327	405	0.608	0.874	0.804	0.583	0.754	0.728
	6096	0.993	438	272	370	0.621	0.963	0.878	0.642	0.845	0.796
W200x22	2286	1.16	69.9	42.4	49.5	0.606	0.858	0.791	0.573	0.707	0.716
	3048	0.871	45.4	28.8	40.3	0.634	1.04	0.947	0.698	0.887	0.86
	3810	0.696	33.4	21.8	34	0.655	1.15	1.05	0.782	1.02	0.961
	4572	0.58	26.4	17.6	29.3	0.669	1.22	1.11	0.838	1.11	1.04
	5334	0.497	21.8	14.8	25.5	0.679	1.26	1.16	0.875	1.17	1.09
	6096	0.435	18.7	12.8	22.5	0.686	1.29	1.18	0.9	1.21	1.14
W250x58	1000	4.29	4550	2380	661	0.523	0.135	1.4	1.33	0.145	0.262
	2000	2.14	1220	675	496	0.552	0.432	0.539	0.409	0.406	0.415
	3000	1.43	601	352	345	0.585	0.71	0.676	0.486	0.573	0.607
	4000	1.07	379	232	280	0.614	0.913	0.836	0.608	0.74	0.757
	5000	0.857	272	173	241	0.636	1.05	0.955	0.704	0.886	0.867
	6000	0.715	212	138	212	0.652	1.14	1.04	0.774	1	0.95
W150x30	1000	2.84	858	460	298	0.537	0.279	0.625	0.532	0.348	0.327
	2000	1.42	247	145	146	0.586	0.714	0.679	0.488	0.591	0.61
	3000	0.947	131	81.9	109	0.626	0.992	0.903	0.662	0.833	0.819
	4000	0.71	87.4	57	88.6	0.653	1.14	1.04	0.775	1.01	0.953
	5000	0.568	65.5	43.9	74	0.67	1.23	1.12	0.843	1.13	1.04
	6000	0.474	52.5	35.8	62.9	0.681	1.27	1.17	0.885	1.2	1.11

Table E.1 Continued

	l (mm)	X	M_u (kNm)	$M_u(1.4l)$ (kNm)	M_{FEA} (kNm)	C_{CAN} (1)	C_{AUS}	C_{DOWS}	C_{D-SSRC}	C_{FEA} (2)	C_{cubic} (3)
W360x39	1000	4.55	1290	675	194	0.521	0.12	1.61	1.54	0.15	0.244
	1200	3.79	908	478	207	0.526	0.169	1.05	0.975	0.228	0.284
	1400	3.25	675	358	193	0.531	0.223	0.765	0.685	0.285	0.303
	1700	2.68	467	252	160	0.539	0.308	0.586	0.486	0.342	0.341
	2000	2.27	345	189	135	0.548	0.396	0.54	0.417	0.39	0.393
	3000	1.52	168	97.6	92.5	0.58	0.667	0.647	0.465	0.55	0.577
	4000	1.14	105	64	74.6	0.608	0.872	0.803	0.582	0.709	0.726
	5000	0.91	75.2	47.4	63.9	0.63	1.02	0.925	0.68	0.849	0.839
	6000	0.758	58.2	37.6	56	0.647	1.11	1.01	0.752	0.963	0.924
W360x33	1000	5.4	993	515	130	0.518	0.0867	2.48	2.39	0.131	0.118
	1200	4.5	694	362	144	0.522	0.123	1.57	1.5	0.207	0.248
	1400	3.85	515	270	138	0.525	0.164	1.09	1.02	0.268	0.281
	1700	3.17	354	188	114	0.532	0.232	0.734	0.652	0.321	0.306
	2000	2.7	260	140	94.1	0.539	0.304	0.591	0.491	0.361	0.339
	3000	1.8	124	70.1	61	0.565	0.546	0.575	0.419	0.491	0.492
	4000	1.35	75.9	44.9	47.6	0.591	0.751	0.707	0.509	0.627	0.637
	5000	1.08	53.2	32.6	40.3	0.613	0.908	0.832	0.605	0.757	0.753
	6000	0.899	40.6	25.6	35.3	0.631	1.02	0.931	0.685	0.871	0.844
W310x21	1000	4.65	294	153	70.6	0.521	0.115	1.71	1.64	0.24	0.234
	1200	3.88	206	108	60.8	0.525	0.162	1.1	1.03	0.295	0.281
	1400	3.32	153	81.3	50.5	0.53	0.214	0.798	0.72	0.33	0.3
	1700	2.74	106	57	36.6	0.538	0.297	0.6	0.502	0.346	0.336
	2000	2.33	78.3	42.8	32.7	0.547	0.383	0.542	0.423	0.417	0.384
	3000	1.55	38	22	21.7	0.578	0.65	0.636	0.457	0.571	0.565
	4000	1.16	23.7	14.4	17.2	0.605	0.857	0.79	0.572	0.725	0.714
	5000	0.931	16.9	10.6	14.6	0.628	1	0.913	0.67	0.863	0.828
	6000	0.776	13	8.41	12.7	0.645	1.1	1	0.744	0.973	0.914
W310x24	1000	4.17	349	183	89.6	0.523	0.142	1.31	1.24	0.257	0.268
	1200	3.48	245	130	75.8	0.529	0.198	0.871	0.796	0.309	0.294
	1400	2.98	183	97.6	63.2	0.534	0.258	0.666	0.577	0.346	0.317
	1700	2.45	127	69	50.2	0.544	0.353	0.552	0.441	0.396	0.366
	2000	2.09	94.1	52.1	42	0.554	0.448	0.541	0.407	0.446	0.426
	3000	1.39	46.4	27.3	28.8	0.588	0.729	0.691	0.497	0.62	0.621
	4000	1.04	29.4	18.1	23.1	0.616	0.931	0.851	0.62	0.787	0.771
	5000	0.835	21.2	13.5	19.6	0.638	1.07	0.968	0.715	0.926	0.88
	6000	0.696	16.5	10.8	17	0.655	1.15	1.05	0.783	1.03	0.962

Table E.1 Continued

	l (mm)	X	M_u (kNm)	$M_u(1.4l)$ (kNm)	M_{FEA} (kNm)	C_{CAN} (1)	C_{AUS}	C_{DOWS}	C_{D-SSRC}	C_{FEA} (2)	C_{cubic} (3)
W410x46	1000	5.35	2020	1050	211	0.518	0.088	2.43	2.34	0.104	0.127
	1200	4.46	1410	736	240	0.522	0.125	1.54	1.47	0.17	0.251
	1400	3.82	1050	550	248	0.526	0.166	1.07	0.997	0.237	0.282
	1700	3.15	720	383	218	0.532	0.235	0.725	0.642	0.303	0.308
	2000	2.68	529	285	184	0.539	0.308	0.587	0.486	0.348	0.341
	3000	1.78	253	143	122	0.566	0.551	0.578	0.42	0.482	0.496
	4000	1.34	155	91.5	95.8	0.591	0.757	0.711	0.512	0.619	0.641
	5000	1.07	109	66.6	81.4	0.614	0.913	0.836	0.609	0.75	0.757
	6000	0.892	82.7	52.3	71.6	0.632	1.03	0.935	0.688	0.866	0.848
W1000X584	4000	1.36	25200	14900	13300	0.59	0.745	0.703	0.505	0.528	0.633
	4600	1.18	20100	12100	12200	0.604	0.845	0.78	0.565	0.606	0.706
	5000	1.09	17700	10800	11600	0.612	0.903	0.827	0.602	0.656	0.749
	6000	0.907	13400	8480	10400	0.63	1.02	0.926	0.681	0.775	0.84
	7000	0.777	10800	6970	9490	0.645	1.1	1	0.743	0.878	0.913
	8000	0.68	9030	5930	8690	0.657	1.16	1.06	0.79	0.962	0.971

1. $C_{CAN} = \dfrac{M_u(1.4l)}{M_u}$

2. $C_{FEA} = \dfrac{M_{FEA}}{M_u}$

3. $C_{cubic} = \dfrac{M_{cr}}{M_u}$, Eq. [6.12]

References

1. American Institute of Steel Construction, (AISC). (2010). *Specification for Structural Steel Buildings*, ANSI/AISC 360-10, AISC, Chicago, IL.

2. Austin, W. J. (1961). "Strength and Design of Metal Beam-Columns." *Journal of the Structural Division*, ASCE, 87(4), 1-32.

3. Bradford, M. A. and Trahair, N. S. (1981). "Buckling of elastically restrained beams with web distortions." *Thin-Walled Structures*, 107(2), 335-370.

4. Bradford, M. A. (1986). "Inelastic Distortional Buckling of I-Beams." *Computers & Structures*, 24(6), 923-933.

5. Bradford, M. A. (1992a). "Buckling of doubly-symmetric cantilevers with slender webs." *Engineering Structures*, 14(5), 327-334.

6. Bradford, M. A. (1992b). "Lateral-Distortional Buckling of Steel I-Section Members." *Journal of Constructional Steel Research*, 23(1-3), 97-116.

7. Canadian Standards Association, (CSA). (2009) *Limit States Design of Steel Structures*, CAN/CSA S16-09, Toronto, Ontario, Canada.

8. CISC. (2011). *Structural Selections Table V9.2*, http://www.cisc-icca.ca/publications/software/sst/ (last accessed on 2011/08/03)

9. Dabbas, A. (2002). "Lateral Stability of Partially Restrained Cantilever Supports." M. Eng. Report: Department of Civil Engineering, University of Ottawa, Ottawa, ON, Canada.

10. Dowswell, B. (2004). "Lateral-Torsional Buckling of Wide Flange Cantilever Beams." *Engineering Journal*, AISC, 41(2), 85-91.

11. CEN, (2005). Eurocode 3: *Design of Steel Structures*, *Part 1-1: General Rules and Rules for Buildings*, ENV 19931-1, Comité Européen de Normalisation Brussels, Belguim.

12. Gardner, L. and Nethercot, D. A. (2005). *Designers Guide to EN -1993-1 Eurocode 3: Design of Steel Structures and General Rules and Rules for Buildings*, Thomas Telford Publishing, London, UK.

13. Grenier, R., Ofner, R. and Salzberger, G. (1999) "Lateral torsional buckling of beam-columns: Theoretical Background." *ECCS-Validation group*, report 5.

14. Hancock, G. J. (1978) "Local, distortional and lateral buckling of I-beams." *Journal of the Structural Division*, 104(11), 1787-1798

15. Hanckock, G. J. and Papandelis, J. P. (1998). *THIN-WALLED user's manual*, Center for Advanced Structural Engineering, University of Sydey, Sydney, Australia.

16. Kalkan I. and Buyukkaragoz, A. (2012). "A numerical and analytical study on distortional buckling of doubly-symmetric steel I-beams." *Journal of Constructional Steel Research*, 70, 289-207.

17. Kerensky, O. A., Flint, A. R. and Brown W. C. (1956). "The basis for design of beams and plate girders in the revised British Standard 153." *Proceedings of Insitituion of Civil Engineers*, Part III, 5, 396.

18. Kirby, P. A. and Nethercot, D. A. (1979). *Design of Structural Stability,* Halsted Press, NY, NY.

19. Lim, N. H., Park N. H., Kang Y. J., and Sung I. H. (2003) "Elastic buckling of I-beams under linear moment gradient." *International Journal of Solids and Structures*, 40(21), 5635-5647.

20. Nethercot, D. A. (1973). "The effective lengths of cantilevers as governed by lateral buckling." *The Structural Engineer,* 51(5), 161-168.

21. Nethercot, D. A. and Rockey K. C. (1972). "A Unified Approach to the Elastic Lateral Buckling of Beams." *Engineering Journal*, AISC, 9(3), 96-107.

22. Ng, M. L. and Ronagh, H. R. (2004). "An Analytical Solution for the Elastic Lateral-Distortional Buckling of I-section Beams." *Advances in Structural Engineering*, 7(2), 189-200.

23. Papangelis, J. P., Hancock, G. J. and Trahair, N. S. (1995). *PREFLEB user's manual*, Center for Advanced Structural Engineering, University of Sydney, Sydney, Australia.

24. Pi, Y. L. and Trahair N. S. (1997). “Lateral-distortional buckling of hollow flange beams.” *Journal of Structural Engineering*, 123(6), 695-702.

25. Pi, Y. L. and Trahair N. S. (2000). “Distortion and Warping at Beam Supports.” *Journal of Structural Engineering*, 126(11), 1279-1287.

26. Poley, S. (1956). “Lateral Buckling of Cantileverd I-Beams Under Uniform Load.” *ASCE Transactions*, American Society of Civil Engineers, 121, 786-790

27. Poon, C. P. and Ronagh, H. R. (2004). “Distortional Buckling of I-Beams by Finite Element Method.” *Advances in Structural Engineering*, 7(1), 71-80.

28. Roberts, T. M. and Jhita, P. S. (1983). “Lateral, Local and Distortional Buckling of I-beam*s.”* *Thin-Walled Structures*, 1(4), 289-308.

29. Salvadori, M. G. (1955). “Lateral Buckling of I-beams.” *ASCE Transactions*, American Society of Civil Engineers, 120, 1165-1177.

30. Serna, M. A., Lopez, A., Puente, I., and Yong, D. J. (2006). “Equivalent Uniform Moment Factors and Lateral Torsional Buckling of Steel Members.” *Journal of Constructional Steel Research*, 62(6), 566-580.

31. SIMULIA, (2010a), *Abaqus/CAE User’s Manual*, Dassault Systemes.

32. SIMULIA, (2010b), *Abaqus Analysis User’s Manual*, Dassault Systemes.

33. Standards Association of Australia (SAA). (1998). *Steel Structures*, AS4100-1998, SAA, Australian Institute of Steel Construction, Sydney, Australia.

34. Suryoatmono, B. and Ho, D. (2002). “The Moment Gradient Factor in Lateral-Torsional Buckling on Wide Flange Steel Sections.” *Journal of Constructional Steel Research*, 58(9), 1247-1264.

35. Timoshenko, S. P., and Gere, J. M. (1961) *Theory of elastic stability*, 2nd Ed., McGraw-Hill, Ne York.

36. Trahair, N. S. (1983). “Lateral Buckling of Overhanging Beams.” *Instability and Plastic Collapse of Steel Structures*, L. J. Morris, ed., Granada Publishing, London, England, 503-515.

37. Trahair, N. S. (1993). *Flexural-Torsional Buckling of Structures*. CRC Press, Boca Raton, FL.

38. Vlasov, V. Z. (1961). *Thin- Walled Elastic Beams*, Israel Program for Scientific Translations, Jerusalem

39. Wong, E. and Driver, R. G. (2010). "Critical Evaluation of Equivalent Moment Factor Procedures for Laterally Unsupported Beams." *Engineering Journal*, AISC, 47(1), 1-20.

40. Zemian, R. D. (2010). *Guide to Stability Design Criteria for Metal Structures*, Structural Stability Council, Jon Wiley and Sons, Inc., NY, NY.

41. Zirakian, T. and Showkati, H. (2007). "Experiments on Distortional Buckling of I-beams." *Journal of Structural Engineering*." 133(7), 109-1017.